COMMONWEALTH OF AUSTRALIA
DEPARTMENT OF EXTERNAL AFFAIRS

AUSTRALIAN NATIONAL ANTARCTIC RESEARCH EXPEDITIONS

ANARE SCIENTIFIC REPORTS

SERIES A (IV) GLACIOLOGY

PUBLICATION No. 102

THE HEAT BUDGET AND HEAT TRANSFER PROCESSES IN ANTARCTIC PLATEAU ICE AND SEA ICE

by

G. E. WELLER

ISSUED BY THE ANTARCTIC DIVISION
DEPARTMENT OF EXTERNAL AFFAIRS, MELBOURNE
1968

Registered at the G.P.O. Melbourne
for transmission by post as a book.

Printed in Australia by
Brown Prior Anderson Pty Ltd 5 Evans Street Burwood Victoria

CONTENTS

LIST OF FIGURES

THE HEAT BUDGET AND HEAT TRANSFER PROCESSES IN ANTARCTIC PLATEAU ICE AND SEA ICE

By

G. E. WELLER

Antarctic Division, Department of External Affairs, Melbourne
Present Address: Department of Meteorology, University of Melbourne

(Manuscript received January 1968)

ABSTRACT

The conventional meteorological heat budget is examined at two types of widely represented Antarctic ice surfaces: blue ice in the coastal ablation zone and annual floating sea ice. This work is extended to a multi-level sub-surface budget study by considering the heat transfer processes in the ice. Whereas phase changes of the water substance, convection and radiation contribute to the heat transfer towards and away from the ice surface in the atmosphere, only conduction and radiation have to be considered in the ice.

Short-wave radiation transmission in the ice, and the effect of absorbed solar radiation on the thermal diffusion process, are examined in detail. The latter effect can be seen in the apparent thermal diffusivity changes in the ice both in depth and time, changes in the heat content and large conduction losses by the ice in periods of strong radiation. These losses are certainly considerably larger than the conducted heat fluxes conventionally computed from changes in the net heat storage of the ice. In slabs of ice of finite thickness, such as sea ice covers, considerable errors result in the energy balance of the surface if the absorbed radiation is not considered.

Monthly components of the heat budget of the sea ice surface are presented for five months. The effect of the sea-ice cover on the heat exchange between the ocean and the atmosphere is estimated. The monthly heat budget components for the blue ice plateau surface are given for twelve months. The study was carried out near Mawson station at latitude 67°34′ S, longitude 62°53′ E.

0. INTRODUCTION

The heat budget at the surface of the Earth in any climatic region is important in the understanding of the climatology of that region. In budget studies it is of interest not only to determine the total heat budget but also the individual components which determine how the available energy at the surface is spent. Thus it matters if the available energy expenditure is in the form of radiation, evaporation, sensible heat fluxes or increases in the sub-surface heat storage.

Both macrometeorological and micrometeorological methods have been used to determine the heat budget of a number of climatic regions. Budyko's (1955, 1963) work on a global scale is perhaps the best known example of the former. In high latitude regions, Vowinckel and Orvig (1965) have filled in details over the Arctic Ocean omitted by Budyko in his atlas. For the Antarctic continent such a study has yet to be made; the scarcity of data in this region has prevented a macrometeorological approach, so far, and the present study is a contribution towards such an undertaking in the future.

Whereas the macrometeorological heat budgets give data for large areas, their accuracy is generally low. The micrometeorological approach with precise instrumentation on the other hand, gives good data although strictly these are applicable to small areas only. Numerous studies of the latter variety have been carried out in all climatic regions, many of them being summarized by the well-known book of Geiger (1959) on the climate near the ground. On the Antarctic continent the pioneering work by Loewe (1956) and Liljequist (1956) in Adélie Land, and on the Maudheim Ice Shelf respectively, were followed by budget studies undertaken by Kopanev (1960) at Mirni, Hoinkes (1961) at Little America, Dalrymple *et al.* (1963) at the South Pole and Lorius (1963) at Charcot. However, most of these are short-term budget studies only. Of the individual heat budget components investigated, the radiation terms are the best known and have been measured at a number of additional localities. Rusin (1961) has constructed radiation maps with a coverage over a large area of the Antarctic continent, based on this work.

The study of the heat budget for climatological purposes is usually restricted to computing the heat flux components at the surface of a chosen locality only. This applies to ice and snow surfaces as well as to the more usually investigated agricultural surfaces. For glaciological purposes, however, the heat budget and energy exchange at different levels in the ice are of equal importance to that at the surface. The thermal history of snow or ice at any depth is affected by these exchange processes and is of interest in determining mechanical and thermal properties, as well as mass and heat transfer processes. Whereas phase changes of the water subtance, convection and radiation contribute to the heat transfer towards and away from the surface in the atmosphere, only radiation and conduction have to be considered in ice.

A brief bibliographical survey of the theoretical and experimental developments in treating the various heat budget components is of interest and will be given now. Since it is not possible to treat here more than a fraction of the enormous number of publications, only major developments with the emphasis on their applicability to heat budget studies in polar regions will be considered.

The application of turbulent air flow theories to micrometeorological problems dates back to the fundamental work by Schmidt (1925) and Lettau (1939), from which a vast body of theoretical models has been developed. A review of some of these can be found in Sutton (1953, 1955 and 1961) while later developments are discussed by Priestley (1959). More recent work includes the treatment of the diabatic wind profile structure by Lettau (1962) and Swinbank (1964) amongst others. An excellent analysis of wind and temperature profile structures over a snow surface at the South Pole has been given by Dalrymple, Lettau and Wollaston (1963) and may well be used as a model for eddy heat flux computations over ice or snow surfaces. Another study of interest is that by Grainger and Lister (1966) who compared six wind profile laws over a large stability range with profile measurements over melting ice surfaces.

Latent heat fluxes are usually the most difficult heat budget component to determine in polar regions since no precise simple instrumentation exists for measuring humidity profiles at low temperatures. No precise continuous profile measurements have been made to date. Latent heat fluxes are usually determined as remainder terms; alternatively, over ice at least, mass balance methods may be used when no melting of the ice occurs. The Bowen ratio method (Bowen 1926) of heat losses by conduction and evaporation, and the similarity method between moisture and momentum transfer, can be used as first approximations but may not be accurate since these methods assume the transfer coefficients for heat, moisture and momentum to be identical.

Solar radiation and its attenuation in the atmosphere has been described by the fundamental work of Ångström (1929, 1930). The attenuation process occurs by Rayleigh scattering, absorption and scattering by dust particles. The most complete and satisfactory explanations of absorption are those by Elsasser (1942) and Möller (1943), and of multiple scattering that of Deirmendjian and Sekera (1954). Recommendations on the measurement of radiation fluxes have been made in the IGY Instruction Manual (1958) on radiation instruments and measurements. A complete and exhaustive analysis of radiation fluxes over an Antarctic snow surface has been carried out by Liljequist (1956) which again could well be used as a model study. Recent developments in radiation monitoring techniques (Funk 1963) have made the measuring of net radiation for heat budget studies relatively easy.

The transfer processes in the ice are restricted to conduction and radiation. Convection can, however, occur in snow where the porosity of the crystal structure permits air circulation in the snow pack (e.g., Yen and Bender 1963). This allows the transfer of sensible heat as well as moisture (e.g., Bergen 1963).

The conduction of heat in homogeneous media has been theoretically established by the classical Fourier methods of temperature analysis for a variety of different boundary conditions, extensively discussed for example by Carslaw and Jaeger (1959). For the case of non-homogeneous or layered media the improved model of heat diffusion by Lettau (1954) has proved very valuable. When the boundaries of a medium through which heat is conducted are not stationary, the complex solution of the temperature equation is best obtained by analog computer methods of the type indicated by Schwerdtfeger (1964).

The light transmission in snow and ice is a well studied phenomenon. A theore-

tical treatment of the problem has been provided by Dunkle and Gier (1953) which considers the radiation in a diffusing medium and applies the results to snow. Comprehensive field and laboratory measurements have been made by Ambach *et al.* (1959, 1962 and 1963), for example. Thomas (1963) summarizes a large number of mono- and polychromatic light extinction measurements in snow and ice.

The present paper discusses the heat budget and heat transfer processes in snow and ice on the Antarctic continent. Apart from providing microclimatological data for meteorological uses, including a possible continental heat budget study, the second and major purpose of this study is to extend the surface heat budget to a multi-level budget in the ice for glaciological purposes. A precise analysis of the sub-surface heat fluxes of conduction and radiation is necessary for this. Particularly, radiation fluxes in the ice may have drastic effects on sub-surface budget considerations and, although radiation transmission in ice is a well studied phenomenon, the consequences of absorbed radiation are less well known. To indicate the nature of the problem, some aspects of radiation absorbed in the ice will be considered now.

Radiation transmitted through the ice does not only supply energy directly but, through absorption, gives rise to a temperature increase of the ice and a heat flux by conduction. The separation of the heat flux, caused by the absorption of radiation, from the genuine heat flux in the ice is of considerable importance in determining the thermal diffusivity of the ice. Dalrymple *et al.* (1963) bave pointed out the effect of absorbed radiation on their diffusivity values of snow at the South Pole but were unable to compute the effect numerically. Cameron *et al.* (1962) have obtained conflicting values of the thermal diffusivity from the same set of ice temperature data by using different methods of computation. It will be shown in this paper that the error lies entirely in ignoring the effect of absorbed radiation.

Direct radiation effects will be shown to be present in the measurement of ice temperatures: a thermal sensor in the ice which is not completely reflecting absorbs solar energy at a different rate from that of the surrounding medium and gives erroneous temperature data. It will also be shown that the presence of a mean annual temperature gradient in the ice, due to absorbed radiation, gives a mean annual temperature at the surface which is different by several degrees from that at 15 metres depth, roughly the depth of penetration of the annual surface temperature wave. This should be of interest in glaciological investigations where the annual mean surface temperature at any location is usually assumed to be identical with the ice temperature in excess of 10 metres depth.

This annual mean temperature gradient is also shown to give rise to large conduction losses at the surface which annually balance the absorbed radiation. These losses are certainly considerably larger at most times, except in radiationless periods, than the conducted heat fluxes conventionally computed from changes in heat content due to temperature pattern changes. Finally, the effect of absorbed radiation is shown to be of considerable consequence in changing the actual heat storage in the ice, which is greatly increased by radiation in the optically more transparent media. In slabs of ice of finite thickness, such as sea-ice covers, considerable errors result in the energy budget at the surface if the absorbed radiation is not considered.

SYNOPSIS

The first section discusses in the introduction the importance of radiation as a mode of energy transfer in the optically transparent medium of ice. Section 1.2 separates the extinction process into scattering and absorption, using the theory of Dunkle and Gier (1953). Knowledge of absorbtion as distinct from extinction of radiation is essential, as the former is responsible for a continuous heat source in a transparent medium exposed to radiation. The procedure of installing light-sensitive devices in an existing transparent medium, such as ice or snow, results in a serious perturbation which has not been adequately considered in the literature, as even the surface of a spherical cavity housing a sensor must possess its own reflecting and scattering properties not representative of the surrounding ice. Theoretical justifications for a vertical borehole installation with optical stops are advanced in 1.3 and the measured extinction values using this physical configuration are given in 1.4. The effect of spectral shift of the light with depth measured with photocells, and the possibility of using thermocouples to measure the radiation extinction, are elaborated in sections 1.5 and 1.6 respectively. Extinction measurements and the numerical analysis into scattering and absorption processes follow for wind-packed snow in 1.7, and for sea ice in 1.8. The lack of distinction between absorption and extinction apparent in the literature, e.g., Thomas (1963), is pointed out. The understanding of the physical processes involved in the extinction of radiation reached from this work, and the measured magnitudes of extinction for the various types of ice and snow investigated, can now be used to determine the radiation effect on the thermal diffusion in ice.

This is described in Section 2. In the Introduction, the classical models of heat diffusion in homogeneous media of semi-infinitely and finitely thick bodies are discussed (e.g., Carslaw and Jaeger 1959). Thc annual temperature pattern in Antarctic blue ice is described in section 2.2 and a Fourier analysis of this data in 2.3. The thermal diffusivity of the ice is computed in 2.4, using a model proposed by Lettau (1954) for non-homogeneous media, and the deviation from expected results is explained in terms of absorbed radiation. Computations of the diffusivity, using the classical methods, show the effect of aborbed radiation on the phase change and amplitude reduction of a temperature wave penetrating into the ice.

The problems associated with measurements of heat flux with thermopile flux-plates (Schwerdtfeger and Weller 1967) are discussed in 2.5. In 2.6 heat flux measurements are used to determine the diffusivity for a number of heat flux waves of different frequencies. The effects of radiation on the annual heat flux wave are analysed. Section 2.7 gives a summary of all diffusivity determinations in plateau icc.

Sections 2.8 and 2.9 give a descriptive analysis of the temperature pattern and heat flux measurements in sea ice respectively. In Section 2.10 the thermal diffusivity in the top layer of the sea ice is determined by separating the effects of absorbed radiation from both the amplitude and phase of a penetrating diurnal temperature and heat flux wave in the sea ice.

The thermal diffusivity gradient in sea ice predicted from theoretical considerations by Schwerdtfeger (1963) is verified in 2.11, using the temperature wave

penetration during a period of no radiation and the classical theoretical slab model. The final conclusions show that the thermal diffusivity of optically transparent ice or snow computed from data which ignore the effect of absorbed radiation depends entirely on the method of computation.

The effect of absorbed radiation on the heat budget and heat transfer in ice is considered in the next two sections. Section 3 describes the meteorological heat budget at the snow—air interface of a composite snow and sea-ice slab floating on sea water, and the transfer processes to obtain the heat budget at the ice—water interface. In the Introduction, heat budget equations are developed for the boundaries of the sea-ice slab. Sections 3.2 and 3.3 describe the micrometeorological instrumentation and sea-ice thickness measuring device. Radiation measurements are described in 3.4 and the penetration of radiation through the snow—ice slab in 3.5. The disappearance of the snow cover over the ice in summer results in a drop of the albedo and allows more shortwave radiation to be absorbed by the ice. This results in changes in heat storage in the ice and increases of the conducted heat flux at the upper boundary. To determine this effect, the conducted heat fluxes at the ice boundaries are computed in 3.6 and the numerical difference of the heat fluxes is compared with the heat storage calculated from an equation given by Untersteiner (1964). An ice heat budget equation is then set up, including a term for absorbed radiation, and errors obtained from the above comparison are discussed. Errors are also computed for the conventional surface heat budget equation which contains no absorbed radiation term.

The meteorological heat budget at the surface is completed by considering temperature and wind speed profiles in 3.8. Stability terms are computed and the effects of the surface crystal sizes and distributions on the roughness parameter are determined, using an empirical equation by Kutzbach (1961). Eddy heat fluxes and the latent heat are computed in 3.9 and 3.10, the first using the classical model of turbulent heat exchange, the latter from mass budget considerations at the lower ice boundary and as a remainder term in the budget equation at the upper boundary.

The heat budgets at both boundaries are considered in 3.11, finding error terms and computing the advection of heat by water currents, using empirical methods by Shumski *et al.* (1963) and Sverdrup (1953). The conclusion discusses the relative importance of all components of heat energy transfer above and inside the ice, including the remarkable effect of absorbed radiation on the heat fluxes and heat storage. It is emphasized that it is essential in heat budget studies in transparent bodies of finite thickness to consider the effects of absorbed radiation.

Section 4 discusses the annual meteorological heat budget at the surface and in blue ice at various depths. The two surface components of the meteorological budget, required for the computation of the sub-surface budgets, are considered first by describing radiation measurements in Section 4.2 and conduction in the ice in 4.3. Sub-surface heat budget equations for the ice are established in detail in 4.4. In 4.5, the means and amplitudes of conductive and radiative heat transfer are computed for various depths. The effects of absorbed radiation on the heat fluxes and stored heat in the ice are computed by comparison with heat fluxes calculated from the classical equations of heat diffusion. In Section 4.6, the surface energy budget is established using the fluxes of sensible and latent heat as a remainder

term. A Fourier analysis is carried out on the data. In Section 4.7 wind and temperature profile data are examined and the diurnal temperature gradient changes are discussed. Sensible heat fluxes are computed. In 4.8, the fluxes of latent heat are computed from mass budget considerations, and the contribution of melting and evaporation are separated for the summer months. The Bowen ratio method is applied to obtain further estimates of the latent heat fluxes. A harmonic analysis of the latent and sensible heat flux components is carried out in 4.9 and error terms are estimated. The annual heat budget is considered at three levels in 4.10. Finally, a comparison with data from other Antarctic stations is given in 4.11 and the difference in net heat storage and conduction, due to absorbed radiation in the different media, is commented on.

In the conclusion, the dominating nature in the heat budget of the radiation fluxes above and inside the ice is pointed out. It is emphasized that a strict solution of the surface budget equation is possible by considering the net change in stored heat only, but that the radiative and conductive components of this net change are large. The conventionally computed conducted heat flux thus must not be misleadingly identified with the total conducted heat flux at any level in the ice.

Appendix I discusses the history of the instrument installations used at the various measuring sites, the instruments and recording equipment, routine adjustments of the equipment and calibration data for the instruments. Appendix II contains maps showing the location of measuring sites, and Appendix III gives 49 tables of basic numerical data used in the computations.

1. RADIATION PENETRATION IN ANTARCTIC PLATEAU ICE AND SEA ICE

1.1. INTRODUCTION

The translucency of ice and snow to solar radiation complicates both the analysis of their heat exchange to the atmosphere at the surface as well as the study of conduction. In isotropic ice, radiation of a given wavelength is absorbed with depth in accordance with an exponential extinction law. This process contributes directly to the thermal energy of the ice and affects both conduction in ice as well as appreciable phase changes in porous ice and snow. Accordingly, extended supra-surface radiation investigations are of importance to both heat and mass balance studies of ice and snow.

Extinction measurements with these aims in mind have been carried out at many localities. Ambach (1963) bas reported on investigations in summer ice in Greenland. Liljequist (1956) has made measurements in Antarctic snow. The necessity for these studies has been emphasized by the analysis made by Dalrymple, Lettau *and* Wollaston (1965) of both South Pole and Maudheim temperature data indicating the importance of non-conductive heat transfer processes. The present set of observations was conducted in the three most frequently occurring types of solid water substance in the Antarctic:

1. Blue ice of density 0·88 gm cm^{-3}. The surface was a flat ice plateau at an elevation of 150 metres, 2 km from the coastal station of Mawson at latitude 67°34′S, longitude 62°53′E. This ice was clear without cryoconite holes.

2. Wind-packed snow of density 0 42 gm cm^{-3}, essentially homogeneous, with a horizontal surface conveniety close to Mawson.

3. Annual sea ice up to 135 cm thick, 1 km from Mawson.

1.2. SCATTERING, ABSORPTION AND EXTINCTION

The radiation absorbed by a diffusing medium depends on the reduction in intensity of the net radiation. It is thus insufficient to determine the total extinction coefficient alone of such a medium. Additionally, the net flux of radiation or the ratio of upward and downward components must be monitored in order to be able to derive the actual absorption of radiation.

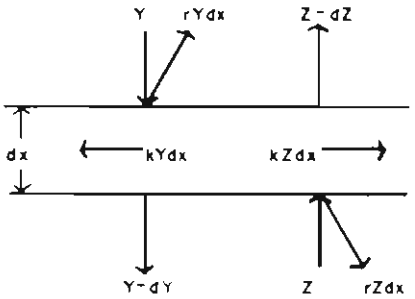

FIG. 1.1. Illustrating the notation adopted by Gier and Dunkle (1953) for component fluxes of radiation at an infinitesimally thick horizontal sheet in a diffusing medium.

Dunkle and Gier (1953) used the model of radiation fluxes in a homogeneous diffusing medium shown in Fig. 1.1 to derive the relation holding between the scattering (or reflection) coefficient r, the absorbtion k, and the extinction μ. Z and Y are respectively considered to be the upward- and downward-directed fluxes of radiation incident on the faces of a sheet of thickness dx. The radiation leaving the sheet downwards is decreased by absorption and increased by partial reflection or scattering of the upward component upwards, hence:

$$dY = -kYdx - rYdx + rZdx \tag{1.1}$$

With due regard to signs indicative of direction, a similar relation holds for the attenuation of the upward-directed component:

$$dZ = kZdx - rYdx + rZdx \tag{1.2}$$

Equations (1.1) and (1.2) may be solved for Y and Z:

$$Y = I_o e^{-\mu x} \tag{1.3}$$

$$Z = \frac{k + r - \mu}{r} I_o e^{-\mu x} \tag{1.4}$$

where I_o is the value of Y at $x = o$ (the surface), and μ is the total extinction coefficient given by:

$$\mu^2 = (k + r)^2 - r^2 \tag{1.5}$$

The ratio of upward to downward components of radiation is given by:

$$\frac{Z}{Y} = \frac{k + r - \mu}{r} = m \tag{1.6}$$

The energy absorbed by a horizontal layer of unit thickness from (1.1) and (1.2) is:

$$\frac{dE}{dx} = \frac{dY - dZ}{dx} = -k(Y + Z) \tag{1.7}$$

Alternatively, differentiation of equations (1.3) and (1.4) shows that

$$\frac{dE}{dx} = \frac{dY - dZ}{dx} = -\mu(Y - Z) \tag{1.8}$$

These fundamental equations of Gier and Dunkle show that, to obtain the absorbed radiation per unit thickness, two procedures of measurement are available. Net radiation and total extinction coefficient or total radiation (sum of upward and downward components) and the absorption coefficient are both acceptable pairs of information.

1.3. INSTRUMENTATION

Special radiometers (Schwerdtfeger *and* Weller, 1967), which were designed with the continuous measurement of downward and net radiation flux even at vanishingly low intensities in mind, were used. With the total radiative energy transfer (the quantity of main interest in connection with the overall heat economy determination), the fact that these radiometers were spectrally non-selective was considered invaluable. Because these approximately spherical instruments were about 7·5 cm in average diameter, their use closer than 1 metre to the surface was precluded. In order to investigate the optical properties of the near surface layers, less bulky light dependent resistors were used.

Limited spectrally sensitive observations were made with photocells and filters, mainly in order to check the validity of calculating a single extinction coefficient effectively weighted to include all optical frequencies.

Finally, the daily perturbation of temperatures at depths in ice and snow, as detected by chromium-shielded thermocouples, was observed to give supporting data in the case of blue ice and snow and, in fact, the only reliable information for sea ice, for which Untersteiner (1961) has used a similar approach.

1.3.1. *Installation of Radiometers*

Sub-surface radiometry is complicated by the difficulty of installing light sensitive instruments at any depth, since the creation of a cavity in ice immediately results in non-representative attenuation and scattering. At greater depths enormous excavations are required if the instruments are to be introduced through horizontal bore-holes. Because of these difficulties, the thermopile radiometers were installed in simple vertical bore-holes 11 cm in diameter. The disadvantages resulting from additional factors requiring consideration in data interpretation were outweighed by the ease with which the radiometers could be both installed as well as withdrawn for periodic inspection and calibration checking.

Suspension of both hemispherically sensitive and net radiometers in vertical bore-holes would ordinarily result in anomalous contributions which would be particularly serious over the solid angles subtended by the top of the hole at the ice surface, and in the case of the net radiometer, the bottom as well. In order to prevent a large flux of reflected and scattered light from the bottom of the bore-hole

from influencing the net radiometers, the bore-hole depth was made twice the instrument level in all cases. All holes were sealed at the top by a polystyrene foam cylindrical insert protected by a white metal disk 15 cm in diameter. The geometry of a typical installation is shown in Fig. 1.2.

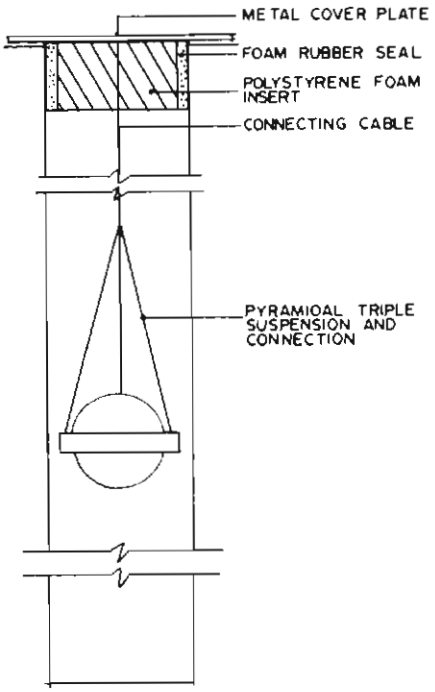

FIG. 1.2. Installation of a radiometer in a vertical borehole, showing the suspension of the radiometer and the cover over the borehole.

Consider a radiometer suspended in a bore-hole with dimensions as shown in Fig. 1.3. The walls of the cylindrical hole at any given depth h are considered to emit light which has been attenuated by passage through a thickness h of ice. The radiation issued from the bore-hole wall at a height x above the radiometer is thus given by:

$$I = I_o e^{-\mu(h-x)} \tag{1.9}$$

where I_o is the intensity at the surface. As seen by the radiometer, therefore, there is an angular distribution of light intensity. The relation between angle of incidence θ and height of an infinitesimally wide cylindrical band in the bore-hole of radius r is given by:

$$x = r \tan \theta \tag{1.10}$$

The flux reaching the radiometer from such a band of the bore-hole wall is:

$$dF = 2\pi I \sin \theta \cos \theta \, d\theta \tag{1.11.}$$

from which the total flux is then simply obtained as

$$F = 2\pi \int I \sin \theta \cos \theta \, d\theta \tag{1.12}$$

The intensity I is, of course, a function of θ specified by equations (1.9) and (1.10).

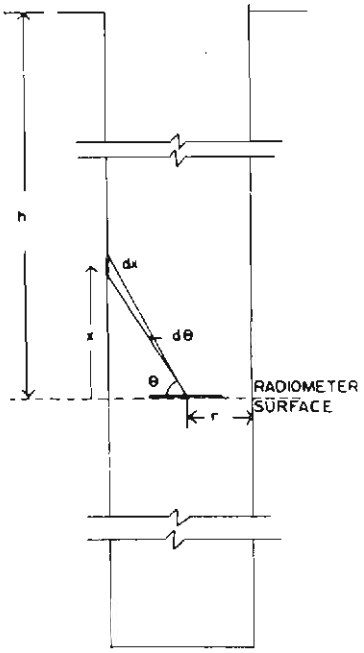

FIG. 1.3. Illustrating the notation used in the deriving of the radiation flux incident on the radiometer surface.

Fig. 1.4. illustrates the graphical method chosen to evaluate equation (1.12). Curve 1 shows the value of $\sin\theta \cos\theta$, i.e., a function proportional to $\frac{dF}{d\theta}$ for a constant value of I, with the scale of θ adjusted to show bore-hole distances linearly. Were the ice perfectly transparent, curve 1 would indicate the relative contributions made by radiating bands of the wall to the total flux reaching the radiometer as a function of depth. To obtain $\frac{dF}{d\theta}$ in relative units, curve 1 is multiplied by the appropriate values of the attenuated light intensity, I, shown on a relative scale with $I_0 = 1$ for extinction coefficients of 0·006, 0·01 and 0·03 cm^{-1}. Curves 2, 3 and 4 result from this operation.

In all cases, it is seen that light emitted from the bore-hole wall, at a distance one radius above the radiometer, causes a maximum value in the radiometer response. However, on the basis of this simplified model, areas beneath the curves 2, 3 or 4 indicate that the total flux is nowhere near representative of the intensity of radiation at the level of the radiometer; in fact, curve 4 would indicate that an installation of this nature in snow would be quite useless.

In order to test the angular distribution of intensity in the actual installation, blackened metal plates were suspended 20 cm above and, where necessary, below the radiometers: some results are shown in Fig. 1.5. The ice, as will be shown later, having had an extinction coefficient of 0·006 cm^{-1} determined for it, a 58% reduction in response of a radiometer to downward radiation would be expected

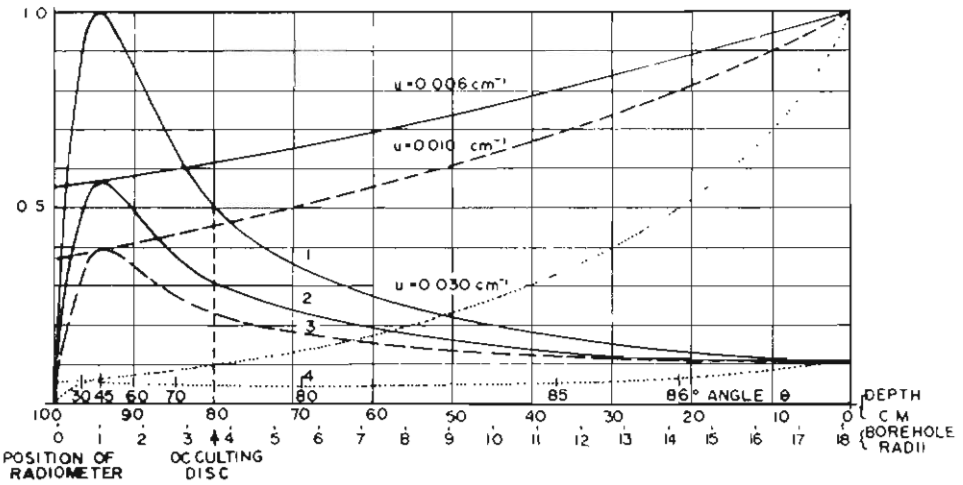

FIG. 1.4. Model of distributed radiation with depth incident at the radiometer surface for various extinction coefficients.

by graphical integration on the basis of the model discussed. However, actual measurements showed a reduction of only 19% when a plate occluded the bore-hole 20 cm above a radiometer suspended 1 metre below the surface. Clearly, a more complex model, involving multiple scattering on the walls of the bore-hole, is necessary. The interesting condition can arise whereby the light seen by the radiometer in fact becomes isotropic. How closely the real installation approaches this can be ascertained by calculating the reduction in isotropic intensity caused by the shading of an 11 cm-diameter disk at a distance of 20 cm. The value of 15% obtained is a much closer approach to the 19% measured than the 58% expected on the assumption of all light proceeding directly down the bore-hole after emerging from the wall. The simple tests performed showed that, at the 1 metre level, only some 4% of the radiation reaching the radiometer was in the nature of an added perturbation. Finally, Fig. 1.5 shows that the measured value of the extinction coefficient remained unchanged, further reinforcing the view that the anomaly introduced by the bore-hole installation, if stopped at the surface, is small. In view of the uncertainties connected even with radiation measurements above the surface, the errors introduced by the bore-hole installation described, i.e., some 4% at 1 metre depth, were regarded as sufficiently small to be neglected in the examination of the data obtained.

1.4. BASIC RESULTS OF RADIOMETER MEASUREMENTS IN BLUE ICE

The results of both downward and net radiation measurements in ice (Tables 45-46)* are summarized as extinction coefficient data in Fig. 1.6. It is seen that, over a period of time extending from March to July, no significant change occurred in the extinction coefficients (μ) which are, moreover, almost identical for down-

*Note: Tables 1-49 (no section designation) are basic data tables and are to be found in Appendix III.

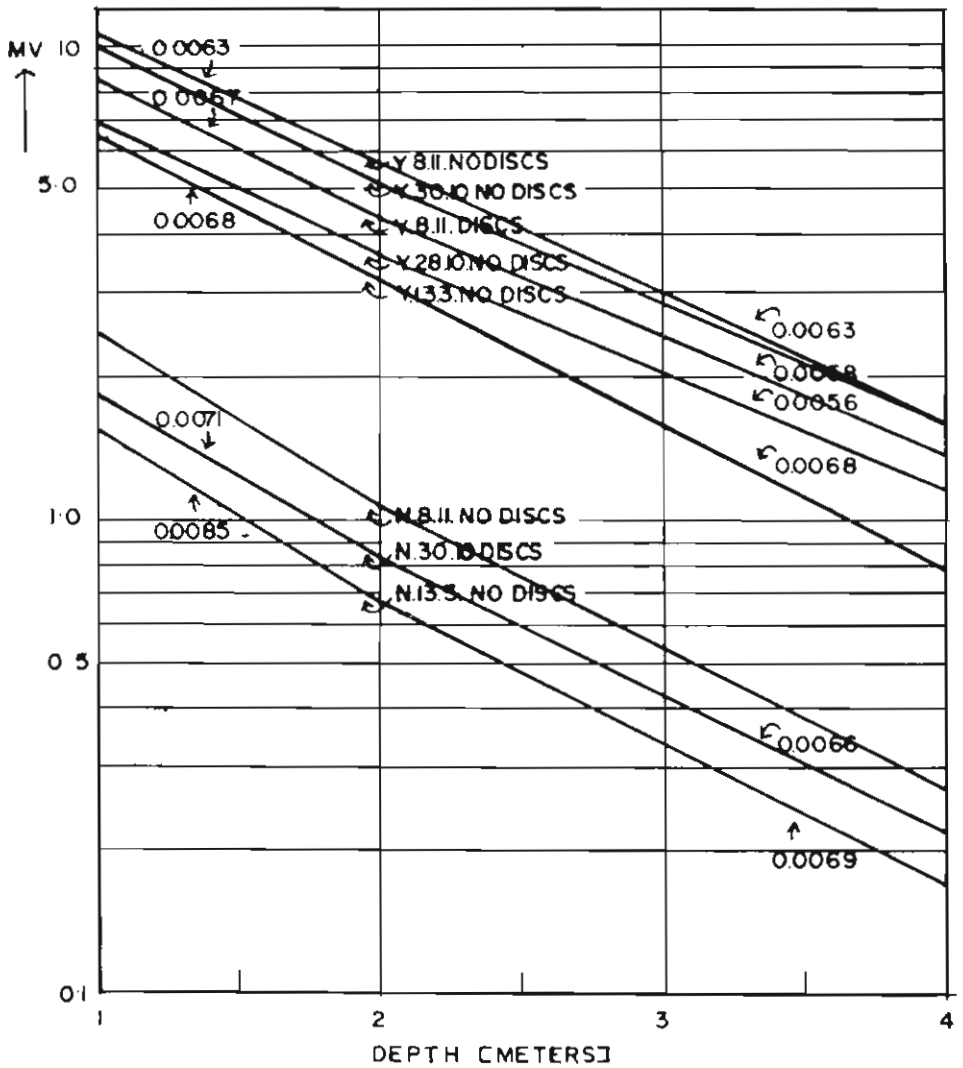

FIG. 1.5. The effect of discs 20 cms above and below radiometers on the extinction coeffieient. Hemispherieal radiometer = Y; net radiometer = N.

ward and net fluxes. The mean value for the period was 0·0067 cm^{-1}. Again, from Fig. 1.6 the March and April data show that the ratio of downward (Y) to net (N) radiation was 3·82. Therefore, since

$$\frac{Y}{N} = 3{\cdot}82$$

and $N = Y - Z$, it follows that

$$\frac{Z}{Y} = 0{\cdot}74.$$

Substituting this latter value in (1.6),

$$\frac{k+r-\mu}{r} = 0{\cdot}74.$$

Since it has been found that

$$\mu = 0{\cdot}0067,$$

equation (1.5) provides a third relationship between μ, k and r, the total extinction, absorption and scattering coefficients. These were then calculated as:

$$\mu = 0{\cdot}0067$$
$$k = 0{\cdot}0011$$
$$r = 0{\cdot}0205,$$

all in units of cm^{-1}.

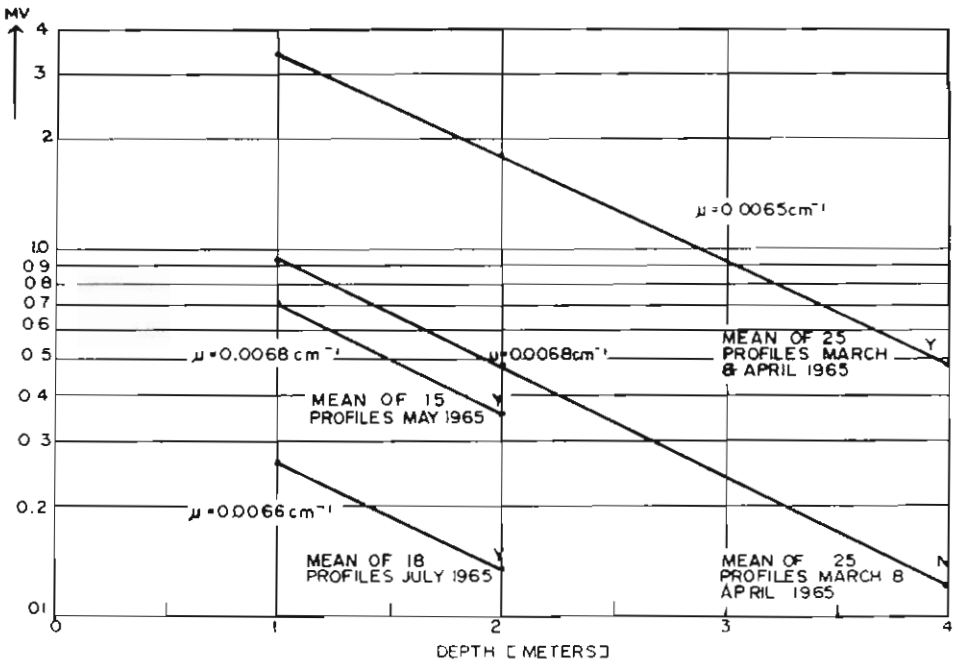

FIG. 1.6. Light extinction in ice: mean profiles from radiometer measurements. Hemispherical radiometer = Y, net radiometer = N.

Before extending the inquiry to the spectral dependence of the extinction coefficient, it is significant to note that the simple data presented so far show that light extinction in the bore-holes themselves follows an exponential law. This fact reinforces the deduction that multiple scattering of light occurred and that, provided the holes were sealed, the light intensities in the bore-holes were representative of those in the ice at the same level.

1.5. CHANGE OF EXTINCTION COEFFICIENT AND SPECTRAL CONTENT OF LIGHT WITH DEPTH IN ICE

The extinction coefficient is a function of the wavelength of the transmitted radiation in ice (e.g., Ambach, 1959). Consequently, a spectral shift would be expected with depth which could alter the total extinction coefficient. Furthermore, the exponential extinction law strictly only applies to homogeneous media. Since, even in blue ablation zone ice, a density gradient exists in the uppermost layers because of evaporation, precipitation, melting and refreezing processes, variations in the specific extinction coefficient μ , where $\int_0^\infty \mu_\nu \, d\nu = \mu$ and ν is the frequency, might be expected.

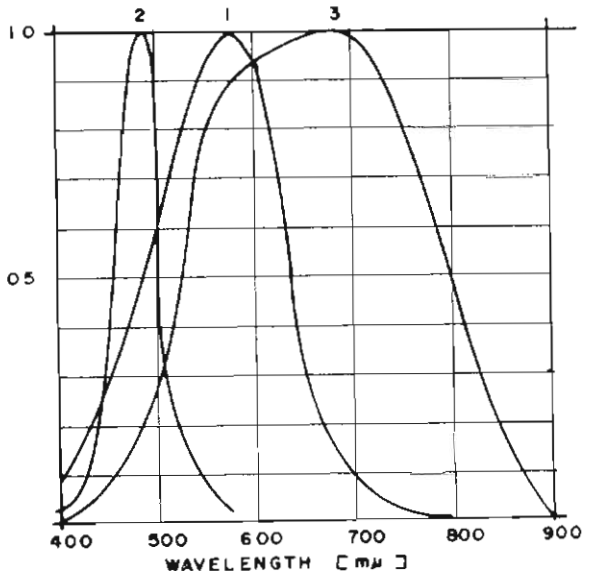

FIG. 1.7. Spectral response of
1. photocell (selenium, International Rectifier A-5)
2. photocell plus blue filter
3. Philips light-dependent resistor.

To investigate both these effects, a photocell and blue filter, and light-dependent resistor, were used in additional measurements. Fig. 1.7, the results of spectrophotometric measurements, shows the spectral ranges investigated on a normalized scale. The photocell was an International Rectifier selenium cell type A-5, normally weighted to the mid-range of the visible spectrum; it was converted to be predominantly blue sensitive by means of a suitable filter. Finally, a Philips light dependent resistor (LDR) extended the range of observations to the red. Figs. 1.8 and 1.9 show the results of extinction measurements for red and blue spectral ranges. The discrepancy between the values of the extinction coefficient obtained for the upward and downward components of the radiation flux shown in Fig. 1.8. gives an indication of the accuracy of the data. Although different rates of extinction

for the two directions would be expected in a non-homogeneous medium, the linearity of the values from 20 to 100 cm in the ice indicates an optically isotropic solid and that the 12% discrepancy was instrumental in origin. The behaviour of the photocell precluded its use in measuring high light intensities. Accordingly, it was used only with the attenuating blue filter near the surface, the mid-optical range without filter only being covered at greater depths. It is seen that the extinction coefficient for predominantly blue light remained constant at 0·007 cm^{-1} for depths of from 2 to 8 metres. Without a selective filter, the photocell measurements, extending from 6 to 10 metres in the ice, give a value of $\mu = 0{\cdot}006$ cm^{-1}.

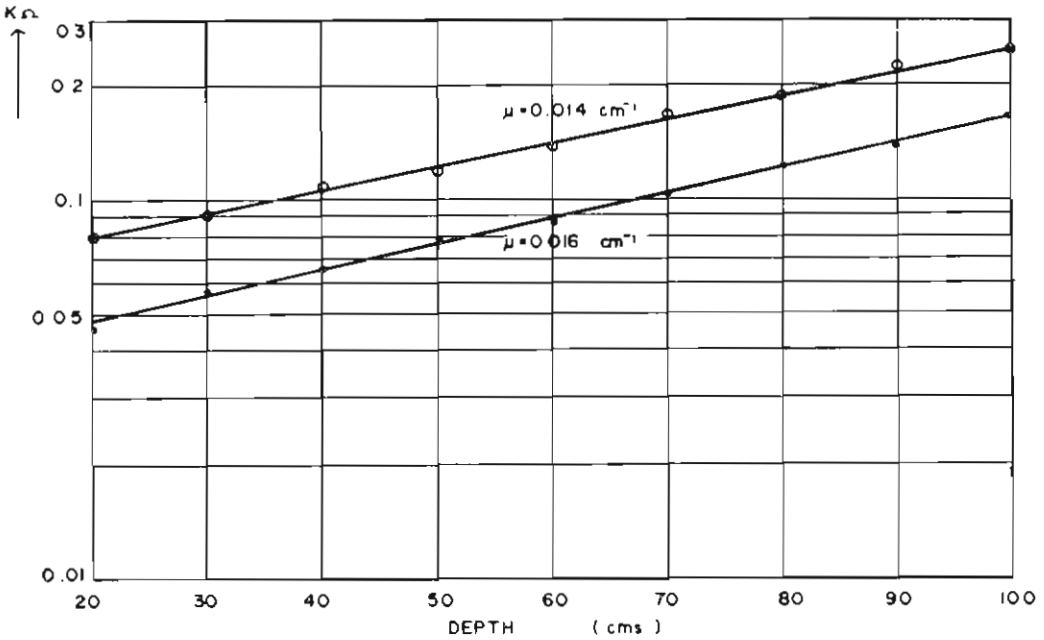

FIG. 1.8. Light extinction in ice measured with Philips light-dependent resistors in vertical boreholes of 3 cm diameter.
Downward flux •
Upward flux O

An approximation of the mean extinction coefficient of the net radiation in the upper 100 cm of the ice was obtained by considering the reduction of radiation at the surface, measured by Kipp solarimeters, and at 1 metre depth, as monitored by the thermopile instruments described earlier. A 4% correction was made to allow for the disturbing bore-hole effect on the instruments at the 1 metre level. On this basis, the mean overall extinction coefficient for the first 100 cm of ice thickness was calculated to be 0·013 cm^{-1}. It is significant to compare this figure with the mean value of 0·015 cm^{-1} obtained by LDR measurements biased to the red region of the visible spectrum. It is clear that the rapid absorption of red light with depth does permit the measurement of a total extinction coefficient at depths below 1 metre in the ablation zone ice described. Fig. 1.10 provides a summary

of this quantity and does, incidently, show that values of μ as high as 0·230 cm^{-1} in parts of the upper 20 cm would not be unexpected. These are of the same order of magnitude as obtained by Ambach and Mocker (1959) in glacier ice.

1.6. MEASUREMENT OF RADIATION EXTINCTION IN ICE WITH THERMOCOUPLES

The simplicity of thermocouples or other temperature sensors in ice makes it attractive to consider their use in determining radiation extinction. Two main instrumental approaches are possible. The first requires the use of a vertical array of highly reflecting temperature sensors so that their measurement of the change in ice temperature is indicative of the attenuation of net radiation. An alternative scheme is to use blackened sensors, in which case a profile of total radiation intensity can be deduced. These two schemes provide the information required for the determination of total extinction, μ, and absorption, k, coefficients as is shown by equations (1.7) and (1.8).

At Mawson, a probe with chromium-plated capsules for the thermocouples was used. One limiting feature of this method is that the sensors must be perfectly reflecting, since the total radiation intensity to which darker sensors respond may be even six times as high as that of net radiation. The increase in ice temperature attributable to radiation as detected by reflecting thermocouples allows

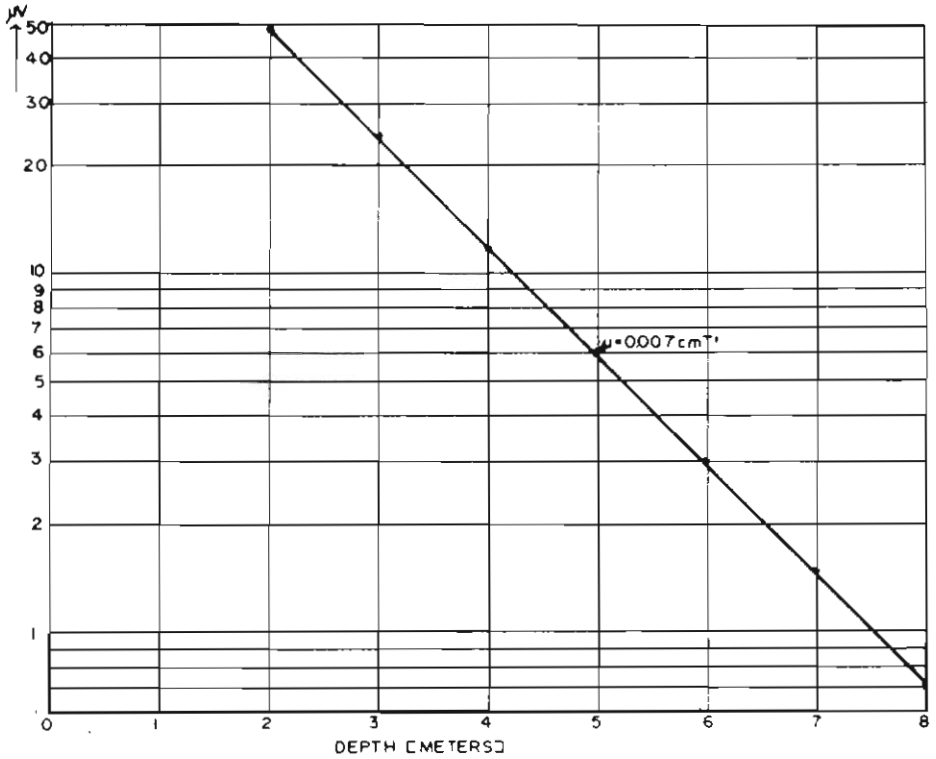

FIG. 1.9. Light extinction in ice measured with photocell and blue filter combination, response peak 490mμ.

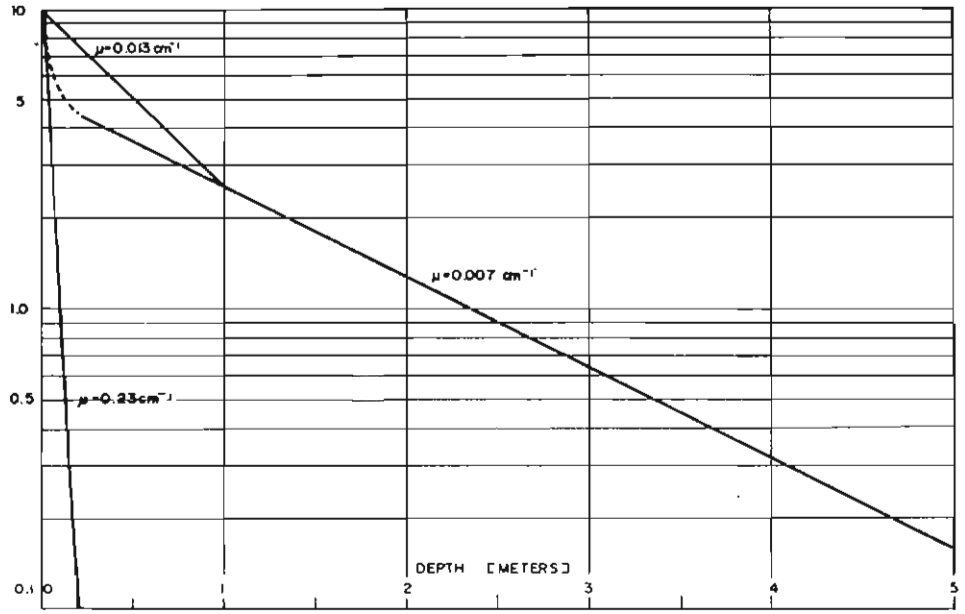

FIG. 1.10. Light extinction in ice: summary of all results including radiometer and photocell measurements.

calculation of the net transfer of light if the specific heat of the surrounding ice is known. On the other hand the magnitude of the excess temperature of blackened thermocouples in ice depends on the thermal diffusivity of the surrounding medium. Since, in the latter case, the reciprocal of the specific heat, as well as the conductivity and density, is the important factor, it is clear that imperfections in the desired characteristics of either reflecting or blackened temperature sensors are serious.

The daily temperature perturbation induced in the ice by solar radiation was detected at depths of 1, 2 and 4 metres by means of the reflecting thermocouples which were part of an extensive probe extending to 8 metres. The mean of 15 profile measurements throughout the year gave an extinction coefficient which was linear with depth and equal to 0·006 cm^{-1}, being in good agreement with the result obtained with radiometers and photocells.

As a further check to ascertain that the temperature rise was representative of the surrounding ice layer and not peculiar to the thermocouple, the absorption of radiation with depth, and hence the perturbation on the temperature profile, was calculated from actual radiation data. In a typical instance, the total downward shortwave radiation above the surface from midnight to noon, when the temperature rise of the thermocouples was observed, was 443 cal cm^{-2}. The albedo of the ice surface was 0·70, so that the net flux of radiation through the surface was 148 cal cm^{-2}. From equation (1.8) the rate of absorption of radiant energy with depth is given by:

$$\frac{dE}{dx} = -\mu(Y - Z).$$

For $\mu = 0{\cdot}013$ cm^{-1} between the surface and 1 metre depth, and $0{\cdot}007$ cm^{-1} below 1 metre depth, the table below summarizes the calculations for ice of density $0{\cdot}90$ gm cm^{-3} and specific heat $0{\cdot}48$ cal gm^{-1} °C^{-1}.

Ice depth	Radiation absorbed	Temperature rise	
		Calculated	Observed
1 metre	$0{\cdot}250$ cal cm^{-3}	$0{\cdot}58$°C	$0{\cdot}9$°C
2	$0{\cdot}130$	$0{\cdot}30$	$0{\cdot}6$
4	$0{\cdot}036$	$0{\cdot}08$	$0{\cdot}2$

The discrepancy between the experimental temperature rise and that expected theoretically on the basis of assumed perfectly reflecting thermocouples is significant. It is clear that in practice the thermocouples were far from perfect reflectors. The detected temperatures were thus perturbed by additional absorption of radiation by the sensors. Thermocouples and similar temperature sensors can thus only be used for extinction measurements with some reservations. It is important to note that in a transparent medium, where the coefficient r is small, the actual coefficient measured by an imperfect temperature sensor (i.e., neither perfectly reflecting nor black) has a value lying between the true values of μ and k. In a more diffusing medium, r would be high, and the method would be meaningless.

1.7. RADIATION EXTINCTION IN WIND-PACKED SNOW

The extinction of light in snow depends strongly on the density and crystal structure and, because of the greater importance of scattering processes, when

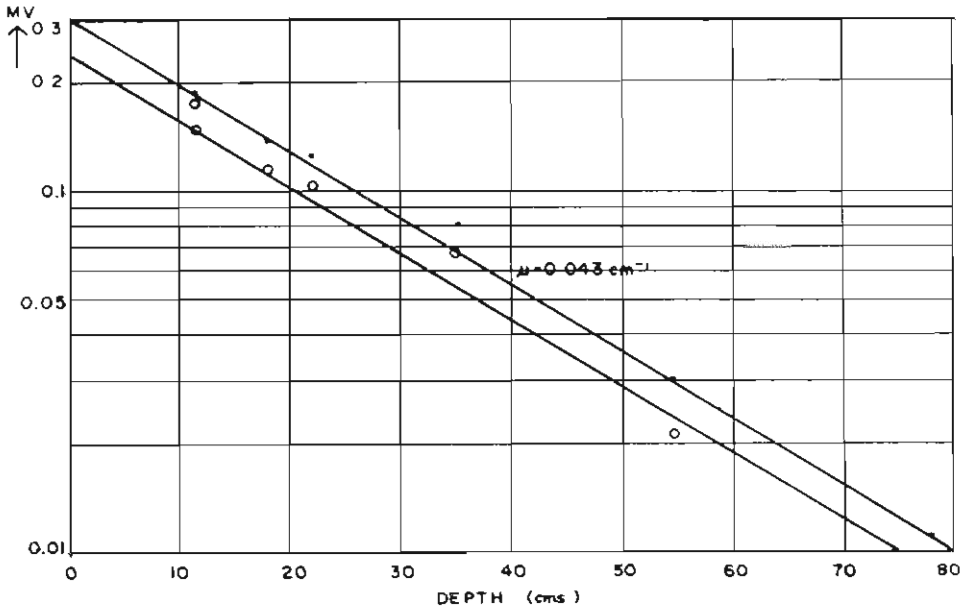

FIG. 1.11. Light extinction in snow of density $0{\cdot}423$ g cm^{-3} measured with photocell in horizontal boreholes 75 cm deep.
Downward flux •
Upward flux O

compared to clear ice, an increased spectral dependence would be expected. A limited review and some optical data for various types of snow has been given by Thomas (1963), although it appears that a proper distinction between absorption, k, and extinction, μ, coefficients has not been made.

Extinction measurements were carried out on the most predominant form of snow at Mawson, wind-packed snow of density 0·42 gm cm^{-3}. Since this type of snow sometimes covered the plateau ice surface and frequently the sea ice, it was deemed necessary to obtain some data for it in order to be able to calculate the total absorption of radiation by the snow-ice cap.

The photocell specified earlier was used in horizontal boreholes 3 cm in diameter cut into the snow from the walls of a trench. In this arrangement, the photocell could be introduced on a 75 cm-long arm and rotated through 360°. During readings, the borehole openings in the trench wall were shaded. After completion of observations, a rigid metre scale was pushed vertically through the snow in order to measure the snow depths precisely.

The results of measurements are shown in Fig. 1.11, and indicate an extinction coefficient of 0·043 cm^{-1}. The ratio of the upward to downward fluxes, m, was found to be 0·80.

Absorption and scattering coefficients were respectively found to be:

$$k = 0{\cdot}005 \text{ cm}^{-1}$$
$$r = 0{\cdot}190 \text{ cm}^{-1},$$

compared to the extinction:

$$\mu = 0{\cdot}043 \text{ cm}^{-1}.$$

It is interesting to compare the relative importance of scattering and absorption in this snow and the blue ice. For snow, the ratio $\frac{r}{k} = 38{\cdot}0$, whilst for ice the value was found to be 18·6, the contribution of scattering being more important by a factor of 2 in the case of snow.

1.8. RADIATION EXTINCTION IN SEA ICE

The permeability of sea ice made long-term installation of radiometers or photocells impracticable, since the boreholes soon filled with brine. One thermopile radiometer was installed in the sea water 150 cm below the surface of the ice whose maximum thickness reached 135 cm. However, gradually the growth of marine deposits made the readings from this instrument of dubious value.

Because of these difficulties, extinction measurements were attempted with the thermocouples installed in the form of a temperature profile probe. This follows a similar procedure to that first used by Untersteiner (1961) at Drifting Station Alpha in 1957. The probe consisted of thermocouples mounted in reflectors and protected from corrosion by a translucent polyethylene sheath. The junctions were located at depth of 15, 30, 45, 60 and 80 cm below the surface.

The maximum temperature rise caused by radiation at noon is shown for a number of days in September, October and November in Fig. 1.12, where the day and month of the observation is indicated by two numbers on the left. The temperature rise of the thermocouples can be seen to decrease exponentially in all cases.

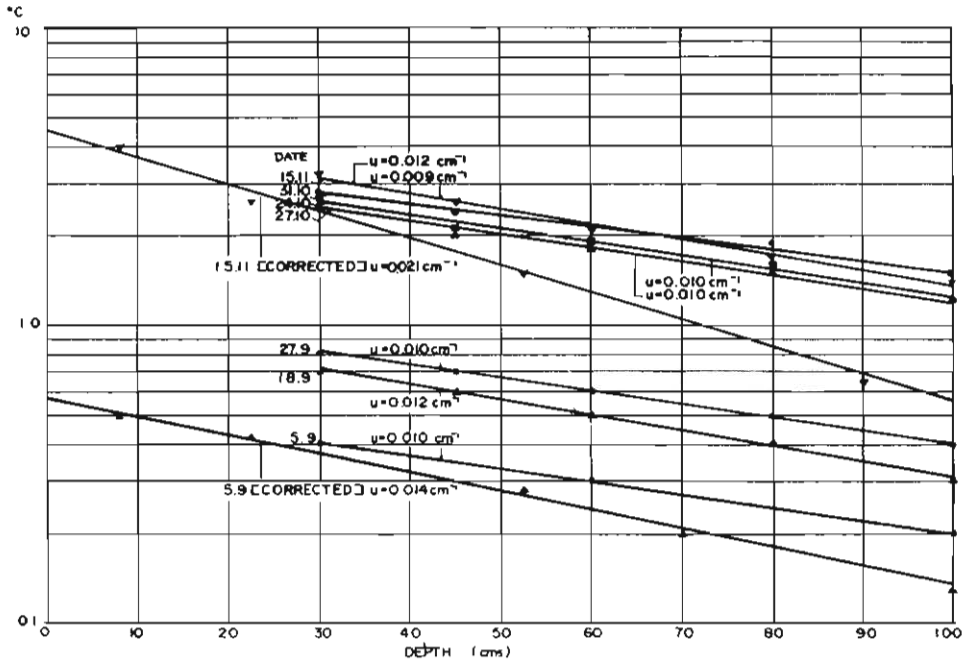

FIG. 1.12. Extinction of light in sea ice measured by the diurnal temperature rise of thermocouples embedded in the sea ice.

The fit of the curves and repetition in time are surprisingly good, considering the non-uniformity of sea ice properties as a function of both depth and time. Even neglecting for the moment the question of optical homogeneity, there is no doubt that the thermal properties, particularly specific heat and hence diffusivity, varied strongly in vertical profile.

As would be expected, temperature increased and salinity decreased with depth, resulting in an overall increase in specific heat in the lower layers of the sea ice. From the experience of examining similar results obtained in clear ablation ice, it became clear that the thermocouples were not perfectly reflecting. Had they been so, it would have been correct to consider ice at depth with a greater specific heat being raised less in temperature for a given absorption of radiation. This would require the normalization of the temperature-rise readings by multiplication with the ratio of specific heat at depth with that of the ice at the surface. When this was done, the "corrected" value of the extinction coefficient became vanishingly small. On the other hand, assuming diffusivity to be the determining factor, as would be the case for black thermocouples, the temperature differences must be divided by the normalizing specific heat ratio. This procedure enables the calculation of an upper bound for the extinction coefficient, which has been shown in Fig. 1.12 for two sets of observations. Ironically, however, the actual value will lie between zero and the extreme bound shown; hence the original result of $\mu = 0{\cdot}010$ cm^{-1} is the more satisfactory.

That this supposition is in fact correct is shown by the value of $\mu = 0{\cdot}012$ cm^{-1} obtained by using the light-dependent resistor described earlier. Extinction readings

taken by Bunt (1960) on the 1956 summer sea ice at Mawson gave a value of 0·013 cm^{-1}. Untersteiner (1961) gives the extinction coefficient of Arctic sea ice a value of 0·015 cm^{-1} and Thomas (1963) a value of 0·011 cm^{-1}. There is thus general agreement between the various observations cited.

1.9. CONCLUSION

The penetration of optical radiation in ice and snow is a relatively well studied phenomenon. The fact, however, that in the more transparent examples of these media, radiation transfer can be the predominant mode of heat flow, is not generally realized. Particularly dramatic is the case of ablation zone ice, where the absence of radiation data to a depth of 8 metres completely negates the value of supposedly heat conduction observations. The thermopile radiometers designed proved to be sufficiently versatile for both temporary and long-term installation, and particularly suitable for parallel operation with the heat flux plate version of the instrument, data from which are given in the next section. In its simple form, in porous snow or ice, the latter is sensitive to convective as well as conduetive heat flow, which a current instrumental development has succeeded in isolating. For the future, then, provision exists for the separate measurement of the fluxes of radiation, conduction and the sum of evaporation and convection separately.

2. THE EFFECT OF ABSORBED SOLAR RADIATION ON THE THERMAL DIFFUSION IN ANTARCTIC PLATEAU ICE AND SEA ICE

2.1. INTRODUCTION

Having examined radiation as a mode of heat energy transfer in the ice in the last section, conduction of heat will be considered next. This involves analysing the propagation of temperature pulses through the ice, the fluctuations in temperature in the upper metres of ice to which absorbed radiation contributes being periodic, due to their solar origin. In the following section this periodieity will be examined by Fourier methods to determine the thermal diffusivity and the effect of absorbed solar radiation on the diffusion process in the ice.

Three separate models will be used which have their equivalents in three types of natural ice bodies:

1. Homogeneous ice of semi-infinite thickness
2. Non-homogeneous ice of semi-infinite thickness
3. Non-homogeneous ice of finite thickness.

The symbols used are:

t = time, sec
z = depth below the surface, cm
T = temperature, °C
B = vertical heat flux conducted in the z direction, cal $cm^{-2}sec^{-1}$
k = heat conductivity at depth z, cal $cm^{-1}sec^{-1}$ $°C^{-1}$
C = heat capacity per unit volume at depth z, cal cm^{-3} $°C^{-1}$
$K = \frac{k}{C}$ = thermal diffusivity at depth z, cm^2sec^{-1}

ν, ω = frequency of temperature or heat flux waves, sec^{-1}
A, a_n, b_n = amplitudes
$\epsilon, \alpha_n, \beta_n, \gamma_n$ = phase angles
n = order of harmonic
the prime ($'$) denotes partial differential with respect to z
($\cdot$) denotes partial differentiation with respect to t.

If the surface temperature in the semi-infinite homogeneous solid $z > 0$ is given by

$$T = A \cos(\omega t - \epsilon) \tag{2.1}$$

and the initial temperature is zero, then the temperature at depth is given by the Fourier solution (Carslaw and Jaeger, 1959) as

$$T = A\, e^{-z\sqrt{\frac{\omega}{2K}}} \cos(\omega t - z\sqrt{\tfrac{\omega}{2K}} - \epsilon) \tag{2.2}$$

The amplitude of the temperature oscillation decreases as

$$e^{-z\sqrt{\frac{\omega}{2K}}} \tag{2.3}$$

and thus falls off more rapidly for large ω. Also there is a progressive lag

$$z\sqrt{\tfrac{\omega}{2K}} \tag{2.4}$$

in the phase of the temperature wave. This lag increases with ω.

A measurement of either the amplitude or phase at depth z is thus sufficient to determine the diffusivity K. A third method of determining the diffusivity is applicable when the vertical flux of heat B is considered at the surface,

$$B = -k\left(\frac{\partial T}{\partial z}\right)_{z=0} = \sqrt{\frac{\omega}{K}}\, kA \cos(\omega t - \epsilon + \tfrac{\pi}{4}) \tag{2.5}$$

and the amplitudes of temperature and heat flux fluctuations are known.

In the non-homogeneous case of heat conduction, i.e., when the heat conductivity and capacity of the medium are functions of depth, the above solutions are no longer applicable. Lettau (1954) has derived an exact solution of this case, where the thermal diffusivity is obtained on the basis of Fourier coefficients of the periodic fluctuations of temperature and heat flux at various depths. The procedure is described and applied in Section 2.4.

The last case of interest is that of a solid bounded by two parallel planes. A slab $0 \leqslant z \leqslant l$ is considered which has zero initial temperature and has the planes $z = 0$ and $z = l$ kept at temperatures zero and sin $(\omega t + \epsilon)$ respectively. A Fourier solution of the diffusion equation exists for these boundary conditions and the amplitudes and phases are given by expressions which are discussed and applied to sea ice in Section 2.11.

All these solutions apply strictly only to conditions of pure heat conduction resulting from temperature changes at the boundaries and are not applicable when other forms of energy transfer take place in the bodies considered. In transparent media, such as ice and snow, the above conditions are, however, not fulfilled since large amounts of energy may be transferred into the medium by radiation. In the

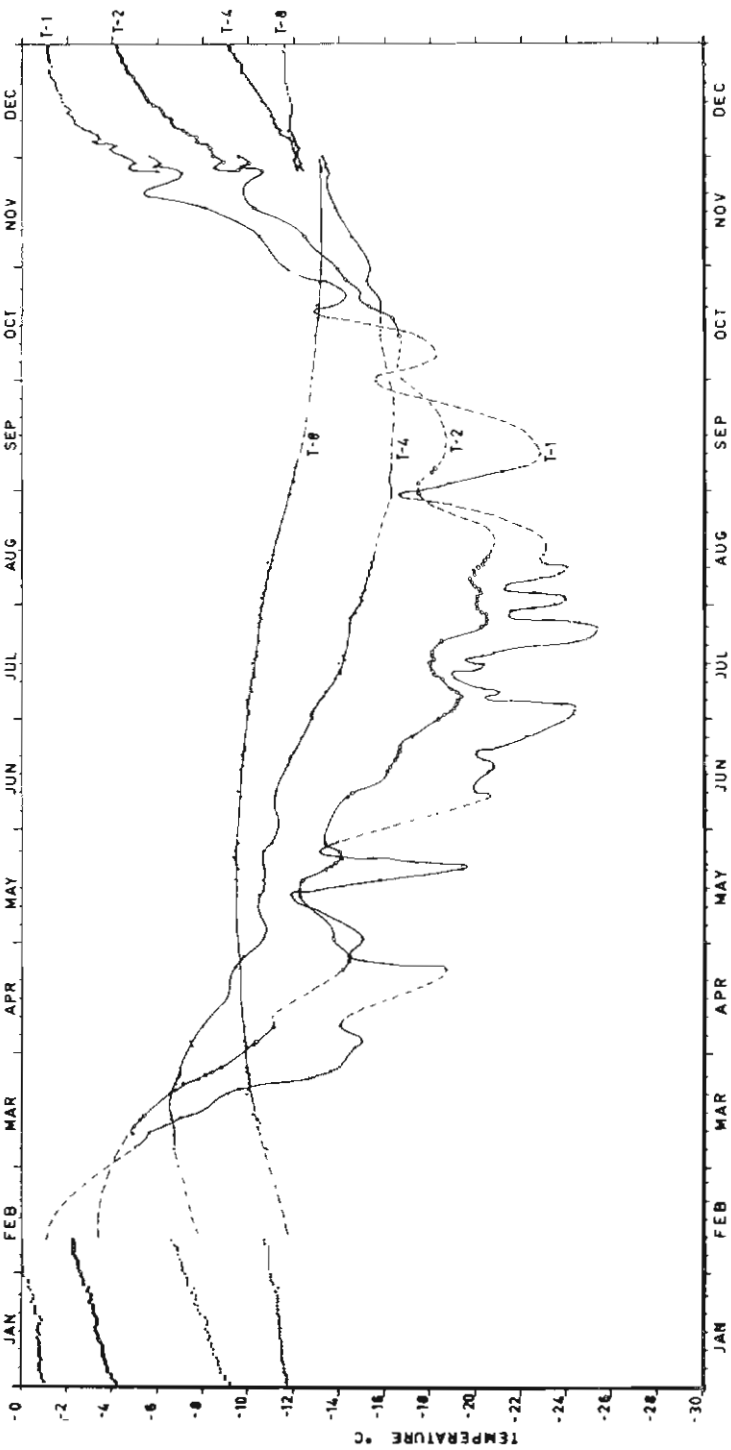

FIG. 2.1. Daily midnight ice temperatures at 1, 2, 4 and 8 metres depth.

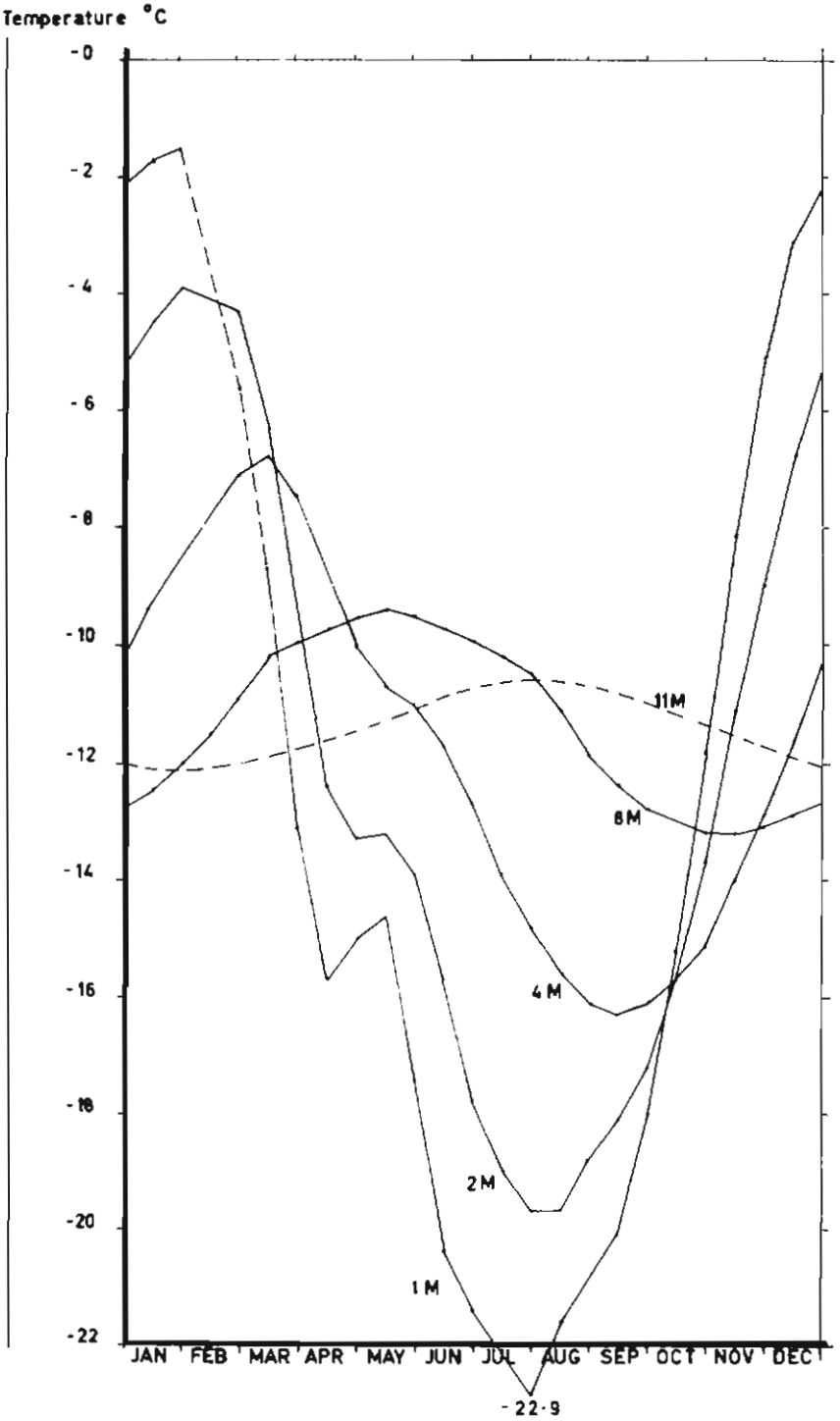

FIG. 2.2. Half-monthly running means of the daily midnight temperatures.

following study the effects of absorbed radiation on the thermal diffusion in fresh-water ice and sea ice will be investigated. The radiation extinction coefficients of these two types of ice were 0·007 cm^{-1} and 0·011 cm^{-1} respectively as determined in Section 1.

2.2. TEMPERATURE PATTERNS IN THE PLATEAU ICE: DESCRIPTIVE ANALYSIS

Ice temperatures were measured on the coastal ice slopes near Mawson at 150 metres altitude during 1965. Copper constantan thermocouples, shielded with chromium-plated 6 mm diameter copper tubes approximately 20 mm long, were used. The thermocouples were sealed in a length of polyethylene tubing and installed in a borehole which was refilled with a snow-water mixture. The reference junction

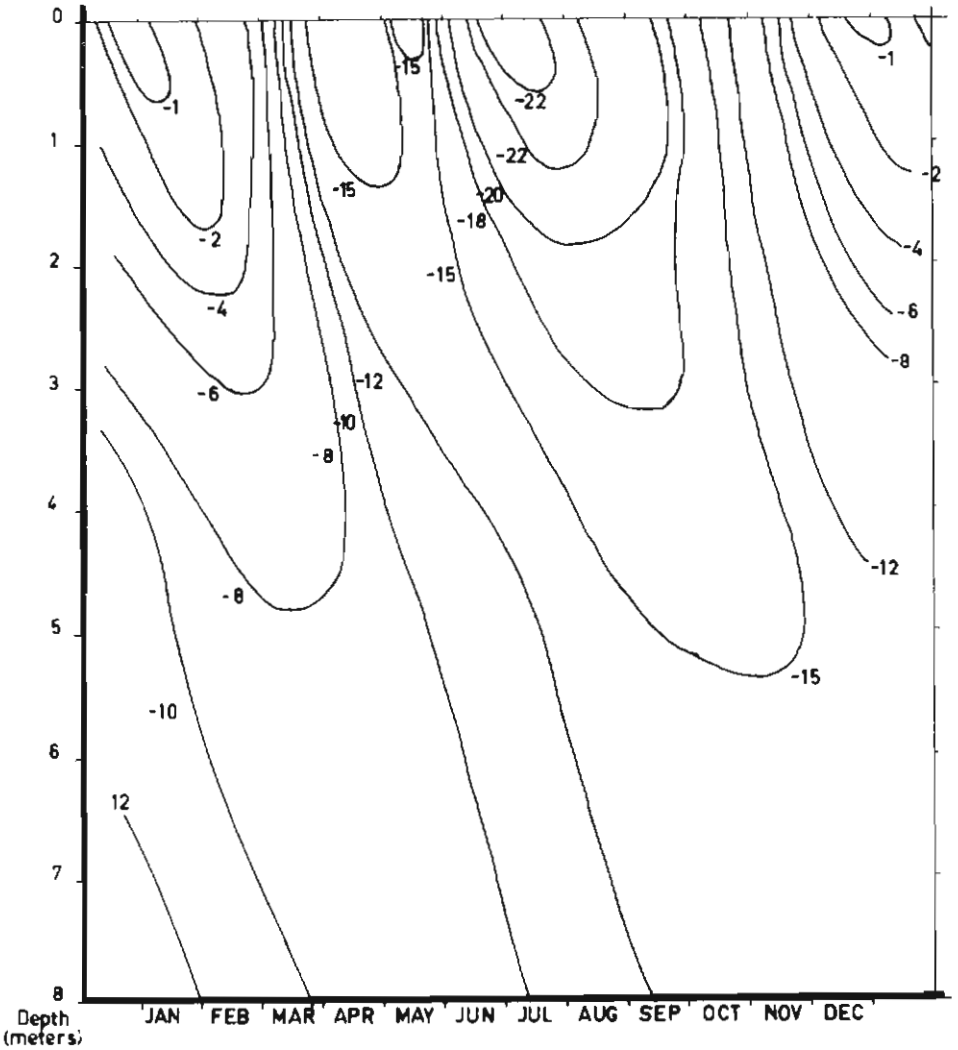

FIG. 2.3. Ice isotherms.

was immersed in a well insulated ice-water bath which was frequently renewed, and recording was by means of a multirange 12-channel Siemens potentiometric recorder which was housed in a heated caravan (Appendix I). Power to drive the recorder was provided by a wind generator, and periods of calms when no recording was made require a certain amount of interpolation of the data.

The daily midnight temperatures observed in the plateau ice at 1, 2, 4 and 8 metres depth (Tables 35-38)* are shown in Fig. 2.1. On 1 December the temperature readings were discontinued and started at a new site approximately 100 metres lower on the plateau. The temperature difference at 8 metres depth can be seen to be 1°C, which corrsponds to the dry adiabatic lapse rate. All subsequent temperature measurements at all levels (Tables 39-40) were corrected to the initial temperature set by subtracting 1°C.

Half-monthly running means are shown in Fig. 2.2. The 11-metre temperatures were largely extrapolated from readings in December, January and February at the new site. Temperature isopleths in a depth-time coordinate system are shown in Fig. 2.3. The penetration of the annual temperature wave is clearly shown in this diagram. Finally, tautochrones showing temperature versus depth for monthly intervals are shown in Fig. 2.4.

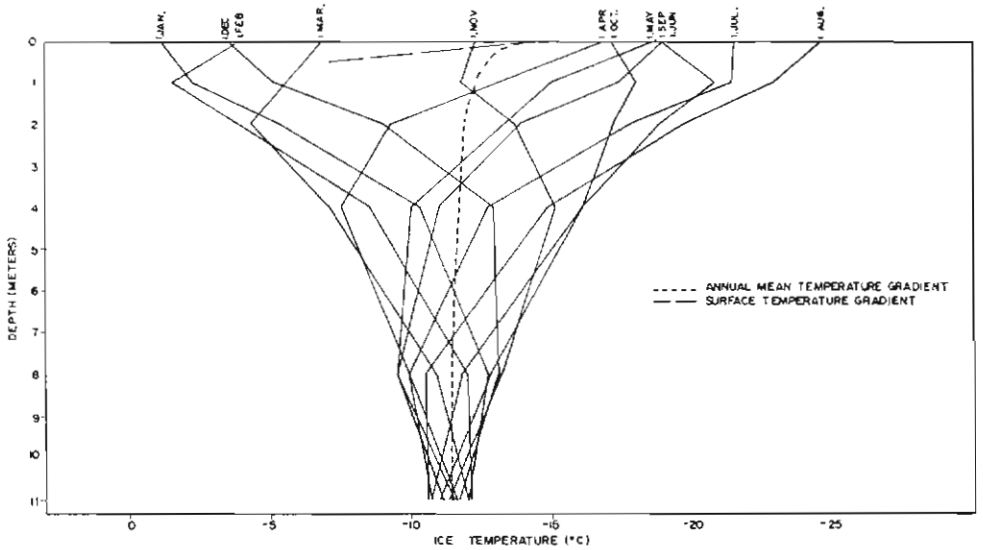

FIG. 2.4. Ice temperature profiles at monthly intervals.

2.3. FOURIER ANALYSIS OF THE PLATEAU ICE TEMPERATURES

It is possible to express the temporal variation of ice temperature at any depth by the Fourier series

$$T = T_m + tT^{\bullet}_{m} + \sum_{n} a_n \cos(n\nu t - \alpha_n) \quad n = 1, 2, 3 \ldots \tag{2.6}$$

where ν = frequency, n = order of harmonic, a = amplitude, α = phase angle and T_m = mean temperature.

* Note: Tables 1-49 (no Seetion designation) are basic data tables and are to be found in Appendix III.

Fourier coefficients for the first twelve harmonics were calculated from the half-monthly running means of temperatures at 1, 2, 4 and 8 metres depth, using an IBM7044 computer. The coefficients for the first three harmonics are shown in Table 2.1.

TABLE 2.1

FOURIER COEFFICIENTS FOR THE ANNUAL ICE TEMPERATURE WAVE AT MAWSON

z (m)	T_m (−°C)	a_1	a_2 (°C)	a_3	α_1	α_2 (rad.)	α_3
1	−12·48	10·34	1·50	0·48	2·70	3·14	0·71
2	−11·92	7·69	0·71	0·48	2·43	2·69	0·08
4	−11·78	4·30	0·16	0·37	1·78	2·27	−1·17
8	−11·37	1·94	0·10	0·18	0·60	−2·49	−1·98

It is interesting to observe the decrease of the annual mean temperature towards the surface. Budd (1966) has solved the diffusion equation containing radiation as an additional heat flux term in the ice to explain this change of temperature with depth, and has used the above results to verify his solution. The annual mean temperature profile can be explained sastisfactorily in terms of absorbed radiation.

2.4. THERMAL DIFFUSIVITY OF THE ICE

A method of ice temperature analysis was selected which is the same as that used by Dalrymple *et al.* (1963) for snow temperature data from the South Pole station, and is based on the model by Lettau (1954) for a non-homogeneous body. The two fundamental equations on which it is based are the equation of heat conduction,

$$B = -k\,T' \tag{2.7}$$

and the equation of heat continuity,

$$B' = -C\,T^{\bullet} \tag{2.8}$$

where B = vertical heat flux, k = heat conductivity at depth z, C = heat capacity per unit volume at depth z, T = ice temperature. The prime ($'$) denotes partial differentiation with respect to z, ($^{\bullet}$) denotes partial differentiation with respect to time t.

From the Fourier series of the ice temperature given in equation (2.6), it is assumed that the dependent variable B follows from a Fourier series similar to that of T, i.e.,

$$B = B_m + tB^{\bullet}_m + \sum_n b_n \cos(n\nu t - \beta_n) \qquad n = 1, 2, 3 \ldots \tag{2.9}$$

By differentiation with respect to z of both (2.6) and (2.9) and introducing

$$\gamma_n = \alpha_n - \beta_n \tag{2.10}$$

i.e., the phase difference between T' and T waves where

$$\tan\gamma_n = -\frac{\alpha'_n}{(lnA)'_n} \tag{2.11}$$

it can be shown (Lettau, 1954) that the thermal diffusivity

$$\overline{K} = \frac{\bar{k}}{\bar{C}} = \frac{n\nu \sin 2\gamma_n}{2\alpha'_n \beta'_n} \tag{2.12}$$

The bar (—) indicates that the values are independent of time.

Equation (2.12) gives a solution for $\bar{K}$, where $\bar{K}$ can vary in any manner with depth. It is thus suitable for non-homogeneous media. The same value of $\bar{K}$ should be obtained for each harmonic n; Lettau has, however, found that in soil the higher harmonics give different results.

Fig. 2.5 shows coefficients α, β and lnA of the first harmonic as a function of depth z. Smoothed curves are drawn through the calculated points and α', β' and lnA' are obtained by drawing tangents to the curves at the points required.

Using equation (2.12), the values of the thermal diffusivity are obtained as shown in Table 2.2.

TABLE 2.2

FOURIER COEFFICIENTS AND DIFFUSIVITY FROM THE FIRST HARMONIC OF ICE TEMPERATURES

z (m)	lnA	$-(lnA)'$	α	α' (rad/m)	γ deg.	β	β' (rad/m)	K cm^{2}sec^{-1}
1	2·34	0·36	2·70	0·30	39 8	2·00	0·42	0·0078
2	2·04	0·30	2·43	0·30	45·0	1·64	0·40	0·0083
4	1·46	0·23	1·78	0·30	52·5	0·86	0·35	0·0092
8	0·66	0·16	0·60	0·30	57·7	—0·41	0·28	0·0107

The amplitude of subsequent harmonics is too small compared with errors in ice temperature measurements to give significant results. The results of the analysis of the first harmonic, however, show the interesting fact that the thermal diffusivity decreases as the ice—air interface is approached. Since density measurements of the ice show no variation in the upper metres, a genuine change in thermal diffusivity of ice seems unlikely. The apparent change in thermal diffusivity must result from shortcomings of the model used, particularly the assumption that there are no energy sinks or sources within the ice. Ice is in fact quite tranparent to shortwave visible radiation, as has been shown in Section 1, and the distribution of the absorbed radiation follows an exponential extinction law from the surface. The least affected value of the thermal diffusivity should be at the 8-metre level where the available energy due to absorbed radiation is negligible. Calculating the thermal conductivity from the diffusivity value at 8 metres depth, using the measured ice density of 0·88 gm cm^3 (Table 48) and specific heat 0·48 cal gm^{-1} deg^{-1}, the conductivity is

$$k = Kpc = 4{\cdot}5 \times 10^{-3} \text{ cal sec}^{-1} \text{ cm}^{-1} \text{ deg}^{-1}.$$

This value compares favourably with values measured elsewhere and the theoretical value of $4{\cdot}85 \times 10^{-3}$cal sec^{-1} cm^{-1} deg^{-1} derived by Schwerdtfeger (1963) for ice at 0°C, the temperature effect on the thermal conductivity being small although not precisely determined to date.

To explain in greater detail the change of diffusivity with depth, the values of 'diffusivity' calculated from phase and amplitude changes of the annual temperature wave will be given now (Table 2.3).* They are computed for the first harmonic from equations (2.4) and (2.3) respectively, taking the data from Table 2.2.

* Strictly, since the two sets of results differ, as will be shown below, the medium does not obey the laws of the homogeneous conductor, and neither of the values can be called "diffusivity".

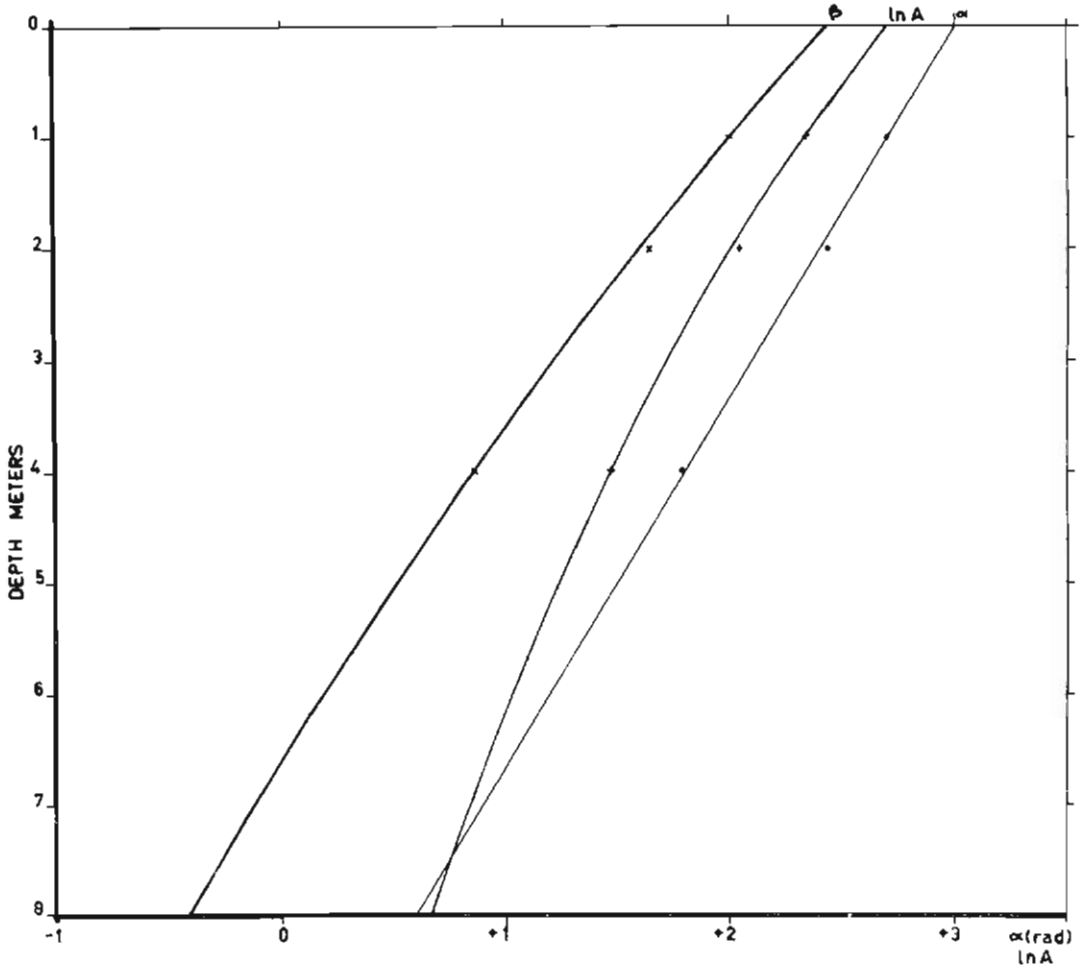

FIG. 2.5. Fourier coefficients of the first harmonic of the ice temperatures.

TABLE 2.3

THERMAL DIFFUSIVITY OF PLATEAU ICE

Depth (metres)	Method of calculation	Diffusivity (cm^2sec^{-1})
1	Amplitude change with depth	0·0077
2	,,	0·0111
4	,,	0·0188
8	,,	0·0390
1	Phase change with depth	0·0111
2	,,	0·0111
4	,,	0·0111
8	,,	0·0111

Thus the radiation effect on the phase change with depth is zero in contrast to a large effect on the amplitude. The absorbed radiation reaches the lower depths as a heat flux only, causing a smaller decrease of the amplitude with depth than expected, and corresponding increases in K as seen above (Table 2.3.). Since only night values of temperature are considered in the initial data, the direct effect of radiation is zero. If direct radiation effects (due to non-perfect reflectivity of thermocouples) had to be considered, then in the upper layers in the ice tbe direct radiation would give increased amplitudes. In the lower layers amplitude changes would be zero, so that one should expect higher K values towards the surface.

The effect of direct radiation thus gives rise to an apparent diffusivity decrease with depth and the effect of heat flux resulting from absorbed radiation gives rise to an apparent diffusivity increase with depth. If radiation is present in ice temperature data which were obtained using non-reflecting thermal sensors, then this data may give fairly uniform diffusivity values with depth, but these values will be too high.

Considering phase changes now: since there is no phase change with depth of the radiation flux (which is in phase with the temperature at the surface), it will be in phase with the heat flux at some particular depth after one eighth of a period or 6 5 weeks for an annual wave. Since the velocity of propagation into the ice is given by classical theory as $2K\omega$, it can be calculated that annual temperature waves penetrate 2·6 metres into the ice in 6·5 weeks. An interesting independent check on this is obtained from Fig. 2.3. which gives approximately 2·5 metres and could thus be used for another diffusivity determination.

At this depth, then, heat and radiation fluxes are in phase and the phase difference between temperature and heat flux waves should be 45°. From Table 2.2. $\gamma = 45°$ indeed at 2 metres depth. The increasing values of γ below 2 metres depth are due to increasing phase difference between the heat and radiation flux.

A graphical analysis of the phase and amplitude relationship of radiation and heat flux is given later for sea ice.

2.5. HEAT FLUX MEASUREMENTS BY FLUX PLATES

The introduction of heat flux plates or similar devices into snow or ice for the purpose of heat flux measurements results in a number of difficulties. Firstly, the plates cannot be made perfectly reflecting, so that radiation errors in transparent media must be expected and all day readings must be radiation-corrected. The most severe limitation of the flux plate, however, lies in the fact that, unless it is perfectly matched in conductivity to the surrounding medium, the temperature regime in its vicinity will be disturbed, which results in different amounts of heat passing through unit cross-section per unit time for flux plate and medium.

Simple analog experiments, using electrically conducting paper across which different potentials could be applied, showed these errors well and will be described elsewhere (Schwerdtfeger, 1967). They basically showed that the flux through a plate is smaller if its conductivity is less than that of the surrounding medium and *vice versa*. The heat flux distortion is controlled by the ratio of the conductivities of flux plate and medium, and the thickness to diameter ratio of the flux plates.

The heat flux plates (Schwerdtfeger and Weller, 1967) were installed in vertical

boreholes at depths of 1, 2 and 4 metres in the plateau ice. The particular version of the flux plates used had approximately 600 pairs of thermo-junctions each. Physical dimensions of the elements were 14 mm thickness and 38 mm diameter, enclosed in a perspex ring 14 mm thick and 76 mm in diameter. The boreholes were filled with snow and refrozen with melt water.

To determine the distortion errors of the set of flux plates used in plateau ice and sea ice, their emf output was compared with that expected from temperature gradient measurements in the ice at the same time. About 100 values were analysed as shown in Fig. 2.6. Only night values were used to avoid radiation errors. The scatter is high, due to inaccuracies in the graphical method of determining the temperature gradient at a point. The grouped means, however, show the flux plate errors for both types of ice. The fact that for a given temperature gradient the flux plate temperature gradient, given as an emf reading, is higher than that of the surrounding, means that less flux is passing through the plate than through the surrounding ice.

In the case of sea ice with a thermal conductivity of $4{\cdot}3 \times 10^{-3}$ cal $cm^{-1}\,deg^{-1}\,sec^{-1}$ at the flux plate depth, compared with plateau ice of conductivity $5{\cdot}3 \times 10^{-3}$ cal $cm^{-1}\,deg^{-1}\,sec^{-1}$, the heat flux distortion is considerably larger instead of being smaller. This initially somewhat unexpected result is undoubtedly due to heat flux focusing by the wide perspex ring surrounding the flux plate element. Correction factors, which have to be applied to determine the temperature gradient in the undisturbed ice from flux plate readings, are 0·75 for plateau ice and 0·60 for sea ice. Table V (Appendix I) gives conversion figures to obtain the heat flux in both types of ice.

2.6. HEAT FLUX MEASUREMENTS IN PLATEAU ICE

The output of the flux plates measured in millivolts was recorded automatically (Table 43). Fig. 2.7. shows an example for the variation of heat flux at various depths. Fluctuations of heat flux have been smoothed out considerably by the time the 4-metre level is reached. At that level the heat flux changes sign at the beginning of April from downward to upward flux towards the surface, as the temperature gradient becomes negative due to surface cooling.

The penetration of the temperature waves can be seen again to be preceded by approximately one eighth of a period by the change in heat flux: Fig. 2.7. may be compared with Fig. 2.1.; a particular example is presented later (Fig. 2.9.) when the phase and amplitude relationship between heat flux and temperature is used to derive the diffusivity of the ice.

The heat flux can also be determined without the aid of flux plates by considering the rate of change of heat content of the ice. The heat flux through the surface can be computed by determining the total heat gained by the ice by a change of temperature profile with depth $\Delta T(z)$:

$$Q = c\rho \int_0^\infty \Delta T(z)\,dz \qquad \text{cal cm}^{-2} \tag{2.13}$$

where ρ the density and c the specific heat of the ice are known. Using the temperature-depth relationship shown in Fig. 2.4, monthly changes in the heat content

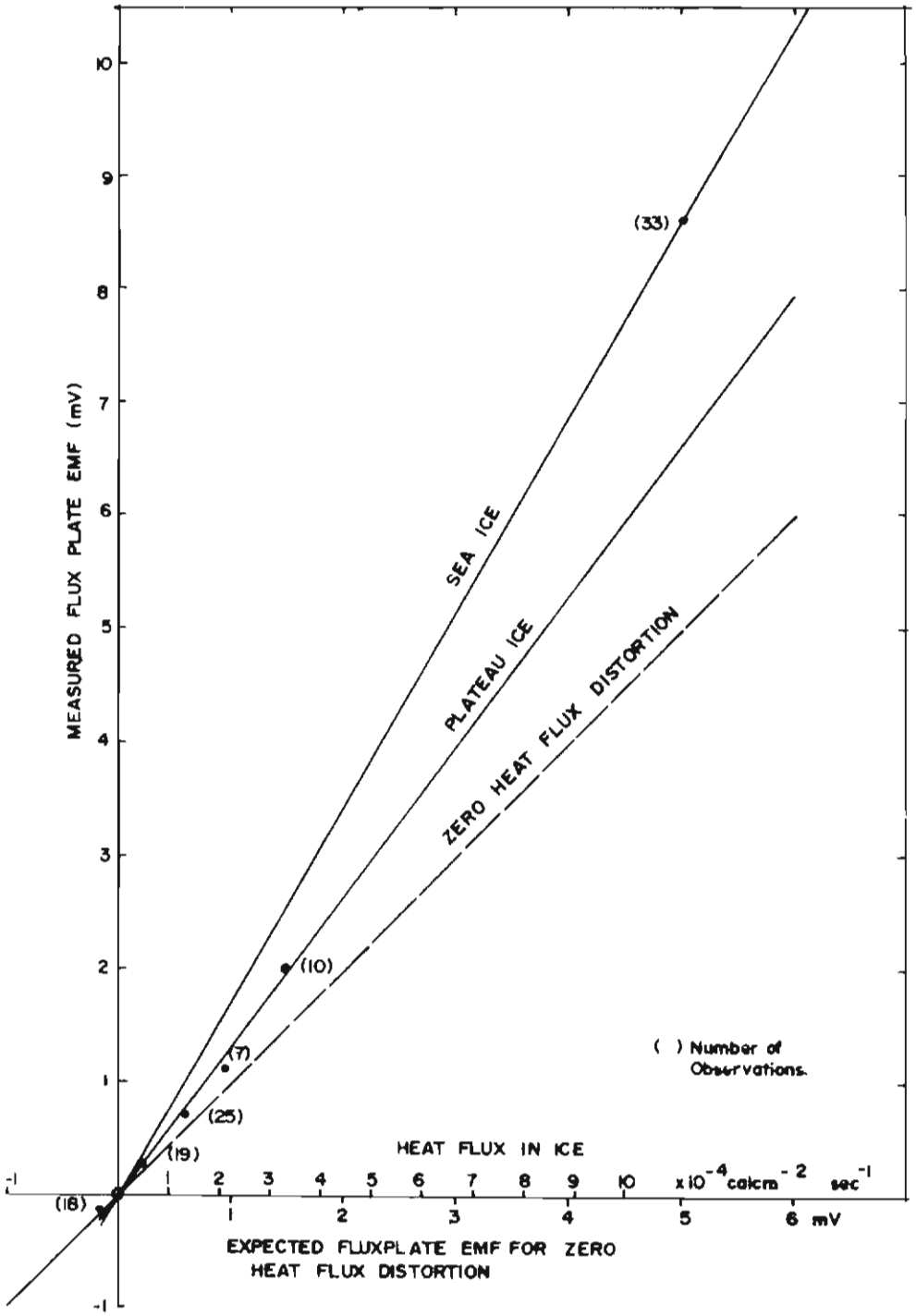

FIG. 2.6. Calibration of flux plates.

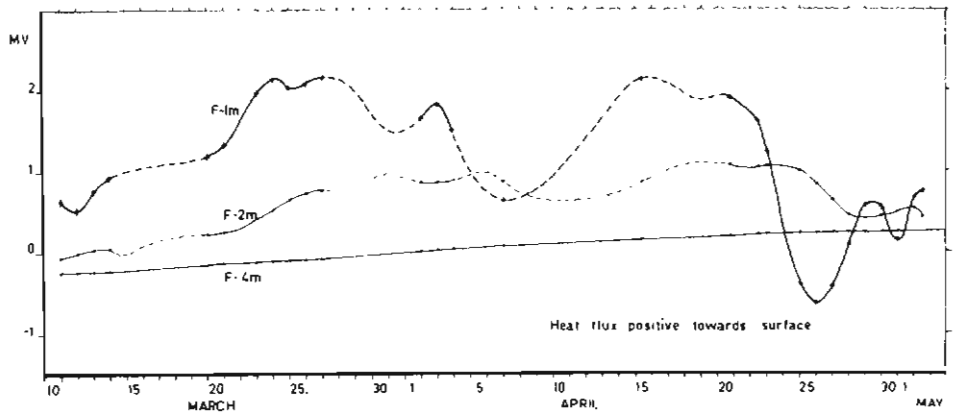

FIG. 2.7. Heat flux in the ice at 1, 2 and 4 metres depth.

of the ice can be computed down to 11 metres. Changes in heat content below 11 metres are neglected. The results are shown in Table 2.5.

TABLE 2.5

MEAN DAILY ICE SURFACE HEAT FLUX (CAL $CM^{-2}DAY^{-1}$)

Jan.	Feb.	Mar.	Apr.	May	Jun.	Jul.	Aug.	Sep.	Oct.	Nov.	Dec.
+10	+4	−26	−20	−7	−23	−20	−1	+2	+20	+36	+25

+ve sign = heat flux downward; −ve sign = heat flux upward

Fig. 2.8 shows the monthly means of the surface temperature and surface heat flux. The phase difference can be numerically determined to be 52 days. The amplitudes of the annual temperature wave (A) and heat flux wave (B) at the surface are approximately 11 °C and 30 cal $cm^{-2}\,day^{-1}$. From equation (2.5) a value of the conductivity is obtained and, using $\rho = 0{\cdot}88$ gm cm^{-3} and $c = 0{\cdot}48$ cal $gm^{-1}\,deg^{-1}$, the diffusivity can be computed. The values obtained are

$$k = 0{\cdot}0118 \text{ cal } cm^{-1}deg^{-1}sec^{-1}$$
$$K = 0{\cdot}028 \text{ } cm^2sec^{-1}.$$

These values are more than twice as high as the expected values for ice of density 0·88 gm cm^{-3}.

From previous considerations this is not surprising: the heat flux at the surface is not solely due to the surface temperature wave but also due to an additional conducted heat flux due to absorbed radiation. A simple calculation can now show the effect of radiation on the heat flux.

From radiation data at Mawson in 1965 (Tables 3 and 5) the mean annual amplitude of the short wave flux directed downward into the ice through the surface is 90 cal $cm^{-2}day^{-1}$. Some of this absorbed radiation is stored in the ice and some is lost by conduction to the surface. The radiation effect on the heat storage will be considered first.

Anticipating the results shown below of a diffusivity determination during a radiationless period, namely $K = 0{\cdot}0118$ cm^2sec^{-1}, and using the annual surface temperature amplitude A of 11 °C, from equation (2.5), an annual amplitude of the heat flux B of only 19·5 cal $cm^{-2}day^{-1}$ is computed. Since the measured heat

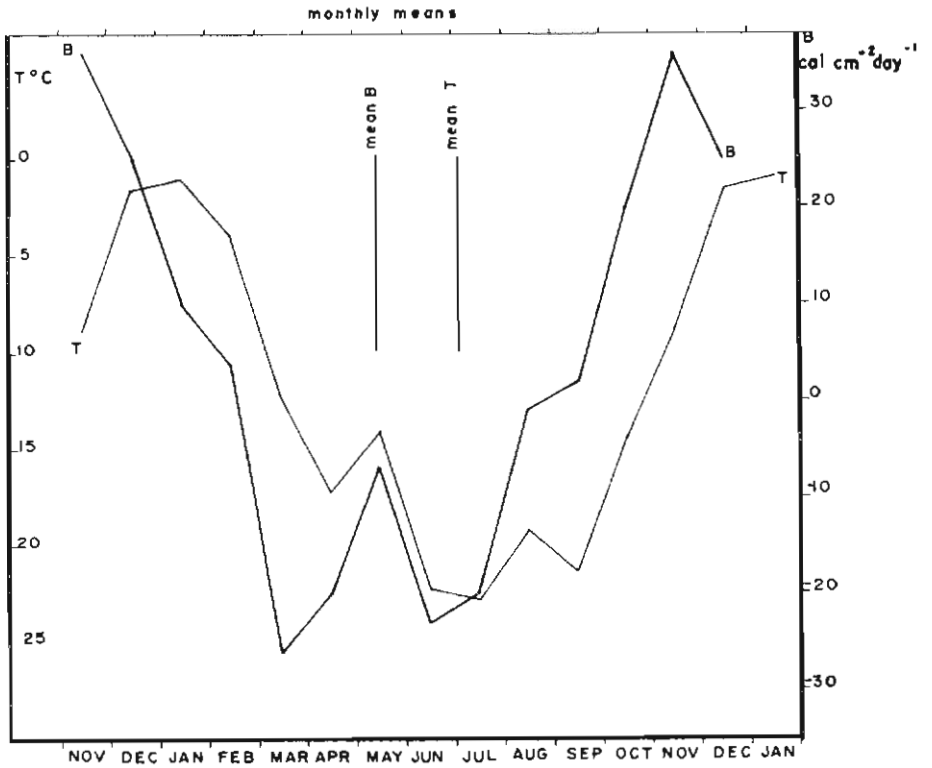

FIG. 2.8. Monthly mean values of surface temperature (T) and heat flux (B).

flux has an amplitude of approximately 30 cal $cm^{-2}day^{-1}$, the absorbed radiation must nearly double the heat storage in the ice and the resulting conducted heat flux, giving high amplitudes of B and hence high values of conductivity and diffusivity. The value of A is not affected by absorbed radiation, since it is extrapolated from ventilated air temperature sensors.

The heat loss of the ice by conduction due to the presence of an annual mean temperature gradient set up by absorbed radiation will be considered next. This gradient is shown in Table 2.1. The surface temperature was extrapolated by considering the mean of the measured air temperatures at 1 and 4 metres height above the ice for the year to obey a logarithmic profile law, and the ice surface temperature to be equal to the air temperature at the height of the mean roughness parameter $z_0 = 0{\cdot}23$ cm (Tables 18-29). This temperature is $-14{\cdot}5$°C. From the discussions in Section 1, one can assume that the curvature of the temperature profile follows a law similar to the curvature of the dashed line in Fig. 1.10, representing the extinction of light in the ice. Using these considerations, the temperature gradient at the surface of the ice is found to be 15°/metre. This leads to a heat loss through the surface by conduction of

$$Q = k\frac{\partial T}{\partial z}t$$
$$= 25{\cdot}0 \text{ kcal cm}^{-2}\text{year}^{-1},$$

or approximately 69 cal $cm^{-2}day^{-1}$. This figure should be compared with the 90 cal $cm^{-2}day^{-1}$ of absorbed radiation. For a balanced energy budget of the ice other forms of energy transfer could play a role such as internal melting in the ice, the water vapour reaching the surface of the ice through melted cavities. It seems likely, however, that the observed difference between heat gain by absorbed radiation and heat loss by conduction is due to the inaccuracy of determining the ice temperature gradient at the surface.

To determine the diffusivity of the ice when there is no radiation present, an isolated sinusoidal temperature pulse and resulting heat flux wave were taken from the recorded data at 1 metre depth in the plateau ice. The period of the temperature and flux pulses was 7 days, masking any diurnal radiation pattern. Moreover, the data were taken from the August records when the incoming radiation is still very low. Flux and temperature pulses are shown in Fig. 2.9.

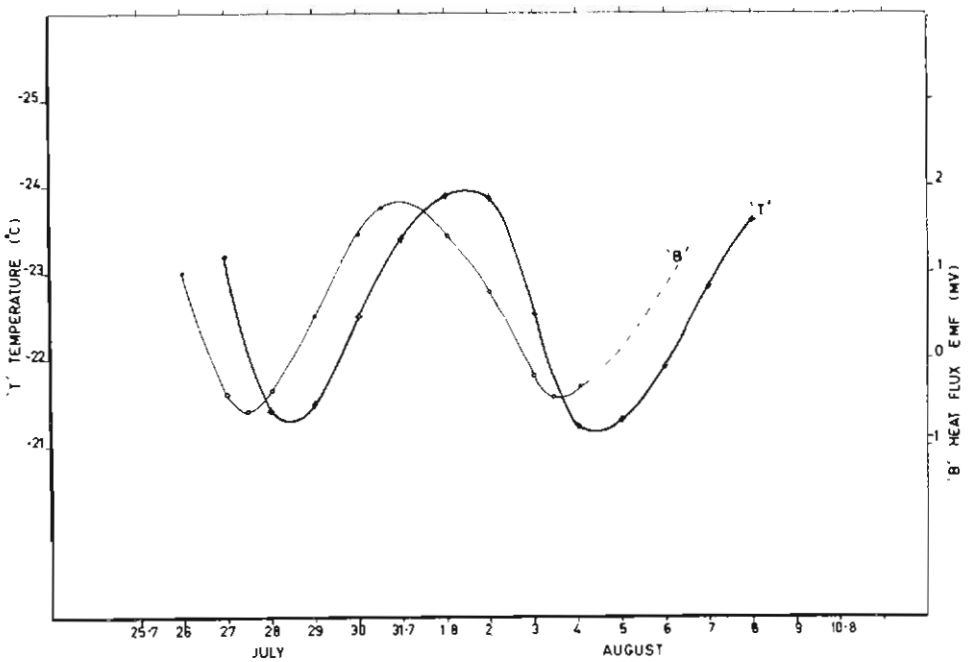

FIG. 2.9. Selected example of waves of heat flux (B) and temperature (T) at one metre depth.

The phase difference between temperature and heat flux waves is approximately one eighth of a period as expected. Amplitudes are 1·4°C and 1·3 mV respectively; the latter figure is converted by means of Table V to $2{\cdot}15 \times 10^{-4}$ cal cm^{-2} sec^{-1}. From these amplitudes the conductivity and diffusivity can be calculated again, using equation (2.5), and are

$$k = 5{\cdot}3 \times 10^{-3} \text{ cal cm}^{-1}\text{deg}^{-1}\text{sec}^{-1}$$

and $$K = 0{\cdot}0118 \text{ cm}^2\text{sec}^{-1}.$$

They agree very well with accepted figures for ice and show again that radiation

effects must be eliminated when the diffusivity of transparent media is to be computed.

2.7. SUMMARY OF DIFFUSIVITY DETERMINATION IN PLATEAU ICE

The results of all plateau ice diffusivity determinations are summarized in Table 2.6.

TABLE 2.6

Depth (m)	Method of computation	Period of waves	Diffusivity cm^2sec^{-1}	Remarks
0	Ampl. of T & B	1 year	0 0247	High due to large amount of heat transmitted by radiation.
1	Ampl. & phase of T (Lettau's method)	1 year	0·0078	Not a true variation of K with depth, but caused by the effect of radiation penetration on the amplitude-depth profile.
2	,,	,,	0·0083	
4	,,	,,	0·0092	
8	,,	,,	0·0107	
1	Ampl. of T	1 year	0·0077	Not true values due to the penetration of radiation. The value at 2m is close to the true value, since radiation and conduction are approximately in phase here.
2	,,	,,	0·0111	
4	,,	,,	0·0188	
8	,,	,,	0·0390	
1	Phase of T	1 year	0·0111	Close to true value because the radiation only has a slight effect on variation of phase with depth > 1 m.
2	,,	,,	0·0111	
4	,,	,,	0·0111	
8	,,	,,	0·0111	
1	Ampl. of T & B	7 days	0·0118	Close to true value, because only conductive heat transfer present (no radiation).

2.8. TEMPERATURE PATTERN IN SEA ICE: DESCRIPTIVE ANALYSIS

In the sea ice, as well as in the plateau ice, the temperatures were measured by thermocouples frozen into the ice at 0, 15, 30, 45, 60, 80 and 100 cm depth (Tables 32-34). All readings were taken at midnight to reduce radiation errors. A thermocouple at 2 metres depth was always in the sea water since the maximum ice thickness reached near the thermocouple probe was only 135 cm. Fig. 2.10. shows half-monthly means for all levels. Curves for all levels were extrapolated to $-1{\cdot}8°C$, the freezing temperature at $33‰$ salinity sea water, at the date at which freezing began at that level. Two warm temperature periods, one in early July, the other in late August, can be traced throughout the sea ice cover. In November, sea ice temperature measurements were discontinued: the ice became unsafe to walk on and broke out late in December.

Fig. 2.11 shows tautochrones of sea-ice temperature against depth for half-monthly intervals. Temperature gradients in the early periods of winter are steep and decrease slowly towards the summer months, when the greater amounts of absorbed radiation again cause deviation from a linear temperature gradient in the top layer.

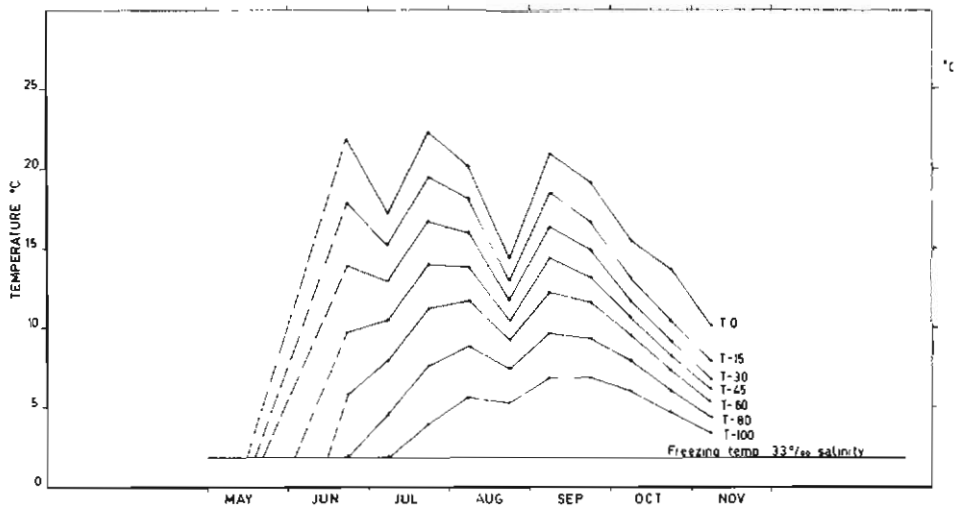

FIG. 2.10. Sea-ice temperatures: half-monthly means of the daily midnight values.

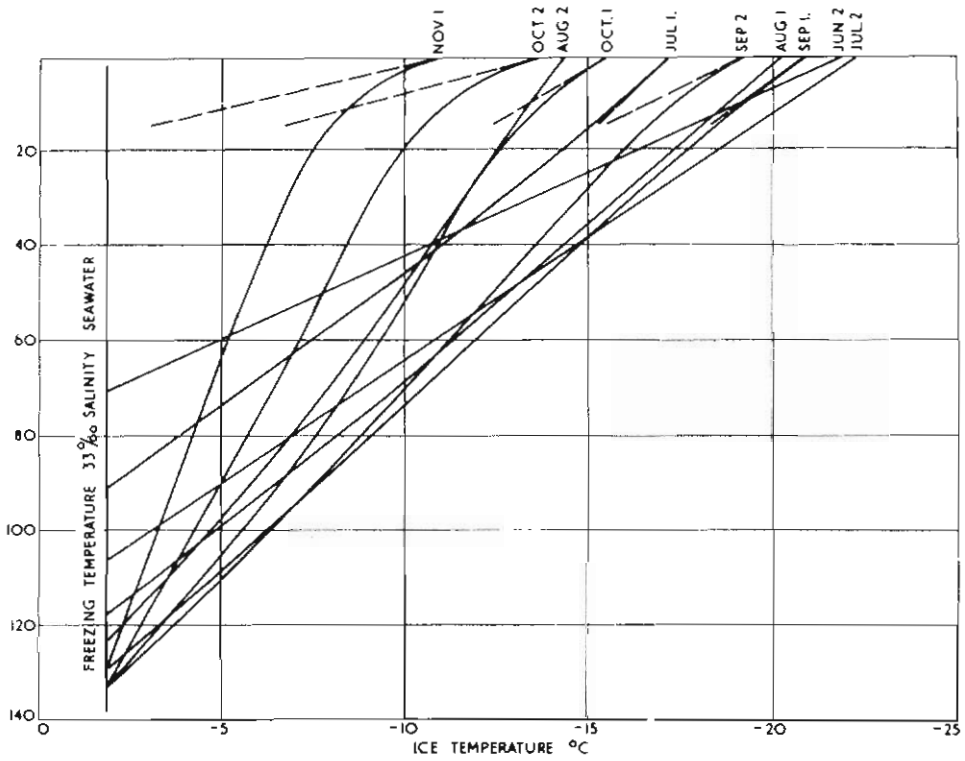

FIG. 2.11. Sea-ice tautochrones for the first and second half of each month and surface temperature gradients (dashed lines).

2.9. HEAT FLUX MEASUREMENTS IN SEA ICE

Heat flux plates were installed in the sea ice at depths of 30 and 60 cm. Sea water was allowed to refreeze the boreholes which had been filled with sea ice shavings after installation of the flux plates. The flux plate at 60 cm depth gave inconsistent readings shortly after installation; presumably the plate was not hermetically sealed and electrolytic emf's were set up. The flux plate at 30 cm depth performed well throughout (Tables 41-42).

One important consequence of heat flux through the sea-ice cover is its effect on the ice growth rate at the ice—water interface. This is shown in Fig. 2.12 where the heat flux at 30 cm depth is plotted, together with the ice growth rate on the same time scale. The phase and amplitude relationship between heat flux and rate of ice growth is obvious. The phase difference is approximately 4-5 days, depending on the frequency of the heat flux wave, with the heat flux leading the waves of rate of ice growth. Schwerdtfeger (1966) has used similar data to derive a lag coefficient for sea ice which is of interest in ice-growth forecasts. The lag coefficient is inversely proportional to the thermal diffusivity, the proportionality constant being derived empirically. For the above data the constant derived was identical with Schwerdtfeger's.

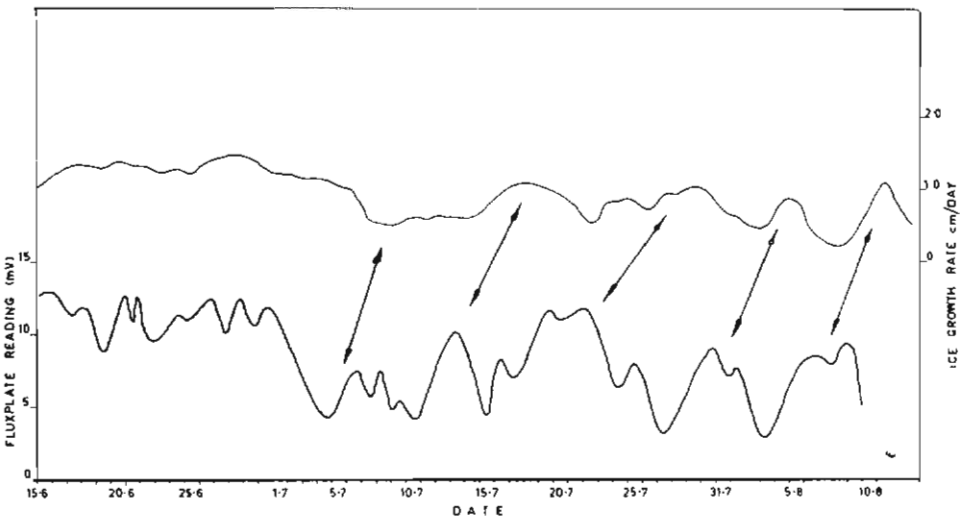

FIG. 2.12. Heat flux at 30 cm depth in the sea ice, and the ice growth rate at the iee—water interface.

Sea-ice thickness measurements were carried out fully automatically every six hours through a series of operations where an electric current was passed through a wire loop through the sea ice to heat it; a weight attached to the wire was wound up by an electric motor to the underside of the sea ice and the number of turns of the motor counted and printed (see Section 3.3). The design of the machine is due to Schwerdtfeger.

With the aid of the flux plates, some of the more detailed aspects of heat flux

in sea ice, such as the diurnal heat flux, could be investigated. Fig. 2.13 shows the diurnal variation in heat flux for October. The amplitude of the diurnal variation is remarkable, a change in sign of heat flux occurring quite frequently. It will have to be examined, now, whether this is a genuine heat flux or whether other effects such as radiation contribute.

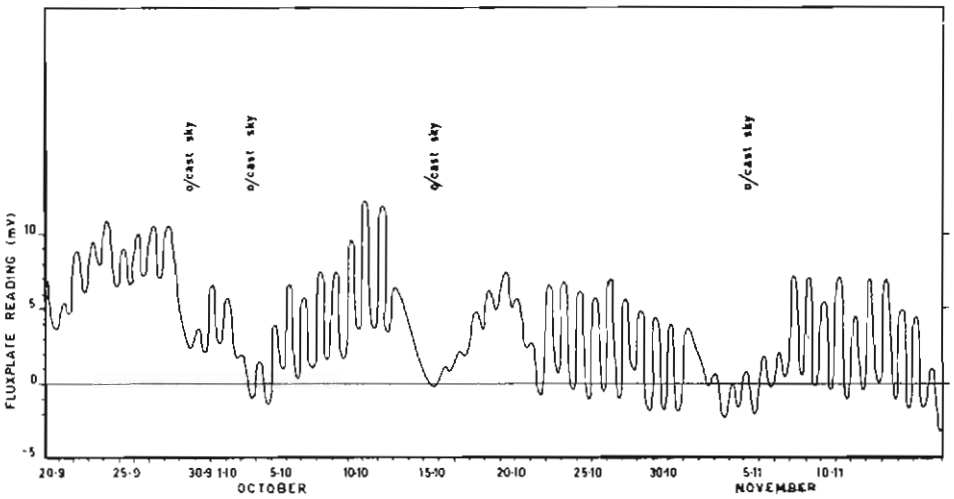

FIG. 2.13. The diurnal variation of the heat flux at 30 cm depth in the sea ice.

2.10. THERMAL DIFFUSIVITY OF SEA ICE

Fig. 2.14 shows the diurnal variation of heat flux and temperature at the 30 cm depth in sea ice. The curves are based on mean values for the month of October calculated for hourly intervals (Table 44). It is apparent that the temperature curve is not a sine wave: the phase difference between minimum and maximum temperature is only 9 instead of 12 hours and there is a hump in the curve at approximately 19 hours. The heat flux curve also shows some deviation from the expected sine wave shape.

If the distortion of the curves is ascribed to radiation penetrating into the sea ice, then, by superimposing a diurnal radiation pattern on assumed perfect sinusoidal temperature and heat flux waves, one should be able to separate the relative amplitudes and phases of these latter by trial and error method, by changing the phases and amplitudes of radiation, temperature and heat flux waves until the results actually measured are obtained.

The shape of the radiation curve for October has been obtained from Weller (1964). Its phase is fixed in relation to solar noon. Using a trial and error method to change its amplitude and the phase and amplitude of an assumed sinusoidal temperature wave, a curve can be obtained by addition of the two components (Fig. 2.15) which closely resembles the mean temperature curve in Fig. 2.14. The immensely strong effect of radiation, both on the phase and amplitude of the temperature curve, is immediately apparent.

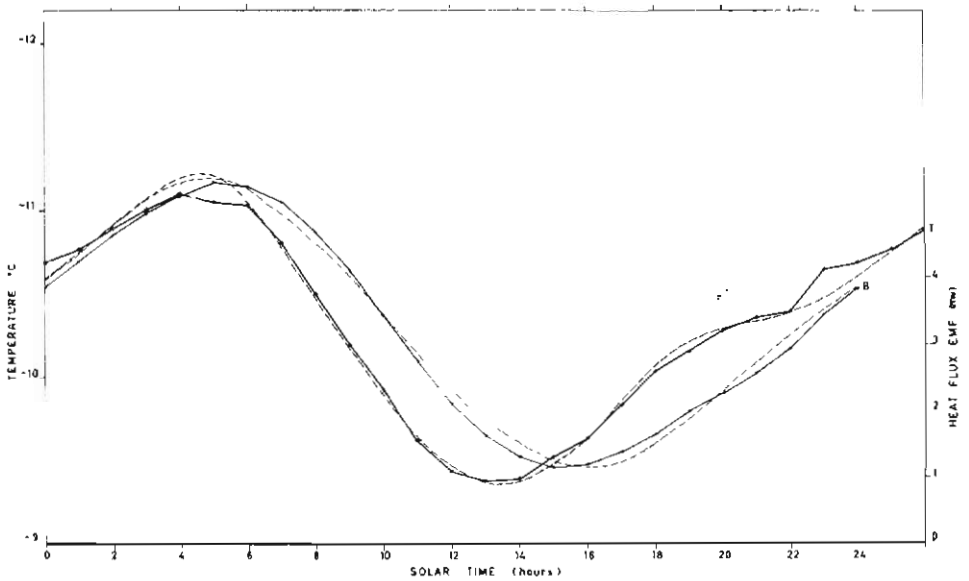

FIG. 2.14. Heat flux and temperature at 30 cm depth in the sea ice. Monthly means for October. (Dashed lines are curves derived by trial-and-error method.)

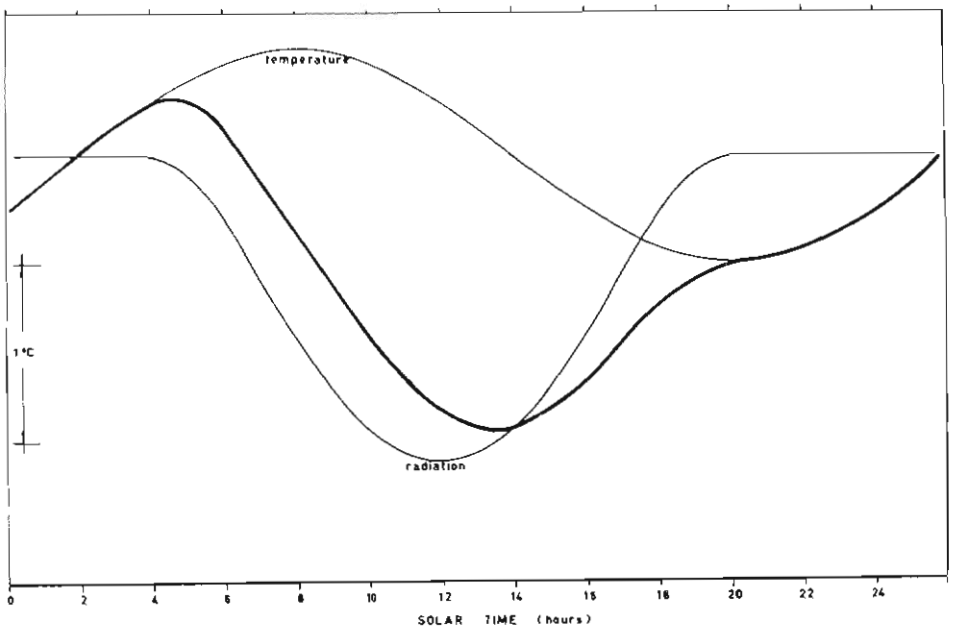

FIG. 2.15. The effect of radiation on the diurnal temperature curve at 30 cm depth derived by trial-and-error method.

Similarly, the heat flux curve can be obtained (Fig. 2.16). The effect of radiation on the heat flux measurements is less severe, since the heat flux plates are only affected by the net (downward minus upward) radiation at any level in contrast to the thermocouples which are affected by the total (upward plus downward) radiation.

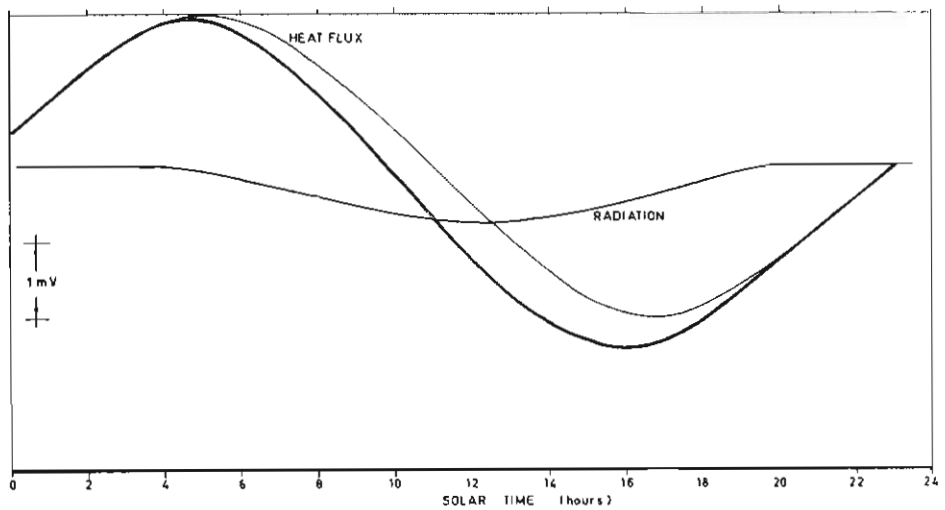

FIG. 2.16. The effect of radiation on the diurnal heat flux curve at 30 cm depth derived by trial-and-error method.

It should be pointed out that the "radiation" curve in both cases indicates the amplitude of the total radiation effect, i.e., the effect of direct radiation on the non-perfectly reflecting thermocouples and flux plates, as well as the effect of absorbed radiation on the temperature rise and heat flux at 30 cm depth. Strictly, there is a slight phase shift between the direct radiation effect and the heat flux and temperature rise at 30 cm depth, resulting from radiation absorption in the top 30 cm. For $K = 0{\cdot}01$ cm^{2}sec^{-1} the depth of penetration is 15 cm in one hour for an amplitude reduction of $\frac{1}{100}$. Also the direct radiation effect is large in the top layers compared with the heat flux effect due to absorbed radiation. The small phase shifts involved are therefore ignored.

Drawing the radiation-corrected waves of temperature and heat flux together now (Fig. 2.17), there appears the correct phase relationship between heat flux and temperature with the heat flux leading the temperature wave by one eighth of a period.

From the amplitudes obtained, namely 0·6°C and $2{\cdot}60 \times 10^{-4}$ cal cm^{-2}sec^{-1} (the peaks of heat flux are $7{\cdot}1 \times 10^{-4}$ and $1{\cdot}9 \times 10^{-4}$ cal cm^{-2}sec^{-1}), the thermal conductivity can now be derived. Some uncertainty is introduced when values of the density and specific heat must be chosen, neither of which was measured. From Schwerdtfeger (1963), the specific heat of sea ice of density 0·9, salinity $6^0/_{00}$ and temperature −12°C (these latter two values are average conditions measured for October for the top 30 cm of sea ice) is 0·67 cal gm^{-1}deg^{-1}.

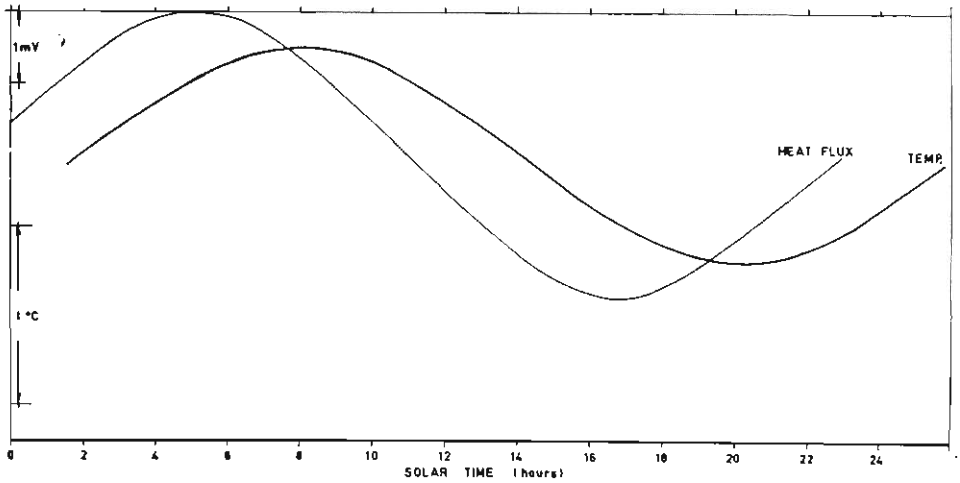

FIG. 2.17. Radiation-corrected curves of the diurnal temperature and heat flux at 30 cm depth in sea ice.

Again, $k = (\frac{B}{A})^2/\omega\rho c$ from equation (3.5), from which

$$k = 4{\cdot}30 \times 10^{-3} \text{ cal cm}^{-1}\text{deg}^{-1}\text{sec}^{-1}$$

and the diffusivity $K = 0{\cdot}0072$ cm^{2}sec^{-1}.

(The classical solution for semi-infinite thickness can be used here, since the depth of penetration for $K = 0{\cdot}007$ cm^{2}sec^{-1} is 65 cm for an amplitude reduction of $\frac{1}{100}$ and the sea-ice thickness is 135 cm.) The value of conductivity given by Schwerdtfeger for ice of the same make is $4{\cdot}69 \times 10^{-3}$ cal cm^{-1}deg^{-1}sec^{-1} or $K = 0{\cdot}0078$ cm^{2}sec^{-1}.

Despite uncertainties in the values assumed for ρ and c, the value obtained for the thermal conductivity is close to the expected value. Radiation effects seem, therefore, to have been successfully eliminated and the above curves (Figs. 2.15-2.17) are essentially correct.

The fluctuations of heat flux shown in Fig. 2.13 are then basically quite realistic, although the amplitudes should be reduced slightly. They demonstrate the powerful effect of the diurnal surface temperature pattern on the sea ice and the direct contribution of solar radiation to its final summer melting and break-up.

2.11. DIFFUSIVITY PROFILE IN SEA ICE

It will now be attempted to determine the change of thermal diffusivity with depth in sea ice. As has been shown above, only data collected during a radiationless period can be used for this purpose. From the smoothed sea ice temperatures (Tables 32-34) a 50-day period warm wave through the sea ice was obtained (Fig. 2.18). This wave occurred in August when radiation effects are still quite small and can be neglected. Average values of daily insolation in August: 40 cal cm^{-2}day^{-1}; in December: 680 cal cm^{-2}day^{-1} (Table 3); also during August, there was a 4-5 cm-thick snow cover on the sea ice (Fig. 3.9).

Small changes of sea-ice thickness due to ice growth were neglected and an

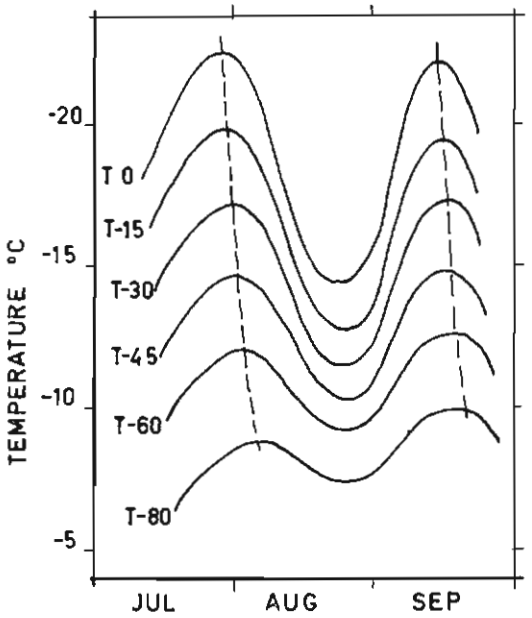

FIG. 2.18. Amplitude and phase changes of a 50-day period warm wave travelling through the sea ice.

average thickness of 125 cm was taken. Salinity profiles were measured (Table 49) and are shown in Table 2.7, together with the average ice temperature at that level for the duration of the wave. From this data and using Schwerdtfeger's (1963) theoretical considerations, values of diffusivity could be derived for various levels.

TABLE 2.7

Depth (cm)	Salinity (‰)	Temperature (°C)	Diffusivity ($cm^2 sec^{-1}$)
0	7	−18	0·0098
30	6	−14	0·0093
60	5	−11	0·0083
100	4	−6	0·0052
125	4	−2	0·0010

To analyse the wave data, the solution given by Carslaw and Jaeger (1959) for a slab with periodic surface temperature was used. A slab $0 \leqslant x \leqslant l$ with zero initial temperature and with the planes $x = 0$ and $x = l$ kept at zero and sin $(\omega t + \epsilon)$ respectively is considered. The solution for temperature is of the form

$$A = \frac{\{\cosh 2hx - \cos 2hx\}^{\frac{1}{2}}}{\{\cosh 2hl - \cos 2hl\}} \tag{2.14}$$

$$\phi = \arg \frac{\{\sinh hx(1+i)\}}{\{\sinh hl(1+i)\}} \tag{2.15}$$

where A is the amplitude, ϕ the phase and $h = \sqrt{\frac{\omega}{2K}}$, K = diffusivity.

Amplitudes are obtained from Fig. 2.18 and are given below:

Depth (cm)	Amplitude (°C)	Relative Amplitude A	Relative Depth x/l
0	4·0	1·00	0
15	3·5	0·87	0·12
30	2·9	0·73	0·24
45	2·4	0·60	0·36
60	1·9	0·47	0·48
80	1·2	0 30	0·64

A solution of equation (2.14) for diffusivities K is easily obtained graphically, using the above data and a series of values of hl and hx. This is shown in Fig. 2.19 where the dotted line represents the actual sea ice amplitude data. Interpolating between the values of hl or K the diffusivity can be obtained for various depths such as shown.

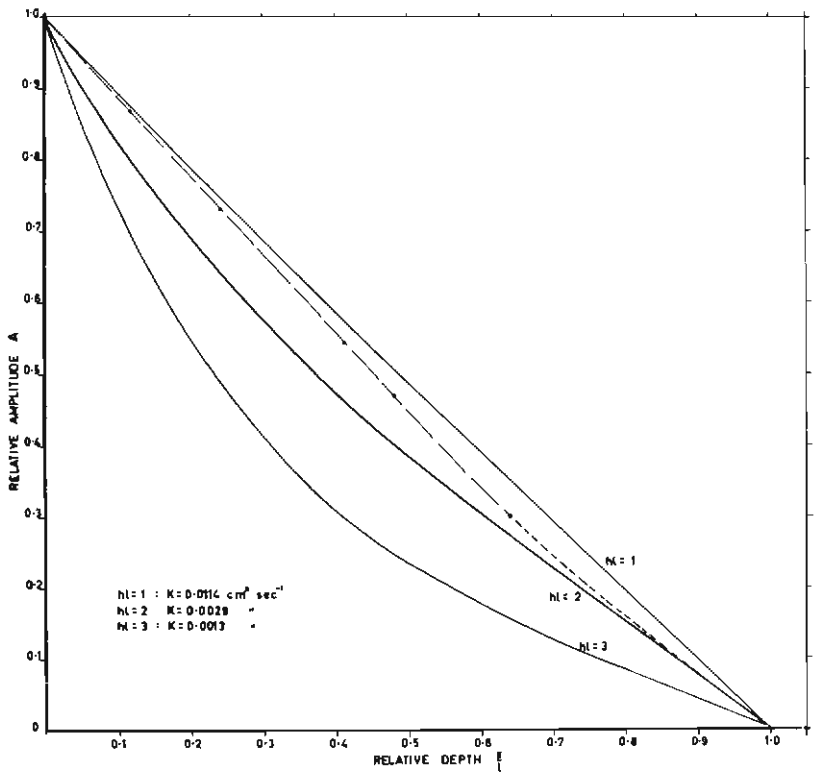

FIG. 2.19. Amplitude decrease of a 50-day period wave travelling through the sea ice (dashed line). Lines h l = 1, 2 and 3 are solutions for a slab model with fixed temperature at the lower boundary; harmonic temperature wave at the surface.

Relative depth	hl	Diffusivity K (cm^2sec^{-1})	Depth (cm)
0·1	1·10	0·0094	12·5
0·2	1·12	0·0091	25
0·4	1·26	0·0072	50
0·6	1·62	0·0043	75
0·8	1·81	0·0035	100
0·9	2·00	0·0029	112·5

These values, together with the data obtained from theoretical considerations above, are shown in Fig. 2.20. The diffusivity decreases with depth, as expected, and agrees generally with the theoretical values. However, the error bars indicate that the method is quite critical in the determination of the amplitude reduction with depth, an error of ± 0·1 °C changing the diffusivity appreciably. The factor that affects the theoretical values most is the salinity, and the error bars in Fig. 2.20 show that a change of ± 1‰ in salinity can also change the diffusivity appreciably, particularly at higher ice temperatures.

A simplification of matters was also introduced by considering a stationary lower boundary. Actually, the boundary advanced approximately 10 cm, due to ice growth in the period considered. This would slightly increase the amplitudes of the

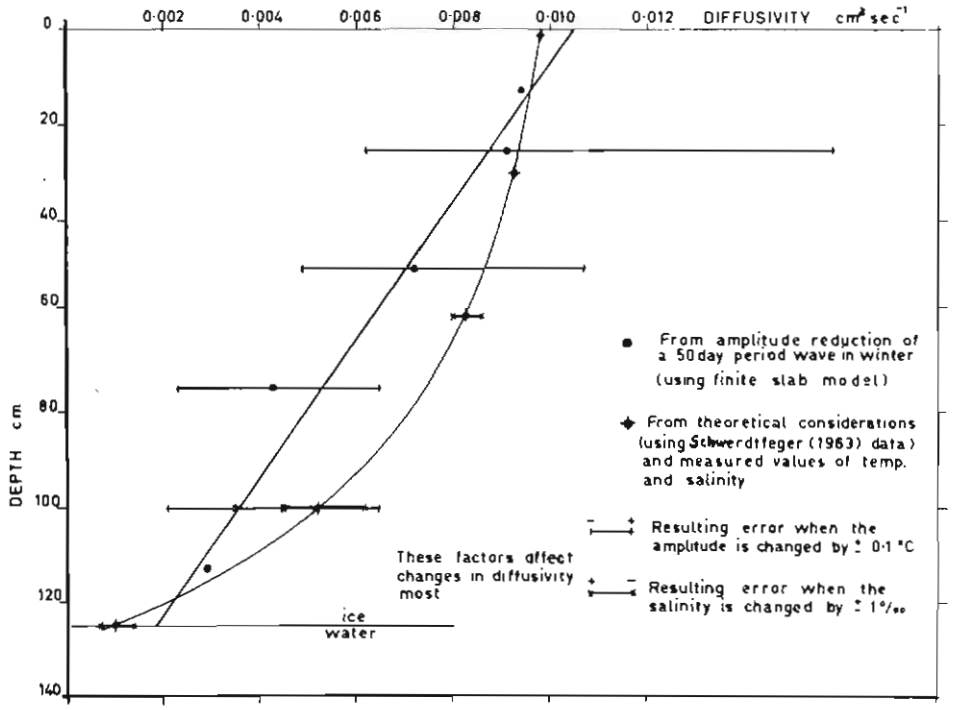

FIG. 2.20. Thermal diffusivity profile through the sea ice.

temperature wave at the lower levels and hence decrease the diffusivity. Compared with the errors of the above method this change would, however, appear to be inconsequential. The accuracy of the available data does not permit diffusivity calculations from phase changes.

2.12. CONCLUSION

It has been shown that, to determine the thermal diffusivity in optically transparent media such as ice, it is necessary to consider the effect of radiation transmitted through the medium. This effect is twofold: firstly, direct radiation on temperature or flux sensors in the ice results in large errors if these sensors are not perfectly reflecting. Secondly, the radiation is absorbed exponentially with depth, and a heat flux results which is additional to that due to temperature pulses at the surface.

If radiation effects are not separated, diffusivity values obtained may be either too high or too low, depending entirely on the method used for computation.

The same considerations apply to snow and other optically translucent media. The consequences of this on heat flux and temperature measurements, particularly in polar regions, are obvious.

3. THE HEAT ENERGY TRANSFER THROUGH A FOUR-LAYER SYSTEM: AIR—SNOW—SEA ICE—SEA WATER

3.1. INTRODUCTION

Heat budget studies of sea ice have been carried out extensively in the ice-covered waters of the Arctic Ocean. Both meteorological methods and glacio-meteorological methods, involving the measuring of ice temperatures and ablation and ice accretion, have been used for this purpose. Untersteiner (1964) has quoted some of these investigations and has compared their results with his own glacio-meteorological heat budget estimate. In an extensive study, Fletcher (1965) has used all available data to evaluate the heat exchange between the surface and the atmosphere in the Arctic. Little information of this nature is, however, available for Antarctic sea ice.

To determine the components of the heat energy exchange between ice and snow surfaces and the lowest layers of the atmosphere, two semi-automatic micro-meteorological stations were set up in the vicinity of Mawson.

The energy exchange at the upper and lower boundaries of a snow-covered annual floating sea ice sheet will be discussed in this Section, as well as the energy transfer processes in the solid layer. The effect of the snow-cover on the sea ice is of considerable importance in altering the optical properties of the ice surface. Since at Mawson it was only a few centimetres thick, however, its thermal capacity was small and its presence was neglected in all heat budget considerations except in the radiation component.

This study uses both meteorological and glacio-meteorological methods to determine the heat budget components, and discusses in detail the effect of absorbed radiation on the heat budget of the ice.

The equation of the energy budget of an ideal body, with semi-infinite extent in the vertical direction and infinite dimensions in the horizontal, is given by the sum of all the energy fluxes at the surface and is usually considered in the form:

$$R + Q + S + E = 0 \tag{3.1}$$

where R = net radiation or radiation balance at the surface
Q = sensible or eddy heat flux at the surface
S = conducted heat flux at the surface
E = latent heat flux at the surface.

The sign convention used is that a negative value indicates a heat flux towards the surface which acts as a heat sink, and a positive value indicates a heat flux away from the surface which acts as a heat source.

In the case of bodies transparent to radiation such as ice or snow, the net shortwave flux above the surface is equal to the net shortwave flux just below the surface, since a two-dimensional surface cannot have any absorbing properties. Since they have opposite sign the term R becomes the net flux of longwave radiation at the surface, since no longwave radiation penetrates ice or snow. The absorbed shortwave radiation can either be stored in the ice or lost by conduction to the surface. The difference between the absorbed radiation and conducted heat flux due to it is equal to the net heat storage change in the ice due to absorbed radiation. This latter term is included when computing the change in heat storage from temperature pattern changes to give the conducted heat flux S, so that the penetrated radiation and resulting heat flux do not necessarily have to be included separately in the energy budget equation of semi-infinite bodies.

In the case of a body with finite thickness, however, such as the case of a sea ice cover under consideration here, not all the radiation energy passing through the upper surface is absorbed by the sea ice but some energy passes through into the water. Also, the water at the lower boundary usually acts as a heat source, due to its high temperature and large thermal capacity. Because of this, the heat flux cannot be simply computed from the change in heat content, as one could do with a semi-infinite body, since part of the radiation flux at the upper boundary and part of the conducted heat flux at the lower boundary may pass through the ice without heating it. Heat fluxes must therefore be computed from temperature gradients and must thus necessarily include a heat flux term which is due to absorbed radiation.

The same considerations apply for transparent semi-infinite bodies, if the heat flux is computed from temperature gradients at the surface. The net annual conducted heat flux at the surface is then not zero but in the case of plateau ice at Mawson (extinction coefficient 0·007 cm^{-1}), approximately of the same magnitude as the annual mean value for the daily absorbed radiation, which is 90 cal $cm^{-2}day^{-1}$. This was shown in the last section.

The energy budget equation at the boundaries of the sea ice cover, therefore, has to be considered in the form:

$$N_L + N_{Sa} + N_{Sb} + Q + S + E = 0 \tag{3.2}$$

where N_L = net flux of longwave radiation

N_{Sa} = net flux of shortwave radiation above the surface
N_{Sb} = net flux of shortwave radiation below the surface;

for the upper boundary:

$$N_{Sa} = -N_{Sb}$$

$$\therefore \quad N_L + Q + S + E = 0; \tag{3.3}$$

for the lower boundary:

$$N_{Sa} = -N_{Sb};$$

also, $N_L = 0$ since the temperature difference between the water and ice at the interface is negligible.

$$\therefore \quad Q + S + E = 0 \tag{3.4}$$

3.2. INSTRUMENTATION

The site where the instruments were installed on the sea ice was approximately 400 metres offshore. Low ice cliffs (2-3 metres) were 400 metres upwind from the instruments, with the prevailing wind a steady SE katabatic with an annual mean velocity of 10 m sec^{-1}. To the south of the instruments, the ice cliffs were 20 metres high and to the north and west the closest islands were 2 kilometres away. The seabottom was 300 metres below the instruments on the sea ice (see maps in Appendix II).

Recording instruments were housed in a heated caravan constructed of fibreglass and expanded polyurethane (Fig. 3.1). A power cable connected the caravan to the mains supply at the main station. The caravan was installed on West Arm of Mawson Harbour (Fig. 3.2), and connected to the instrument set on the sea ice through 500 metres of 16-pair telephone cable.

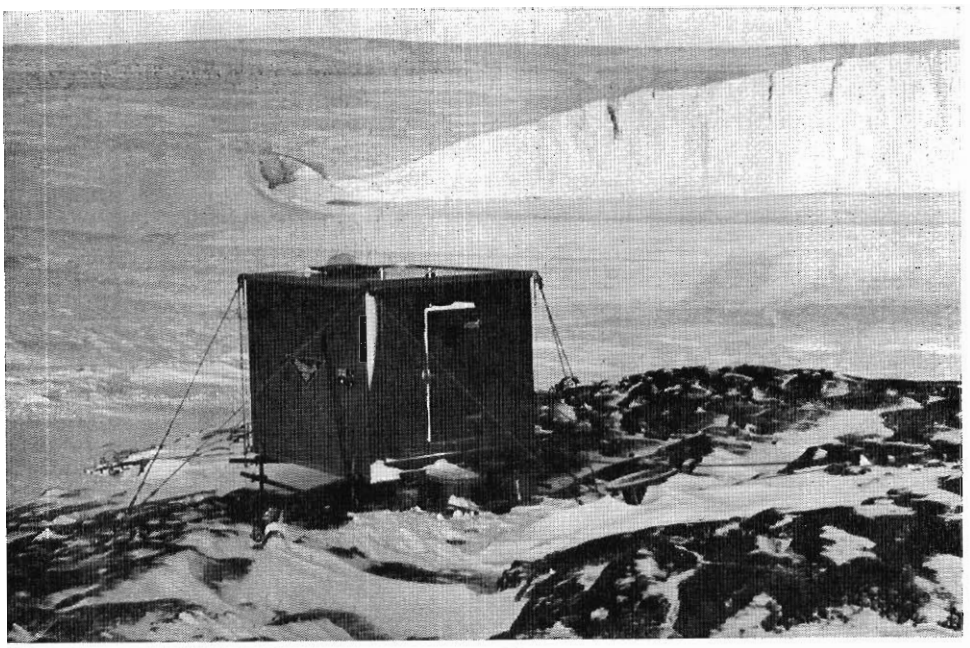

FIG. 3.1. Instrument caravan on West Arm, Mawson harbour.

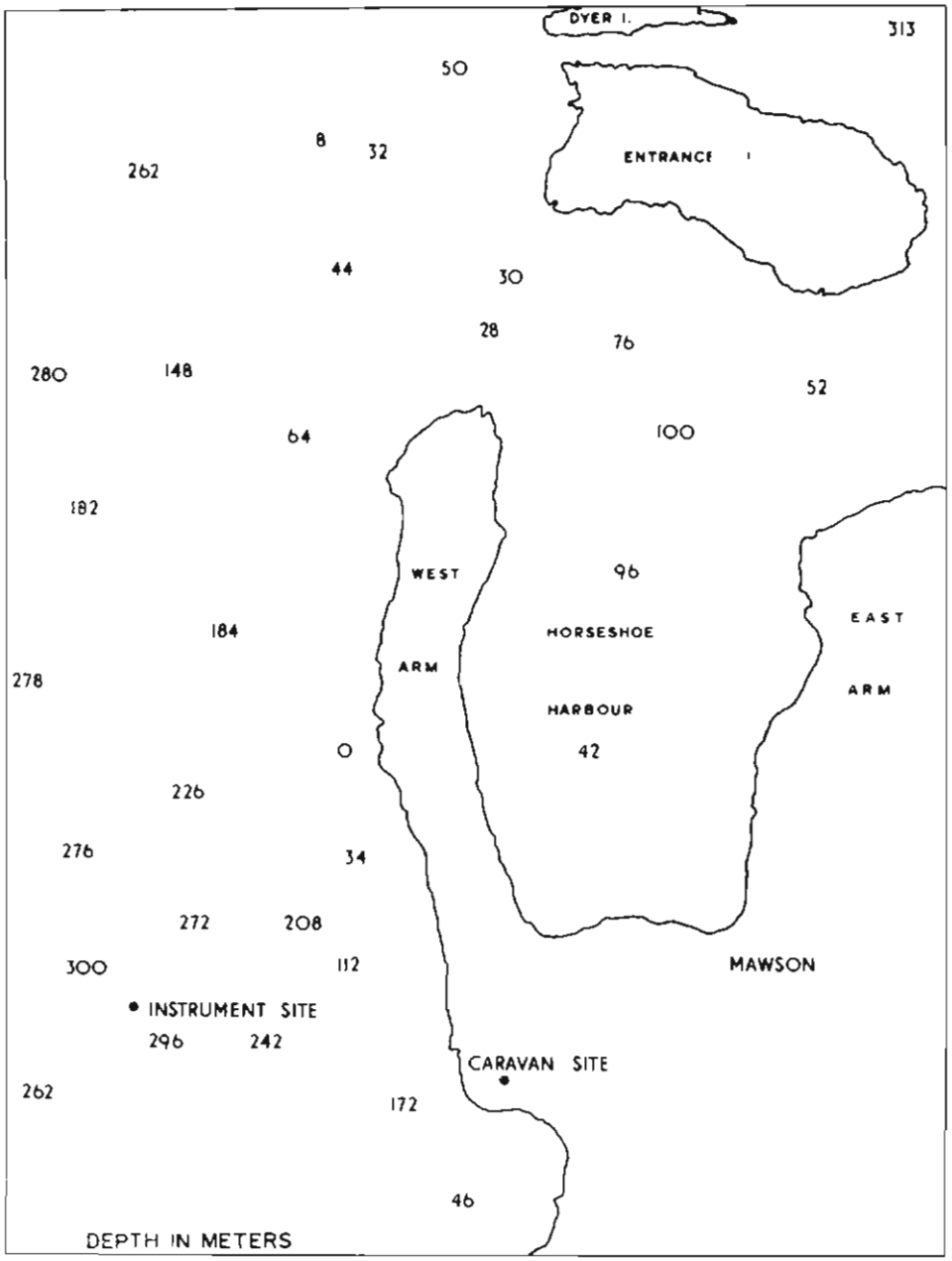

FIG. 3.2. Instrument and caravan sites in West Bay.

The radiation instruments at the instrument site are shown in Fig. 3.3: Two Kipp solarimeters facing upwards and downwards respectively, to measure the shortwave radiation fluxes in both directions, and a CSIRO net radiometer to measure the flux of longwave and shortwave radiation. The instrument mast is shown in Fig. 3.4 and was located 20 metres from the radiation instruments. It could be adjusted for height and had radiation-shielded thermocouples at 0·5, 1, 2 and 4 metres height on crossbars and anemometers (Beckmann and Whitley) at 1, 2 and 4 metres height. A central post halfway between the mast and radiation scaffold held a terminal box for instrument connections. Subsurface instruments included a thermocouple probe with radiation-shielded thermocouples in a closed polyethylene tube at 0, 15, 30, 45, 60, 80, 100, 200 and 400 cm depth. Heat flux plates were installed at 30 and 60 cm depth and a net radiometer was installed at 150 cm depth, just below the sea ice cover. An automatic sea-ice thickness measuring device, which will be described below, was situated some distance off. For size comparison the black dot on the ice slope in the left half of Figures 3.3 and 3.4 is a Volkswagen car.

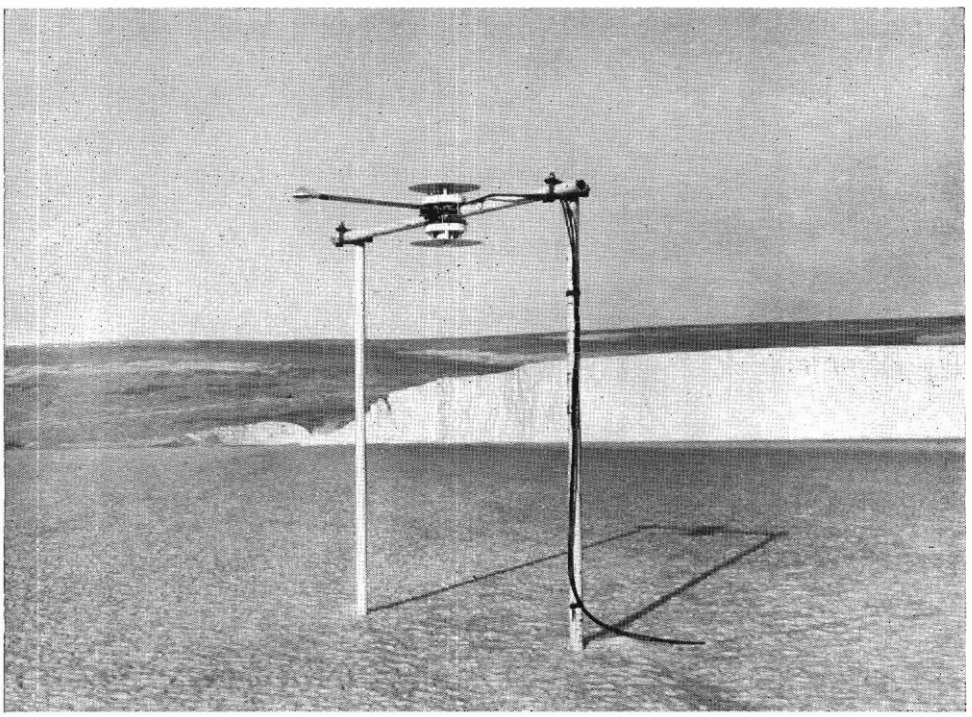

FIG. 3.3. Radiation instruments on the sea ice.

Recording equipment inside the caravan included a Siemens Kompensograph 3-range, 12-channel potentiometric recorder. All temperature, heat flux and radiation data were recorded on this potentiometer, a relay switching the sea-ice thermocuples into the recorder for one cycle every half hour. Specially designed

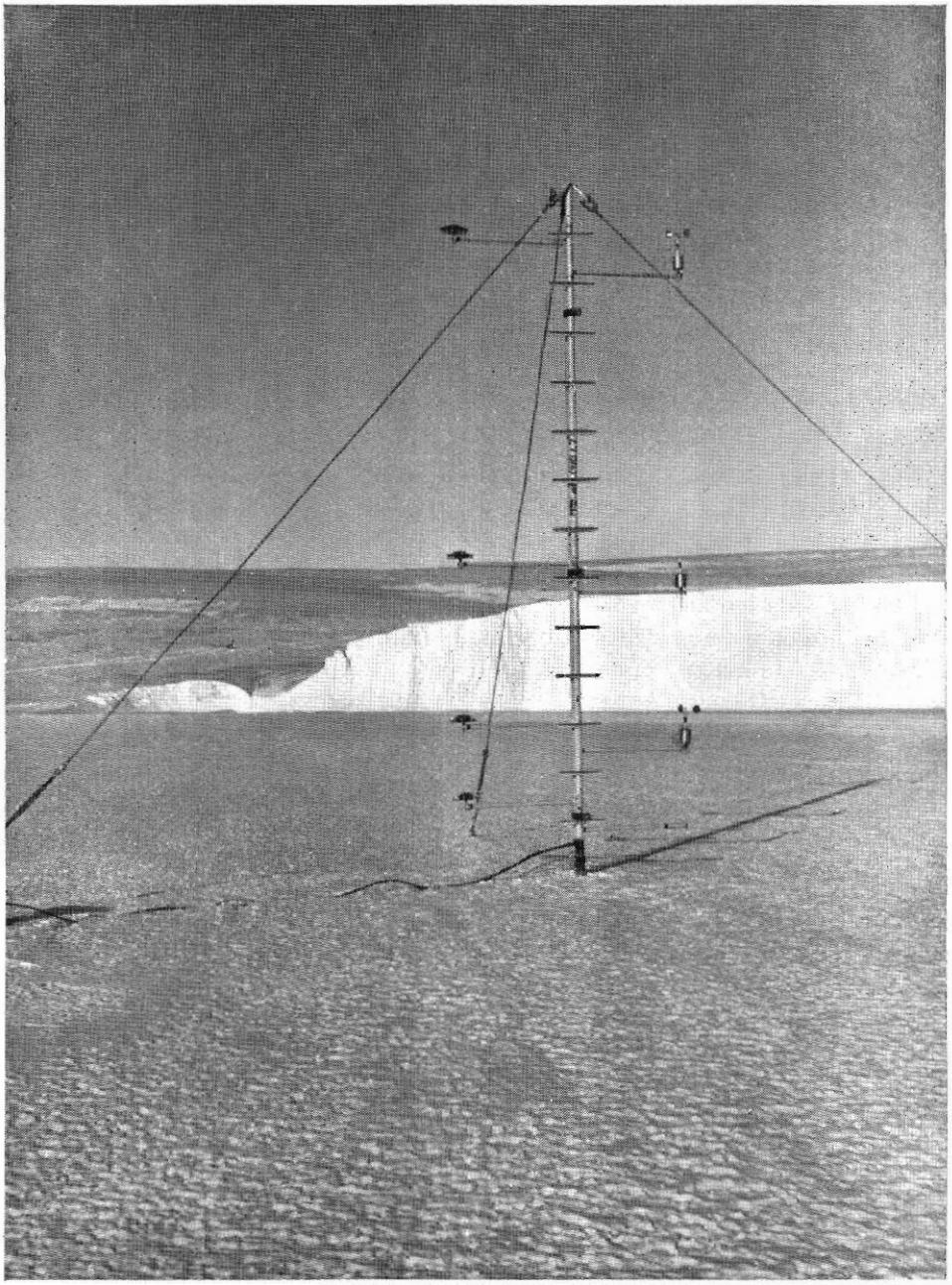

FIG. 3.4. Instrument mast on the sea ice.

amplifier-binary divider circuits for the Beckmann and Whitley anemometers fed one single pulse for every four revolutions of the anemometer rotors into two 2-channel Sodeco digital counters. A synchronous motor/relay device actuated the printing mechanism of these counters every 30 minutes, printing the integrated wind run at the three anemometer levels, as well as the date and time. The reference junction for the temperature thermocouples was immersed in an ice-water bath in a carefully insulated vacuum flask. Temperature drift of the reference bath occurred only rarely and could be detected immediately by observing the apparent simultaneous drift of the sea-water temperature. The programmer of the automatic sea-ice thickness measuring device was also housed in the caravan. Heating of the caravan was by a thermostatically controlled electric fan-heater. A more detailed description of the equipment is given in Appendix I.

3.3. ICE THICKNESS MEASUREMENTS

Sea-ice thickness measurements were carried out automatically every six hours throughout the winter. The machine which enabled this is shown in Fig. 3.5 and was designed by Dr. P. Schwerdtfeger. Its operation was as follows: through a programmer (a synchronous motor, driving cams which operated microswitches) all operations were initiated and terminated. The first operation closed a circuit including a wire loop through the sea ice (Fig. 3.6). Current passed through the loop and heated the wire and the degree of heating could be controlled by a Variac transformer. The motor inside the spherical housing was switched on next, then a solenoid clutch engaged the wire drum driven via rough plastic friction drive faces, and the weight at the lowest part of the wire loop was wound against the

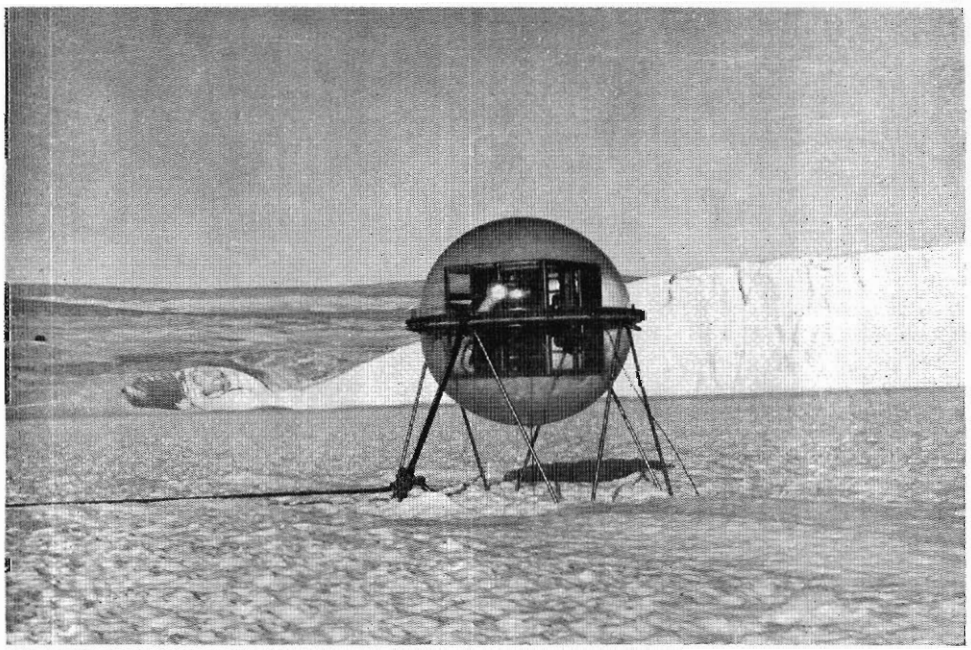

FIG. 3.5. Automatic sea-ice thickness measuring device.

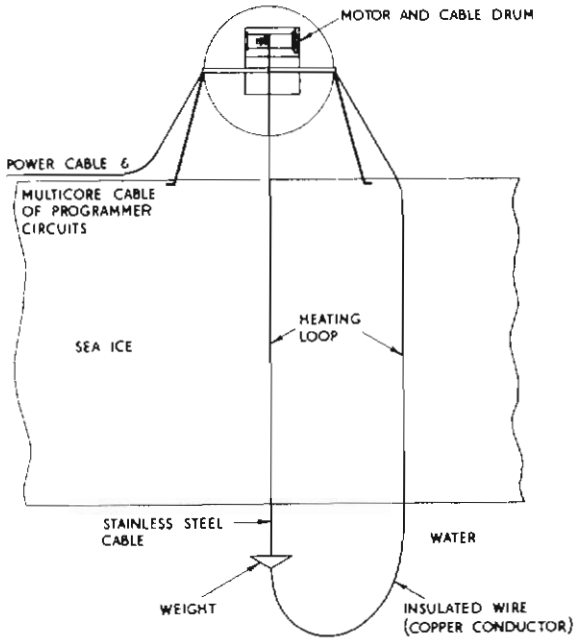

FIG. 3.6. Schematic representation of the automatic sea-ice thickness measuring device.

underside of the ice. A star-wheel cam on the wire drum actuated another micro-switch which closed the counting circuits of a Sodeco digital counter which then counted the number of fractions of wire drum revolutions. Two printing operations followed, then all operations were switched off and the weight sank down again. The counting registers were automatically cleared.

Thickness could be measured to 0 5 cm accuracy. The machine performed free of troubles throughout: occasional manual checks were perfomed by drilling through the ice and measuring the thickness, with a metre stick, with a collapsible crossbar pulled up against the underside of the ice. A 60-watt light globe kept the 60 cm diameter bubble warm and the motor operating.

Results of measurements are shown in Fig. 3.7. Intial freeze rates were as high as 5 cm per day. The machine was dismantled before the breakout on 10 May and re-installed after freezing began again. At no stage was bottom-melting observed until the end of October. The machine was dismantled in November; measurements after this period were made manually.

3.4. RADIATION MEASUREMENTS

Kipp solarimeters measured the downward-directed and surface-reflected fluxes of shortwave radiation. A CSIRO net radiometer measured the net flux of shortwave and longwave radiation. Calibration of all these three instruments was carried out in the standard fashion by shading and unshading the element and comparing the difference in these readings with the output of a Linke-Feussner actinometer pointed at the sun.

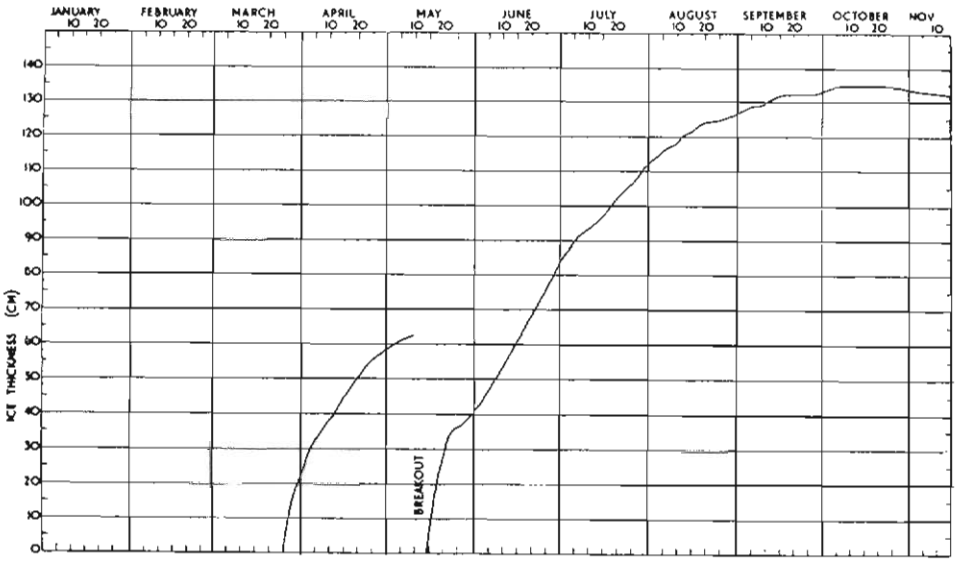

FIG. 3.7. Sea-ice thickness in West Bay.

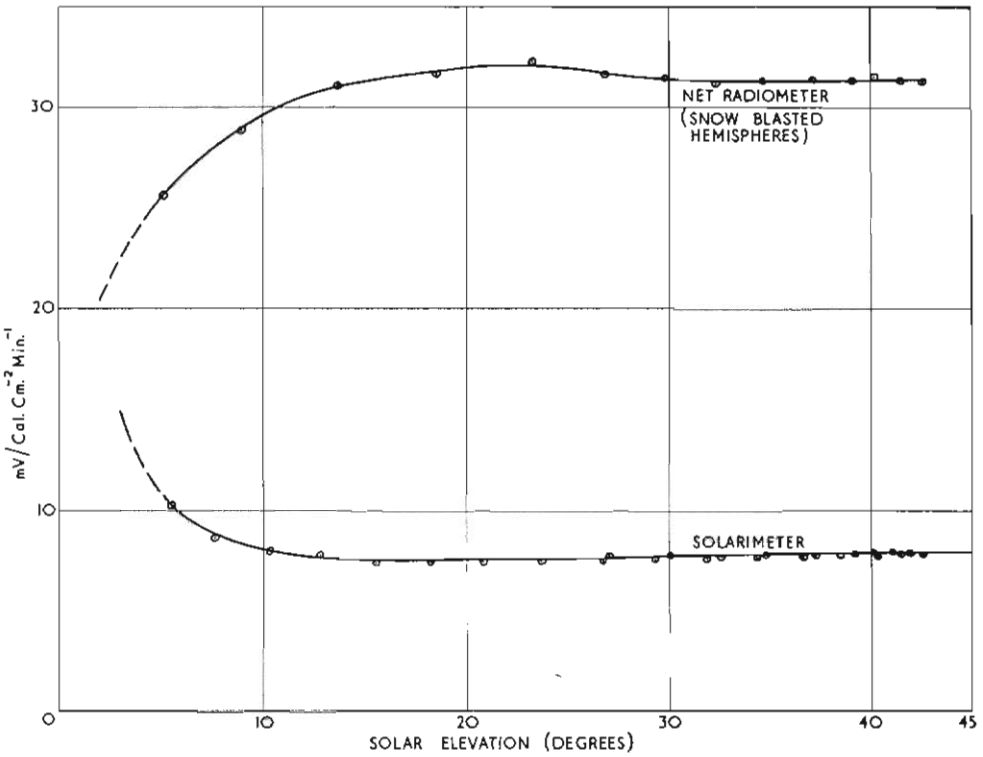

FIG. 3.8. Calibration factors of the Kipp solarimeter and the CSIRO net radiometer (referred to 20°C).

The results of the shortwave calibrations (Table II)* are given in Fig. 3.8 the factors being constant at solar elevation angles larger than 15°. The factors responsible for the non-linear behaviour at lower angles have been adequately described elsewhere, e.g., Weller (1964). Since the polyethylene hemispheres of the net radiometer were constantly bombarded by drift-snow particles, which resulted in the upwind portion of the hemispheres becoming quite translucent, the instrument was calibrated with these hemispheres, and all calibration factors apply for snow-damaged hemispheres only.

The effect of change of solar azimuth on the calibration factors of the Kipp solarimeter was not considered; also, the calibration factor of the net radiometer for longwave radiation was used as stated on the CSIRO calibration certificate (Table I).

For the reduction of the data, calibration factors corresponding to the noon solar elevation were used throughout the day, and temperature coefficients of sensitivity of $-0{\cdot}2\%\,°C^{-1}$ and $+0{\cdot}1\%\,°C^{-1}$ were taken together with the monthly mean temperature for the solarimeters and radiometer respectively.

Adding the daily radiation fluxes of Tables 3, 4 and 6, now, the following mean monthly values are obtained (Table 3.1).

TABLE 3.1

MEAN MONTHLY VALUES OF RADIATION FLUXES AND ALBEDO
(cal $cm^{-2}day^{-1}$)

	Net radiation (all-wave)	Global radiation	Albedo %
June (16-30)	+126	0	90
July	+104	−5	90
August	+75	−39	75
September	+67	−169	70
October	−43	−394	56
November (1-15)	−118	−545	52

(+ve value = outgoing radiation; −ve value = incoming radiation)

The net radiation loss during June/July is approximately 20% higher than at the surface of a semi-infinite freshwater ice plateau 2 kilometres away (Section 4). Correspondingly, by November, the net radiation gain of the sea ice has increased to be 25% higher than the plateau ice surface. The first effect is due to longwave radiation and will be discussed in detail later; the second is due to a considerably higher net shortwave flux compared with the plateau ice, as the albedo of the sea ice decreases.

Daily noon values of the albedo are given in Fig. 3.9, together with the thickness of the snow cover on the sea iee. June and July values were not calculated, since the errors involved in the ealibration factors at low solar elevation are too high. It is, however, a well-known fact that the albedo of snow and ice surfaces increases with decreasing solar elevation (e.g., Liljequist 1956). During calibration of the solarimeters, when the exact calibration factors were known, the albedo was

* Note: data tables with Roman numerals contain basic calibration data and can be found in Appendix I.

also calculated. The results of one of these tests are shown in Fig. 3.10 for a partly snow-covered surface and it can be seen that at solar elevations less than 10° there is a sharp increase of the albedo as expected. Use of these figures was made to extrapolate a mean value of the albedo for June and July, taking the albedo to change in a similar fashion. Values of 90% for June and July were adopted.

Fig. 3.9 shows then that, while there is a snow cover exceeding 2 cm in thick-

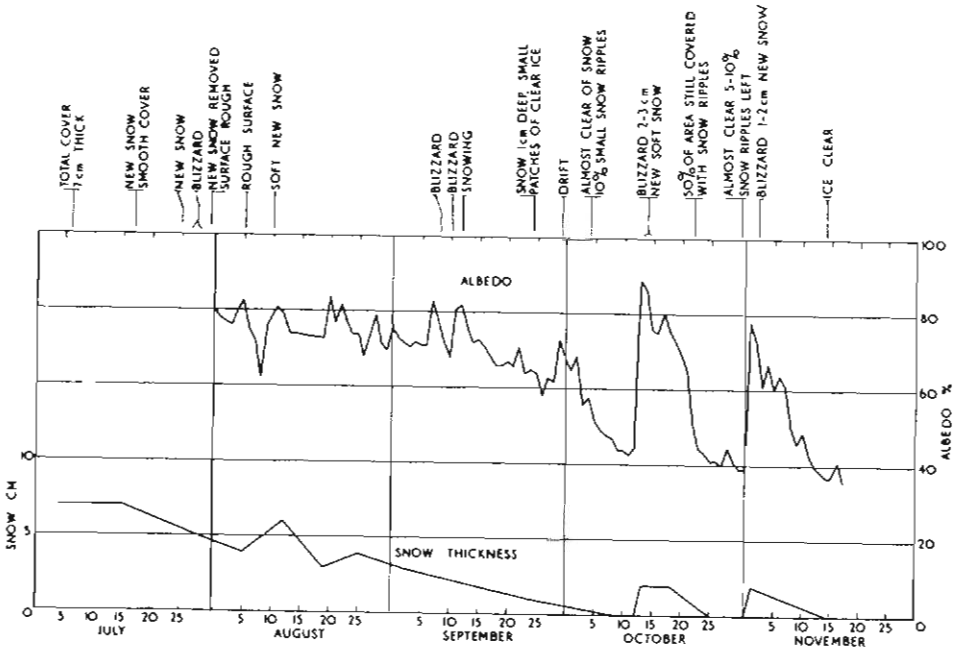

FIG. 3.9. Snow cover and noon albedo of the sea-ice surface.

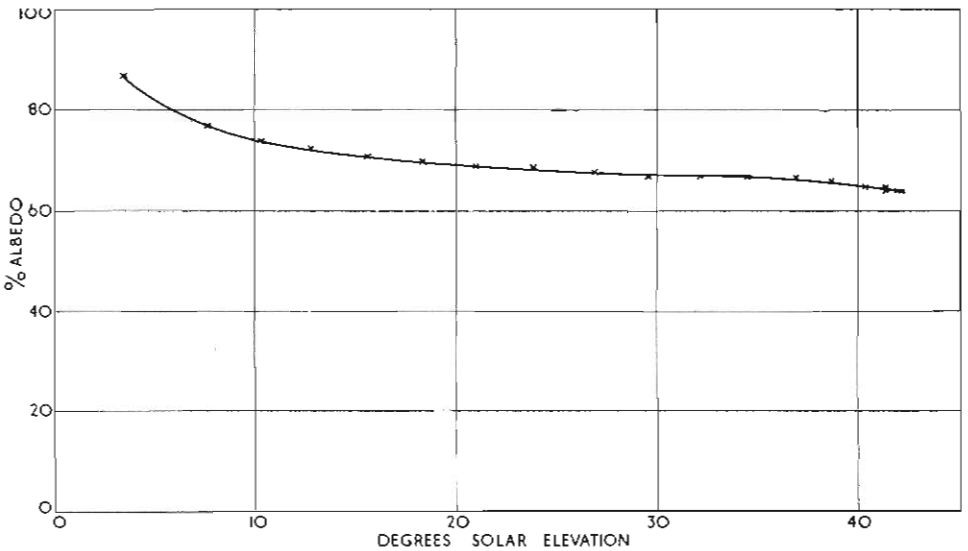

FIG. 3.10. The change of the albedo of an ice surface with change in solar elevation.

ness, the albedo is approximately constant at solar elevations larger than 10° and has a value of 75%. This applies for August and for brief periods in October and November when blizzards deposited new snow on the sea ice. When the snow is completely removed, the albedo of the ice surface sinks to 37%. This more than doubles the possible amount of radiation that can be transmitted downwards through the transparent ice. The day to day fluctuation of the albedo is not only due to small changes in the surface structure, but a systematic investigation showed that the albedo with an overcast sky is 11% higher than with a clear sky. Cloud conditions are thus important as is well known (e.g., Hanson 1960).

3.5. RADIATION TRANSMISSION THROUGH THE SNOW-COVER AND SEA ICE

Both the sea ice and the snow covering it are partially transparent to shortwave radiation. It is essential to compute the amount of radiation absorbed by the ice, as this leads to a modification of the temperature profile and subsequent change of the heat flux to the surface.

Results of extinction measurements of shortwave radiation in the sea ice and snow at Mawson gave extinction coefficients (Section 1) for sea ice and snow of 0·011 cm^{-1} and 0·043 cm^{-1} respectively. The amounts of radiation energy absorbed by a composite snow and sea ice body will now be evaluated, using these extinction coefficients. The physical data are set out in Table 3.2.

TABLE 3.2

RADIATION FLUXES AND PHYSICAL DIMENSIONS OF THE SNOW/SEA ICE BODY

	Global radiation cal $cm^{-2}day^{-1}$	Albedo %	Snow thickness cm	Sea ice thickness cm
June (15-30)	0	90	7	72
July	−5	90	6	98
August	−39	75	4	120
September	−169	70	2	130
October	−394	56	1	134
Nov. (1-15)	−545	52	1	132

In Table 3.3 the mean values of the monthly net fluxes of shortwave radiation (N_S) at the three interfaces are shown, and the amount of radiation abosorbed A (as a percentage of the net shortwave flux and in cal $cm^{-2}day^{-1}$) is given.

TABLE 3.3

SHORTWAVE RADIATION ABSORBED IN SNOW AND SEA ICE

	Net flux at air—snow interface N_s cal/ cm^2/day	Radiation absorbed by snow A %	Radiation absorbed by snow A cal/ cm^2/day	Net flux at snow—ice interface N_s cal/ cm^2/day	Radiation absorbed by sea ice A %	Radiation absorbed by sea ice A cal/ cm^2/day	Net flux at ice—water interface N_s cal/ cm^2/day
June (16-30)	0	26	0	0	55	0	0
July	0·5	23	0·1	0·4	63	0·3	0·1
August	9·7	16	1·6	8·1	74	6·0	2·1
September	50·8	8	4·1	46·7	76	35·5	11·2
October	173·2	4	6·9	106·3	78	83·0	23·3
Nov. (1-15)	261·5	4	10·5	251·0	77	193·0	58·0

The snow—sea ice body can be seen to be quite transparent; 22% of the net shortwave flux at the air—snow interface passes through the ice into the sea water, and 78% of the shortwave radiation is absorbed. The amount of radiation absorbed is high and exceeds 200 cal $cm^{-2}day^{-1}$ in the first half of November. This absorbed heat energy increases the net stored heat in the ice and modifies the magnitude of the heat flux considerably. Both these processes will be considered in greater detail later.

3.6. HEAT CONDUCTION IN THE SEA ICE

The conduction of heat in the sea ice was determined from measurements of the temperature gradients in the ice, and calculations of the thermal conductivity based on measurements of the physical characteristics of the ice. The thermal conductivity of sea ice depends on temperature, salinity and density in a manner which is described by Schwerdtfeger (1963).

Fig. 3.11 shows curves of the sea ice temperatures for half-monthly means computed from Tables 32-34. The tangents to the curves at the upper and lower boundaries of the ice were used to determine the temperature gradients at the two

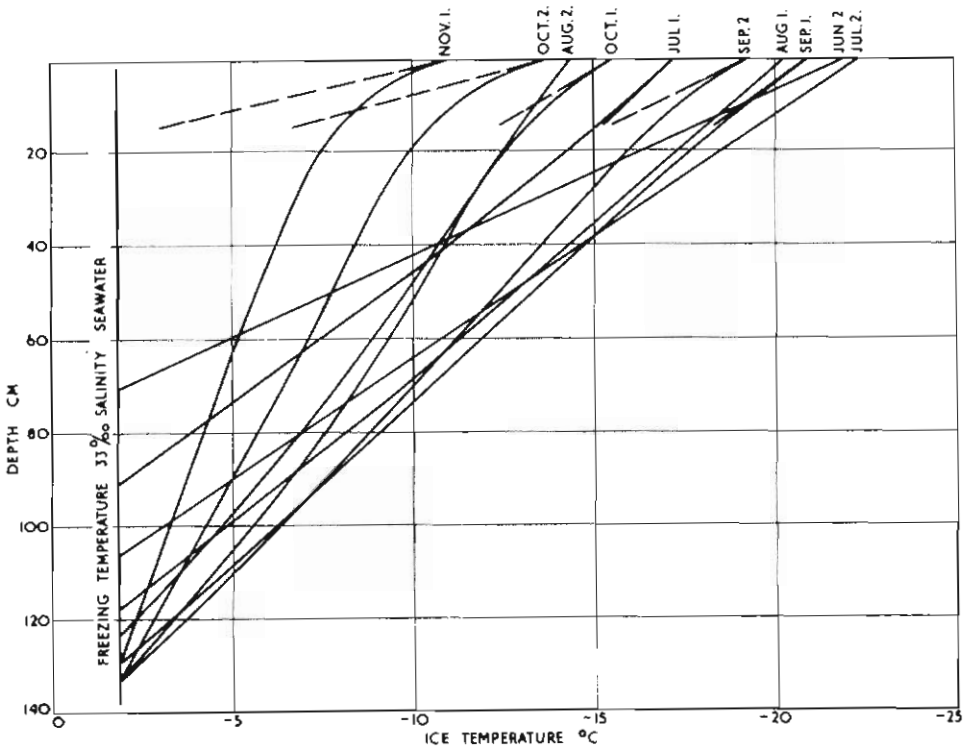

FIG. 3.11. Sea-ice temperatures and surface temperature gradients (dashed lines). Means of daily midnight values for the first and second half of eaeh month.

boundaries. Salinity data were obtained from hydrometer measurements (Table 49) which enabled a mean salinity chart to be drawn up (Fig. 3.12). Values derived for the thermal conductivities of the sea ice at the upper and lower boundaries were $4{\cdot}70 \times 10^{-3}$ and $4{\cdot}42 \times 10^{-3}$ cal $cm^{-1}deg^{-1}sec^{-1}$ respectively. Variations of these values for the individual half-monthly periods considered were less than 2%. The values of the temperature gradients and conducted heat fluxes are summarized in Tables 3·4 and 3·5.

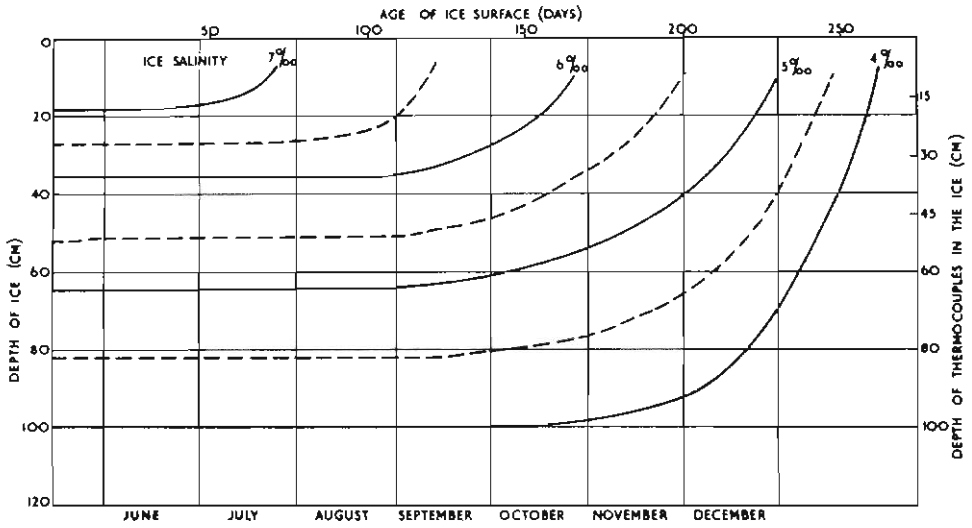

FIG. 3.12. Salinity of the sea ice as a function of ice depth and age.

TABLE 3.4

TEMPERATURE GRADIENTS AND CONDUCTED HEAT FLUXES AT THE UPPER AND LOWER BOUNDARIES OF THE SEA ICE COVER

	Upper Boundary		Lower Boundary	
	Temp. grad. (°C/cm)	Heat flux (cal $cm^{-2}day^{-1}$)	Temp. grad. (°C/cm)	Heat flux (cal $cm^{-2}day^{-1}$)
Jun. 2	0·267	−108	0·283	108
Jul. 1	0·133	−54	0·183	70
Jul. 2	0·192	−78	0·183	70
Aug. 1	0·142	−58	0·158	60
Aug. 2	0·100	−41	0·117	45
Sep. 1	0·167	−68	0·150	57
Sep. 2	0·250	−102	0·133	51
Oct. 1	0·208	−85	0·108	41
Oct. 2	0·466	−189	0·067	25
Nov. 1	0·525	−212	0·058	22

The sign convention used is again that of positive value: heat flux away from boundary; negative value: heat flux towards the boundary.

TABLE 3.5

MONTHLY MEANS OF DAILY CONDUCTED HEAT FLUXES AT THE UPPER AND LOWER BOUNDARIES OF SEA ICE

	Upper boundary	Lower boundary	Heat loss (−) or gain (+) of sea ice by conduction only
June (2nd half)	−108	+108	0
July	−66	+70	+4
Aug.	−50	+52	+2
Sept.	−85	+54	−31
Oct.	−137	+33	−104
Nov. (1st half)	−212	+22	−190

The conducted heat flux towards the upper surface increases markedly in the summer months, despite the fact that heat fluxes of small magnitude only are conducted upwards from the lower surface. This implies large heat losses of the ice as shown numerically in the last column of Table 3.5. Examining the slopes of the temperature curves of Fig. 3.11, it is apparent that most of the heat loss occurs in the top 30 cm of the sea ice. But this is obviously the layer in which a large proportion of the radiation which penetrates the surface is absorbed, since the usual exponential extinction law applies.

It now remains to compute the difference between the net heat loss to the surface by conduction and the heat gain of the ice by absorbed radiation. The difference between these two terms should give the net heat gain or loss of the ice. This term can also be derived independently from the temperature curves of Fig. 3.11 and salinity data, and thus provides an error check.

3.7. HEAT STORAGE IN THE SEA ICE

Untersteiner (1964) gives a nomograph for determining the change in heat storage in sea ice. It is based on the approximate expression:

$$Q = 0{\cdot}9(T_2 - T_1)\ (0{\cdot}5 + \frac{4{\cdot}1S}{T_1 T_2}) \tag{3.5}$$

where Q denotes the amount of heat in cal cm^{-3}, T_1 and T_2 are the initial and final temperatures in °C, and S is the salinity of ice in parts per thousand. Because of its simplicity of application, this equation was used and was found to be quite accurate for the temperature and salinity regime considered here. The initial and final mean temperature and the mean salinity were considered for 15 cm-thick slabs for the whole cover, and the change in heat content calculated for half-monthly intervals. For the considerations used here, monthly changes of heat content of sea ice are required.

Fig. 3.13 shows the change in heat storage per day, as a function of depth and time. The monthly mean values computed for the layers 0—60 cm and 60 cm to lower boundary, and for the whole sea ice cover, are given in Table 3.6.

TABLE 3.6

MONTHLY MEANS OF DAILY HEAT STORAGE CHANGES IN SEA ICE FOR 0-60 CM AND 60 CM TO LOWER BOUNDARY

(cal $cm^{-2}day^{-1}$)

	0-60 cm	60 cm to lower boundary	Total ice cover
June (2nd half)	+2·1	−3·8	−1·7
July	−7·2	−9·8	−17·0
Aug.	+5·2	−2·2	+3·0
Sept.	+1·1	−2·1	−1·0
Oct.	+13·2	+12·4	+25·6
Nov. (1st half)	+6·9	+7·9	+14·8

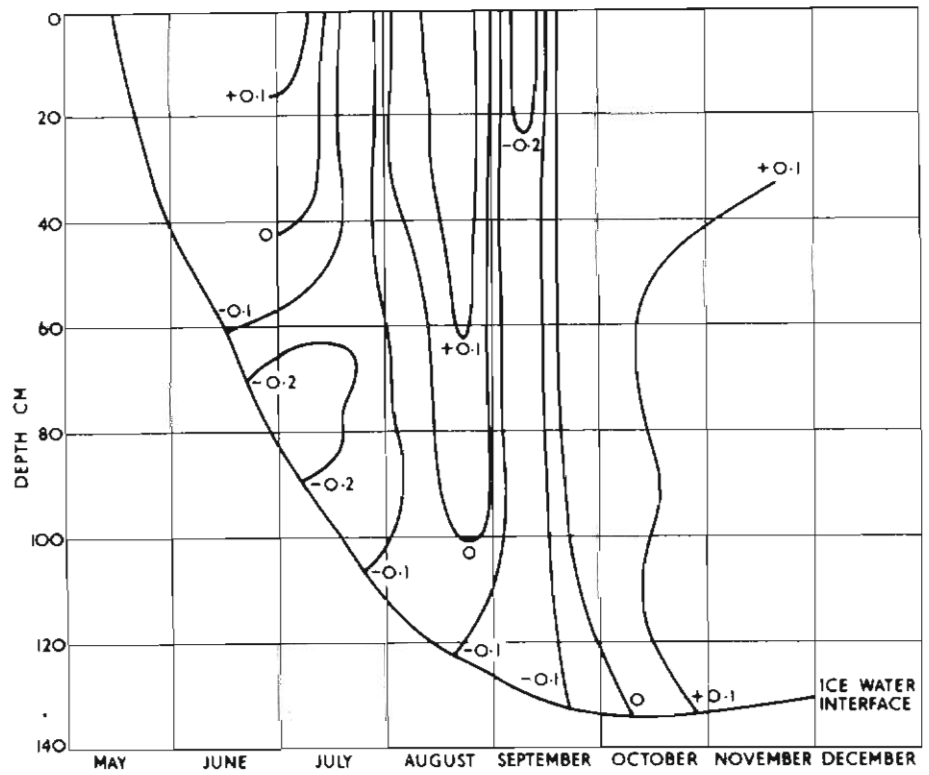

FIG. 3.13. Rate of change of heat storage in the sea ice, cal $cm^{-3}day^{-1}$.

The energy budget of the ice can now be written in another form:

$$R_A + S_N = H \tag{3.6}$$

where R_A = radiation energy absorbed by the ice
S_N = net heat loss or gain of the sea ice by conduction
H = net change in heat storage of the ice.

Positive values indicate heat gain, negative values heat loss by the ice. Table 3.7

gives the values of all three terms (R_A from Table 3.3, S_N from Table 3.5, H from Table 3.6).

TABLE 3.7

HEAT BUDGET OF THE SEA ICE
(cal cm^{-2}day^{-1})

	R_A	S_N	$R_A + S_N$	H	Δ
June (2nd half)	0	0	0	−2	2
July	0	+4	+4	+17	−13
Aug.	+8	+2	+10	+3	7
Sept.	+40	−31	+9	−1	10
Oct.	+150	−104	+46	+26	20
Nov. (1st half)	+203	−190	+13	+15	−2

The last column in Table 3.7 indicates the magnitude of errors involved in the computations. Since both R_A and H can be determined quite accurately, the error lies mainly in the determination of S_N, where errors are introduced in obtaining the temperature gradients at the two surfaces.

Considering the magnitude of the terms, there is quite good agreement and the above considerations are substantiated. Considerable errors are therefore introduced into energy budget studies carried out for sea ice unless the effect of absorbed radiation is considered. A simple example will demonstrate this by considering two possible approaches:

1. The absorbed radiation is ignored and the heat flux is computed from the mean temperature gradient at some depth in the ice;

then $R + S + Q + E = 0$.

For October: $R = -43$ cal cm^{-2}day^{-1} (Table 3.1)

$S = -29$ cal cm^{-2}day^{-1} (from Fig. 3.11 at 60 cm depth)

$\therefore \quad Q + E = +72$ cal cm^{-2}day^{-1} (remainder).

2. Both absorbed radiation and the temperature gradient at the surface are considered (correct method);

then $N_L + S + Q + E = 0$.

For October: $N_L = +130$ cal cm^{-2}day^{-1} (Table 3.10)

$S = -137$ cal cm^{-2}day^{-1} (Table 3.5)

$\therefore \quad Q + E = \quad +7$ cal cm^{-2}day^{-1} (remainder).

The errors introduced into the remainder term are thus large, and a completely false value of the conducted heat flux at the surface is obtained by ignoring the absorbed radiation effects.

3.8. TEMPERATURE AND WIND SPEED PROFILES

Temperatures and wind speeds were recorded continuously. The copper-constantan thermocouples measuring the air temperatures at 4, 2, 1 and 0·5 metres were protected with chromium-plated radiation shields. However, these devices were not totally suecessful in reducing radiation errors, which depend on the incident radiation (both from above and below) and the wind speed. With profile measurements, the errors in the temperature gradient at 2 metres height due to

radiation were $0{\cdot}01°m^{-1}$ at wind speeds greater than 2 m sec^{-1} for the period considered (Table III). At wind speeds less than 2 m sec^{-1} the radiation error increased rapidly; no daily mean wind speeds less than 2 m sec^{-1} were, however, measured.

For eddy heat flux computations, the gradients of potential temperature are required and the difference in potential temperature between the upper and lower thermocouples was approximately $0{\cdot}01°m^{-1}$. Since corrections on the temperature profile, due to radiation errors, and potential temperature conversion are of opposite sign and equal magnitude, both corrections were disregarded.

Wind speeds were recorded at the 1-, 2- and 4-metre level as integrated wind runs for half-hourly periods. Due to instrumental difficulties, the 2-metre level anemometer was unusable for long periods of time, and extrapolation was necessary. Mast heights were adjusted frequently to correct for the small changes at the surface due to snow accumulation or ablation. As has been seen above, the maximum thickness of snow was however only 7 cm.

The shape of the wind profile in the air layer close to the ground depends on the stability of the air layer which can be expressed in terms of the Richardson number. For neutral stability (Richardson number zero) the wind profile has been found to follow a logarithmic law, but with increasing or decreasing Richardson numbers the deviation from the logarithmic law increases. The Richardson number is given by:

$$R_i = \frac{g\Delta z\Delta\theta}{T_m(\Delta V)^2} \tag{3.7}$$

where g = acceleration of gravity, Δz = height difference, $\Delta\theta$ = potential temperature difference, T_m = layer mean temperature and ΔV = wind speed difference.

The Richardson number is referred to the geometric mean height of two levels.

Since, for most of the period of observation, only small diurnal patterns in the wind and temperature gradients were present (these only become significant in the late summer months), mean daily values of temperature and wind speed difference were used and corresponding R_i-numbers computed (Tables 12-16).

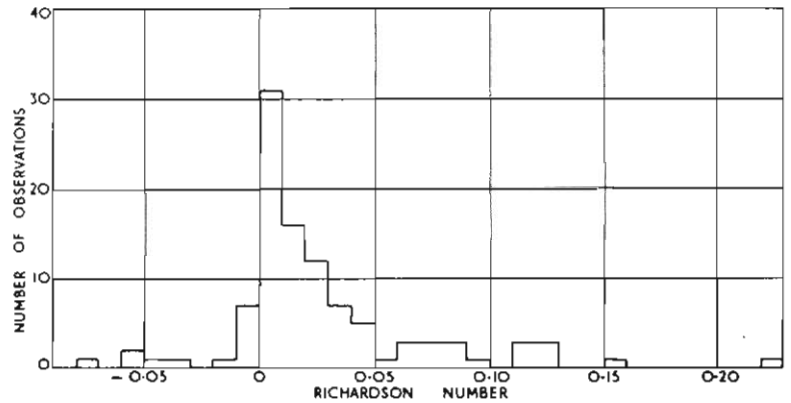

FIG. 3.14. Frequency distribution of the Richardson number daily means at the 2-metre level over the sea ice.

The frequency distribution of Richardson numbers computed for the 2-metre level (Table 17) is shown in Fig. 3.14. The air stratification over the sea ice is mostly neutral and near-neutral, with 80% of observations in the range $-0{\cdot}05 < R_i < 0{\cdot}05$.

From the exhaustive studies by Grainger *and* Lister (1966) of wind structure over cold surfaces, it appears that no wind profile law is applicable at all stabilities. However, for the above stability range the logarithmic law would be most suitable

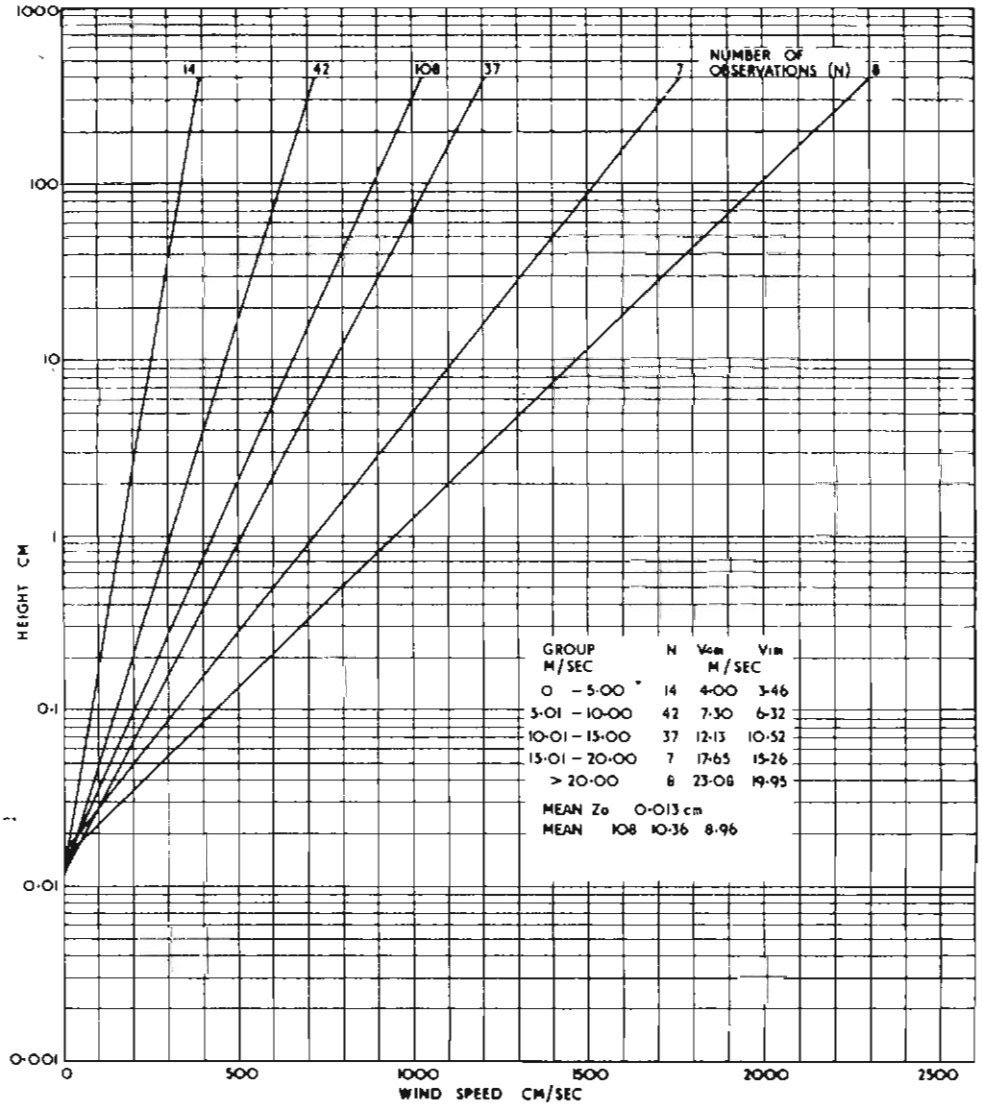

FIG. 3.15. Grouped means of the daily mean wind speed profiles over the sea ice.

and it is hence used for all further data reduction. Taking all wind speed measurements, now, and computing group means for intervals of 5 m sec^{-1}, the logarithmic wind structure can be shown to give roughness parameters for the various profiles which are remarkably constant (Fig. 3.15).

The roughness parameter is a measure of the surface roughness and is the height (z_0) at which the wind speed is zero. From the logarithmic law:

$$u = \frac{u^*}{k} ln \frac{z}{z_0} \tag{3.8}$$

where u = velocity, k = von Karman constant (0·428), z = height, u^* = friction velocity.

Daily mean values of the roughness parameter are shown in Fig. 3.16. These values are considerably smaller than those of an ice surface. It will now be shown whether the day-to-day fluctuations of the roughness parameter in Fig. 3.16 are acceptable.

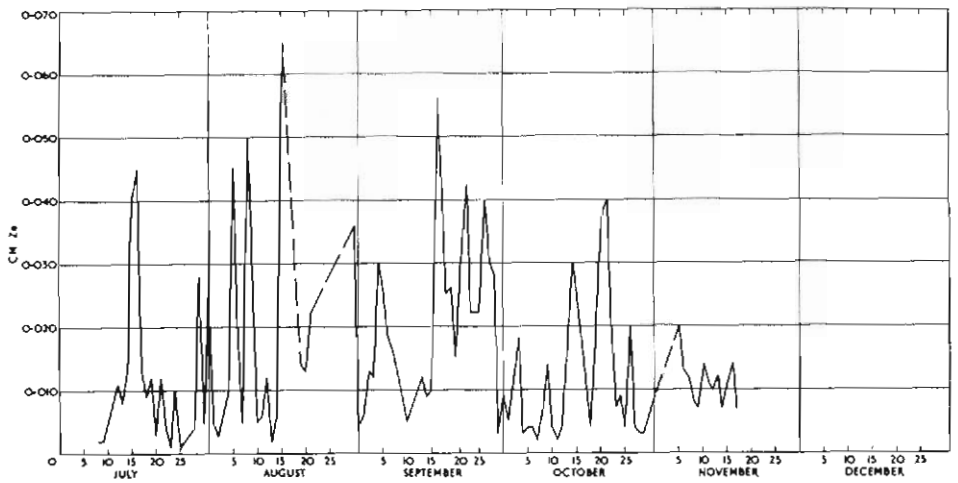

FIG. 3.16. Daily mean roughness parameter, z_0.

From extensive measurements of artificially controlled surface roughness, using bushel baskets on a frozen lake surface, Kutzbach (1961) has derived an empirical expression for the surface roughness z_0 which has been reduced by Lettau (1967) to the form:

$$z_0 = \frac{0{\cdot}5h^*}{A} \tag{3.9}$$

where $A = \frac{\text{specific area}}{\text{lateral silhouette area}}$, and specific area $= \frac{1}{\text{obstacle density}}$, h^* = height of obstacle.

Taking various possible surface crystal arrangements now, the first of which can be represented schematically thus:

1. Height of obstacle: 0·5 mm
   Width of obstacle: 1 mm
   Lateral cross-sectional area: 0·25 mm²
   Obstacle density: 100 per cm².
   Therefore: $z_0 = 0{\cdot}06$ cm.

2. Similarly, a second arrangement:
   Dimensions as for 1:

   Obstacle density: 25 per cm².
   Therefore: $z_0 = 0{\cdot}015$ cm.

This small change in the surface arrangement of the obstacles (crystals) can cause large changes in the roughness parameter. The value for case 2 is close to the mean sea ice value of 0·013 cm. Case 1 gives the upper limit of measured roughness parameters.

3. Consider the typical cusped blue ice surface at the plateau station, now: this surface has the shape shown in Fig. 3.17a:

   Height of obstacle: 2 cm
   Lateral cross-section: 5 cm²
   Obstacle density: 1 per 25 cm².
   Therefore: $z_0 = 0{\cdot}2$ cm.

This latter figure is close to the actually measured value of 0·23 cm for the plateau ice.

Since the actual sea ice surface frequently resembled case 3 in macrostructure, but had a microstructure resembling either case 1 or 2 (see Figs. 3.3-3.5), and since the roughness parameters under these conditions rarely exceeded 0·04 cm, it seems likely that the microstructure of the surface is the dominating factor affecting the roughness parameter.

Thus, for an idealized sastrugi-covered surface of the shape shown in Fig. 3.17b, the roughness parameter should be less than the computed value and quite small compared with the size of the obstacles.

The lateral silhouette area is approximately 700 cm² if the spacing is as shown in Fig. 3.17c.

The obstacle density is 8 for 7·2 m²;
therefore: $z_0 = 1{\cdot}17$ cm.

At Byrd station, the roughness parameter for smooth snow surfaces and sastrugi-covered surfaces is almost the same and does not exceed 0·02 cm (Budd, Dingle and Radok, 1964). The conclusion of the authors that the roughness parameter is controlled by the microstructure of the surface is supported by the above considerations.

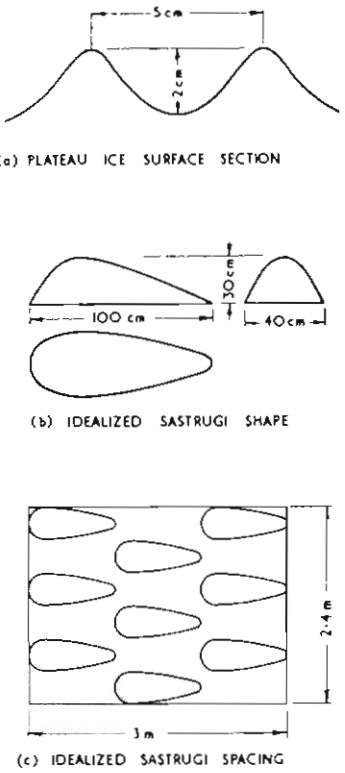

FIG. 3.17. Ice surface and sastrugi forms.

3.9. EDDY HEAT FLUX

The heat exchange coefficient has been computed from a formula given by Lettau (1949):

$$A = \frac{A_a}{(1 + R_i)^2} \text{ g cm}^{-1}\text{sec}^{-1} \tag{3.10}$$

(Strictly, the equation is $A = \frac{A_a}{(1+x)^2}$, where x is similar but not equal to R_i, because the actual wind shear u' enters R_i, but the adiabatic wind shear u'_a enters x, so that $x = \frac{(u')^2}{(u'_a)^2} \cdot R_i$)

R_i is the Richardson number and A_a the exchange coefficient for adiabatic conditions.

$$A_a = k\rho u^* z \tag{3.11}$$

where k = von Karman's constant (0·428), ρ the air density, u^* the friction velocity and z the height above the surface. The exchange coefficient is thus corrected for non-adiabatic conditions and the average correction for all profiles used is 5%. The maximum correction is 33%.

From these data, the flux of sensible heat can now be computed according to the well-known equation:

$$Q = c_p A \frac{d\theta}{dz} t \qquad \text{cal cm}^{-2} \tag{3.12}$$

c_p is the specific heat of air at constant pressure (0·24 cal $g^{-1}deg^{-1}$), A is the exchange coefficient for non-adiabatic conditions (g $cm^{-1}sec^{-1}$), $\frac{d\theta}{dz}$ the gradient of potential temperature and t the time. From daily mean values of A and $\frac{d\theta}{dz}$, the sensible heat can be calculated (Tables 12-16). The use of daily means for the early summer months, when there is a diurnal pattern of the temperature and temperature gradients, is justified by an analysis of the plateau ice data for December (Section 4) which showed that the daily sensible heat flux for six-hourly periods is only 3% different from the daily sensible heat flux calculated from 24-hourly mean values of the parameters involved (Table 30). It is assumed that the exchange coefficients for momentum and heat have equal magnitude, and that the daily mean temperatures follow a logarithmic law. The following monthly means of sensible heat transfer are thus obtained:

TABLE 3.8

MONTHLY MEANS OF SENSIBLE HEAT TRANSFER
(cal $cm^{-2}day^{-1}$)

June (2nd half)	—
July	−9
August	−10
September	−19
October	−27
November (1st half)	+22

(− ve values: heat flux towards the surface)

The sensible heat transfer is fairly constant throughout the winter months and small, due to the relatively small inversions above the sea ice. Proper inversions due to radiational cooling of the surface did not develop, since there was always a constant large heat supply to the surface from the sea water below. The positive value of sensible heat transfer in November is due to the temperature gradient converting from weak inversions to lapse conditions during the day, due to solar heating.

3.10. LATENT HEAT

No direct measurements of the latent heat flux at the upper surface were made, since no suitable instruments were available. Also, ablation measurements were not carried out since, almost constantly, drift snow was blowing over the sea ice, making any mass change readings meaningless for latent heat determinations. On the lower boundary, however, the latent heat of freezing or melting could simply

be determined by observing the advance or decay of the sea-ice cover. The temperature at the lower boundary was constant at $-1{\cdot}8°C$, and latent heat values, based on this and on a constant salinity of 4 parts per thousand of the sea ice at the lower boundary, gave a latent heat of ice formation of $70{\cdot}4$ cal gm^{-1} (Schwerdtfeger 1963). From this, then, the latent heat at the lower boundary was computed for monthly means:

TABLE 3.9

LATENT HEAT FLUX AT LOWER SEA ICE BOUNDARY
(cal $cm^{-2}day^{-1}$)

June (2nd half)	−93
July	−59
August	−29
September	−15
October	−2
November (1st half)	+6

(−ve values = heat release at the boundary)

Only in November did the ice boundary begin to recede, and positive latent heat values resulted.

3.11. HEAT BUDGET

The heat energy budget at the two boundaries of the sea ice will be considered now. At the air—ice and ice—water interfaces the heat budget can be written in the following form again:

$$N_L + S + E + Q = 0,$$

where N_L = the net longwave radiation at the interface
S = the conduction heat flux at the interface
Q = the flux of sensible heat at the interface
E = the latent heat flux at the interface.

The following sign convention will be used as before: −ve values = heat flux towards the surface, i.e., surface acts as heat sink; +ve values = heat flux away from surface; i.e., surface acts as heat source.

TABLE 3.10

HEAT BUDGET AT ICE–AIR INTERFACE
(cal $cm^{-2}day^{-1}$)

	N_L	S	Q	E
June (2nd half)	+126	−108		
July	+105	−66	−9	−30
August	+85	−50	−10	−25
September	+118	−85	−19	−14
October	+130	−137	−27	+34
November (1st half)	+144	−212	+22	+46

E is calculated as a remainder term.

TABLE 3.11

HEAT BUDGET AT ICE–WATER INTERFACE

(cal $cm^{-2}day^{-1}$)

	N_L	S	E	Q
June (2nd half)	0	+108	−93	−15
July	0	+70	−59	−11
August	0	+52	−29	−23
September	0	+54	−15	−39
October	0	+33	−2	−31
November (1st half)	0	+22	+6	−28

Q is calculated as a remainder term.

The magnitudes of the remainder terms require some quantitative investigation. The negative values of latent heat flux in July and August indicate hoar frost deposition on the snow surface. This is the actual condition one should expect at a coastal station; however, the ablation measurements close by at 150 metres altitude on blue ice show that small ablation occurs even in the winter months (Table 47). Thus, in July, 5 mm of ice evaporated giving a latent heat flux of +10 cal $cm^{-2}day^{-1}$ (using the latent heat of sublimation of ice of 677 cal gm^{-1}). Unfortunately, these ablation measurements cannot include hoar frost deposition since hoar frost may be removed as drift particles. Hoar frost deposition was frequently observed on the instruments at the sea-ice installation in July and August and usually exceeded 0·5 mm per day. While direct estimates of the amount deposited are not possible, a deposit of 14 mm per month is required to give the latent heat fluxes for July and August. This seems a possible order of magnitude. The ablation rates on the ice plateau are controlled by entirely different heat energy fluxes.

After September, the latent heat flux at the surface became positive but no melting occurred before the end of November. In October, the latent heat flux at the sea-ice surface can evaporate 1·7 cm of ice. At 150 metres altitude, the actually observed ablation was 2·6 cm of ice. No precise error estimate can be affixed to the latent heat flux values, but the above checks have shown their general validity.

An attempt to determine the accuracy of the remainder term Q for the underside of the ice is more difficult. All monthly mean values are negative and show sensible heat transfer from the water to the ice, the transfer increasing in summer. Both horizontal and vertical temperature gradients are presumably small, and the water flow velocities are probably fairly constant throughout the year. The increase in the transfer of sensible heat must then be due to water warming as summer is approached. Only small warming is necessary to bring about this change, as will be attempted to be shown below. It is interesting to note here that considerable smaller ice growth rates during the winter months are possible in areas between islands, where stronger currents under the sea-ice cover transfer large amounts of heat energy to the sea ice and prevent its rapid growth. Wishart (1964) describes some of these ice thickness measurements at Mawson in 1963.

A waterflow meter did not arrive in time when the expedition sailed, so no

direct flow measurements are available. Mean sea water temperatures were $-1{\cdot}9 \pm 0{\cdot}1$°C for August and September, and $-1{\cdot}8 \pm 0{\cdot}1$°C for October. The freezing temperature for 35 parts per thousand salinity sea water is $-1{\cdot}9$°C, and for 33 parts per thousand, $-1{\cdot}8$°C.

As a rough approximation of the sensible heat transfer, the classical equation of eddy heat transfer, as used for the air eddy heat flux, will be used now. Untersteiner (1965) has determined a roughness parameter of $z_0 = 2$ cm for the underside of large sea-ice floes, and typical water flow velocities of 15 cm sec^{-1} at 4 metre depth below the sea ice. Assuming a logarithmic profile, a friction velocity of 1·2 cm sec^{-1} is obtained. For a turbulent heat transfer of 20 cal cm^{-2}day^{-1} a vertical temperature gradient of 0·03°C/100 metres is then required.

The applicability of this equation is probably dubious; it gives, however, the rough indication that only minute vertical temperature gradient changes are required to alter the heat flux considerably.

Heat energy may also be transported to the underside of the ice by advection, and some estimates are available for the heat transport by sea currents to the underside of floating ice shelves. Thus, Shumskiy and Zotikov (1963) estimate the heat supplied for melting at the lower boundary of the Ross Ice Shelf to be approximately 2·5 cal cm^{-2}day^{-1} at between 100 and 200 kilometres inwards from the shelf edge, and approximately 5 cal cm^{-2}day^{-1} near the edge. These values were computed from an empirical equation for turbulent flow of liquids along flat plates, using flow velocities of 15 to 20 cm sec^{-1}.

Sverdrup (1953) estimates a heat supply to the Maudheim Ice Shelf of 70 cal cm^{-2}day^{-1} due to the existing shallow surface currents of 20 cm sec^{-1} velocity, assuming a sea water temperature 0·3°C higher in the annual mean than the ice melting temperature. (In summer, the water temperature is 0·8° above the freezing point near the Maudheim shelf.) For the Maudheim Ice Shelf to remain in mass equilibrium, about 12 per cent of the heat supply of the surface current, i.e., 8·5 cal cm^{-2}day^{-1}, must reach the underside of the ice shelf to compensate for accumulation gains at the surface. This is not greatly different from the value of 5 cal cm^{-2}day^{-1} given by Shumskiy for the Ross Ice Shelf.

Assuming that the surface currents at Mawson are similar to those at the Maudheim Ice Shelf, and using the Sverdrup values of the heat supplied by these currents, namely 2450 cal sec^{-1} per centimetre width of ice shelf, it can be computed that, for a temperature difference of 0·1°C between the ice melting point and the water temperature, and an average sea-ice cover extending 100 km offshore, an average of 7 cal cm^{-2}day^{-1} is supplied to the underside of the ice. The temperature difference is taken from the water temperature measurements at Mawson quoted above. Mellor (1960) states that there is usually open water 100 km east of Mawson (the direction of coastal currents are easterlies), even in winter.

The amount of radiation absorbed by the sea water from June to November is 2·0 k cal cm^{-2}. This energy can increase the temperature of a column of water 100 metres deep by approximately 0·2°C. Increasing the temperature difference, then, to 0·2°C and decreasing the extent of the sea ice cover to 50 km gives a heat supply to the underside of the iee of 28 cal cm^{-2}day^{-1}. The computed values

agree well with the winter and spring data obtained for Mawson from heat budget considerations.

The final heat budget components are presented graphically in Fig. 3.18. The individual components represent the total heat energy transfer of that component for the period 1 July to 15 November in k cal cm^{-2}. The longwave radiation emitted by the surface was computed from the Stefan-Boltzmann law, taking the mean ice surface temperature for the period considered and the emissivity of ice to be 0·96. Note that the radiation fluxes in the ice are net fluxes.

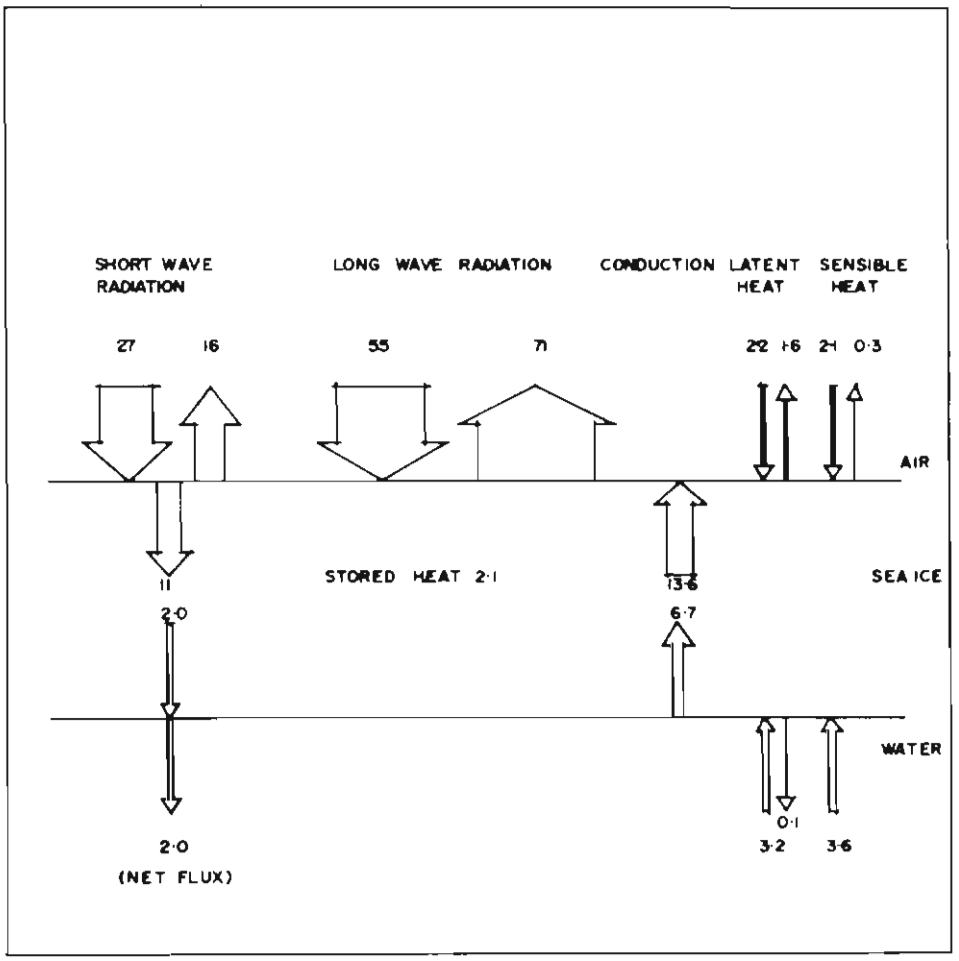

FIG. 3.18. The heat budget components at the boundaries of a floating sea-ice cover for the period 1 July to 15 November, k cal cm^{-2}.

An estimate of how the presence of the sea ice affects the energy exchange between the ocean and the atmosphere can now be attempted. This is shown in Table 3.12, where the heat exchange between the ocean and the atmosphere for

an open water surface, estimated by Kort (1962) for the Mawson sector of the coast, is compared with the above data. The period considered is from June to August.

TABLE 3.12

WINTER HEAT BUDGETS FOR THE OPEN AND ICE-COVERED OCEAN CLOSE TO MAWSON
(cal $cm^{-2}day^{-1}$)

	R	Q	E	Total heat to atmosphere
Open water	84	166	160	410
Ice covered water	100	−10	−30	60

The total amount of heat given by the water to the atmosphere is seven times higher when there is no sea-ice cover. Considering the extent of the ice cover in winter over the Southern Ocean this must have a significant overall effect on the heat input into the atmosphere over the Southern Ocean. These results show the same tendency as experiments by Badgley (1966) on older and thicker sea ice in the Arctic which indicate that the annual heat loss of open water is about two orders of magnitude greater than that of old ice.

3.12. CONCLUSION

For the heat budget of the ice, then, the turbulent heat exehange is of relatively little importance for the upper boundary of the ice. In winter, with large longwave net radiation losses of the surface, most of the radiation energy is supplied by conduction from the water below; also, some latent heat contributes. When summer approaches, the picture changes completely. With the disappearance of the snow-cover, large amounts of absorbed radiation result in large conducted heat fluxes to the surface, while the longwave heat loss changes little. Energy becomes available, then, at the surface to produce evaporation, and some of the conducted heat energy is also lost at the surface through turbulent mixing with the atmosphere. Due to the large reservoir of heat stored in the relatively warm water, the conducted heat flux in winter is very high compared with the plateau ice heat fluxes. The heat available to the air at the surface considerably modifies the temperaure structure over the ice, resulting in only small sensible heat flux gains by the surface.

At the lower boundary, the predominant heat fluxes are conduction losses which in winter are compensated by latent heat fluxes due to ice growth. The reduced ice-growth rates and even ice melting, as summer is approached, involve small positive latent heat fluxes. The conduction losses are balanced by the only other form of heat flux available: this is the transfer of sensible heat which increases considerably for the summer months, and is due to increased advection of heat by water currents.

Finally, the ice cover as a whole acts as an effective insulator in the heat exchange between ocean and atmosphere, reducing the heat supply to the atmosphere by an order of magnitude.

4. THE ANNUAL HEAT ENERGY TRANSFER ABOVE AND INSIDE ANTARCTIC BLUE ICE

4.1. INTRODUCTION

The study of heat budgets for climatological and microclimatological purposes is usually restricted to computing the heat flux components at the surface of a chosen locality. This applies to ice and snow surfaces as well as to the more usually investigated agricultural surfaces. For glaciological purposes, however, the energy exchange at different levels in the ice is of equal importance to that at the surface. The thermal history of snow and ice at any depth is affected by these exchange processes and is of interest in determining mechanical and thermal properties, as well as mass and heat transfer processes.

In this study, before the meteorological surface heat budget is established in the conventional fashion, a separate budget equation for the total ice mass is set up, and the heat fluxes in the ice are considered at various depths. Whereas phase changes of the water substance, convection and radiation contribute to the heat transfer towards and away from the surface in the atmosphere, only radiation and conduction have to be considered in the ice.

The annual heat budgets were determined above and inside blue ice, the surface of which was practically free of snow throughout the year. The location was on an ice plateau, briefly described in Section 1, and 2 km inland from Mawson station at an altitude of 150 metres (see maps in Appendix II). The surface slope upwind of the site was very small, and both advection and the effect of a mountain range 10 km upwind were presumed to be unimportant in the meteorological heat budget. The ice thickness at the site was approximately 200 metres.

Power was supplied by a wind generator, and mechanical difficulties with this generator necessitated the removal of the instruments in November to a new site closer to the main station where power was available. This new site was on a slightly sloping ice plateau at 50 metres altitude.

The instruments installed at the first site are shown in the two photographs below. Fig. 4.1 shows the radiation instruments, with the caravan and wind generator in the background, looking south. Fig. 4.2 shows the mast with anemometers and radiation-shielded thermocouples at 0·5, 1, 2 and 4 metres height, looking north out to sea.

4.2. RADIATION

The net flux of shortwave and longwave radiation was measured continuously by a CSIRO net radiometer. In addition, downward- and upward-directed fluxes of shortwave radiation were measured by Kipp solarimeters. The calibration and data reduction technique has been described at length for the 1961/62 Mawson radiation data (Weller 1964) and also briefly in Section 3. Similar methods were used for the 1965 data. (Calibration factors are given in Table II.)

From the daily noon values (Table 5), a mean albedo for the whole year was computed as 69%. On the occasions (14% of all observations) when a thin snow layer covered the surface the albedo increased to a mean value of 84%. From the values of albedo and incident shortwave radiation measured at the surface (Table

3), the amount of radiation absorbed by the ice was computed and appears in Table 4.1 below.

At Mawson, as elsewhere, in the Antarctic the radiation balance of the ice surface (Table 7) is negative for the greater part of the year. The total radiation loss of the ice is 8 k cal/cm²/year, and even in summer the radiation balance remains negative up to an elevation of the sun of 17 degrees on clear days (Weller 1964).

All the monthly radiation data are given in Table 4.1, the accuracy of the data is estimated to be within ± 5%.

TABLE 4.1
MEAN MONTHLY RADIATION FLUXES
(cal $cm^{-2}day^{-1}$)

	N	G	A	$G(1-A)$
January	−69	−617	0·67	−203
February	−40	−433	0·66	−147
March	49	−204	0·63	−75
April	75	−76	0·75	−19
May	86	−10	0·71	−3
June	92	0	—	0
July	85	−5	0·79	−1
August	79	−39	0·72	−11
September	79	−169	0·71	−49
October	3	−394	0·64	−142
November	−88	−616	0·66	−209
December	−86	−675	0·66	−229
Mean	22	−270	0·69	−91

N = net flux of all wave radiation
G = global radiation (shortwave downward flux)
A = albedo
$G(1-A)$ = shortwave radiation absorbed by the ice.

The sign convention used is: negative values, heat flux towards the surface (i.e., ice surface acts as a heat sink); positive values, heat flux away from the surface (i.e., surface acts as a heat source).

4.3. CONDUCTED HEAT FLUX IN THE ICE

The usual approach is used initially to compute the conducted heat flux through the surface of the ice by determining the net heat gain or loss of the ice by a change of the temperature profile with depth $\Delta T(z)$:

$$S = \rho c \int_0^\infty \Delta T(z)\, dz \tag{4.1}$$

where ρ is the density and c the specific heat of the ice. Later it will be shown that S is not the total conducted heat flux at the surface but only a net effect.

Measured temperature profiles down to 11 metres depth (Tables 35-40) gave a temperature-depth relationship (Fig. 2.4) from which monthly changes in the heat content of the ice could be computed, extrapolating the temperature profiles to depths greater than 11 metres.

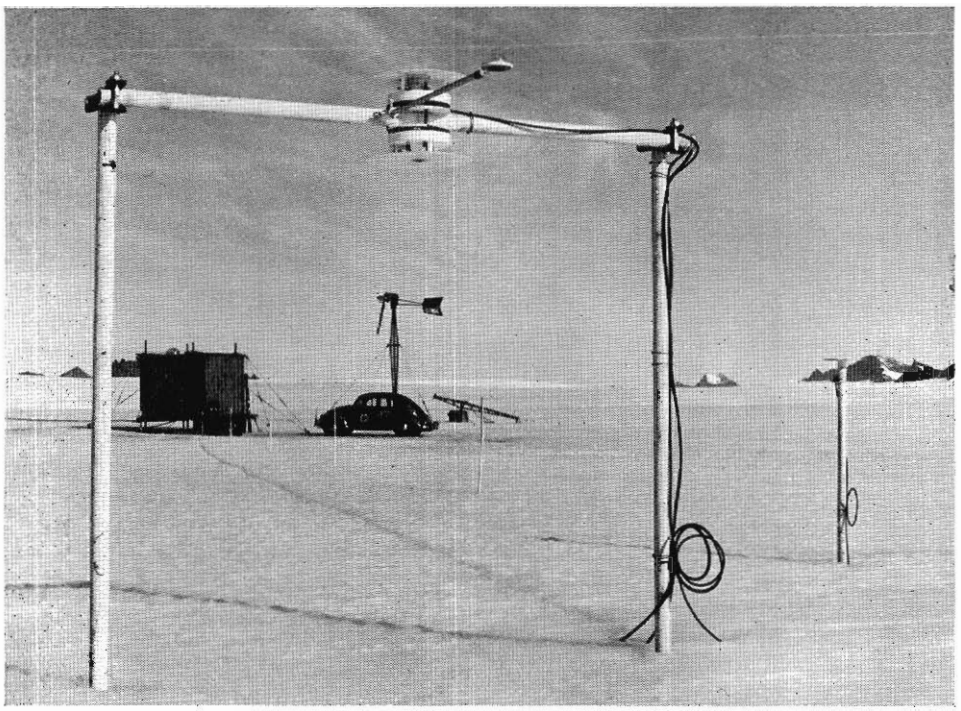

FIG. 4.1. Radiation instruments, wind generator and instrument caravan, looking south.

From a number of measurements (Table 48) the ice density was determined as 0·88 gm cm^{-3}, corresponding to an air bubble content of 4% (Schwerdtfeger 1963) and the specific heat value used was 0·48 cal $deg^{-1}gm^{-1}$. Heat flux plates were used successfully in the ice to determine the thermal diffusivity and the amplitude of the diurnal heat flux fluctuations (Section 2). The thermal diffusivity of the ice was 0·011 cm^2sec^{-1}.

4.4. SUB-SURFACE HEAT BUDGET EQUATIONS

Apart from conduction and shortwave radiation, other forms of energy transport do not take place in the ice, so that the changes in heat storage of the ice can be determined from these two processes. Longwave radiation and sensible and latent heat loss or supply at the ice—air interface do not enter the computations directly, but are accounted for by corresponding changes in the conducted heat flux in the ice.

If R_A is the radiation absorbed by the ice below depth z', $S_{A_{z'}}$, the heat flux to the surface resulting from this absorbed radiation, and $\Delta H_{A_{z'}}$, the net change in heat storage, due to absorbed radiation below level z', then a balance equation for the absorbed radiation and resulting changes can be written:

$$R_{A_{z'}} + S_{A_{z'}} = \Delta H_{A_{z'}} \tag{4.2}$$

Similarly, the heat flux at depth z', due to temperature pulses at the surface which are propagated downwards into the ice, can cause a change in the heat content of

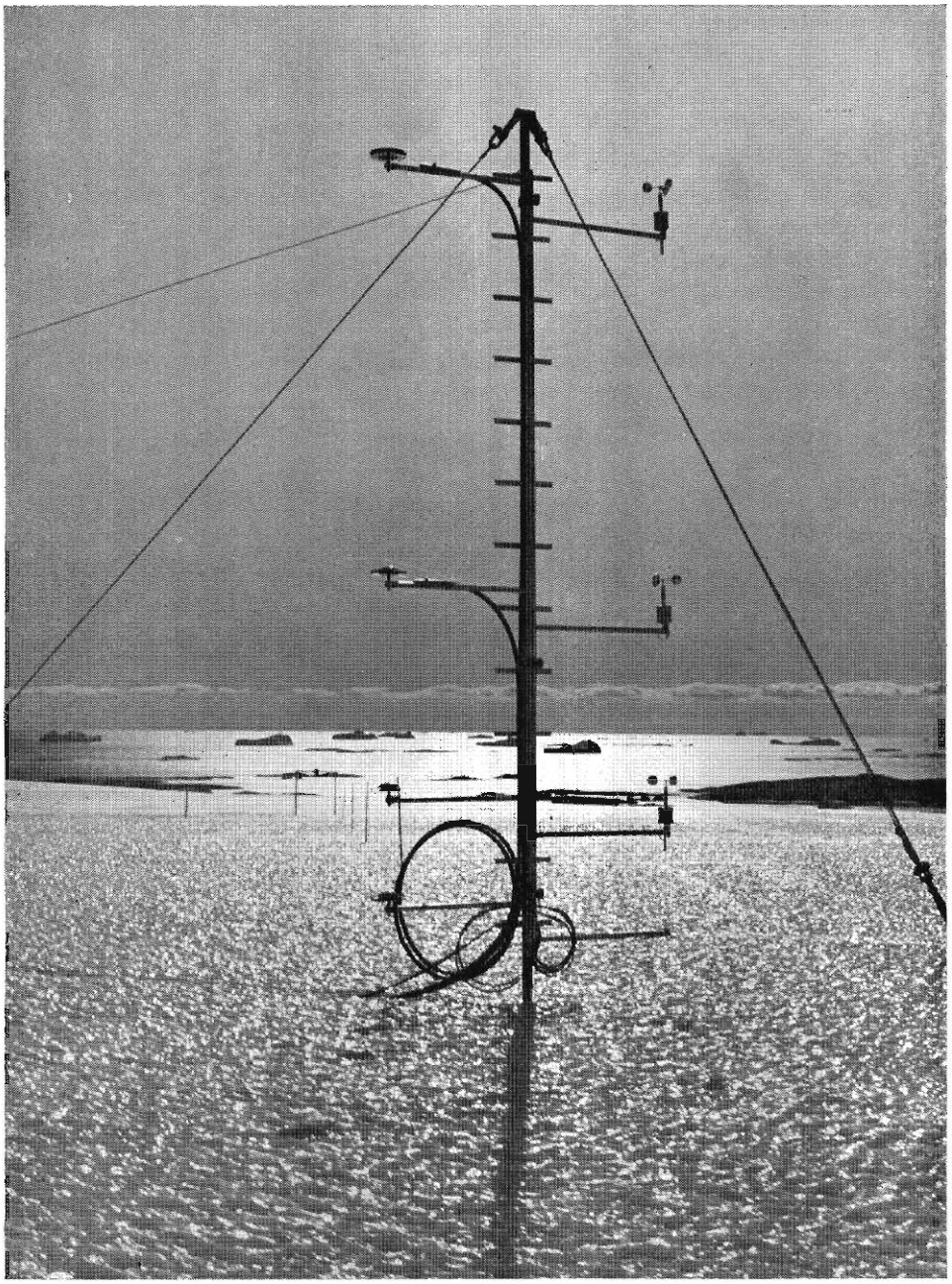

FIG. 4.2. Instrument mast looking north, out to sea.

the ice. If $S_{T_{z'}}$ is the heat flux due to surface temperature changes only at depth z' and $\Delta H_{T_{z'}}$ the change in net heat storage below level z', then $S_{T_{z'}} = \Delta H_{T_{z'}}$ (4.3)

The heat budget equation of the ice below level z' can therefore be written:

$$R_{A_{z'}} + S_{A_{z'}} + S_{T_{z'}} = \Delta H_{A_{z'}} + \Delta H_{T_{z'}} \tag{4.4}$$

If the surface budget is considered, then $z' = 0$. Instead of computing R_{A_0}, S_{A_0} and S_{T_0}, the net change in heat content, which is simply obtained as a change in the tautochrone pattern in the ice, $\Delta H_{A_0} + \Delta H_{T_0}$, can be used as the only necessary sub-surface component in the surface budget equation.

Since it is not easy in most cases to separate the effects of absorbed radiation and surface temperature pulse, the following budget equation can be writtten for the ice mass below depth z':

$$R_{z'} + S_{z'} = \Delta H_{z'} \tag{4.5}$$

where
$$R_{z'} = R_0 e^{-\mu z} \tag{4.6}$$

is the net flux of shortwave radiation directed downwards at depth z', or the radiation absorbed by the ice mass below depth z' (R_0 = net shortwave radiation at the surface, μ = extinction coefficient).

$$S_{z'} = kt\left(\frac{dT}{dz}\right)_{z'} \tag{4.7}$$

is the total conducted heat flux at depth z', including the total heat flux which results from absorbed radiation (k = thermal conductivity, t = time).

$$\Delta H_{z'} = \rho c \int_{z'}^{\infty} \Delta T(z)\,dz \tag{4.8}$$

is the net heat gain or loss of the ice below depth z', or the conduction of heat through the level at depth z' resulting from this heat storage change. It includes the conducted heat due to changes in the net heat storage by absorbed radiation.

Although is has been shown above (equation 4.5) that it is not necessary to consider the radiative and conductive heat flux components separately in the surface heat budget, if the net heat change in the ice is known, they are of interest in the sub-surface heat budgets and will be considered numerically now.

4.5. COMPARISON OF CONDUCTIVE AND RADIATIVE HEAT TRANSFER IN THE ICE AND SUB-SURFACE HEAT BUDGETS

The distribution of the absorbed radiative energy with depth was described in Section 1. The mean extinction coefficient between the surface and 1 metre depth was 0·013 cm^{-1} and 0·007 cm^{-1} below 1 metre. The net flux of shortwave radiation at any depth can be computed from these extinction coefficients and the surface radiation values in Table 4.1.

The annual mean values of the conductive and radiative terms will be evaluated first for the surface. The mean annual temperature gradient at the surface was determined as approximately 15°/metre. This leads to a heat loss through the surface by conduction of 25 k cal $cm^{-2}year^{-1}$, using a thermal conductivity of the ice of $5{\cdot}3 \times 10^{-3}$ cal $cm^{-1}deg^{-1}sec^{-1}$, corresponding to the diffusivity value quoted above. This is an average heat loss of 70 cal $cm^{-2}day^{-1}$ which should be compared with the 90 cal $cm^{-2}day^{-1}$ absorbed radiation heat gain shown in Table

4.1. The total annual heat gain of the ice is considered zero and the ice heat balance equation (equation 4.5) can be regarded to balance within the error limits of determining the surface temperature gradient.

The monthly temperature gradients at the surface cannot be determined with sufficient accuracy; the heat flux at the surface can, however, be written as a remainder term in the balance equation. This has been done in Table 4.2. Similarly, the components have been computed for 1 and 4 metres depth.

TABLE 4.2

HEAT ENERGY BUDGET OF THE ICE

(cal $cm^{-2}day^{-1}$)

	R_0	S_0	ΔH_0	R_1	S_1	ΔH_1	R_4	S_4	ΔH_4
January	203	−193	10	51	−37	14	6	2	8
February	147	−142	4	37	−29	8	4	6	10
March	75	−101	−26	19	−31	−12	2	2	4
April	19	−39	−20	5	−23	−18	1	−5	−4
May	3	−10	−7	1	−7	−6	0	−2	−2
June	0	−23	−23	0	−20	−20	0	−6	−6
July	1	−21	−20	0	−16	−16	0	−8	−8
August	11	−12	−1	3	−11	−8	0	−10	−10
September	49	−47	2	12	−12	0	1	−7	−6
October	142	−122	20	36	−23	13	4	−4	0
November	209	−173	36	52	−39	23	6	0	6
December	229	−204	25	57	−35	22	7	1	8
Year	91	−91	0	23	−23	0	3	−3	0

(Positive values denote heat gain; negative values heat loss of the ice.)

The amplitude of the annual radiative flux into the ice at the surface (R_0) is thus approximately four times higher than the amplitude of the conductive heat flux resulting from the net changes in heat storage in the ice (ΔH_0).

Numerically, it has been shown then that, during the summer months when the magnitude of the absorbed radiation is high, surface temperature gradients cannot be used to compute the sub-surface heat flux. The heat flux terms derived in this way (e.g., for short-term heat budget studies) may be an order of magnitude too high, unless the absorbed radiation is considered also in the heat budget equation at the surface.

At 1 metre depth the amplitude of the annual radiative flux is approximately twice the amplitude of the conductive heat flux due to changes in the net heat storage in the ice, while the radiative flux at 4 metres depth is still one third of the conductive heat flux.

It will now be shown how the absorbed radiation affects the net storage of heat in the ice. From the Fourier solution of a sinusoidal temperature wave at the surface of a semi-infinite body, the amplitude of the heat flux at the surface is given by

$$B = A\sqrt{\omega\rho ck}$$ (e.g., Carslaw and Jaeger 1959, also equation 2.5)

where B = amplitude of the heat flux, A = amplitude of the temperature wave, ω = frequency, ρ = density, c = specific heat, k = thermal conductivity. For the

Mawson ice: $\rho = 0{\cdot}88$ gm cm^{-3}, $c = 0{\cdot}48$ cal gm^{-1}deg^{-1} and $k = 5{\cdot}3 \times 10^{-3}$ cal cm^{-1}deg^{-1}sec^{-1}. The amplitudes of the annual temperature wave at the surface and at 1 and 4 metres depth were taken as the difference between the mean annual temperature at 8 metres depth and the smoothed winter minimum temperatures. This procedure avoids radiation effects and, from the equation by Carslaw and Jaeger, heat conduction due to the surface temperature wave can be computed. The effect of absorbed radiation on the net heat storage can then be obtained by comparing the observed annual heat flux with that computed, the difference being due to heat storage changes caused by absorbed radiation. The data are set out in Table 4.3.

TABLE 4.3

CONDUCTED HEAT FLUXES DUE TO NET CHANGES IN STORED HEAT BY THE SURFACE TEMPERATURE WAVE AND ABSORBED RADIATION

Depth	Temperature amplitude A	Heat flux amplitude computed B	Heat flux amplitude measured	Ratio of heat flux due to net change in heat storage by absorbed radiation to heat flux due to surface temperature wave
(metres)	(°C)	(cal cm^{-2}day^{-1})	(cal cm^{-2}day^{-1})	
0	11·0	19·5	30	0·54
1	10·6	18·8	23	0·22
4	4·8	8·5	10	0·18

The net heat storage in the ice and resulting heat flux are increased by half by absorbed radiation. At 4 metres depth the contribution of absorbed radiation to the net heat stored in the ice below 4 metres depth is still 15 per cent. Thus radiation effects are still significant at this depth and their importance as a method of heat transfer, even at depths greater than 4 metres in the ice, are obvious.

4.6. SURFACE HEAT ENERGY BUDGET: FIRST DETERMINATION

The measured values of the radiation and conduction heat fluxes at the surface can now be used in the energy budget equation

$$R + S + E + Q = 0 \tag{4.9}$$

to determine the flux of latent and sensible heat as a remainder term. R = net flux of radiation or radiation balance at the surface, S = conducted heat flux at the surface, E = latent heat flux at the surface, Q = eddy heat flux or flux of sensible heat at the surface. The sign convention used is: positive values, heat flux away from; negative values, heat flux towards the surface.

The geothermal heat contribution and the frictional heat created by the ice motion can be disregarded; in general they do not even reach the ice surface (Robin 1955). The annual net storage of heat is assumed zero. Table 4.4 gives the monthly means of the heat fluxes.

TABLE 4.4

HEAT ENERGY FLUXES: MONTHLY MEANS
(cal cm^{-2}day^{-1})

	MAWSON 1965		
	R	S	$E+Q$
January	−69	10	59
February	−40	4	36
March	49	−26	−23
April	75	−20	−55
May	86	−7	−79
June	92	−23	−69
July	85	−20	−65
August	79	−1	−78
September	79	2	−81
October	3	20	−23
November	−88	36	52
December	−86	25	61
Year	22	0	−22

Fig. 4.3. shows the monthly means of the heat fluxes.

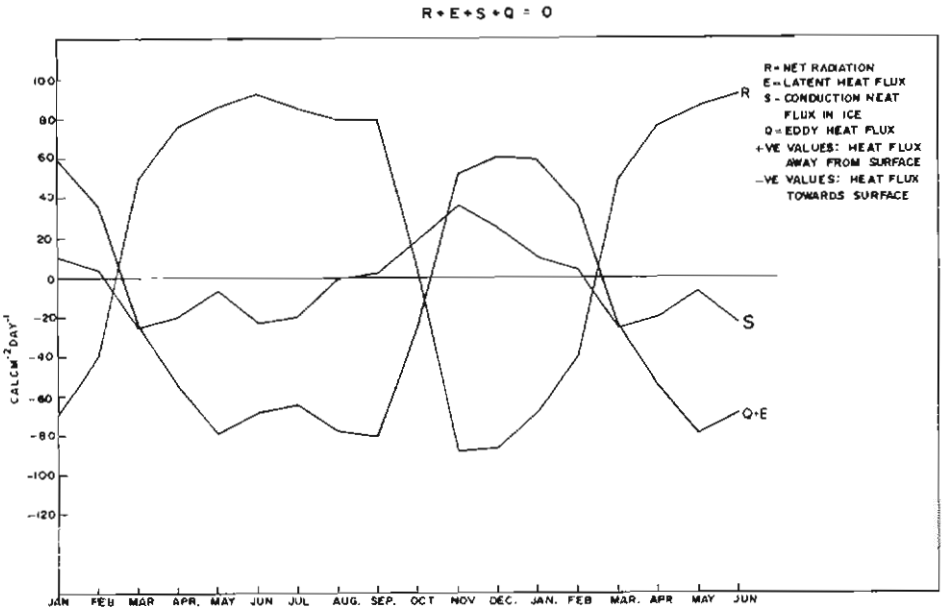

FIG. 4.3. Monthly means of the heat budget components. $Q + E$ is computed as the remainder of equation $R + E + S + Q = 0$.

The temporal variation of any of the heat budget components can be expressed by the Fourier series:

$$C = C_m + \sum_n \alpha_n \cos(n\nu t - \alpha_n) \qquad n = 1,2,3 \ldots \tag{4.10}$$

where C = heat budget component (R, S, E or Q), a = amplitude, α = phase angle, n = order of harmonic, ν = frequency, t = time, subscript m = annual mean.

The Fourier coefficients of the first six harmonics were computed with an IBM 7044 computer and are given in Table 4.5.

TABLE 4.5

FOURIER COEFFICIENTS OF THE HEAT BUDGET COMPONENTS AT MAWSON

(Amplitudes in cal $cm^{-2}day^{-1}$, phase angles in radians)

	R $R_m = 22{\cdot}08$		S $S_m = 0{\cdot}0$		$E+Q$ $E+Q_m = -22{\cdot}08$	
n	a_n	α_n	a_n	α_n	a_n	α_n
1	96·92	−2·989	24·12	0·727	64·71	−0·131
2	18 21	−2·588	4·84	1·699	10·80	−0·818
3	17·78	0·021	4·02	−1·997	21·62	−2·554
4	15·29	0·512	8·85	−2·955	20·24	−1·531
5	1·18	−2·294	2 36	0·782	15·27	−0·802
6	3·91	−2·504	0·77	0·841	17·65	−0·109

The equations of the first two harmonics of the heat budget components can therefore be expressed thus:

$$R = 22{\cdot}08 + 96{\cdot}92\cos(2\pi t - 2{\cdot}989) + 18{\cdot}21\cos(4\pi t - 2{\cdot}588)$$
$$S = 24{\cdot}12\cos(2\pi t + 0{\cdot}727) + 4{\cdot}84\cos(4\pi t + 1{\cdot}699)$$
$$E + Q = -22{\cdot}08 + 64{\cdot}71\cos(2\pi t - 0{\cdot}131) + 10{\cdot}80\cos(4\pi t - 0{\cdot}818)$$

(The datum line $t = 0$ is on the 15th January, $t = 0{\cdot}5$ on the 15th July.)

More precise expressions for the heat budget components should include at least the first four harmonics which all have amplitudes more than 10% of the first harmonic.

It will now be attempted to separate the latent and sensible heat fluxes from the E + Q term, neither quantity having been measured continuously throughout the year. The latent heat flux was determined from mass loss considerations in the winter months, when there was only evaporation and no melting at the surface. The sensible heat flux was measured for some months in winter and summer, and computed as a remainder for the other months. Simultaneous latent and sensible heat flux determinations allow an error estimate of the budget.

4.7. LATENT HEAT FLUX

Mass budget methods were used to determine the flux of latent heat at the surface. From an ablation stake grid of 9 stakes (Table 47) the weekly mass loss at the surface through evaporation was determined for all months when there was no surface melting. This includes the period April to October. The mean value of the standard deviation of the weekly ablation values

$$\sigma = \sqrt{\frac{\Sigma v_i^2}{n-1}} \tag{4.11}$$

was 0·14 cm of ice for that period. Taking the density of ice as 0·88 gm cm^{-3} and the latent heat of evaporation as 680 cal gm^{-1}, the latent heat flux was computed for monthly intervals. This latent heat flux does not include latent heat release due to hoar frost deposition which, however, was only very rarely observed. On a few

occasions in winter it was detected in small amounts on instruments; its contribution to the heat balance of the surface can be assumed to be negligible.

During the melting period the latent heat flux (consisting of the latent heats of melting and evaporation) was determined as a remainder in the heat budget equation.

A rough estimate of the relative contributions of melting and evaporation to the energy and mass loss at the surface can be obtained by initially considering the ablation to be due to melting only, and the meltwater to run off. The remaining heat energy of the latent heat flux can be used for evaporation, and the ablation rate due to evaporation can then be computed. By successive approximations the following values are obtained from the total ablation rates of 13·4 cm in December and 11·6 cm in January:

	Energy required for melting	Mass loss by melting	Energy required for evaporation	Mass loss by evaporation
	cal $cm^{-2}day^{-1}$	cm ice	cal $cm^{-2}day^{-1}$	cm ice
December	24	10·3	55	3·1
January	23	9·8	32	1·8

These values are upper limits of the contribution of evaporation. Ambach's (1963) values over the Greenland ice cap indicate considerably smaller contribution of evaporation to the ablation under similar conditions.

Estimates of the latent heat flux were also obtained by the Bowen ratio method where the Bowen ratio

$$r_\beta = \frac{c_p(T_2 - T_0)p_0}{0{\cdot}622L(e_2 - e_0)} \tag{4.12}$$

in the first approximation, and

$$E = \frac{Q}{r_B} \tag{4.13}$$

Using the monthly mean values of the temperature at 2 metres height, T_2 (Table 10) and at the surface, T_0 (extrapolated profiles from tables 18-29), the surface pressure p_0 (Table 1), vapour pressures e_2 and e_0 (from relative humidity values in Table 1 and assuming saturation at the surface respectively, and eddy heat flux Q (Tables 18-29), values of the latent heat flux E can be computed. (L = latent heat of evaporation, c_p = specific heat of air at constant pressure.) Values were computed for July, December and January only when the eddy heat flux was accurately known from profile measurements.

	r_B	Q	E	E (from mass budget, or as remainder)
July	−5·28	−75	14	10
December and January	−0·055	−7	127	44

For July, the computed values agree well with the values obtained from the ablation data, but the summer values calculated are too high by a factor of three, suggesting that the similarity between heat and moisture transfer does not apply for the two-monthly means, if at all in summer. Monthly means give even worse results, and are probably due to large errors resulting in the computation when the values of Q are small.

4.8. EDDY HEAT FLUX

The eddy heat flux or flux of sensible heat was computed from temperature and wind speed profile measurements (see Appendix I for instrumentation) for the months May to August and December and January. Computing the Richardson number for the geometric mean height of two metres from wind and temperature data at the 4-metre and 1-metre level above the ground, the air was found to be mostly in neutral or near-neutral stability (84% of all profiles were in the range $-0{\cdot}1 < \mathrm{Ri} < 0{\cdot}1$, Table 31). Logarithmic wind speed profiles were hence used in the eddy heat flux computations. The roughness parameter of the surface had a mean value of 0·23 cm. The classical equation of sensible heat transfer was used

$$Q = c_p A \frac{d\theta}{dz} t \tag{4.14}$$

with the exchange coefficient A corrected for non-adiabatic conditions

$$\mathrm{A} = \frac{A_a}{(1 + R_i)^2} \tag{4.15}$$

where Q = eddy heat flux, c_p = specific heat of air at constant pressure, $\frac{d\theta}{dz}$ = vertical gradient of potential temperature, t = time, A_a = exchange coefficient for adiabatic conditions, R_i = Richardson number.

It is assumed that the exchange coefficients of heat and momentum have equal magnitude.

Temperature profiles during the winter months, when there were usually conditions of temperature inversions, show the logarithmic structure of the temperature variation in the lower four metres (Fig. 4.4). The largest inversion measured was 6·6°C betwen the heights of 4 and 0·5 metres, and inversions greater than 6°C were frequent.

Since the diurnal change of temperature and temperature gradient is negligible

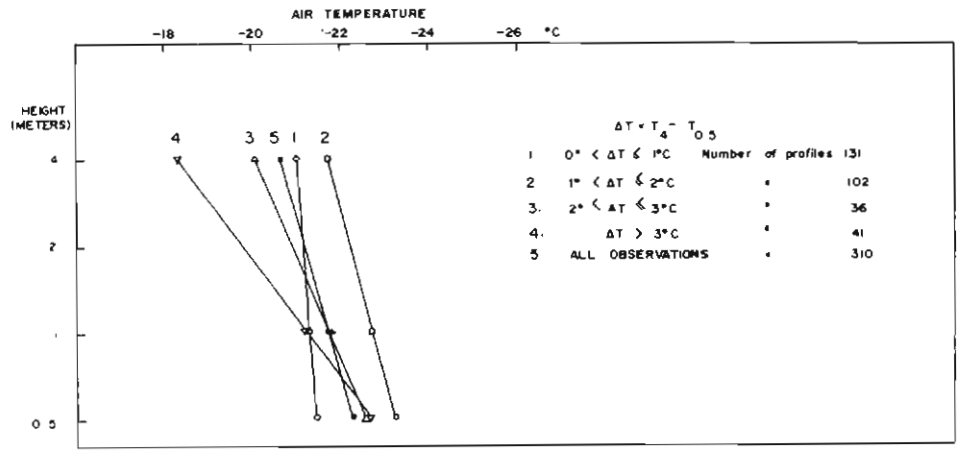

FIG. 4.4. Grouped means of air temperature profiles during the winter months.

in the winter months, daily values of the gradient of potential temperature and wind speed were used to compute the daily eddy heat flux (Tables 18-21).

In summer, the diurnal amplitude of the temperature variation increases to over 3°C (Table 11) and is associated with a diurnal pattern in the katabatic wind speed, temperature maxima and wind speed minima both occurring in the mid-afternoon. Profiles of temperature and wind speed were hence computed for six-hour periods (4 a.m. to 10 a.m., etc.), the night period being the time of strongest katabatic winds and the afternoon period (10 a.m. to 4 p.m.) the time of weakest katabatics.

Fig. 4.5 shows air temperature profiles for Deeember and January for the six-hour periods. During the night period, there are moderately strong inversions changing to lapse rate conditions in the afternoon. The transition periods show small inversions in December and small lapse rates for January. The eddy heat flux was computed for the six-hour periods (Tables 22-29), but comparison in December with the eddy heat flux, computed from daily values of the gradients (Table 30), show only a difference of 3% in the monthly mean values.

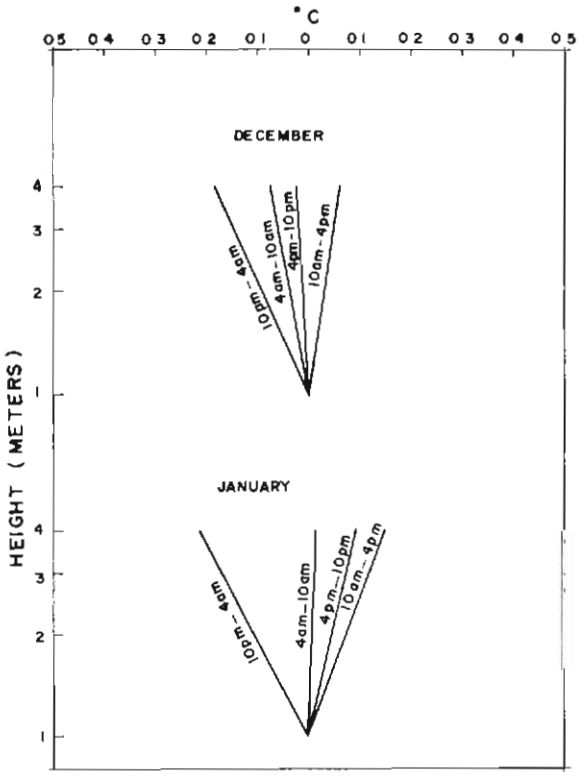

FIG. 4.5. Air temperature difference between the 4-metre and 1-metre height for six-hour periods in summer.

4.9. SURFACE HEAT ENERGY BUDGET—SECOND DETERMINATION

Data are now available for the monthly components of conduction and radiation for the whole year, and latent heat flux for the winter months and sensible heat flux

TABLE 4.6

COMPARISON OF EDDY HEAT FLUXES OBTAINED BY DIFFERENT METHODS
(cal $cm^{-2}day^{-1}$)

	Measured values (from profile data)	Number of days of measurement	Obtained as remainder term
May	—55	9	—121
June	—61	13	—85
July	—65	22	—75
August	—42	14	—104

for some winter and summer months. The missing monthly data for the latter two components are computed as remainders in the budget equation. A check on the errors involved in this method can be carried out by comparing the eddy heat flux computed as a remainder term, with the eddy heat flux measured during the winter months. The data are set out in Table 4.6.

The agreement between the two sets of values is good only for July where 22 days of observations are available, but too low for the other months when only little data are present. The measured data are possibly selective, since the wind generator did not supply sufficient power to the recording instruments at wind speeds less than 7 m/sec, and the instruments had to be switched off after prolonged periods of calm conditions when the batteries became discharged. Many of the light to moderate wind speed periods, with large inversions and high heat transfer by eddy diffusion, must therefore have been eliminated from the data, thus possibly accounting for the low values of the measured eddy heat flux.

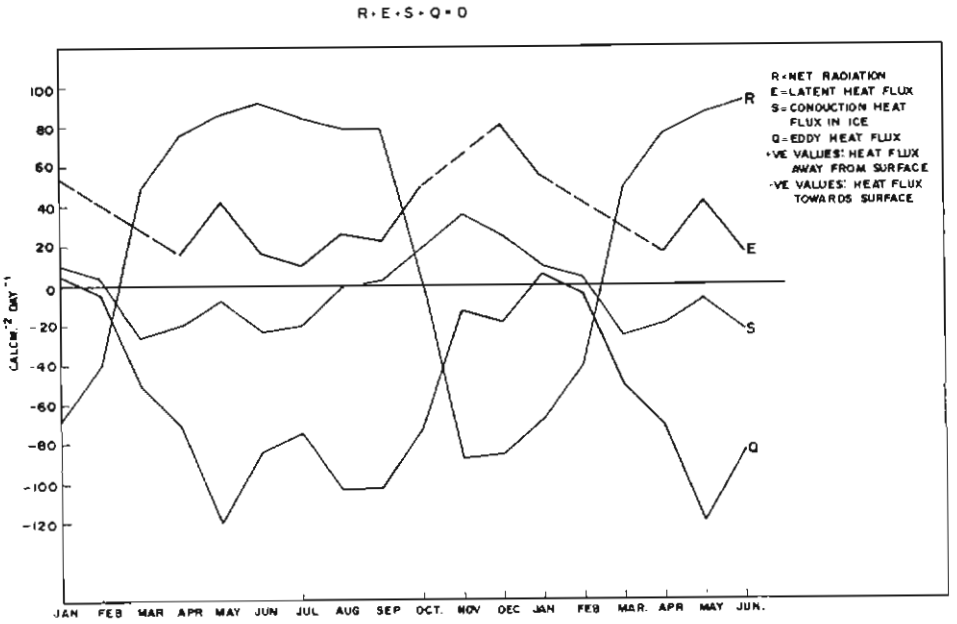

FIG. 4.6. Monthly means of the heat budget components.

The error term in the budget equation is probably of the order of ± 10 cal $cm^{-2}day^{-1}$, as indicated by the July error. This is small compared with the magnitude of the individual heat budget components considered. The fiual values of the budget components are shown in Fig. 4.6 and Table 4.7.

TABLE 4.7

HEAT BUDGET COMPONENTS AT MAWSON

(cal $cm^{-2}day^{-1}$)

	R	S	E	Q
January	−69	10	54	5
February	−40	4	41	−5
March	49	−26	28	−51
April	75	−20	16	−71
May	86	−7	42	−121
June	92	−23	16	−85
July	85	−20	10	−75
August	79	−1	26	−104
September	79	2	22	−103
October	3	20	50	−73
November	−88	36	65	−13
December	−86	25	80	−19
Year	22	0	38	−60

The Fourier coefficients for the last two terms are computed separately now:

TABLE 4.8

FOURIER COEFFICIENTS OF THE HEAT BUDGET COMPONENTS

(Amplitude in cal $cm^{-2}day^{-1}$, phase angles in radians)

	E $E_m = 37{\cdot}50$		Q $Q_m = -59{\cdot}58$	
n	a_n	α_n	a_n	α_n
1	24·58	0·300	54·97	−0·157
2	10·26	1·273	14·03	−0·367
3	1·80	−2·275	15·67	2·840
4	8·01	2·891	8·45	−1·193
5	4·24	0·446	5·40	−2·636
6	6·19	−3·035	9·12	0·268

The equations of the two heat budget components can now be written again for the first two harmonics:

$$E = 37{\cdot}50 + 24{\cdot}58\cos(2\pi t + 0{\cdot}300) + 10{\cdot}26\cos(4\pi t + 1{\cdot}273)$$
$$Q = -59{\cdot}58 + 54{\cdot}97\cos(2\pi t - 0{\cdot}157) + 14{\cdot}03\cos(4\pi t - 0{\cdot}367)$$

Higher harmonics including the sixth are significant again and exceed 10% of the amplitude of the first harmonic.

4.10. THE MULTI-LEVEL ANNUAL HEAT BUDGET

The magnitudes of the total yearly heat budget components at three levels were computed, and are shown graphically in Fig. 4.7. The longwave radiation emitted

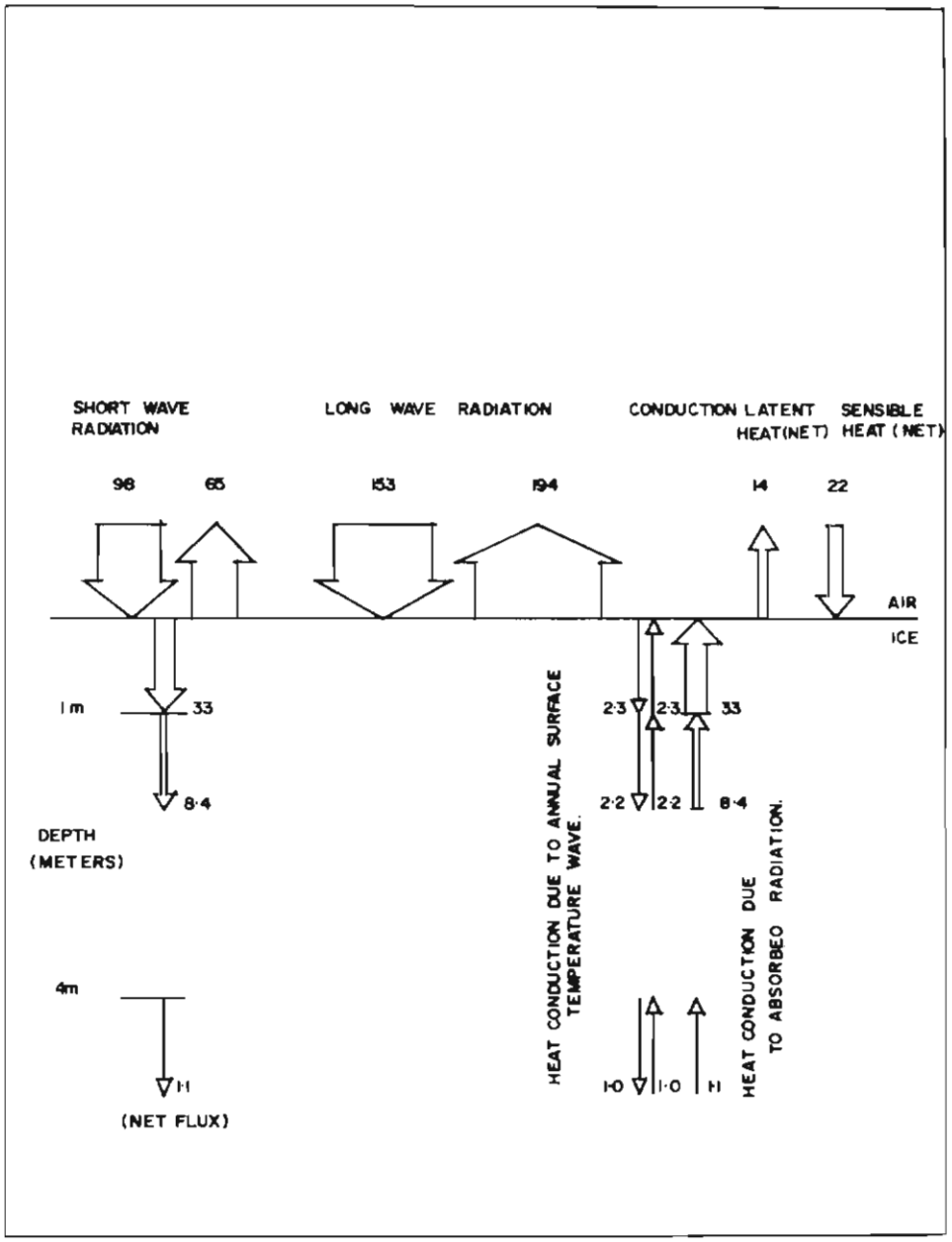

FIG. 4.7. Yearly heat budget components above and inside the ice, k cal cm^{-2}.

by the surface was calculated from the Stefan-Boltzmann law, using an emissivity of the ice surface of 0·96 and the annual mean surface temperature. The sub-surface shortwave radiation fluxes are net fluxes and represent radiation which is actually absorbed by the ice beneath the various levels given. The annual conduction fluxes, due to absorbed radiation, have equal magnitude but opposite sign to the radiative fluxes. The conducted heat fluxes, due to the annual surface temperature wave, are also shown at various levels. At the surface, they are an order of magnitude smaller than the heat flux due to absorbed radiation, and at 4 metres depth they have only about the same magnitude as the latter. The net annual heat storage in the ice is zero.

4.11. COMPARISON WITH OTHER ANTARCTIC DATA

The midwinter energy fluxes at four Antarctic stations are given by Dalrymple *et al.* (1963). They are the mean values for June and July and are compared in Table 4.9 with the mean June/July values of the energy fluxes at the site described above, and also over the annual sea ice surface described in Section 3. The data given by Dalrymple are rounded off to the closest whole numbers.

TABLE 4.9

SUMMARY OF MIDWINTER ENERGY FLUXES AT SIX ANTARCTIC STATIONS

$R + S + Q + E = 0$, cal cm^{-2}day^{-1}

Station (Altitude)	Year	R	S	Q	E
South Pole (2,800m)	1958	+57	−3	−51	−3
Mirny (36m)	1957	+51	−3	−98	+50
Maudheim (37m)	1950–51	+46	−7	−30	−9
Little America (44m)	1957	+33	−3	−13	−17
Mawson (150m)	1965	+89	−22	−80	+13
Mawson sea ice (0m)	1965	+115	−87	−10	−18

The effect of persistent winds on the eddy heat flux is apparent: at the coastal stations under the influence of steady katabatic winds (Mirny and Mawson) the eddy heat flux is roughly four times higher than at Maudheim and Little America, which are both situated outside the influence of the katabatic on ice shelves. At the South Pole station, where there are moderate prevailing winds, the eddy heat flux has intermediate magnitude.

The thermal characteristics of the solid layer determine the conducted heat flux in that layer. Only at Mawson does the solid layer consist of ice, giving annual amplitudes of conducted heat fluxes four times higher than in the snow medium of the other stations. If there is a large heat source under the ice, such as in the case of sea ice floating on relatively warm water, the conducted heat flux becomes very high, of course, as shown for the Mawson sea ice. Radiation losses at the surface increase accordingly, but little cooling of the surface due to radiation losses result because heat energy is replaced from the water below by conduction. No pronounced surface inversions can develop, therefore, and the eddy heat flux is small despite the presence of strong katabatic winds.

The optical transparency of the solid layer also affects the conducted heat flux as has been shown above. For snow the extinction coefficient is high and the total effect of absorbed radiation on the heat flux is considerably smaller than in ice. Subtracting the radiation effect from the heat flux at Mawson, the latter becomes about twice as high only as the heat flux at Maudheim station where there is a similar annual temperature amplitude at the surface. This is the result that would be expected from theoretical considerations, using the thermal diffusivities of the solid media at the two stations.

Annual radiation losses are similar at the coastal stations and somewhat higher at the inland station at the South Pole. The eddy heat fluxes generally show the same tendency to increase during the winter when inversions are strongest, but while at the South Pole and at the ice-shelf stations there is usually a deposit of hoar frost throughout most of the year with release of latent heat, Mirny and Mawson on the coast show latent heat losses by evaporation. The heat budget at Mawson resembles that at Mirny closest and probably applies for most of the coast of Eastern Antarctica where there are strong katabatic winds.

4.12. CONCLUSION

The radiation fluxes above and inside blue ice are the dominating methods of heat energy transfer. Both amplitudes and annual mean values are large compared with the other heat fluxes.

The absorbed radiation causes net changes in the stored heat in the ice as well as changes of the temperature gradients, particularly near the surface where absorption is greatest. A strict solution of the heat budget equation is shown to be possible by considering the sub-surface heat fluxes in terms of the net change in stored heat only. This procedure avoids having to compute the absorbed radiation and heat flux resulting from this absorbed radiation separately.

These latter components are computed, however, to determine their contribution to the heat transfer in the ice. The amount of heat stored annually in the ice is almost doubled by absorbed radiation and changes in the surface temperature gradients give conducted heat fluxes an order of magnitude higher than the conducted heat fluxes due to the annual surface temperature wave. The effects of absorbed radiation are still large at depths exceeding 4 metres.

5. ACKNOWLEDGEMENTS

During 1961 the author carried out radiation measurements over ice and snow surfaces at Mawson, a station of the Australian National Antarctic Research Expeditions (ANARE) in Antarctica. On returning from Antarctica he was invited by Dr. U. Radok, Head of the Department of Meteorology at the University of Melbourne, to participate in a complete heat budget study of Antarctic ice in the coastal areas just then projected by Dr. P. Schwerdtfeger, of the same department, as part of the ANARE glaciological programme. The detailed planning, development and testing of instruments was carried out over two years by Dr. Schwerdtfeger and the author before leaving Melbourne with the 1965 ANARE expedition to carry out the work at Mawson during that year.

It is with pleasure that the author acknowledges his indebtedness to Dr. Peter

Schwerdtfeger who, not only encouraged all aspects of the study, but also gave assistance and advice without which this research would not have been possible. He also wishes to thank Mr. W. Budd, Dr. U. Radok and Dr. F. Loewe who read different parts of the manuscript and offered many suggestions for improvement. Mr. G. Martin, electronics engineer at Mawson in 1965, was of invaluable help in maintaining and improving the electronics of the remote stations; Mr. I. Hore has done most of the tedious data reduction; and Mr. J. Straede has provided a programme for the computer treatment of some of the data. Thanks are due to the members of the wintering party at Mawson in 1965 who assisted on many occasions, and to the Acting Director of the Antarctic Division who has authorized the publication of this paper.

6. REFERENCES

AMBACH, W. (1959). Ein Beitrag zur Kenntnis der Lichtstreuung im Gletschereis. *Archiv für Meteorologie, Geophysik und Bioklimatologie*. Serie B, Band **9**, Heft 3/4, 441.

AMBACH, W. (1963). Untersuchungen zum Energieumsatz in der Ablationszone des Grönlandischen Inlandeises. Expedition Glaciologique Internationale au Groenland (EGIG) (1957-60), Vol. 4, No. 4. 311pp.

AMBACH, W., *and* MOCKER, H. (1959). Messungen der Strahlungsextinktion mittels eines kugelförmigen Empfängers in der oberflächennahen Eisschicht eines Gletschers und im Altschnee. *Archiv für Meteorologie, Geophysik und Bioklimatologie*. Band **10**, 1. Heft, 84.

AMBACH, W., *and* HABICHT, H. L. (1962). Untersuchungen der Extinktionseigenschaften des Gletschereises und Schnees. *Archiv für Meteorologie, Geophysik und Bioklimatologie*. Band **11**, 4. Heft, 512.

ÅNGSTRÖM, A. (1929). On the atmospheric transmission of sun radiation and on dust in the air, I. *Geografisker Annaler* **11**: 156.

ÅNGSTRÖM, A. (1930). On the atmospheric transmission of sun radiation, II. *Geografisker Annaler* **12**: 130.

BERGEN, J. (1963). Vapor transport as estimated from heat flow in a Rocky Mountain snowpack. IUGG International Association of Scientific Hydrology, Publ. No. 61, 62.

BOWEN, I. S. (1926). The ratio of heat losses by conduction and by evaporation from any water surface. *Physical Review* **27**: 779.

BUDD, W. (1966). Ablation from an Antarctic ice surface. Proceedings of International Conference on Low Temperature Science, Hokkaido, August 1966.

BUDD, W., DINGLE, R., *and* RADOK, U. (1964). Byrd snow drift project. University of Melbourne, Meteorology Department, Publ. No. 6, 100pp.

BUDYKO, M. I. (1955). Atlas of heat balance. Published by the Chief Administrator, Hydrometeorological Service USSR, 41pp.

BUDYKO, M. I. (1963). Atlas of the heat balance of the earth. Published by the Geographic Committee, Academy of Science, USSR. 69pp.

BUNT, J. S. (1960). Introductory Studies: hydrology and plankton, Mawson, June 1956–February 1957. *ANARE Reports* (B) **3**. Pub. No. 56.

CAMERON, R. L., *and* BULL, C. B. (1962). The thermal diffusivity and thermal conductivity of glacial ice at Wilkes Station, Antarctica. American Geophysical Union, Antarctic Researeh, Geophysical Monograph No. 7, 178.

CARSLAW, H. S., *and* JAEGER, J. C. (1959). Conduction of heat in solids. 2nd ed. Oxford Clarendon Press.

COLLINS, B. G., *and* KYLE, T. G. (1966). The spectral variation of the sensivity of a polyethylene-shielded net radiometer. *Pure and Applied Geophysics* **63**: 231.

DALRYMPLE, P., LETTAU, H., *and* WOLLASTON, S. (1963). South Pole micrometeorological program: data analysis. American Geophysical Union. Antarctie Research, Monograph No. 9, 13.

DEIRMENDJIAN, D., *and* SEKERA, Z. (1954). Global radiation resulting from multiple scattering in a Rayleigh atmosphere. *Tellus* **6**: 382.

DUNKLE, R. V., *and* GIER, J. T. (1953). Radiation in a diffusing medium with application to snow. California University Institute of Engineering Researeh Contract DA-11-190-Eng-3, 14pp.

ELSASSER, W. M. (1942). Heat transfer by infrared radiation in the atmosphere. Harvard Meteorological Studies No. 6.

FUNK, J. P. (1962). A net radiometer designed for optimum sensitivity and a ribbon thermopile used in a miniaturized version. *Journal of Geophysical Research* **67**: 2753.

FUNK, J. P. (1963). Improvements in polythene-shielded net radiometers. Paper published in Proceedings of Symposium on Engineering Aspeets of Environment Control for Plant Growth. CSIRO.

GEIGER, R. (1959). Thc elimate near the ground. Third printing. Harvard University Press, Cambridge, Mass.

GRAINGER, M. E., *and* LISTER, H. (1966). Wind speed, stability and eddy viscosity over melting ice surfaces. *Journal of Glaciology* **6**: 101.

HANSON, K. J. (1960). Radiation measurements on the Antarctic snowfield, a preliminary report. *Journal of Geophysical Research* **65** (3).

HOINKES, H. C. (1961). Studies in glacial meteorology at Little Ameriea V, Antarctica. I.U.G.G. International Association of Scientific Hydrology, Publ. No. 55, 29.

HOINKES, H. C., *and* UNTERSTEINER, N. (1952). Wärmeumsatz und Ablation auf Alpengletschern, II. *Geografisker Annaler* **35**: 116.

IGY INSTRUCTION MANUAL (1958). Radiation instruments and measurements. *Annals of the IGY* **5** (6).

KOPANEV, I. D. (1960). Snow cover of thc Antarctic. Leningrad, USSR Chief Administrator of Hydrometeorological Service.

KUTZBACH, J. E. (1961). Investigation of the modification of wind profiles by artificially controlled surface roughness. Annual Report 1961 Univcrsity of Wisconsin, Department of Meteorology, 71.

LETTAU, H. (1939). Atmosphärische Turbulenz. Akademische Verlagsgesellschaft, Leipzig.

LETTAU, H. (1949). Isotropic and non-isotropic turbulence in the atmospheric surface layer. Gcophysical Rescarch Papers No. 1, Air Force Cambridge Rcsearch Laboratory, Cambridge, Mass.

LETTAU, H. (1954). Improved model of thcrmal diffusion in the soil. *Transactions, American Geophysical Union*, **35**: 121.

LETTAU, H. (1962). Notcs on diabetic profile structure. Madison, Wisconsin. Section 10, 195-226, Final Report, Contract DA-36-039-SC-80282. October 1962.

LILJEQUIST, G. H. (1956). Energy exchange of an Antarctic snow-field. Norwegian-British-Swedish Antarctic Expedition 1949-52. Scientific Results **3** (1).

LOEWE, F. (1956). Contributions to the glaciology of the Antarctic. *Journal of Glaciology* **2**: 657.

LORIUS, C. (1963). Considérations sur le bilan thermique de la station Charcot. IUGG International Association of Scientific Hydrology, Publ. No. 6I, 7.

MELLOR, M. (1960). Sea-ice measuremcnts at Mawson and Davis, 1954-58. *ANARE Interim Reports* No. 19. Publ. No. 55.

MÖLLER, F. (1944). Das Strahlungsdiagramm. *RfW Berlin 1943 und Meteorologische Zeitschrift* **61**: 37.

PRIESTLEY, C. H. B. (1959). Turbulent transfer in the lowcr atmospherc. University of Chicago Press, Chicago 1959.

ROBIN, DE Q. (1955). Ice movement and temperature distribution in glaciers and ice sheets. *Journal of Glaciology* **2**: 523.

RUSIN, N. P. (1961). Meteorologicheskii i radiatsionyi Rekhim Antarktidy. Gydrometeorolocheskoye Izdatelstvo, Leningrad.

SCHMIDT, D. (1925). Masscnaustausch in freier Luft und verwandte Erscheinungen. Probleme der kosmisehen Physik 7. Hamburg. H. Grand, 1925.

SCHWERDTFEGER, P. (1960). Observations on cstuary ice. *Canadian Journal of Physics* **38**: 1391.

SCHWERDTFEGER, P. (1963). Theorctical derivation of the thermal conductivity and diffusivity of snow. Publication No. 61 of the IASH Commission of Snow and Ice. 75.

SCHWERDTFEGER, P. (1964). An analogue computer for solving growth problems of floating ice. *Gerland's Beiträge zur Geophysik* **73**, Heft 1, 44.

SCHWERDTFEGER, P. (1966). On the response of a sea-ice cover to changes in surIace temperature. *Journal of Glaciology* **6**: 439.

SCHWERDTFEGER, P. (1967). The measurement of heat conduction in the ground. Presented to ANZAAS Conference, Melbourne, Australia, January 1967.

SCHWERDTFEGER, P., *and* POUNDER, E. R. (1963). Energy exchange through an annual sea-ice cover. International Association of Scientific Hydrology, Publ. No. 61, 109.

SCHWERDTFEGER, P., *and* WELLER, G. (1967). The measurement of radiative and conductive heat transfer in ice and snow. *Archiv für Meteorologie Geophysik und Bioklimatologie* Serie B, Band **15**, 1-2, 24.

SHUMSKIY, P. A., *and* ZOTIKOV, I. A. (1963). On the bottom melting of the Antarctic ice shelves. International Association of Scientific Hydrology, General Assembly of Berkeley. Publ. No. 61, 225.

SUTTON, O. G. (1953). Micrometeorology. McGraw-Hill, New York.

SUTTON, O. G. (1955). Atmospheric Turbulence. Wiley, New York.

SUTTON, O. G. (1961). The challenge of the atmosphere. Harper, New York (Chapters 6 and 7).

SVERDRUP, H. U. (1953). The currents off the coast of Queen Maud Land. *Norsk Geografisk Tidsskrift* **14**: 239.

SWINBANK, W. C. (1964). The exponential wind profile. *Quarterly Journal of the Royal Meteorological Society* **90**: 119.

THOMAS. C. W. (1963). On the transfer of visible radiation through sea ice and snow. *Journal of Glaciology* **4**: 481.

UNTERSTEINER, N. (1961). On the mass and heat budget of Arctic Sea Ice. *Archiv Meteorologie Geophysik und Bioklimatologie*, Serie A, **12**: 151.

UNTERSTEINER, N. (1964). Calculations of temperature regime and heat budget of sea ice in the Central Arctic. *Journal of Geophysical Research* **69**: 4755.

UNTERSTEINER, N. (1964). A nomograph for determining heat storage in sea ice. *Journal of Glaciology* **5**: 352.

UNTERSTEINER, N., *and* BADGLEY, F. I. (1965). The roughness parameters of sea ice. *Journal of Geophysical Research* **70**: 4573.

VOWINCKEL. E., *and* ORVIG. S. (1965). The heat budget over the Arctic Ocean. Publications in Meteorology No. 74, McGill University, Montreal. 22pp.

WELLER. G. (1964). Radiation fluxes over an Antarctic ice surface. *ANARE Scientific Reports* (A) **4**. Publ. No. 96.

WELLER. G. (1967). The effect of absorbed solar radiation on the thermal diffusion in Antarctic freshwater ice and sea ice. *Journal of Glaciology* **6**: 859.

WELLER, G., *and* SCHWERDTFEGER, P. (1967). Radiation penetration in Antarctic plateau and sea ice. WMO Technical Note No. 87, Proceedings of Symposium on Polar Meteorology, Geneva, September 1966.

WISHART, T. (1964). On the growth and decay of sea ice. Mawson 1963. Glaciology report, Meteorology Department, University of Melbourne (unpublished).

YEN, Y., TIEN, C., *and* BENDER, J. (1963). On the isothermal flow of air through a snow pack with variable permeability. IUGG International Association of Scientific Hydrology, Publ. No. 61, 51.

APPENDIX I

INSTRUMENTATION

1. HISTORY OF THE INSTRUMENT INSTALLATION

The measurements which have been described above, and which have provided the basic data shown in the tables of Appendix III, have been made at four different locations in the vicinity of Mawson:

Site 1. Sea ice station (see maps in Appendix II).

Location: 400 metres offshore, in West Bay due west of Mawson station, sea bottom 300 metres below water surface; obstacles upstream of prevailing wind direction: 2-3 metre high ice cliffs 400 metres upwind, 8 degree coastal ice slope south of cliffs, 1500 metres altitude reached 80 km inland.

History:

25.3.65.	Sea ice begins freezing.
27.3.	Automatic sea-ice thickness-measuring device installed in Mawson harbour.
27.4.	Sea-ice thickness 55 cm in West Bay. Caravan and instrument set installed on sea ice. Power cable connection back to main station.
10.5.	Sea ice breaking up from north. Caravan and instruments taken ashore.
11.5.	All sea ice, except in Mawson harbour, breaks up and goes out.
19.5.	Caravan installed on a rock surface of West Arm.
10.6.	Sea-ice thickness 55 cm in West Bay. Automatic sea-ice thickness-measuring device installed in West Bay.
12.6.	Instrument set installed on sea ice in previous position and connected to caravan through 16-pair telephone cable.
17.11.	Instrument set taken ashore.
7.12.	Open pools of water along coast, shallow puddles of water on sea ice.
14.1.66.	Sea ice breaks up in West Bay.

Site 2. Plateau station (150 metres altitude).

Location: 2 km south of Mawson at 150 metres altitude. Flat ice plateau extending 2-3 km upwind of the station, then gradually rising to a chain of mountains (maximum height 1500 metres) 10 km upwind. Surface: blue ice, no permanent

snow cover, large melt streams during summer. Ice thickness: approximately 200 metres. Power supply for the station: one 1·5 kW wind generator.

History: 19.1.65. Caravans and equipment come ashore from the expedition ship.
22.1. Wind generator tower and instrument tower erected.
25.1. Caravan installed.
1.2. Instruments installed and connected.
9.2. Wind generator installed.
3.3. Electronics difficulties solved; recording commences.
29.5. Wind generator blades broken by blizzard.
15.8. Wind generator blades broken by blizzard.
8.9. Caravan completely destroyed by explosion; air vent of battery compartment blocked by drift snow in blizzard; hydrogen from batteries ignited by relay spark. For the rest of the year only spot readings with a portable potentiometer were carried out at this site, using the undamaged set of instruments still in position.

NOTE: Unusual conditions of calm weather during 1965 frequently necessitated switching the recording equipment off. The average annual wind speed at Mawson was 9·0 m/sec during 1965 compared with 11·1 m/sec during 1964, and 10·0 m/sec for the 10-year period 1956-1965.

Site 3. Plateau station (50 metres altitude).

Location: 500 metres south of Mawson station on a gently sloping ice plateau (1-2 degree slope), 8 degree slope south of station. Ice thickness: approximately 40 metres. Blue ice surface as at 150 metres altitude; no permanent snow cover. Power supply to station by power cable from main station.
History: This site was chosen for its convenient vicinity to the main station, making power available for more continuous recording than possible with wind generator power.

17.11.65. Instruments and caravan installed (all equipment coming from the sea-ice station which was closed on 17.11.65).
21.11. Recording commences.
6.12. Extremely strong melting: all bore holes fill with water, making it necessary to remove radiometers and discontinue light extinction measurements.
8.2.66. End of the ANARE 1965 expedition activities.

Site 4. Meteorological station Mawson.

The routine surface observations by the meteorological staff at Mawson have been used to supplement the data.
Temperature, wind speed, humidity, sunshine and cloud-cover data were observed at site 4 (see map). A set of radiation instruments was also operated for part of

the year, close to the micrometeorological station at site 3. Values of global radiation and net flux of all-wave radiation from this set of instruments were used when no other data were available.

NOTE: The data collected cover the period March 1965 to February 1966. All data tables of Appendix III show the 1966 data in the January and February columns; 1965 data in the March to December columns.

2. INSTRUMENTS AND RECORDING EQUIPMENT USED

Site 1. Instrument shelter: fibreglass-polyurethane caravan 2·1 × 2·1 × 2 7 metres, raised on four steel scaffold legs 50 cm above the grond. Power: 240 V AC, 50 c/s through 9 × 100 metres cable from station mains supply; Cannon environmental connectors; Variac transformers at either end to step up the voltage.
Instruments: Wind speed: three light-weight Beckman & Whitley three-cup anemometers at 1, 2 and 4 metres height, ANARE designed amplifier/binary divider circuits, giving one counting pulse for every four revolutions of the anemometer rotors. Two two-channel Sodeco six-digit pulse counters and printers, one channel being a date and time counter.

Temperature: Single-junction copper-constantan thermocouples above the surface at 0·5, 1, 2 and 4 metres height, provided with chromium-plated circular radiation reflection shields. Below the surface at 0, 15, 30, 45, 60, 80, 100 and 400 cm depth, enclosed in a polyethylene tube, and provided with 5 mm diameter tubular chromium-plated radiation reflectors. Reference junction in an ice-water bath enclosed by a vacuum flask and polyurethane thermal insulator.

Radiation: Two Kipp solarimeters facing upwards and downwards respectively, one net radiometer (CSIRO), one University of Melbourne subsurface radiometer below the ice—water interface.

Additional instruments: Two University of Melbourne heat-flux plates at 30 and 60 cm depth in the ice; also a device for measuring the sea-ice thickness automatically every six hours.

Recording equipment: One Siemens 12-channel recorder with ranges

1. —0 25 to 1·25 mV
2. —2·5 to 12·5 mV
3. —8 to 40 mV.

Through a relay unit the eight sea-ice temperature sensors were switched into the recorder every half hour for one cycle while air-temperature sensors were disconnected.

Frequency of recording: 48 seconds between dot-printing operations. Two operations for individual channels, 48 sec. This applies for all air temperature, radiation and heat flux measurements. Every half hour gave one cycle of sea-ice temperatures. Sodeco counters: printing every 30 minutes of integrated half-hourly wind runs at all three levels. Sea-ice thickness, every six hours.

Site 2. Instrument shelter: similar caravan as used at Site 1. Power: 50 V DC from a 1·5 kW Dunlite wind generator through two sets of eight 6-Volt 120 amphour

batteries with transparent cases and inbuilt hydrometer floats. 240 V AC, 130 Watt through X-tal power supply to run the recording equipment.

Instruments: wind speed and temperature sensors as at site 1. Ice temperature thermocouples at 0, 0·5, 1, 2, 4, 6 and 8 metres depth. Radiation instruments above the surface as at Site 1. Below the surface: University of Melbourne net radiometers and hemispherical radiometers (measuring downward flux) at 1, 2 and 4 metres depth, flux plates at 1, 2 and 4 metres depth. Also an ablation stake-grid of 12 stakes.

Recording equipment: one Siemens 12-channel potentiometric dot recorder with ranges:

1. —0·25 to 1·25 mV
2. —0·5 to 2·5 mV
3. —2·5 to 12·5 mV
4. —5·0 to 25·0 mV

Frequency of recording: 48 seconds between dot-printing operations. Two Sodeco counters as at site 1 with half-hourly print-out. One Hartmann and Braun 12-channel potentiometric recorder, range —1 to +4 mV, dot-printing sequence 5 seconds.

Site 3. Instrument shelter: the same caravan as previously used at Site 1. Power: 240 V AC, 50 c/s through 3 × 100 metres power cable from the station mains. Instruments: Wind speed, air temperature and radiation: the same instruments as used at Site 1. Ice temperatures: a copper-constantan thermocouple probe with thermocouples at 0, 0·5, 1, 2, 4, 6, 8 and 11 metres depth. Reference temperature: ice-water bath. Net and hemispherical subsurface radiometers at 1, 2 and 4 metres depth: the same as used at Site 2. Heat flux plates at 1 and 2 metres depth. Also an ablation stake-grid of 12 ablation stakes.

Recording equipment: one Siemens recorder (ex-Site 1); two Sodeco counters (ex-Site 1); one Siemens recorder (ex-Site 2).

Frequency of recording: Siemens recorders: 48 sec.; Sodecos: half-hourly integrated wind runs.

Site 4. Temperature: mercury and alcohol thermometers, clockwork thermograph. Humidity: clockwork hair hygrograph checked twice weekly against aspirated psychrometer readings. All the above instruments in standard meteorological screen at approximately 2 metres height above the ground.

Wind speed and direction: Dines anemograph (daily charts) at 10 metres height. Cloud observation visual. Duration of sunshine: Campbell-Stokes glass hemisphere sunshine recorder.

Radiation instruments: one CSIRO net radiometer; one Kipp solarimeter measuring global radiation; one Kipp solarimeter with equatorial shade-ring measuring diffuse sky radiation.

Temperature, humidity, wind speed and cloud cover: three-hourly observations. Duration of sunshine: continuous recording, daily integrated values. Radiation: daily integrated values from recorder with 5 second dot-printing sequence.

3. ROUTINE ADJUSTMENTS OF THE EQUIPMENT

The following routine adjustments of the equipment were carried out regularly:

Function	Frequency	
	in winter	in summer
1. Instrument mast height—adjusted	monthly	fortnightly
2. Cyclic interchange of anemometers	fortnightly	fortnightly
3. Levelling of radiation instruments	monthly	
4. Replacement of net radiometer hemispheres	monthly	
5. Renewing ice-water reference temperature mixture	daily or every second day	

4. CALIBRATION OF INSTRUMENTS

Calibration data for the instruments are given, with short comments on the calibration technique used in Tables I–V below.

TABLE I

CALIBRATION FACTORS OF RADIATION INSTRUMENTS SUPPLIED BY MANUFACTURERS

1. Linke & Feussner Actinometer CM 1 Serial No. 630062
   12·8 mV/g cal $cm^{-2}min^{-1}$ (at 20°C)
2. Kipp solarimeter CM 3 No. 2038
   7·9 mV/g cal $cm^{-2}min^{-1}$ (at 20°C)
3. Kipp solarimeter CM 3 No. 2047
   7·9 mV/g cal $cm^{-2}min^{-1}$ (at 20°C)
4. Kipp solarimeter CM 3 No. 2060
   7·9 mV/g cal $cm^{-2}min^{-1}$ (at 20°C)
5. Kipp solarimeter CM 3 —
   7·9 mV/g cal $cm^{-2}min^{-1}$ (at 20°C)
6. CSIRO net radiometer Inst. No. 421
   Shortwave 0 39_8 mV/mW cm^{-2} (at 20°C)
   Longwave 0·39_6 mV/mW cm^{-2}
7. CSIRO net radiometer Inst. No. 433
   Values lost.

TABLE II

CALIBRATION OF RADIATION INSTRUMENTS

1. Effect of solar elevation.

Calibration factors (mV/cal $cm^{-2}min^{-1}$) at 20°C.

Solar elevation	Kipp (Sea ice)	Kipp (Plateau)	CSIRO (Sea ice)*	CSIRO (Plateau)*
45	7·9	7·7	31·3	29·3
40	7·9	7·7	31·3	29·3
35	7·8	7·7	31·3	29·3
30	7·7	7·7	31·5	29·6
25	7·6	7·7	31·7	30·0
20	7·6	7·7	31·8	30·8
15	7·6	7·7	31·2	31·4
10	8·0	7·8	29·5	31·7
5	11·0	9·1	25·2	26·0
3	15·0	13·5	22·1	—
Calibration Dates (Mawson 1965/66)				
	19.1.66	13.3.65	19.1.66	13.3.65
	22.1.66	13.5.65	22.1.66	13.5.65

* Hemispheres damaged by drift snow on windward side.

2. Effect of solar azimuth.

Solar elevation	Ratio of Kipp output: sun incident parallel to element/sun incident perpendicular to element orientation
42	1 02
24	1·04
18	1·06
13	1·11
5 5	1·37
2	2 27

Calibration days: 13.3.65 and 22.1.66

3. Calibration of Linke & Feussner Actinometer: on 12.11.64 at the CSIRO Aspendale laboratories against a silver-disc actinometer (No. 53): 13·32 mV/cal cm^{-2}min^{-1} at 20°C.

TABLE III

RADIATION ERRORS AND POTENTIAL TEMPERATURE CORRECTIONS OF AIR TEMPERATURE THERMOCOUPLES

The air temperature thermocouples were provided with radiation shields, but were not artificially ventilated. At low wind speeds errors resulted which are shown below. The errors were determined at the University of Melbourne, comparing ventilated with unventilated thermocouples over a wheat field. The thermocouples were provided with the radiation shields used at Mawson; extrapolation was carried out for the different albedo values.

1. Global radiation at Mawson.

Global radiation at noon: $G \leqslant 0{\cdot}15$ cal cm^{-2}min^{-1}: 5 May–10 August
$G \geqslant 0{\cdot}6$ cal cm^{-2}min^{-1}: 20 Sept.–22 March
$G \geqslant 1{\cdot}2$ cal cm^{-2}min^{-1}: 25 Nov.–20 Jan.

2. Radiation error on the temperature gradient at 2 metres height.

$G = 1{\cdot}2$ cal cm^{-2}min^{-1} $A = 70\%$		$G = 0{\cdot}6$ cal cm^{-2}min^{-1} $A = 70\%$		$G = 0{\cdot}15$ cal cm^{-2}min^{-1} $A = 70\%$	
Wind speed m sec^{-1}	Error on temp. grad. °C m^{-1}	Wind speed m sec^{-1}	Error on temp. grad. °C m^{-1}	Wind speed m sec^{-1}	Error on temp. grad. °C m^{-1}
1	−0·09	1	−0·06	1	0·02
2	−0·06	2	−0·04	2	0·01
3	0·03	3	0·02	3	0·01
4	0·01	4	0·01	4	0·01
>4	<0·01				

3. The correction to obtain potential temperature gradients at 2 metres height is −0 01°C m^{-1}.

All temperature gradients need not be corrected for wind speeds $\geqslant$ 4 m/sec throughout the year—since radiation and potential temperature corrections cancel. For the period September–March all temperature data at wind speeds $\leqslant$ 2 m/sec are discarded since the errors eannot be determined with sufficient accuracy to allow eorrections to be made.

TABLE IV

BECKMAN AND WHITLEY ANEMOMETER COUNTER EQUIVALENTS
(SUPPLIED BY THE MANUFACTURERS)

R.P.S.	M/Sec	R.P.S.	M/Sec	R.P.S.	M/Sec
3·0	4·84	7 0	10 58	11·0	16·91
1	5·01	1	11·02	1	17·09
2	5·15	2	11·18	2	17·21
3	5·28	3	11 31	3	17·36
4	5·46	4	11·49	4	17·53
5	5 59	5	11·67	5	17·65
6	5·73	6	11·80	6	17·81
7	5·91	7	11·92	7	17·99
8	6 04	8	12·07	8	18·16
9	6·17	9	12·24	9	18·31
4·0	6·36	8·0	12·39	12·0	18·41
1	6·54	1	12·52	1	18·64
2	6·62	2	12·69	2	18·71
3	6·80	3	12 81	3	18·88
4	6·97	4	13·00	4	19·07
5	7·11	5	13·16	5	19·18
6	7·26	6	13·31	6	19·38
7	7·38	7	13·46	7	19·51
8	7·52	8	13·60	8	19·66
9	7·70	9	13·72	9	19·81
5·0	7·88	9 0	13·91	13·0	19·93
1	8·01	1	13·04		
2	8·14	2	14·18		
3	8·32	3	14·35		
4	8·46	4	14·48		
5	8·58	5	14·61		
6	8·76	6	14·80		
7	8·89	7	14·93		
8	9·03	8	15·07		
9	9·21	9	15·24		
6·0	9·34	10 0	15·39		
1	9·53	1	15·55		
2	9·66	2	15·75		
3	9·79	3	15·87		
4	9·96	4	16·01		
5	10·11	5	16 16		
6	10·28	6	16·31		
7	10·41	7	16·46		
8	10·56	8	16·64		
9	10·68	9	16·76		

TABLE V

CALIBRATION OF SUBSURFACE INSTRUMENTS

I. Heat flux plates.

1. Water-tank calibrations (applying a constant temperature difference across the 1·5 cm-thick flux-plate elements).

Temp. difference °C	Flux plate emf mV
−1	−15·0
0	0·0
1	15·0
2	30·0

i.e., for all flux plates used, the temperature sensitivity is 22·5 mV/°C cm^{-1} (± 3%).

2. Calibrations in iee (comparing measured temperature gradients multiplied by the thermal conductivity of ice, with the emf output of the heat flux plates).

Measured flux plate emf mV	Heat flux $\times 10^4$ cal $cm^{-2}sec^{-1}$	
	Sea ice	Plateau iee
1	1·30	1·67
2	2·60	3·34
3	3·90	5·00
4	5·20	6·67
5	6·50	8·34
6	7·80	10·00
7	9·10	11·67
8	10·40	13·34
9	11·70	15·00
10	13·00	16·67

II. Radiometers.

Calibrations were carried out in vertical boreholes (on 12.3.65 and 27.10.65); output of all instruments was compared at 1 metre depth. Absolute calibration values were obtained by comparison with a Kipp solarimeter element, alternately facing up and down in the borehole.

$H_1 = 82{\cdot}5$ mV/cal $cm^{-2}min^{-1}$ $N_1 = 96{\cdot}8$ mV/cal $cm^{-2}min^{-1}$
$H_2 = 90{\cdot}0$,, $N_2 = 118{\cdot}0$,,
$H_3 = 95{\cdot}0$,, $N_3 = 90{\cdot}0$,,

(H = hemispherical downward flux; N = net flux at 1, 2 and 4 metres depth)

APPENDIX II

MAPS

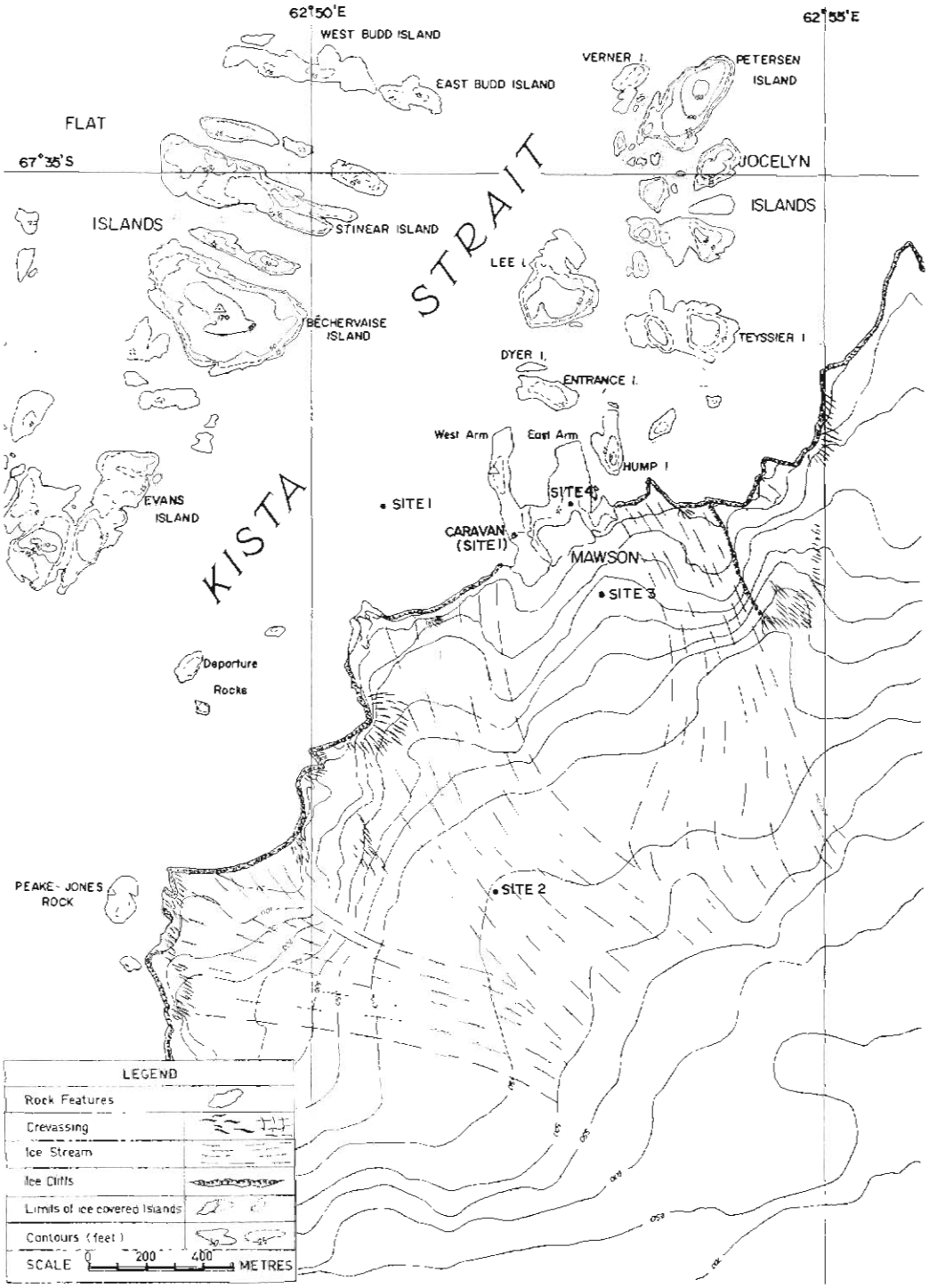

MAP 1

Details of the location of the four instrument sites.

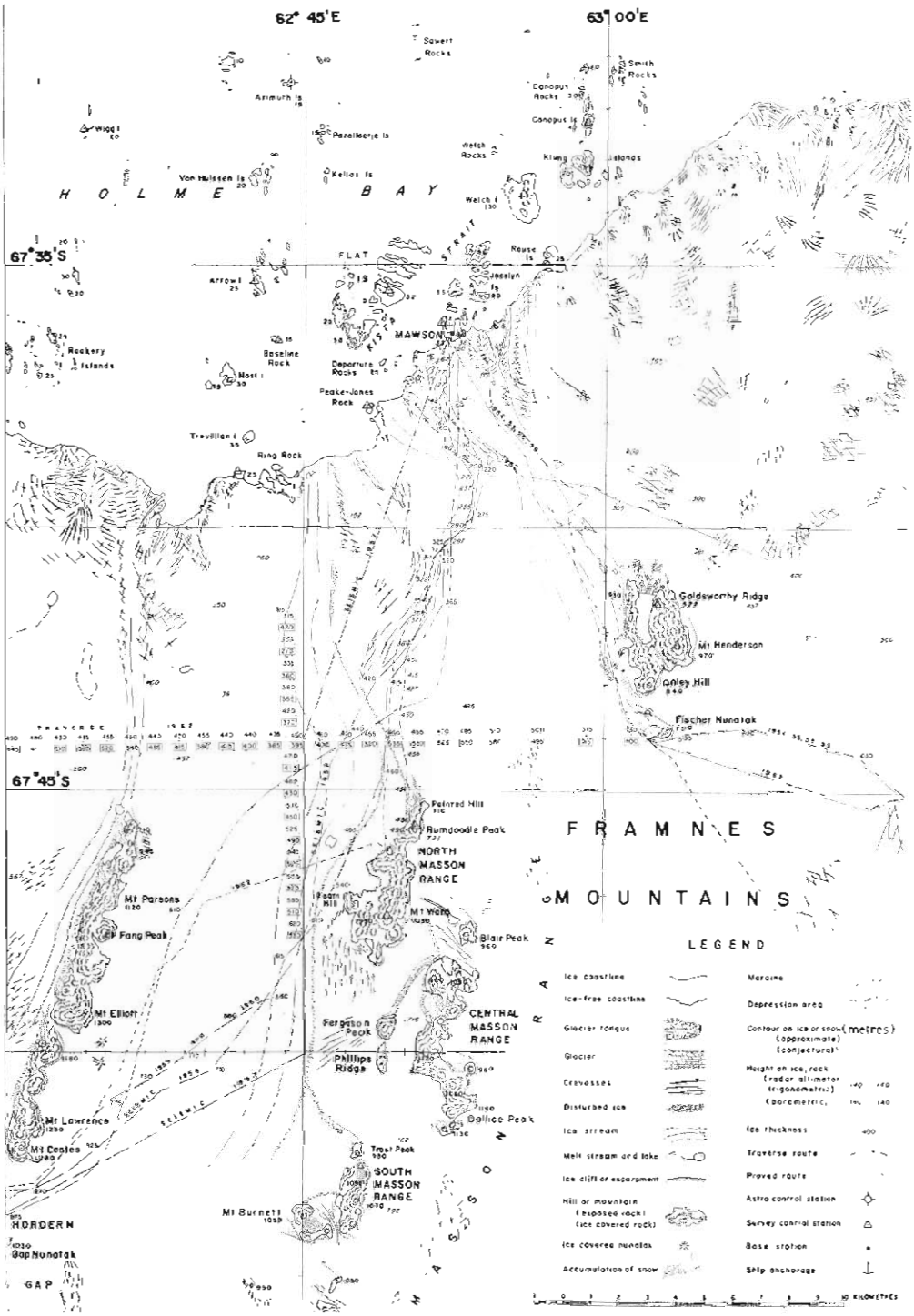

MAP 2
Area around Mawson.

APPENDIX III

DATA TABLES

Contents

Tables 12-16: Column 2: V_4 wind speed at 4 metres height
,, 3: V_1 wind speed at 1 metre height
,, 4: z_0 roughness parameter
,, 6: u^* friction velocity
,, 7: A_a exchange coefficient for adiabatic temperature profiles at 2 metres height
,, 8: $\frac{d\theta}{dz}$ potential temperature gradient at 2 metres height
,, 9: T air temperature at 2 metres height
,, 10: Ri Richardson number at 2 metres height
,, 11: A exchange coefficient for non-adiabatic conditions
,, 12: Q daily eddy heat flux

All the above are mean daily values. All temperature data at wind speeds less than 2 m sec^{-1} have been deleted (see Table III, calibration data).

17 Frequency distribution of daily mean Richardson numbers: sea ice.
18 Eddy heat flux: plateau: May: daily values.
19 Eddy heat flux: plateau: June: daily values.
20 Eddy heat flux: plateau: July: daily values.
21 Eddy heat flux: plateau: August: daily values.
(Tables 18-21: Columns 1-12 same as for Tables 12-16; all the above are mean daily values for site 2.)
22 Eddy heat flux: plateau: December 10 p.m.-4 a.m. period.
23 Eddy heat flux: plateau: December 4 a.m.-10 a.m. period.
24 Eddy heat flux: plateau: December 10 a.m.-4 p.m. period.
25 Eddy heat flux: plateau: December 4 p.m.-10 p.m. period.
26 Eddy heat flux: plateau: January 10 p.m.-4 a.m. period.
27 Eddy heat flux: plateau: January 4 a.m.-10 a.m. period.
28 Eddy heat flux: plateau: January 10 a.m.-4 p.m. period.
29 Eddy heat flux: plateau: January 4 p.m.-10 p.m. period.
(Tables 22-29: Columns 1-12 same as for Tables 12-16, but for 6-hourly mean values. All at site 3.)
30 Comparison between eddy heat flux computations for daily means and sum of 6-hourly means: plateau: December.
31 Frequency distribution of Richardson numbers at all three measuring sites.
32 Daily midnight sea-ice temperatures: May to July.
33 Daily midnight sea-ice temperatures: August to September.
34 Daily midnight sea-ice temperatures: October to November.
(Columns 2-8 and 9-15 give the ice temperatures at 0, 15, 30, 45, 60, 80 and 100 cm depth below the surface.)
35 Daily midnight plateau-ice temperatures: 1 metre depth.
36 Daily midnight plateau-ice temperatures: 2 metres depth.
37 Daily midnight plateau-ice temperatures: 4 metres depth.
38 Daily midnight plateau-ice temperatures: 8 metres depth.
(Tables 35-38: March to November, at site 2. Values in brackets are graphically extrapolated.)
39 Daily midnight plateau-ice temperatures: November to December.
40 Daily midnight plateau-ice temperatures: January to February.
(Columns 2-9: ice temperatures at 0, 0·5, 1, 2, 4, 6, 8 and 11 metres depth.)
41 Daily midnight heat flux plate readings: sea ice: 30 cm depth (conversion factors in Table V.)
42 Daily maximum and minimum heat flux plate readings: sea ice 30 cm depth (Columns 2, 4, 6, 8, 10 and 12: local time = solar time minus two hours, time in hours. Conversion factors in Table V.)
43 Daily midnight heat flux plate readings: plateau ice: 1, 2 and 4 metres depth. (Columns 2, 3 and 4, etc., are heat fluxes at 1, 2 and 4 metres depth. Conversion factors in Table V.)
44 Temperature and heat flux in sea ice: 30 cm depth: monthly means of hourly values for October. (column 1: solar time.)
45 Light extinction in plateau ice: March to April.

46 Light extinction in plateau ice: May to December.
(H_1, H_2 and H_4 are hemispherical downward fluxes, N_1, N_2 and N_4 are net fluxes of radiation at 1, 2 and 4 metres depth. Conversion factors in Table V.)

47 Ablation: plateau.
(Columns 1-5: site 2, columns 6-10: site 3.)

Column 4: $m = \sqrt{\frac{\Sigma V_i^2}{n(n-1)}}$ standard deviation of arithmetic mean.

Column 5: $\sigma = \sqrt{\frac{\Sigma V_i^2}{n-1}}$ standard deviation.

48 Ice density.

49 Sea-ice salinity.

TABLE 1

GENERAL METEOROLOGICAL DATA—MAWSON 1965—MONTHLY MEANS

1.	Jan.	Feb.	Mar.	Apr.	May	Jun.	Jul.	Aug.	Sep.	Oct.	Nov.	Dec.	Year	Mean for period 1956-65
2. Air temperature (°C) 2 m height	+0·1	−2·8	−11·1	−16·1	−12·9	−21·1	−21·7	−18·1	−20·3	−13·5	−7·7	−0·5	−12·2	−11·1
3. Wind speed (m/sec) 10 m height	8·4	9·4	9·2	7·5	10·5	6·1	8·0	10·5	9·8	10·5	9·8	8·4	9·0	10·0
4. Relative humidity (%) 2 m height	58	56	47	58	60	55	67	68	67	60	59	60	59	60
5. Sunshine (hours)	9 5	6·2	4·5	3·8	0·8	0	0·4	1·6	4·9	8·1	10·1	9·3	4·9	5·0
6. Total cloud cover (⅛ths)	4·5	4·8	4·2	4·4	4·6	2·6	3·5	5·0	3·7	4·0	4·5	4·7	4·2	4·6 (1962-5)
7. Sea level pressure (mb)	990·9	996·3	985·3	990·6	993·5	992·7	987·4	987·7	983·7	982·5	976·0	991·9	998·2	
8. Number of days of strong winds (> 11 m/sec)	22	26	28	24	27	21	29	30	29	31	30	29	326	
9. Number of days of gales (> 17 m/sec)	6	8	6	13	13	5	10	17	16	20	13	11	138	
10. Number of days of drifting snow	0	2	0	11	13	0	16	19	14	11	16	7	106	

TABLE 2

ANNUAL EXTREMES OF METEOROLOGICAL PARAMETERS

	1965
1. Maximum temperature	+8·8°C on 8 December
2. Minimum temperature	−34·6°C on 22 July
3. Maximum pressure	1016·4 mb on 23 May
4. Minimum pressure	942·7 mb on 2 November
5. Maximum wind speed	60·0 m/sec on 16 August

TABLE 3

GLOBAL RADIATION
cal $cm^{-2}day^{-1}$

1 Date	2 Jan.	3 Feb.	4 Mar.	5 Apr.	6 May	7 Jun.	8 Jul.	9 Aug.	10 Sep.	11 Oct.	12 Nov.	13 Dec.
1	795	364	(160)	134	29·4	1·5	0	13	82	330	205	810
2	705	477		112	25·3	1·0	0	12	110	123	387	845
3	728	591	(410)	161	22·6	1·0	0	13	129	207	419	853
4	489	487		157	16·1	0	0	15	87	352	337	806
5	656	461	(145)	(55)	17·9	0	0	18	138	340	447	376
6	785	585	(140)	59	18·5	0	1·0	13	143	374	593	576
7	840	472	(135)	(140)	16·7	0	1·5	20	61	372	369	794
8	790	556	317	(130)	26·5	0	0	34	61	362	675	848
9	706		(130)		5·0	0	0	23	162	387	679	846
10	658	(275)	(125)			0	0	24	152	410	506	867
11	760		235			0	1·9	27	94	427	695	880
12	711		309			0	2·7	24	108	322	726	755
13	545		286			0	1·6	43	164	193	681	683
14	535		285	(105)	15·4	0	1·5	45	193	191	734	865
15	369				7·5	0	1·0	17	157	299	735	880
16	556	(235)	(105)	(35)	10·1	0	1·0	21	179	370	519	416
17	558		(100)		11·2	0	4·4	27	125	339	732	773
18	436	(540)			9·9	0	4·0	37	224	467	436	620
19	695	(530)			5·2	0	2·7	42	234	492	725	463
20	475	(520)			6·9	0	5·0	32	126	438	768	748
21	445		270		3·0	0	5·8	42	236	318	740	886
22	757		236	29	5·2	0	4·6	34	126	478	571	886
23	714	(190)	82	23	3·4	0	4·2	46	261	520	716	487
24	417		228	46	1·7	0	6·7	80	222	523	601	520
25	732	(475)	222	42	3·9	0	5·7	83	279	531	536	439
26	712		207	58	3·9	0	5·2	56	204	492	780	377
27	430			56	4·3	0	7·6	46	208	555	793	526
28	335	(170)		50	2·3	0	12·0	55	268	411	787	401
29	672			22	2·3	0	12·3	87	236	478	803	379
30	530		(180)	21	0	0	10 7	109	299	585	811	461
31	631		(175)		0·3		13·0	60		562		862
Mean	617	433	204	76	10·2	0	5·0	39	169	394	616	675

TABLE 4

NOON ALBEDO: SEA ICE
per cent

1 Date	2 Jan.	3 Feb.	4 Mar.	5 Apr.	6 May	7 Jun.	8 Jul.	9 Aug.	10 Sep.	11 Oct.	12 Nov.	13 Dec.
1								78	73	65	78	
2									72	69	73	
3								76	71	56	61	
4								80	72	58	67	
5								83	71	52	60	
6								75	71	49	64	
7							72	72	83	48	61	
8							64	62		47	50	
9								76	72	44	46	
10									68	44	49	
11							69	81	81	43	43	
12								79	82	45	40	
13							79	74	76	89	38	
14							82	74	72	86	37	
15							75		73	76	37	
16							78		71	75	41	
17							63			80	36	
18							68		66	76		
19							80	73	66	73		
20							64	84	67	69		
21							62	77	66	65		
22							84	82	71	51		
23							82	77	64	45		
24							83	74	65	43		
25							85	74	64	41		
26								68	58	41		
27									63	40		
28							71	79	62	45		
29							65	72	73	41		
30							83	70	68	39		
31							80	76		38		
Mean							75	75	70	56	52	

TABLE 5

NOON ALBEDO: PLATEAU ICE
per cent
(S indicates snow cover over the ice surface)

1 Date	2 Jan.	3 Feb.	4 Mar.	5 Apr.	6 May	7 Jun.	8 Jul.	9 Aug.	10 Sep.	11 Oct.	12 Nov.	13 Dec.
1	64	59			87			73	70			59
2	67	53		66	74			69	62			56
3	65	55		63				69				57
4	72	56		64				67	69			56
5	63	55							65			66
6	76	59		83S	64		87	69	62			65
7	73	54			68		79	79	84S			56
8	73	55	63		60		75	71	82S			60
9	70	54	67		75S			68				62
10	70			77S	74S			79S				64
11	70		60		56		75	79S				59
12	70		64		57		79	78S				65
13	73		63		60			77S				68
14	66		62		59		76					69
15	73				68		89S					70
16	69				66		93S					79
17	63						77S					51
18	69						82S					71
19	62											79
20	70		62		68		91S					64
21	71				76		81S				61	62
22	63		63	94S	63						66	61
23	66		61	93S	81						59	70
24	68		64	79S	93S		87S				60	72
25	62		63	76S			83S				71	75
26	63		65	65	96S		78S	69			53	77
27	71			64			68	74			57	72
28	64			59			69	71			57	73
29	59			76			67	66			59	76
30	59			87			76				57	73
31	56						71					60
Mean	67	56	63	75	71		79	72	71		60	66

TABLE 6

NET ALL-WAVE RADIATION: SEA ICE
cal $cm^{-2}day^{-1}$

1 Date	2 Jan.	3 Feb.	4 Mar.	5 Apr.	6 May	7 Jun.	8 Jul.	9 Aug.	10 Sep.	11 Oct.	12 Nov.	13 Dec.
1							140	85	40	75	—	
2							154	23	109	20	—	
3							61	80	71	−26	—	
4							—	105	78	−26	−34	
5							112	94	107	−13	−56	
6							130	78	50	0	—	
7							82	160	—	− 38	−48	
8							64	141	—	−56	−101	
9							54	—	—	− 31	−164	
10							78	—	64	−27	−132	
11							91	102	13	−33	−161	
12							131	149	18	−62	−214	
13							83	142	48	− 40	−118	
14							36	152	122	—	−145	
15						76	75	—	116	−17	−232	
16						151	73	—	55	18	−10	
17						84	141	—	—	43		
18						68	163	—	100	86		
19						86	157	92	101	85		
20						128	161	15	42	20		
21						112	163	66	93	—		
22						155	114	24	35	−64		
23						107	33	60	88	−66		
24						160	138	96	64	−87		
25						160	115	46	104	−91		
26						153	9	25	52	−91		
27						97	39	7	90	−114		
28						152	141	3	40	−96		
29						161	150	32	−18	−267		
30						164	108	83	58	−210		
31							114	33		−160		
Mean						126	104	75	67	−43	−118	

TABLE 7

NET ALL-WAVE RADIATION: PLATEAU
cal $cm^{-2}day^{-1}$

1 Date	2 Jan.	3 Feb.	4 Mar.	5 Apr.	6 May	7 Jun.	8 Jul.	9 Aug.	10 Sep.	11 Oct.	12 Nov.	13 Dec.
1	−125	−97	(4)	55	126	70	117	9	16	88	−29	−116
2	−93	−87		33	26	118	115	20	113	28	−54	−133
3	−100	−99	(54)	92		119	69	76	149	−13	−69	−130
4	−48	−85				55	16	107	73	35	−34	−160
5	−97	−90	(8)	(22)	34	106	111	96	146		−66	−62
6	−41	−91	(8)	46	101	111	106	74	126	(50)	−83	−117
7	−38	−81	(8)	55	84	115	53	175	23	68	−38	−184
8	−19	−72	34	(144)	174	56	47	148	23	34	−38	−145
9	−52		(8)		24	16	49	46	127		−98	−94
10	−40	(−12)	(8)		24	105	64	35	67		−48	−72
11	−52		16		37	70	75	106	37	64	−69	−54
12	−46		35		162	61	103	162	12		−104	−50
13	−144		45		181	107	58	164	43	(−16)	−80	−61
14	−88		51	(154)	164	115	20	164	131	(−16)	−91	−147
15	−55				79	51	49	16	126	(−20)	−91	−13
16	−37	(−6)	(12)	(18)	98	108	51	−1	106		−70	−12
17	−85		(12)		165	76	102	42	33		−103	−59
18	−33	(12)			178	85	123	79	138		−51	−98
19	−97	(15)	107		175	82	116	90	141		−110	−59
20	−71	(18)	59		133	104	118	17	41		−103	−120
21	−21		90		3	82	123	66	96	(−30)	−120	−96
22	−67		110	(20)	2	120	86	38	40		−97	−94
23	−88	(0)	39	(20)	9	74	35	60	104		−134	−49
24	−40		68	94	12	119	143	123	64	−5	−123	−47
25	−64	(32)	86	75	20	120	75	172	127	−1	−104	−41
26	−78		66	163	163	108	10	83	88	−21	−131	−43
27	−59			165	147	67	39	2	120	−13	−125	−61
28	−68	(4)		131	73	106	167	28	25	−37	−127	−53
29	−99			16	28	115	158	105	−26	−34	−128	−54
30	−92		(124)	56	28	128	115	151	70	−25	−132	−88
31	−100		(126)		38		113	10		−70		−152
Mean	−69	−40	49	75	86	92	85	79	79	3	−88	−86

TABLE 8

DAILY MEAN AIR TEMPERATURES: METEOROLOGICAL SCREEN
(°C. Temperatures negative, unless positive sign shown)

1	2	3	4	5	6	7	8	9	10	11	12	13
Date	Jan.	Feb.	Mar.	Apr.	May	Jun.	Jul.	Aug.	Sep.	Oct.	Nov.	Dec.
1		+1·3	3·8	15·2	17·3	10·1	24·7	23·8	20·3	16·4	10·6	3·9
2		+2·1	2·4	16·2	12·9	15·4	24·6	17·4	23·1	13·0	7·1	4·7
3		+1·1	3·0	13·1	12·0	19·3	18·8	14·9	26·4	10·3	5·5	4·8
4		+0·6	5·4	14·1	10·9	21·3	13·0	20·8	23·7	10·7	6·1	1·9
5		1·6	4·7	13·2	8·0	21·3	15 0	24·3	24·2	13·5	7·8	+0·4
6		3·3	5·0	12·5	10·9	22·8	19·6	26·0	25·6	11·9	7·8	+2·9
7		3·6	5·3	14·7	11·7	24·5	18·8	25·5	24·7	13·8	10·3	+5·4
8		4·2	7·2	15·6	12·6	24·8	14·9	26·9	20·8	15·1	13·6	+5·1
9		3·5	8·3	19·7	7·9	18·2	14·8	22·6	22·4	16·2	12·9	+3·7
10		1·3	7·2	18·8	6·5	20·0	14·1	20·0	20·4	18·9	12·2	+0·7
11		0·0	7·9	18·6	7·7	22·1	18·4	22·5	17·1	20·2	11·6	1·0
12		+0·3	9·2	16·4	11·1	19·1	23·9	21·1	19 0	19·3	12·8	1·6
13		0·2	10·2	19·1	14·8	21·9	22·4	21·7	21·3	13·7	11·3	0·6
14		1·1	10·1	22·2	16·4	20·8	14·5	24·2	23 2	11·1	11·2	0·3
15		1·8	12·2	25·5	17·3	18·3	18·1	19·7	18·2	5·6	10·4	1·4
16		0·9	7·4	19·6	19·0	21·8	21·6	14·4	15·5	8·0	6·0	2·2
17		+1·9	8·3	20·4	21·1	17·4	22·9	13·7	9·2	11·4	6·2	1·0
18		0·9	10·8	22·7	23·9	18·9	27·6	14·8	12·3	13·0	7·2	1·6
19		5·4	12·2	24·3	23 6	17·6	30·2	18 8	17·6	15·1	4·9	0·4
20		7·1	14·2	21·9	18·5	21·9	31·0	11·2	14·7	16·3	6·6	+1·6
21		7·1	17·2	15·6	9·9	22·8	32·8	7·8	16·5	12·1	6·0	+1·0
22		7·9	17·2	10·2	7·4	23·5	31·6	9·0	19·9	10·2	5·1	+0·2
23		6·9	17·6	6·8	5·6	21·1	24·9	9·5	22·0	13·8	3·0	2·1
24		7·1	18·4	6·8	8·1	22·3	23·9	10·6	21·1	12·9	3·5	0·6
25		5·7	19·6	5·9	10·7	22·8	23·5	13·8	21·4	12·9	1·8	1·8
26		4·3	19·3	9·9	16·1	25·6	16·8	16·9	23·4	13·4	3·1	0·8
27		4·1	16·4	12·5	13·8	23·7	15·6	13·6	23·6	13·7	4·7	+0·9
28		3·8	14·5	13·7	15·4	25·5	20·8	13·2	22·9	13·0	4·4	+0·7
29		—	11·0	13 5	11·0	25·1	25·1	14·5	17·1	8·8	3·6	+0·2
30		—	12·9	12·3	8·8	25·9	26·7	19 2	15·0	11·3	4·3	+1·6
31		—	17·1	—	8·2	—	24·2	18·6	—	11·7	—	+0·9
Mean		2·7	10·8	15·8	12·9	21·2	21·8	17·8	20·1	13·1	7·4	0·2

TABLE 9

DAILY MEAN AIR TEMPERATURES: SEA ICE, 2M HEIGHT
(Minus °C)

1	2	3	4	5	6	7	8	9	10	11	12	13
Date	Jan.	Feb.	Mar.	Apr.	May	Jun.	Jul.	Aug.	Sep.	Oct.	Nov.	Dec.
1							25·1	23·6	20·1	16·4	11·6	
2							24·0	17·5	22·5	13·4	6·8	
3					13·9		18·9	14·3	25·9	10·4	5·1	
4					12·7		13·4	20·6	23 4	10·8	6·1	
5					9·1		15·2	24·0	23·5	13·4	8·5	
6					12·4		19·7	25·3	24·6	11·7	7·9	
7					13·1		19·0	25·9	25·6	13·8	10·6	
8					13·9		14·5	26·4	21·3	15·6	12·8	
9					9·2		14·6	24·6	21·6	15·4	13·6	
10					7·3		13·0	22·7	21·3	19·0	12·6	
11							17·9	23·4	17·2	20·4	11·3	
12							23·5	22·2	18·3	20·0	13·4	
13							23·3	23·9	21·2	16 6	12·1	
14							14·2	24·9	23·2	14·5	12·2	
15							17·9	21·4	18·7	5·1	11·6	
16							21·5	19·7	16·6	8·1	6·8	
17						15·7	22·4	14 9	9·8	11·2	7·0	
18						17·9	27·2	14·7	12·3	12·8		
19						16·5	29·8	18·5	17·4	15·5		
20						20·3	30·7	12·2	16·4	16·3		
21						21·9	32·5	7·9	17·1	12·4		
22						22·5	31·7	9·3	20·1	10·4		
23						20·6	25·9	9·6	21·9	14·0		
24						21·6	23·8	10·4	20·5	12·9		
25						22·6	24·0	13·5	21·2	13·1		
26						25·3	18·3	16·9	23·3	13·9		
27						23·6	19·1	14·0	23·8	13·2		
28						25·3	20·9	14·7	23·3	13·5		
29						25·1	24·7	14 2	17·0	9·2		
30						26·0	26·7	18·6	14·8	10·9		
31							24·0	18·5		12·5		
Mean					11·5	21·8	21·9	18 3	20·1	13·4	10·0	

TABLE 10

DAILY MEAN AIR TEMPERATURES: PLATEAU, 2M HEIGHT
(All temperatures negative unless positive sign shown)

1 Date	2 Jan.	3 Feb.	4 Mar.	5 Apr.	6 May	7 Jun.	8 Jul.	9 Aug.	10 Sep.	11 Oct.	12 Nov.	13 Dec.
1	+1·5	2·8		20·8	19·6		27·8	24·5	20·8			3·0
2	+2·4	2·3		20·7	16·2		28·0	18·0	25·2			4·6
3	+1·4	2·2		14·7			19·9	16·6				3·7
4	+2·2	2·8		15·3			13·3	23·4	24·9			2·8
5	+2·3	4·4			8·5		15·9	26·1	26·3			0·8
6	+2·9	3·6		13·5	11·7		21·2	26·9	26·6			+1·5
7	+1·7	5·2		17·3	12·1		16·4	28·9	25·6			+4·0
8	+0·7	6·9	8·5		12·0	23·6	16·8	26·5	22·3			+4·3
9	0·7	9·3	10·5		9·1	17·9		24·0				+3·0
10	+1·1		8·4		6·8			20·9				+1·2
11	+0·5		10·1		10·1			24·2				0·6
12	+0·2		12·6		12·9			22·1				1·3
13	1·7		12·1		16·5			22·7				0·4
14	2·6		12·4		18·8		16·7					+1·3
15	3·0					21·0	19·1					0·0
16	+0·8				21·2	23·2	23·5					3·3
17	+1 9					19·6	24 1					1·1
18	+1·3					21·4						2·7
19	0·6		13·2			19·2						1·1
20	1·3		15·8		21·1	24·6	32·6					+0·8
21	1·2		19·9		11·3	24·8	33·9				3·0	+1·7
22	0·7		18·3	9·7	7·1	24·7					5·7	+1·8
23	2·5		19·8	7·1	5·8	23·5					3·5	2·5
24	2·7		20·5	7·0	9·3	22·6	27·4				4·4	+0·7
25	2·1		21·3	8·1	9·9	24·0	25·0				2·3	2·5
26	1·7		21·5	11·6	17·9		17·0	17·4			2·0	1·0
27	4·6		20·9	15·4	16·1		15·9	13·5			4·9	+0·8
28	2·8			16·3			22·9	13·2			3·9	+0·3
29	+0·1			16·9		27·8	26·5	15·7			4·7	0·6
30	1·9			16·2		28·5	28·4	21 8			4·0	+1·1
31	1·3						25·9					+1·9
Mean	0·3	4·4	15·6	15·5	13·4	23·1	22·6	21·5	24·5		3·8	0·2

TABLE 11

DIURNAL TEMPERATURE AMPLITUDE IN SUMMER
(Monthly means of hourly values at 2 metres height)

°C

1 Hour	2 Dec.	3 Jan.
0	−2·9	−3·0
1	−3·2	−3·1
2	−3·2	−3·3
3	−3·1	−3·5
4	−2·6	−3·2
5	−2·3	−3·0
6	−1·9	−2·2
7	−1·3	−1·6
8	−0·6	−0·9
9	0·1	−0·1
10	0·8	0·9
11	1·4	2·1
12	1·9	2·9
13	2·1	3·6
14	2·7	3·3
15	3·2	3·1
16	2·3	3·0
17	1·3	2·1
18	0·9	1·4
19	1·0	0·3
20	0·0	−0·6
21	−0·9	−1·7
22	−2·2	−2·2
23	−2·7	−2·7
Amplitude (°C)	3·2	3·5

TABLE 12

EDDY HEAT FLUX: SEA ICE, JULY

1 Date	2 V_4 cm sec^{-1}	3 V_1 cm sec^{-1}	4 z_0 cm	5 $ln\ z/z_0$	6 u^* cm sec^{-1}	7 A_a	8 $d\theta/dz$ °C m^{-1}	9 T °K	10 Ri	11 A	12 Q cal cm^{-2}day^{-1}
1											
2											
3											
4											
5											
6											
7											
8	1250	1107	0·002	10·82	43·8	5·15	+0·0176	258	0·014	5·01	−18·3
9	1054	935	0·002	10·82	37·0	4·34	+0·0034	258	0 004	4·31	−3·0
10	926	810	0·005	9·90	35·1	4·12	+0·0151	260	0·018	3·98	−12·5
11	898	780	0·008	9·43	35·4	4·15	+0·0240	255	0·029	3·92	−19·5
12	275	238	0·011	9·11	11·2	1·31	+0·0101	249	0·127	1·03	−2·2
13	221	193	0·008	9·43	8·8	1·03	+0·0031	250	0·063	0·92	−0·6
14	826	713	0·013	8·95	34·1	4·00	−0·0079	259	−0·010	4·08	+6·7
15	817	716	0 040	7·82	39·2	1·60	+0·0074	255	0·007	4·54	−7·0
16	533	469	0·045	7·72	26·0	3·05	+0·0105	251	0·024	2·91	−6·3
17	615	531	0·013	8·95	25·4	2·98	+0·0167	251	0·040	2·76	−9·5
18	392	341	0·009	9·31	15·7	1 84	+0·0034	246	0·022	1·76	−1·2
19	560	483	0·012	9·02	22·9	2·69	+0·0130	243	0·040	2·49	−6·7
20	505	443	0·004	10·12	18·8	2·21	−0·0012	242	−0·006	2·24	+0·6
21	426	368	0·012	9·02	17·5	2 05	+0·0243	240	0·130	1·61	−8·1
22	748	658	0·004	10·12	27·8	3·26	+0·0074	241	0·016	3·16	−4·8
23	773	696	0·001	11·52	25·9	3·04	+0·0220	247	0·052	2·75	−12·5
24	653	565	0·010	9·21	26·3	3·08	+0·0136	249	0·031	2·90	−8·2
25	1287	1147	0·001	11·52	42·6	5·00	+0·0312	249	0·027	4·75	−30·7
26											
27											
28	407	356	0·004	10·12	15·1	1·77	+0·0057	252	0·039	1·64	−1·9
29	792	676	0·028	8·18	35·4	4·16	+0·0105	248	0·013	4·05	−8·8
30	612	538	0·005	9·90	23·3	2 73	+0·0394	246	0·116	2·19	−17·8
31	661	565	0·026	8·25	29·4	3·45	+0·0274	249	0 050	3·13	−17·7
Mean			0·012				+0 0135		0·038	3·00	−8·7

TABLE 13

EDDY HEAT FLUX: SEA ICE, AUGUST

1 Date	2 V_4 cm sec^{-1}	3 V_1 cm sec^{-1}	4 z_0 cm	5 $ln\ z/z_0$	6 u^* cm sec^{-1}	7 A_a	8 $d\theta/dz$ °C m^{-1}	9 T °K	10 Ri	11 A	12 Q cal cm^{-2}day^{-1}
1	1474	1292	0·005	9·90	55 9	6·45	0·0037	249	0·002	6·42	−4·9
2	2140	1888	0·003	10·40	77·7	8 98	0 0159	255	0·004	8·92	−29·4
3											
4	372	326	0·010	9·20	15·2	1·76	0·0108	252	0·073	1·53	−3·4
5	386	325	0·045	7·70	18·1	2·09	0·0141	249	0·068	1·83	−5·3
6	1356	1162	0·020	8·52	58·5	6 76	0·0087	248	0·004	6·71	−12·1
7	1286	1129	0·005	9·90	48·8	5·64	0·0300	247	0·020	5·42	−33·6
8	438	369	0·050	7·60	20 8	2·40	0·0120	247	0·044	2·20	−5·5
9	1000	856	0·028	8 18	44·8	5·18	0·0275	248	0·022	4·97	−28·3
10	505	442	0·005	9·90	19·1	2 20	0·0020	250	0·009	2·16	−0·9
11	489	427	0·006	9·71	18·8	2·17	−0·0010	250	−0·005	2·19	+0·5
12	692	600	0·012	9·02	28·5	2·29	0·0146	251	0·028	2·17	−6 6
13											
14	706	618	0·006	9·71	27·2	3·14	0·0050	248	0·011	3·07	−3·2
15	1151	968	0·065	7·33	56·5	6 53	0·0217	252	0·011	6·40	−28·7
16											
17											
18											
19	837	722	0·014	8·87	34·9	4·03	0·0037	255	0·005	4·00	−3·1
20	1350	1170	0·013	8·95	56·0	6 47	0·0040	261	0·002	6·45	−5·3
21	1091	936	0·022	8·42	47·6	5·50	−0·0043	265	− 0·003	5·53	+4·9
22											
23											
24											
25											
26											
27											
28											
29											
30	511	432	0·036	7·94	23·3	2·69	0·0277	254	0·079	2·31	−13·2
31	518	456	0·004	10·12	19·3	2·83	0 0022	254	0·009	2·19	−1·0
Mean			0·019				0·0110		0·021	4·14	−10·0

TABLE 14

EDDY HEAT FLUX: SEA ICE, SEPTEMBER

1 Date	2 V_4 cm sec^{-1}	3 V_1 cm sec^{-1}	4 z_0 cm	5 $ln\ z/z_0$	6 u^* cm sec^{-1}	7 A_a	8 $d\theta/dz$ °C m^{-1}	9 T °K	10 Ri	11 A	12 Q cal cm^{-2}day^{-1}
1	804	701	0·006	9 71	30·9	3·58	0·0077	253	0·013	3·49	−5·6
2	541	467	0·013	8·95	22·3	2·59	0·0269	250	0·085	2·12	−11·8
3	685	591	0·012	9·02	28·1	3·26	0·0182	247	0·037	3·04	−11·5
4	1094	933	0·030	8·10	49·3	5·72	0·0143	250	0·009	5·62	−16·6
5	978	835	0·026	8·25	43·3	5·03	0·0182	249	0·015	4·88	−18·4
6	496	426	0·018	8·62	21·2	2·46	0·0315	248	0·111	1·99	−13·0
7	1045	900	0·016	8 74	44·1	5·12	0·0034	247	0·003	5·10	−3·6
8											
9											
10	1960	1720	0·005	9·90	74·5	8·65	0·0417	252	0·012	8·45	−73·0
11											
12											
13	1383	1198	0·012	9·02	56·9	6·60	0·0134	252	0·006	6·52	−18·1
14	1087	945	0·009	9·31	43·5	5·05	0·0265	250	0·022	4·84	−26·6
15	1563	1360	0·010	9·21	63·3	7·35	−0·0148	254	−0·006	7·44	+22·8
16	1328	1118	0·056	7·48	64·0	7·43	0·0083	256	0·003	7·38	−12·7
17	1703	1445	0·040	7·82	79·2	9·20	0·0023	263	0·001	9·20	−4·4
18	1113	954	0·025	8 29	49·3	5·72	−0·0006	261	0	5·72	+0·7
19	1703	1457	0·026	8·25	75·5	8·75	0·0025	256	0 001	8·75	−4·5
20	2038	1758	0·015	8·80	85·5	9·92	0·0145	257	0·003	9·86	−29·6
21	894	761	0·030	8·10	40·3	4·68	0·0661	256	0·062	4·15	−56·8
22	1045	883	0·042	7·78	48·6	5·65	0·0093	253	0·006	5·59	−10·8
23	626	537	0·022	8·42	27·3	3·17	0·0735	251	0·154	2·38	−36·2
24											
25	625	535	0·022	8·42	27·2	3·16	0·0346	252	0·073	2·74	−19·6
26	1426	1209	0·040	7·82	66·2	7·69	0·0244	250	0·009	7·55	−38·2
27	856	730	0·030	8·10	38·6	4·48	0·0432	249	0·046	4·10	−36·7
28	850	725	0·028	8·18	38·0	4·41	0·0380	250	0·041	4·07	−32·0
29	1871	1650	0·003	10·40	68·0	7·89	0	256	0	7·89	−0
30	943	820	0·009	9·31	37·7	4·37	0·0286	258	0·031	4·11	−24·3
31											
Mean			0·022				0·0213		0·029	5·48	−19·2

TABLE 15

EDDY HEAT FLUX: SEA ICE, OCTOBER

1 Date	2 $V_{.1}$ cm sec^{-1}	3 V_1 cm sec^{-1}	4 z_0 cm	5 $ln\, z/z_0$	6 u^* cm sec^{-1}	7 A_a	8 $d\theta/dz$ °C m^{-1}	9 T °K	10 Ri	11 A	12 Q cal cm^{-2}day^{-1}
1	1161	1020	0·005	9·90	44·2	4·97	0·0173	257	0·014	4·84	−17·3
2	1126	976	0·011	9·11	45·9	5·17	0·0044	260	0·003	5·14	−4·7
3	1464	1260	0·018	8·62	62·6	7·05	0·0071	263	0·003	7·01	−10·3
4	1254	1104	0·003	10·40	45·5	5·12	0·0284	262	0·020	4·93	−29·0
5	490	431	0·004	10·12	18·2	2·05	0·0247	260	0·113	1·65	−8·5
6	750	659	0·004	10·12	27·9	3·14	0·0195	261	0·038	2·92	−11·8
7	1141	1006	0·003	10·40	41·4	4·66	0·0240	259	0·021	4·48	−22·3
8	1070	933	0·007	9·55	41·8	4·71	0·0290	257	0·025	4·49	−27·0
9	622	538	0·014	8·87	25·9	2·92	0·0368	258	0·084	2·49	−19·0
10	1237	1085	0·004	10·12	46·0	5·18	0·0228	254	0·017	5·00	−23·6
11	892	788	0·002	10·82	31·2	3·51	0·0532	253	0·085	2·98	−32·8
12	1060	935	0·004	10·12	39·6	4·46	0·0171	253	0·017	4·31	−15·3
13	2395	2061	0·019	8·57	103·0	11·60	0·0171	256	0·003	11·53	−40·8
14											
15											
16											
17											
18	552	487	0·004	10·12	20·6	2·32	0·0256	260	0·091	1·95	−10·3
19	1193	1024	0·021	8·46	51·8	5·83	0·0410	257	0·023	5·58	−47·3
20	1906	1620	0·038	7·87	88·1	9·92	0·0154	257	0·003	9·86	−31·4
21	2410	2043	0·040	7·82	112.0	12·60	0·0253	261	0·003	12·52	−65·5
22	1461	1256	0·020	8·52	63·1	7·10	0·0235	263	0·009	6·98	−34·0
23	1215	1060	0·007	9·55	47·5	5·35	0·0244	259	0·016	5·18	−26·2
24	1085	942	0·009	9·31	43·3	4·88	0·0334	260	0·027	4·63	−32·0
25	715	628	0·004	10·12	26·6	2·99	0·0605	260	0·129	2·35	−29·4
26	1158	995	0·020	8·52	50·0	5·63	0·0197	259	0·012	5·50	−22·4
27	490	432	0·004	10·12	18·3	2·06	0·0490	260	0·221	1·38	−14·0
28	1635	1442	0·003	10·40	59·5	6·70	0·0065	259	0·003	6·66	−9·0
29	2068	1825	0·003	10·40	75·2	8·46	0·0099	264	0·003	8·42	−17·2
30											
31	648	563	0·009	9·31	25·9	2·92	0·0182	260	0·041	2·69	10·1
Mean			0·011				0·0251		0·039	5·21	−27·4

TABLE 16

EDDY HEAT FLUX: SEA ICE, NOVEMBER

1 Date	2 V_4 cm sec^{-1}	3 V_1 cm sec^{-1}	4 z_0 cm	5 $ln\ z/z_0$	6 u^* cm sec^{-1}	7 A_a	8 $d\theta/dz$ °C m^{-1}	9 T °K	10 Ri	11 A	12 Q cal cm^{-2}day^{-1}
1											
2											
3											
4											
5	1351	1160	0·020	8·52	58·5	6 50	+0·0160	264	+0 007	6·42	−21·3
6	882	763	0·013	8·95	36·5	4·05	−0·0055	265	· 0·006	4·10	+4·7
7	1364	1180	0·012	9·02	56·0	6·22	− 0·0120	262	+0·006	6·15	+15·3
8	578	501	0·008	9·43	22·8	2·53	−0·0685	260	−0·199	3·64	+51·6
9	869	756	0·007	9·55	33·9	3·76	−0·0386	259	−0·051	4·15	+33·2
10	1302	1126	0·014	8·87	54·3	6·03	−0 0296	260	−0·015	6·22	+38 0
11	705	611	0·011	9·11	28·7	3·18	−0·0435	262	−0·079	3·70	+33·4
12	1178	1022	0·010	9·21	47 5	5·27	−0·0590	260	−0 040	5·70	+69 5
13	1367	1184	0·012	9·02	56·2	6 25	+0·0028	261	+0 001	6 24	−3·6
14	815	800	0·007	9·55	35·8	3·98	−0·0485	261	−0·057	4·44	+44·5
15	1110	961	0·011	9·11	45·2	5 02	−0·0618	261	− 0·046	5·50	+70·4
16	1124	970	0·014	8·87	46·8	5·20	+0·0368	266	+0·025	4·95	· 37·7
17	1028	897	0·007	9 55	40·2	4·46	+0 0078	266	+0 007	4·40	−7·1
18											
19											
20											
21											
22											
23											
24											
25											
26											
27											
28											
29											
30											
31											
Mean			0·011				−0·0233		−0·034	5·05	+22·4

TABLE 17

FREQUENCY DISTRIBUTION OF RICHARDSON NUMBERS (DAILY MEANS): SEA ICE

1	2	3	4	5	6	7	8	9	10	11	12	13	14	15	16	17	18	19	20	21	22
< 010	·010 to −·001	0	·001 to ·01	·011 to 02	·021 to ·03	·031 to ·04	·041 to ·05	·051 to 06	061 to ·07	·071 to ·08	·081 to ·09	·091 to ·10	·101 to ·11	·111 to ·12	·121 to ·13	·131 to ·14	·141 to ·15	·151 to ·16	·161 to ·17	171 to 18	>0 18
−·199	− 010	0	·004	·014	·029	040	·050	·052	·063	073	·085	·091		·116	·127			·154			221
−·051	−·006	0	·007	·018	·024	·040	·044		·068	·079	·084			·111	·130						
−·015	− 005		002	·016	·022	·031	·046		·062	·073	·085			·113	·129						
−·079	−·003		·004	·013	027	039	·041														
−·040	−·006		·004	020	·022	·037	·041														
− 057	−·006		·009	011	·028	031															
·046			·005	011	·022	·038															
			·002	·013	·021																
			009	·015	·025																
			·009	·012	·023																
			·003	014	·027																
			006	·020	025																
			·003	·017																	
			·001	·017																	
			·001	·016																	
			·003	012																	
			·006																		
			·009																		
			·003																		
			·003																		
			·003																		
			·003																		
			·003																		
			009																		
			·003																		
			·003																		
			·007																		
			·006																		
			·001																		
			·007																		
7	6	2	30	16	12	7	5	1	3	3	3	1	0	3	3	0	0	1	0	0	1

TABLE 18

EDDY HEAT FLUX: PLATEAU, MAY

1 Date	2 V_4 cm sec^{-1}	3 V_1 cm sec^{-1}	4 z_0 cm	5 $ln\ z/z_0$	6 u^* cm sec^{-1}	7 A_a	8 $d\theta/dz$ °C m^{-1}	9 T °K	10 Ri	11 A	12 Q cal cm^{-2}day^{-1}
1											
2											
3											
4											
5											
6											
7											
8	1051	824	0·730	4·91	71·8	8·23	+0·071	261	+0 021	7·90	−116·0
9											
10											
11											
12											
13	730	(584)	0·380	5·57	44·9	5 15	+0·130	257	+0·098	4·27	−114·2
14	544	(435)	0 380	5·57	33·4	3·82	+0·172	254	+0 238	2 50	−89·1
15											
16	437	351	0 380	5·57	27·0	3·10	+0·068	252	+0·145	2 37	−33 4
17											
18											
19											
20	960	(768)	0·380	5·57	59·0	6·75	+0·001	252	+0 001	6·75	−1·5
21	(250)	209	0·380	5·57	16·1	1·84	+0·045	262	+0·189	1·30	−12·2
22	1430	(1143)	0·380	5·57	87 8	10·05	+0·059	266	+0·012	9 80	−120·7
23	865	(692)	0·380	5·57	53·2	6·10	+0 034	267	+0 017	5·90	−41·0
24	961	(770)	0·380	5·57	59 2	6·79	−0·026	264	−0·011	6·93	+37·1
25							+0·062		0·079		−54·5
26											
27											
28											
29											
30											
31											
Mean							+0·062		0·079		−54·5

TABLE 19

EDDY HEAT FLUX: PLATEAU, JUNE

1 Date	2 V_4 cm sec^{-1}	3 V_1 cm sec^{-1}	4 z_0 cm	5 $ln\ z/z_0$	6 u^* cm sec^{-1}	7 A_a	8 $d\theta/dz$ °C m^{-1}	9 T °K	10 Ri	11 A	12 Q cal cm^{-2}day^{-1}
1											
2											
3											
4											
5											
6											
7											
8	(620)	517	0·380	5·57	39·7	4·68	0·035	249	0·035	4·38	−31·5
9	(1130)	942	0·380	5·57	72·4	8·55	−0·024	255	−0·006	8·65	+42·5
10											
11											
12											
13											
14											
15	403	(322)	0·380	5·57	24·7	2·92	0·030	252	0·077	2·52	−15·8
16	750	(600)	0·380	5·57	46·1	5·45	0·120	250	0·089	4·60	−114·2
17	1233	(986)	0·380	5·57	75·8	8·95	0·119	253	0·032	8·41	−207·0
18	990	(792)	0·380	5·57	60·9	7·19	−0·008	252	−0·003	7·24	+11·3
19	1150	(920)	0·380	5·57	70·7	8·35	−0·015	254	−0·004	8·40	+26·2
20	842	(674)	0·380	5·57	51·8	6·11	−0·026	248	−0·015	6·30	+33·8
21	712	(570)	0·380	5·57	43·8	5 17	0·005	248	0·004	5·13	−5·7
22	877	(702)	0·380	5·57	53·9	6·35	0·092	248	0·050	5·78	−109·8
23	455	(364)	0·380	5·57	28·0	3·30	0·242	250	0·485	1·50	−75·3
24	(1005)	837	0·380	5·57	64·3	7·60	0·178	250	0·068	6·66	−245·5
25	(808)	673	0·380	5·57	51·7	6·10	0·087	249	0·052	5·52	−98·7
26											
27											
28											
29											
30											
31											
Mean							0·064		0·066		−60·7

TABLE 20

EDDY HEAT FLUX: PLATEAU, JULY

1 Date	2 V_4 cm sec^{-1}	3 V_1 cm sec^{-1}	4 z_0 cm	5 $ln\ z/z_0$	6 u^* cm sec^{-1}	7 A_a	8 $d\theta/dz$ °C m^{-1}	9 T °K	10 Ri	11 A	12 Q cal cm^{-2}day^{-1}
1	1270	1052	0·11	8·20	66·5	7·78	0·015	245	0·004	7·72	—24·2
2	1057	868	0·17	7·75	58·4	6·82	0·034	245	0·017	6·60	—45·8
3	1390	1130	0·23	7·46	80·0	9·36	0·097	253	0·022	8·97	—180·2
4	2392	1958	0·18	7·70	133·0	15·56	—0·026	260	0	7·78	+37·9
5	467	387	0·10	8·29	24·1	2·82	0·324	257	0·850	0·83	—55·6
6	984	808	0·16	7·82	53·9	6·30	0·130	252	0·069	5·52	—148·2
7	789	641	0·23	7·46	45·3	5·30	0·133	257	0·099	4·39	—120·7
8	1126	940	0·80	8·52	56·5	6·62	0·065	256	0·030	6·25	—83·8
9											
10											
11											
12											
13											
14	642	522	0·23	7·46	36·9	4 32	0·040	256	0·043	3·98	—32·9
15	763	642	0·06	8·79	37·2	4·36	0·006	254	0·009	4·28	—5·8
16	648	542	0·08	8·52	32·6	3·82	0·034	250	0·048	3·48	—24·2
17	565	476	0·06	8·79	27·5	3·22	0·152	249	0·320	1·85	—58·5
18											
19											
20	513	416	0·24	7·41	29·7	3·48	0·236	241	0·436	1·69	—107·5
21	533	440	0·16	7·82	29·2	3·42	0·139	239	0·268	2·13	—61·5
22											
23											
24	479	390	0·16	7·82	26·2	3 06	0·307	246	0·713	1·04	—66·2
25	1333	1098	0·15	7·90	72·3	8·46	0·099	248	0·030	8·00	—165·0
26	1744	1463	0·07	8·65	86·5	10·12	0·018	256	0·004	10·04	—38·3
27	1518	1274	0·07	8·65	75·2	8 80	0·030	257	0·009	8·65	—54·3
28	786	652	0·08	8·52	39·5	4·62	0·069	250	0·069	4·05	—58·1
29	820	680	0·11	8·20	42·8	3·02	0·018	247	0·017	2·92	—11·2
30	665	555	0·08	8·52	33·4	3·90	0·066	245	0·095	3·26	—44·5
31	511	407	0·40	6·92	31·7	3·70	0·146	247	0·233	2·43	—73·5
Mean			0·15				0·097		0·154		—64·6

TABLE 21

EDDY HEAT FLUX: PLATEAU, AUGUST

1 Date	2 V_4 cm sec^{-1}	3 V_1 cm sec^{-1}	4 z_0 cm	5 $ln\ z/z_0$	6 u^* cm sec^{-1}	7 A_u	8 $d\theta/dz$ °C m^{-1}	9 T °K	10 Ri	11 A	12 Q cal cm^{-2}day^{-1}
1	1387	1135	0·180	6·32	76·9	8·85	0·029	249	0·008	8·72	−52·5
2	2070	1648	0·380	5·57	126·6	14·56	0·002	255	0	14 55	−6·5
3	1076	930	0·019	8·57	46·4	5·35	0·040	256	0·028	5·07	−42·1
4	505	426	0·070	7·26	25·1	2 89	0·071	250	0·177	2 09	−31·0
5											
6	1403	1170	0·110	6·80	73 6	8 46	0·054	246	0·016	8·21	−91·8
7	1547	1312	0·034	7·99	70·3	8·09	0·025	244	0 008	7·96	−40·8
8	563	456	0·270	5·91	33·0	3 80	0·070	247	0·103	3·12	−45·5
9	1369	1150	0·070	7·26	67·8	7 80	0·044	249	0 015	7·58	−69·4
10	948	813	0·019	8·57	40·6	4·67	0·019	252	0·018	4·51	−18·0
11	585	496	0·034	7·99	26·6	3 06	0·064	249	0·142	2·35	−30·9
12	894	752	0·070	7·26	44·3	5·09	0·105	251	0·083	4·33	−94·0
13	370	308	0·110	6·80	19·4	2·23	0 253	250	0·833	0·66	−34·5
14											
15											
16											
17											
18											
19											
20											
21											
22											
23											
24											
25											
26	1083	873	0·270	5·91	63·2	7·27	0 068	256	0·003	7·24	−11·4
27	1810	1528	0 070	7·26	90 1	10·36	0·012	260	0 002	10·32	−25·4
28											
29											
30											
31											
Mean			0·122				0 057		0·103		−42·4

TABLE 22

EDDY HEAT FLUX: PLATEAU, DECEMBER
10 p.m.-4 a.m. period

1 Date	2 V_4 cm sec^{-1}	3 V_1 cm sec^{-1}	4 z_0 cm	5 $ln\ z/z_0$	6 u^* cm sec^{-1}	7 A_a	8 $d\theta/dz$ °C m^{-1}	9 T °K	10 Ri	11 A	12 Q cal cm^{-2}
1	885	725	0·180	6·32	49·1	5 30	+0·072	265	0·044	4·87	−18·2
2	862	653	0·230	6·10	45·8	4·95	+0·027	266	0·019	4·77	−6·7
3	958	786	0·180	6·33	53·1	5·73	+0·040	264	0·021	5·50	−11·4
4	914	751	0·180	6·33	50·8	5·49	+0·070	266	0·040	5·07	−18·4
5	1175	982	0·090	7·05	59·6	6 44	+0·018	270	0·007	6·35	−5·9
6	1038	856	0·150	6·51	56·3	6 08	+0·026	271	0·012	5·94	−8·0
7	1437	1120	0·720	4·94	97·0	10 48	−0·010	274	0·002	10·52	+5·5
8	876	730	0 110	6·84	45 7	4 94	+0 264	277	+0·179	3·55	−48·7
9											
10											
11	790	665	0·070	7·28	39·1	4 22	+0·094	269	0·090	3·55	−17·3
12											
13	705	575	0·230	6·10	40·3	4 35	+0·016	269	0·014	4·23	−3·5
14	613	484	0·530	5·27	39·3	4·24	+0·052	271	0·049	3·85	−10·4
15	691	576	0·090	7 05	35·0	3·78	+0·151	268	0·180	2·72	−21·4
16	802	679	0·050	7 62	38·1	4 11	+0·003	268	0·003	4·09	−0·6
17	962	795	0·110	6·84	49·7	5·37	+0·009	269	0·005	5·32	−2·5
18	782	635	0·270	5·94	45·8	4 95	+0·019	269	0·013	4·82	−4·8
19	1099	915	0·110	6·84	57·3	6·19	+0·043	271	0·019	5·96	−13·3
20	1369	1137	0·110	6·84	71·1	7·68	+0·181	272	0·052	6·94	−65·1
21	1130	940	0·110	6·84	58·8	6·35	+0·048	271	0·020	6·11	−15·2
22	381	321	0·070	7 28	18·9	2 04	+0·068	271	0 276	1·25	−4·4
23	1062	880	0·110	6·84	55·1	5·95	+0·045	269	0·022	5·69	−13·3
24											
25	600	492	0·180	6·33	33·3	3·60	+0 127	269	0·167	2·64	−17·4
26											
27											
28	1405	1189	0·050	7·62	66·8	7·21	+0·037	273	0·012	7·04	−13·5
29	1581	1247	0·530	5·27	101·3	10 94	+0 017	271	0·002	10·90	−9 6
30	1706	1444	0·034	8·02	77·1	8·33	+0·043	273	0·010	8·17	−18·3
Mean			0·187				+0·061		0·052	5·41	−14·3

TABLE 23

EDDY HAT FLUX: PLATEAU, DECEMBER
4 a.m.-10 a.m. period

1 Date	2 V_4 cm sec^{-1}	3 V_1 cm sec^{-1}	4 z_0 cm	5 $ln\ z/z_0$	6 u^* cm sec^{-1}	7 A_a	8 $d\theta/dz$ °C m^{-1}	9 T °K	10 Ri	11 A	12 Q cal cm^{-2}
1	765	622	0·230	6·10	43·6	4·71	+0·022	268	0·017	4·56	−5·2
2											
3	840	695	0·110	6·84	43·5	4·70	+0·028	267	0·022	4·50	−6·5
4	952	789	0·110	6·84	49·4	5·34	+0·001	269	0·001	5·33	−0·3
5	1292	1072	0·110	6·84	67·1	7·25	−0·048	272	−0·015	7·47	+18·6
6											
7	1250	1040	0·110	6·84	65·1	7 03	+0·060	277	−0·020	6·76	−21·1
8	527	450	0·027	8·25	23·3	2·52	+0·150	277	0·392	1·30	−10·2
9											
10	873	745	0·035	7·99	39·9	4·31	+0·047	274	0 042	3·97	−9·7
11	1176	1016	0·014	8·89	48·9	0·28	+0·039	271	0·024	5 03	−10·2
12											
13	513	428	0·090	7·05	26·0	2·81	−0·063	272	−0·136	3·77	+12·3
14	888	785	0·004	10·16	33·1	3·57	−0·002	272	−0·003	3·55	+0·4
15	418	349	0·090	7·05	21·2	2·29	−0·005	272	−0·016	2·37	+0·6
16	728	616	0·035	7·99	33·0	3·56	−0·002	269	− 0·003	3·54	+0·4
17	742	596	0·340	5·71	44·7	4·83	+0·021	271	0·015	4·69	−5·1
18	1016	829	0·230	6·10	58·2	6·29	+0·005	269	0·002	6·26	−1·6
19	1396	1172	0·070	7·28	68·9	7·44	+0·009	272	0·003	7·40	−3·5
20	1218	954	0·640	5·06	80·7	8·72	+0·108	274	0·024	8·31	−46·7
21	1080	895	0·110	6·84	56·0	6·05	+0·050	273	0·023	5·78	−15·0
22	653	541	0·110	6 84	33·9	3·66	+0·070	274	0·087	3·10	−11·3
23	878	730	0·110	6·84	45·7	4·94	0	269	0	4·94	0
24	484	383	0·540	5·24	31·3	3·38	−0·072	271	−0·107	4·24	+15·9
25	1076	895	0·110	6 84	56·0	6·05	+0·015	270	0·007	5·97	−4·7
26											
27	1910	1612	0·050	7·62	90·5	9·77	+0·169	272	0·030	9·21	−81·0
28	1400	1182	0·050	7·62	66·4	7·17	0	274	0	7·17	0
29	1530	1302	0·035	7 99	69·7	7·53	+0·032	271	0 010	7·38	−12·3
30											
31											
Mean			0·140				+0·026		0·018	5·27	−8·2

TABLE 24

EDDY HEAT FLUX: PLATEAU, DECEMBER
10 a.m.-4 p.m. period

1 Date	2 V_4 cm sec^{-1}	3 V_1 cm sec^{-1}	4 z_0 cm	5 $ln\ z/z_0$	6 u^* cm sec^{-1}	7 A_a	8 $d\theta/dz$ °C m^{-1}	9 T °K	10 Ri	11 A	12 Q cal cm^{-2}
1											
2											
3											
4	667	538	0·270	5·94	38·8	4·19	−0·141	274	−0·134	5·59	+41·0
5	1216	1010	0·110	6·84	63·2	6·83	+0·057	274	0·020	6·57	−19·4
6											
7	680	534	0·650	5·06	45·2	4·88	+0·055	279	0·038	4·53	−13·0
8											
9											
10											
11											
12											
13											
14											
15											
16	626	496	0·540	5·24	40·5	4·37	−0·003	271	−0·003	4·40	+0·7
17	553	476	0·020	8·55	23·8	2·57	−0·044	274	−0·111	3·25	+7·4
18	733	614	0·070	7·28	36·1	3·90	−0·013	272	−0·014	4·01	+2·7
19	1045	860	0·180	6·33	58·1	6·27	+0·010	273	0·004	6·22	−3·2
20	923	775	0·070	7·28	45·6	4·92	+0·005	276	0·003	4·89	−1·3
21	477	396	0·110	6·84	24·8	2 68	−0·068	278	−0·156	3·76	+13·3
22											
23	410	332	0·270	5·94	23·9	2·58	−0·050	272	−0·126	3·38	+8·8
24											
25											
26	2084	1765	0·034	8·02	94·2	10·17	−0·080	273	−0·013	10·44	+43·4
27											
28	1238	1016	0·180	6·33	68·7	7·42	+0·005	275	0·002	7·39	−1·9
29	1160	970	0·070	7·28	57·0	6·16	+0·012	274	0·005	6·10	−3·8
30											
31											
Mean			0·198				−0·020		−0·037	5·42	+5·7

TABLE 25

EDDY HEAT FLUX: PLATEAU, DECEMBER
4 p.m.-10 p.m. period

1 Date	2 V_4 cm sec^{-1}	3 V_1 cm sec^{-1}	4 z_0 cm	5 $ln\ z/z_0$	6 u^* cm sec^{-1}	7 A_u	8 $d\theta/dz$ °C m^{-1}	9 T °K	10 Ri	11 A	12 Q cal cm^{-2}
1											
2	436	354	0·270	5·94	25·5	2·75	−0·190	270	−0·425	8·31	+82·0
3											
4											
5											
6	1114	925	0·110	6·84	57·9	6·25	+0·056	277	0·024	5·96	−17·3
7											
8											
9											
10	270	216	0·380	5·59	16 5	1·78	+0·011	276	0·058	1·59	−0·9
11											
12											
13											
14											
15	290	226	0·730	4·94	19 6	2·12	+0·072	273	0 270	1·31	−4·9
16	431	356	0·110	6·84	22·3	2·41	0	271	0	2·41	0
17	486	386	0·460	5·41	30·5	3·29	−0·021	274	- 0·032	3·51	+3·8
18	887	741	0·090	7 05	45·0	4·86	0	271	0	4·86	0
19	1128	923	0·180	6·33	62·4	6·74	+0·043	272	0·016	6·53	−14·6
20	890	745	0·090	7·05	45·2	4·88	+0·024	274	0·017	4·72	−5·9
21	320	263	0·180	6·33	17 8	1·92	−0·070	277	−0·313	4·07	+14·8
22											
23	467	406	0·009	9·36	18·6	2·01	−0·014	272	−0·058	2·27	+1·7
24											
25											
26	2200	1870	0·035	7·99	100·2	10 82	+0·138	271	0·020	10·40	−74·6
27	504	411	0·230	6 10	28 8	3·11	+0·060	276	0·103	2·56	−8·0
28											
29	1663	1352	0·230	6·10	94·9	10·25	+0·010	273	0·002	10·21	−5·3
30											
31											
Mean			0·222				+0 009		−0·023	4·91	−2·1

TABLE 26

EDDY HEAT FLUX: PLATEAU, JANUARY
10 p.m.-4 a. m. period

1 Date	2 V_4 cm sec^{-1}	3 V_1 cm sec^{-1}	4 z_0 cm	5 $ln\ z/z_0$	6 u^* cm sec^{-1}	7 A_a	8 $d\theta/dz$ °C m^{-1}	9 T °K	10 Ri	11 A	12 Q cal cm^{-2}
1	758	615	0·270	5·91	44·5	4·85	+0·036	270	0·026	4·61	−8·6
2	737	605	0·180	6·32	41·0	4·46	−0·019	273	−0·016	4·61	+4·6
3	905	720	0·450	5·40	57·1	6·22	+0·188	272	0·083	5·30	−51·8
4	682	540	0·530	5·23	44·2	4·81	+0·024	273	0 018	4·64	−5 8
5											
6											
7											
8											
9	732	570	0·730	4 91	49·7	5 41	+0·185	269	0·109	4·40	−42·3
10	240	195	0·270	5·91	14·1	1 53	+0·072	271	0·525	0·66	−2·5
11	885	706	0·380	5·57	54·3	5·91	+0·133	268	0·066	5·20	−36·0
12	830	671	0·270	5·91	48·6	5·30	+0·053	270	0·033	4·97	−13·7
13	955	774	0·270	5·91	56·0	6 10	+0·099	269	0·046	5·58	−28·7
14	1152	950	0·150	6·50	62·6	6·82	+0·012	270	0·004	6·77	−4·2
15	1956	1622	0·110	6·80	102·2	11 12	+0·029	269	0·004	11 03	−16·6
16	1890	1570	0·110	6·80	98·9	10 78	+0·096	272	0·014	10·49	−52·3
17	1338	1098	0·180	6·32	74·4	8 10	+0·147	273	0·038	7·52	−57·5
18	958	785	0 180	6·32	53·2	5 80	+0·130	273	0·066	5·11	−34·6
19											
20	1165	965	0·110	6·80	60·8	6·62	+0·007	271	0 003	6·58	−2·4
21	1143	909	0 450	5·40	72·0	7 85	+0·075	271	0·021	7·53	−29·4
22											
23	891	691	0·850	4·77	62·1	6·76	+0·103	269	0·039	6·26	−33·6
24	1262	972	0·950	4·66	89·3	9·72	+0·021	269	0·004	9·64	−10·5
25											
26											
27	1160	885	1·100	4·50	84·2	9·16	0	266	0	9·16	0
28	1130	845	1 600	4·13	87·5	9·54	+0·082	269	0 016	9·24	−39·4
29	1107	871	0·530	5·23	71·4	7 77	+0·101	270	0·029	7·34	−38·5
30	1124	905	0·340	5 68	68·2	7 42	+0 017	269	0·005	7·35	−6 5
31	1025	785	1·100	4·50	74·7	8·14	+0·048	269	0·013	7·93	−19 8
Mean			0·483				+0·071		0·050	6·60	−23·0

TABLE 27

EDDY HEAT FLUX: PLATEAU, JANUARY
4 a.m.-10 a.m. period

1 Date	2 V_4 cm sec^{-1}	3 V_1 cm sec^{-1}	4 z_0 cm	5 $ln\ z/z_0$	6 u^* cm sec^{-1}	7 A_a	8 $d\theta/dz$ °C m^{-1}	9 T °K	10 Ri	11 A	12 Q cal cm^{-2}
1	472	384	0·230	6 08	27·0	2·94	—0·038	273	—0·075	3·44	+6·8
2	551	438	0·450	5·40	34·8	3·79	—0 024	274	—0·028	4·01	+5·0
3	961	771	0·380	5·57	59·4	6·46	+0·037	272	0·015	6·27	—12·0
4	790	638	0·270	5·91	46·2	5·03	+0·019	274	0·013	4·90	—4·8
5											
6											
7											
8											
9	762	617	0·270	5 91	64·7	7·05	+0·055	272	0·019	6·79	—19·4
10	510	411	0·270	5·91	29·8	3·25	—0·046	272	— 0·075	3·80	+9·1
11	765	624	0·230	6·08	43·4	4·73	—0·003	269	—0·002	4·75	+0·7
12	864	705	0·230	6·08	49·6	5·40	+0·010	271	0·006	5·34	—2·8
13	1437	1190	0·110	6·80	75·0	8·17	+0·029	271	0·007	8·06	—12·2
14	1445	1180	0·230	6·08	83·0	9·05	+0·003	270	0·001	9·03	—1·4
15	2112	1760	0·090	7·00	107·7	11·71	+0·056	270	0·007	11·55	—33·6
16	1553	1283	0·150	6·50	84·5	9·20	—0·034	274	—0·007	9·35	+16·5
17	1400	1155	0·150	6·50	76·0	8 28	+0·029	275	0·007	8·17	—12·3
18	1050	862	0·180	6·32	58·5	6·37	—0·005	273	—0·002	6·40	+1·7
19											
20	1456	1211	0·090	7·00	74 1	8·07	—0 018	272	—0·004	8·22	+7·7
21	1114	898	0·340	5·68	67·7	7·37	+0·027	272	0·009	7·24	—10·2
22											
23	959	795	0·110	6·80	50·0	5·44	—0·052	269	—0·030	5·78	+15·6
24	1292	998	0·840	4·77	89·5	9·75	—0·011	270	—0·002	9·80	+5·6
25	845	648	0·950	4·66	59·5	6 48	—0 036	270	—0·015	6·68	+12·5
26	825	679	0·180	6·32	46·0	5·01	—0·082	268	—0·056	5·69	+24·0
27	1010	835	0·150	6·50	55·0	5·99	—0·030	268	—0·015	6·18	+9·6
28	1134	923	0·230	6·08	65·0	7·07	+0·041	269	0·014	6·88	— 14·7
29	825	675	0·180	6·32	45·7	4·97	0	271	0	4·97	0
30	1013	755	1·800	4·02	80·5	8·76	—0·016	270	—0·003	8·83	+7·3
31	992	817	0·150	6·50	53·8	5·85	—0·018	269	—0·008	6·00	+5·6
Mean			0·330				—0·004		—0·009	6·72	+0·2

TABLE 28

EDDY HEAT FLUX: PLATEAU, JANUARY
10 a.m.-4 p.m. period

1 Date	2 V_4 cm sec^{-1}	3 V_1 cm sec^{-1}	4 z_0 cm	5 $ln\ z/z_0$	6 u^* cm sec^{-1}	7 A_a	8 $d\theta/dz$ °C m^{-1}	9 T °K	10 Ri	11 A	12 Q cal cm^{-2}
1											
2											
3											
4											
5											
6											
7											
8											
9											
10											
12											
13	1440	1188	0·150	6·50	78·4	8·54	0	273	0	8·54	0
14	1460	1211	0·110	6·80	76·4	8·32	—0·036	272	—0·009	8·47	+15·8
15	2520	2026	0·340	5·68	152·6	16·60	—0·036	270	—0·002	16·67	+31·2
16	955	865	0·001	11·50	32·2	3 50	—0·017	275	—0·046	3·85	+3·4
17	1045	855	0·180	6·32	58·0	6·32	—0·017	276	—0·007	6·41	+5·7
18	408	329	0·340	5·68	24·8	2·70	—0·050	276	—0·118	3·47	+9·0
19											
20											
21	855	690	0·270	5·91	50·0	5·45	—0·038	273	—0·021	5·69	+10·9
22											
23	715	549	0·950	4·66	50·5	5·50	—0·207	273	—0·116	7·37	+79·2
24	1183	939	0·450	5·40	74·5	8 12	—0·037	272	—0·010	8·28	+15·9
25											
26											
27											
28	1108	882	0·450	5·40	70·1	7·65	—0·031	272	—0·008	7·78	+12·5
29											
30	643	485	1·400	4·27	48·6	5·30	—0·079	273	—0·048	5·87	+24·1
31											
Mean			0·422				—0·050		—0·035	7·49	+18·9

TABLE 29

EDDY HEAT FLUX: PLATEAU, JANUARY
4 p.m.-10 p.m. period

1 Date	2 V_4 cm sec^{-1}	3 V_1 cm sec^{-1}	4 z_0 cm	5 $ln\ z/z_0$	6 u^* cm sec^{-1}	7 A_a	8 $d\theta/dz$ °C m^{-1}	9 T °K	10 Ri	11 A	12 Q cal cm^{-2}
1	278	213	1·100	4·50	20·3	2·21	−0·125	277	−0·430	6·80	+44·2
2											
3											
4											
5											
6											
7											
8	245	198	0·270	5 91	14·3	1·56	+0·039	274	0·273	0·96	−1·9
9											
10	320	256	0·380	5·57	19·7	2·14	−0·026	274	−0·096	2·62	+3·5
11											
12											
13	1163	955	0·180	6·32	64·7	7·05	+0·017	272	0·006	6·97	−6·2
14	1694	1410	0·110	6·80	88·8	9·67	0	270	0	9·67	0
15	2326	2045	0·004	10·14	86·5	9 42	+0·030	271	0·006	9·31	−14·5
16	864	702	0·230	6·08	49·5	5·39	+0·005	275	0·003	5·36	−1·4
17	418	346	0·110	6·80	21·8	2·37	−0·021	275	−0·063	2·70	+2·9
18											
19											
20	915	695	1·200	4·41	67·5	7 35	+0·005	272	0·002	7·32	−1·9
21											
22	276	206	1·600	4·13	21·4	2·33	−0·153	274	−0·478	8·07	+64·2
23	825	630	1·100	4·50	60·0	6·53	0	271	0	6·53	0
24											
25	548	483	0·004	10·14	20·3	2 21	−0·106	272	−0·370	5·57	+30·7
26	386	285	1·900	3·96	30·8	3 36	−0·090	272	−0·137	4·51	+21·1
27	1024	788	0·950	4·66	72·5	7·90	+0 021	269	0·006	7·81	−8·5
28	888	731	0·150	6·50	48·2	5·25	+0·043	271	0·027	4 98	−11·1
29											
30	394	307	0 720	4 93	26 6	2 90	−0·048	272	−0·099	3·57	+8·9
31	537	415	0·850	4·77	37·2	4·05	−0·112	273	−0·116	5·18	+30 2
Mean			0·639				−0·031		−0·086	5·70	+9·4

TABLE 30

COMPARISON BETWEEN EDDY HEAT FLUX COMPUTATIONS FOR DAILY MEANS AND SUM OF 6-HOURLY MEANS PLATEAU, DECEMBER

Date	Period considered hrs	Q (Daily means) cal $cm^{-2}day^{-1}$	Q (Sum of 6-hour means) cal $cm^{-2}day^{-1}$
1	12	−22·9	−23·4
2	12	−54·7	75·3
3	12	−26·4	−17·9
4	18	19·0	22·3
5	18	−9·4	−6·7
6	12	−25·2	−25·3
7	18	−39·5	−28·5
8	12	−51·8	−58·9
9			
10	12	−8·3	−10·6
11	12	−31·5	−27·5
12			
13	12	9·5	8·8
14	12	−9·5	−10·0
15	18	−24·1	−25·7
16	24	0	1·1
17	24	7·8	3·6
18	24	0	−7·7
19	24	−35·2	−34·6
20	24	−102·8	−119·0
21	24	10·2	2·1
22	12	−15·5	−15·7
23	24	4·2	−2·8
24	6	15·7	15·9
25	12	−31·6	−22·1
26	12	−31·2	−30·2
27	12	−69·4	−89·0
28	18	−15·7	−15·4
29	24	−32·2	−33·0
30	6	−18·2	−18·3
31			
Mean		−17·1	−17·6

TABLE 31

FREQUENCY DISTRIBUTION OF RICHARDSON NUMBERS AT ALL THREE MEASURING SITES

$< -0{\cdot}5$	$-0{\cdot}5$ to $-0{\cdot}4$	$-0{\cdot}4$ to $-0{\cdot}3$	$-0{\cdot}3$ to $-0{\cdot}2$	$-0{\cdot}2$ to $-0{\cdot}1$	$-0{\cdot}1$ to 0	0 to 0·1	0·1 to 0·2	0·2 to 0·3	0·3 to 0·4	0·4 to 0·5	0·5 to 0·6	0·6 to 0·7	0·7 to 0·8	$> 0{\cdot}8$	Total
I. Plateau 50 m height, Nov.-Jan., 6-hour periods															
0	3	2	0	10	40	86	5	3	1	0	1	0	0	0	151
II. Plateau 150 m height, May-Aug., 24-hour periods															
					6	38	5	3	1	2	0	0	1	2	58
III. Sea ice, Jul.-Nov., 24-hour periods															
				1	13	82	7	1							104
Total:															
0	3	2	0	11	59	206	17	7	2	2	1	0	1	2	313

TABLE 32

DAILY MIDNIGHT SEA-ICE TEMPERATURES: MAY TO JULY
(Minus °C)

	MAY							JULY						
1	2	3	4	5	6	7	8	9	10	11	12	13	14	15
Date	T_0	T_{-15}	T_{-30}	T_{-45}	T_{-60}	T_{-80}	T_{-100}	T_0	T_{-15}	T_{-30}	T_{-45}	T_{-60}	T_{-80}	T_{-100}
1	13·1	9·6	6·3	3·0				25·1	21·4	17·5	13·6	9·6	4·3	1·8
2	10·8	8·7	6·4	3·6				23·8	20·9	17·3	13·5	9·7	4·6	1·8
3	11·2	8·1	6·0	3·7				15·2	16·1	15·0	12·5	9·5	4·9	1·8
4	9·6	8·0	6·0	3·9				12·3	12·3	11·4	10·0	7·9	4·3	1·8
5	8·4	6·7	5·3	3·6				17·6	15·0	11·5	9·4	7·3	4·4	1·8
6	11·5	8·2	6·0	4·0				15·7	14·2	12·0	9·5	7·2	4·0	1·8
7	11·6	8·5	6·2	4·0				17·6	14·5	11·8	9·3	7·2	4·2	1·8
8	12·4	9·8	7·1	4·5				14·2	12·6	11·3	9·3	7·2	4·2	1·8
9	7·3	7·4	6·2	4·2				13·3	12 3	10·9	9·0	7·0	4·2	1·8
10	10·6	8·3	6·2	3·8	(Mean)			14·7	12·2	10·5	8·7	6·9	4·3	1·8
11								18·0	14·1	11·2	8·8	6·8	4·3	1·8
12				JUNE				21·2	16·7	13 2	10·1	7·5	4·5	1·8
13								16 8	16·4	14·2	11·3	8·3	4·6	1·8
14	21·9	16·6	12·0	7·3	2·6	1·8	1·8	14·5	13·7	12·5	11·8	8·6	5·5	1·8
15	19·0	14·4	10 9	7·1	3·2	1·8	1·8	17·1	13·4	11·3	9·4	7·6	5·0	1·8
16	20·0	16·4	12·2	7·8	3·6	1·8	1·8	17·6	15·1	12·9	10·4	8·1	5·2	2·2
17	17·3	13·9	11·0	7·7	3·5	1·8	1·8	21·2	16·9	13·9	11·2	8·6	5·4	2·3
18	16·3	14·7	11·6	7·9	4·0	1·8	1·8	25 1	20·3	16·2	12·8	9·6	5·0	2·6
19	17·6	14·5	11·0	7·4	3·8	1·8	1·8	26·3	22·2	18·2	14·3	11·0	6·8	2·9
20	21·9	17·0	12·3	8·0	4·1	1·8	1·8	28 0	23·5	19·4	15·4	11·9	7·5	3·0
21	22·4	18·0	13·4	9·1	5·1	1 8	1·8	29·3	25·0	21·0	16·6	12·9	8·2	3·4
22	23·1	18·7	14·4	10·0	5·7	1·8	1 8	26·4	24·4	21·3	17·5	13·6	8·8	3·9
23	21·3	17·1	13·7	10·1	6·1	1·8	1·8	22·8	21·0	18·6	16·2	13·3	9·3	4·4
24								23·5	20·5	17·7	15·0	12·4	8·6	4·3
25	23·8	19·1	14·9	10·7	6·7	2·0	1·8	20·1	19·7	17·9	15·6	12·9	9·2	5·0
26	26·0	21·0	16·3	11·9	7·6	2·4	1·8	16·8	16·6	15·7	14·2	12·3	9·2	5·5
27	23·5	19·5	15·7	12·0	8·0	2·9	1 8	15·6	14·5	13·6	12·2	10·6	8·0	4·6
28	24·6	21·0	16·8	12·5	8·4	3·2	1·8	19·2	16·0	13·6	11·6	9·7	7·3	4·2
29	25·5	21·3	17·0	12·9	8·9	3 6	1·8	22·0	18·0	15·1	12·4	10·1	7·3	4·1
30	25·6	21·9	17·7	13·5	9·3	4·0	1·8	21·2	19·1	16·5	13·7	10·9	7·7	4·4
31								21·1	18·5	16·2	13 6	11·2	7·9	4 5
Mean	21·9	17·8	13·8	9·7	5·7	2·3	1·8	19·7	17·3	14·7	21·1	9·5	6·0	2·9

TABLE 33

DAILY MIDNIGHT SEA-ICE TEMPERATURES: AUGUST TO SEPTEMBER
(Minus °C)

	AUGUST							SEPTEMBER						
1	2	3	4	5	6	7	8	9	10	11	12	13	14	15
Date	T_0	T_{-15}	T_{-30}	T_{-45}	T_{-60}	T_{-80}	T_{-100}	T_0	T_{-15}	T_{-30}	T_{-45}	T_{-60}	T_{-80}	T_{-100}
1	19·6	18·3	16·3	14 0	11·6	8·4	5·0	17·3	15·2	13 4	11·5	9·7	7·4	5 0
2	15·7	15 6	14·7	13·1	11 3	8 4	5·1	22 2	17·9	15·0	12·4	10·3	7·9	5·3
3	17·3	15 0	13 5	12·2	10·5	8·3	5·2	24·3	20·4	17·0	14·1	11·5	8·5	5·6
4	19·6	16·6	14·4	12·2	10·2	7·7	4·9	22·4	19·3	17·0	14·6	12·3	9·2	6·2
5	21 0	18·1	15 3	12 8	10·5	7·6	4·7	24 1	20·5	17 5	15·0	12·5	9·6	6·5
6	22·7	19 4	16·4	13·5	11·2	8·2	5·0	25·2	21·7	18 6	15·8	13·3	10·2	7·0
7	23 4	20·2	17·4	14·5	11·8	8·6	5·2	21 5	20·3	18·3	16·2	13·7	10·7	7·3
8	25·8	21 7	18 0	15 1	12·3	8·7	5·3	19·5	18 2	16·9	15·3	13·4	10·7	7·6
9	20·4	19·9	18 5	16 3	13·9	10 5	6·9	23 3	19·7	17·1	15·0	13·0	10·4	7·4
10	18·6	17·2	16·0	14·3	12·5	9·7	6 4	19·3	18·4	17·4	15·7	13·8	11·1	8·1
11	19 0	17·2	15·3	13·3	11·5	8 7	5·7	19·1	16 5	15·0	13·7	12·3	10·1	7·4
12	20·8	17·5	15·5	13·5	11 6	9·0	5·8	17·2	15·8	14·6	13·3	11·9	9 7	7·2
13	21·0	18 4	16·0	13·7	11·5	8·8	5 7	19·6	17·1	15·2	13·4	11·7	9·5	7·0
14	21·7	19·6	16 5	14·2	12·1	9·2	6·2	20·0	18·6	16 3	14·1	12·1	9 6	7·0
15	16 5	16 6	16·0	14 3	12·6	9·8	6 7	18·7	17 3	15·9	14·2	12·4	10·0	7·3
16	14·8	14·6	14·1	13·2	12·0	9·7	6·9	16·1	15·4	14·6	13·5	12·0	9·8	7·3
17	14·2	13 5	12 6	11·6	10·3	8·4	6·0	13·0	12·2	12·2	11·9	11·2	9 4	7·2
18	16 5	13·7	12·2	11 0	9·6	7·6	5·4	15·6	13·3	11·9	11·0	10·0	8·6	6·6
19	16 4	14 9	13·4	11·7	9·9	7·7	5·3	18·6	15·5	13 3	11·5	10·0	8·2	6·3
20	12·2	12·4	12·0	11·2	9·7	7·8	5·4	15·5	14·3	13·2	12·0	10·5	8·6	6 4
21	11·5	11·2	10·6	10·0	9·2	7·6	5·3	18·8	15·5	13·5	11 8	10·3	8·5	6·3
22	11·0	10·4	10·0	9·3	8·4	7·1	5·2	20·2	16·5	14·4	12·5	10·8	8 6	6·4
23	10·2	10·2	9·8	9·1	8·2	6·9	5·2	23 0	18 7	15·7	13·3	11·3	8·8	6·3
24	13·2	11·0	9·7	8·7	7·7	6·4	4·7	20·7	17·8	16·0	14 0	12·0	9·3	6·7
25	15 9	13·0	11 1	9·2	8·0	6·4	4·8	22·4	18·8	16·3	14·1	12·1	9·4	6·7
26	14·6	13·3	11·7	10·0	8·3	6·3	4 5	24·0	20·0	17·2	14·7	12·5	9·8	7·0
27	12 7	11·9	11 0	9·8	8·5	6·6	4·6	24 8	20 6	17·7	15·4	13·2	10·4	7·4
28	13·3	12·1	11·1	9·9	8·7	7·1	5·1	21·0	19·6	17·6	15 5	13·3	10·5	7·5
29	16·6	13·2	11·2	9·5	8·2	6·5	4·7	16·7	16·1	15 4	14 2	12·7	10·3	7·5
30	18·7	15·5	13·1	10·9	8·9	6·9	5 0	18·2	15·5	14·0	12·8	11·6	9·7	7·3
31	17·5	15·1	13·2	11·5	9·6	7·5	5·2							
Means	17 2	15·5	13·8	12 1	10·4	8·0	5·4	20 0	17·5	15·6	13·7	11·9	9 4	6·8

TABLE 34

DAILY MIDNIGHT SEA-ICE TEMPERATURES: OCTOBER TO NOVEMBER
(Minus °C)

	OCTOBER							NOVEMBER						
1	2	3	4	5	6	7	8	9	10	11	12	13	14	15
Date	T_0	T_{-15}	T_{-30}	T_{-45}	T_{-60}	T_{-80}	T_{-100}	T_0	T_{-15}	T_{-30}	T_{-45}	T_{-60}	T_{-80}	T_{-100}
1	17·5	15 5	14·0	12 6	11·4	9 4	7·1	9 8	8 6	7·9	7·0	6·3	5·1	4·1
2	12·7	13·2	12·9	12·2	11·2	9·2	7·0	7·1	7 3	7·1	6·6	5·9	4·8	4·3
3	11·6	11·5	11·3	11·1	10·2	8 8	7 0	7·2	6·0	5·8	5 6	5·2	4 3	3·5
4	13·8	11 2	9·8	9·4	8·8	7 8	6·2	8 0	6·3	5·9	5 6	5·2	4 5	3·6
5	15 5	11·9	10·5	9·6	8·7	7·5	5·9	10 0	7·2	6·3	5·9	5·3	4 6	3·8
6	15·1	12·0	10·5	9·5	8·6	7 2	5·6	9·0	6·8	6 0	5 4	4·8	4·2	3·3
7	17 5	12·6	10·5	9 3	8·3	7 0	5·3	12·0	8·4	6·9	5 7	4·9	4·1	3·3
8	16·0	13·1	11·2	9·7	8·5	7·0	5 3	14·5	9·2	7·3	6·3	5·2	4·2	3·3
9	17 6	13·1	11·2	9 8	8·6	7·1	5·2	12·5	9·2	7·6	6·4	5·2	4·2	3·2
10	22·3	16·0	12·6	10·5	8·9	7·0	5·2	13·8	9·3	7·6	6·5	5·3	4·2	3·3
11	21·7	16 2	13·2	11 3	9·5	7·3	5·2	12·6	8·8	7·3	6·3	5·4	4·2	3·2
12	16·4	15·2	13·5	11 5	9·8	7·6	5·3	14 5	9 5	7·4	6 3	5·3	4 2	3·3
13	14·1	14 3	13·5	12 4	11·1	9·1	7·2	13·6	8 5	7·0	6·2	5·2	4·1	3·2
14	11·4	12 0	11·6	11 2	9·9	8 6	6 4	12·7	7·5	6 5	6 0	5 2	4·2	3·3
15	9 3	9 1	9·2	8 9	8 4	7·2	5 6	11·7	7·3	6·2	5 6	4·9	3·9	3·0
16	10·5	9·5	9·0	8 5	8·0	6·9	5·5	9 0	6·2	5 7	5 4	4·8	4·0	3·2
17														
18	15·3	11 8	10 1	8 8	7·8	6 5	5·0							
19	16·8	12·8	10·9	9 3	8·0	6 5	5 0							
20	15·0	13 0	11·3	9 7	8·3	6·6	5·0							
21	10 6	11·1	10 1	9 5	8·6	7 0	5 2							
22	15·7	11·4	9·4	8 5	7·8	6·6	5·1							
23	15·3	11·5	9·4	8·3	7·4	6·1	4 6							
24	14·8	10·5	9 0	8·2	7·2	6·0	4·5							
25	14·7	10·1	8·6	8 0	7·1	5·8	4·3							
26	15·4	11·2	9·1	8·0	7·0	5·7	4·4							
27	14 0	10·1	8·5	7·8	6·9	5 5	4·2							
28	13·0	10 3	9 0	8·0	7·0	5·6	4·3							
29	11·6	8·1	7·5	7·1	6·3	5·2	3 8							
30	12 2	7·7	7·0	6·6	6·0	5 0	3·8							
31	10·8	7·5	6·8	6·2	5·7	4 7	3·6							
Mean	14 6	11·7	10·4	9·4	8·4	6 9	5 3	11 1	7·9	6·8	6·1	5·3	4·3	3·4

TABLE 35

DAILY MIDNIGHT PLATEAU-ICE TEMPERATURES: 1 M DEPTH
(Minus °C)

1 Date	2 Jan.	3 Feb.	4 Mar.	5 Apr.	6 May	7 Jun.	8 Jul.	9 Aug.	10 Sep.	11 Oct.	12 Nov.	13 Dec.
1			(5·4)	14 6	15·0	(16·4)	24·3	23·9	(18 0)	(15 7)	(11·3)	
2			(5·3)	14·6	(14·9)	(16·9)	24·3	23 9	18·7	(16·2)	(11·1)	
3			(5·2)	15·0	(14·7)	(17·5)	24·4	22·5	(19·6)	(16·8)	(11·0)	
4			5·1	14·9	(14·5)	(18·1)	23·6	21·2	(20·4)	(17·5)	(10 9)	
5			5·1	(14·8)	14·2	(18·6)	21·5	21·3	21·1	(18·0)	(10·8)	
6			(5·1)	14 4	(13·9)	(19·2)	20·4	21·8	21·9	(18·2)	(10·7)	
7			5·2	14·0	(13·6)	(19·7)	21 0	22 8	(22·4)	(18·2)	(10·6)	
8			5 3	(14·0)	(13·3)	20·2	20·3	23·6	(22 7)	(18·2)	10·4	
9			5·5	(14 1)	(12·9)	20·6	(19·7)	23·6	(22·8)	(18·1)	(10·2)	
10			5·8	(14·3)	(12·6)	19·9	19·4	24·0	(22·8)	(17·9)	(10·0)	
11			6 2	(14·7)	(12·3)	(19·9)	19 0	23·0	(22·7)	(17·7)	(9·8)	
12			6·5	(15·1)	11·9	(19·9)	18 9	22·8	(22·6)	17 4	(9·4)	
13			6 9	(15·5)	11·8	(20·0)	20·0	22·9	(22·5)	(17·0)	(9·0)	
14			7·3	(15·9)	13·0	(20·2)	20 2	(23·0)	(22·4)	(16·2)	(8·7)	
15			(7·8)	(16·3)	13·5	20·4	20·3	(23·1)	(22·2)	(15·4)	(8·4)	
16			(8·1)	(16·7)	14·4	20·5	19·5	(23·1)	(22·0)	(14·4)	(8·0)	
17			(8·3)	(17·0)	15·7	20·7	20 2	(23·0)	(21·7)	13·4	(7·5)	
18			(8·5)	(17·5)	(17·0)	20·6	20 7	(22·9)	(21·4)	(12·9)	(6·6)	
19			8·8	(17·9)	(18·3)	20·2	(21·6)	(22·6)	(21·0)	(12·9)	(5·6)	
20			9·0	18·1	19 4	20·0	22 8	(22 3)	(20·5)	13·6	(5·3)	
21			9·4	(18·4)	19·4	20·0	24·4	(22·0)	(20·0)	(14·0)	(5·4)	
22			10·0	18·6	17 2	20·9	(24·9)	(21·6)	(19·4)	(14·2)	(5·9)	
23			10·8	18·7	15·5	21·3	(25·1)	(21·3)	(18·8)	(14·3)	(6·5)	
24			12·4	17·0	13·6	21·8	25·3	(20 7)	(18·1)	(14·2)	(6·9)	
25			13·0	15 0	13·1	22·2	25 3	(20·2)	(17·5)	(14·0)	(7·0)	
26			13·6	14·4	13·3	(22·6)	24·5	19·5	(17·0)	(13·8)	7·1	
27			14·0	(14·4)	13·8	(23 0)	23·2	(18·6)	(16·3)	13·2	5 8	
28			(14 1)	(14 5)	(14·2)	(23·4)	21·4	(17 8)	(15 9)	(12·5)	(6 1)	
29			(14·2)	(14·8)	(14 8)	23·7	21·5	(16·9)	(15·6)	(12·0)	(5·9)	
30			(14·3)	15·0	15·3	24·0	22·5	(16·6)	(15·5)	11·7	(5·6)	
31			(14 4)		15·9		23 4	(17·1)		(11·5)		
Mean			8 7	15·7	14 6	20·4	22·1	21·6	20·1	15·2	8·3	

TABLE 36

DAILY MIDNIGHT PLATEAU-ICE TEMPERATURES: 2 M DEPTH
(Minus °C)

1 Date	2 Jan.	3 Feb.	4 Mar.	5 Apr.	6 May	7 Jun.	8 Jul.	9 Aug.	10 Sep.	11 Oct.	12 Nov.	13 Dec.
1			(5·1)	9·9	13·7	(13·4)	18 6	20·0	(17·4)	(16·6)	(13·6)	
2			(5·0)	10·2	(13·7)	(13·5)	18·9	20·0	17·4	(16·5)	(13 4)	
3			(5·0)	10·3	(13·7)	(13·6)	19·0	20·2	(17·6)	(16·5)	(13·3)	
4			5·0	10·5	(13·6)	(13·7)	19·1	20·1	(17·8)	(16·5)	(13·0)	
5			5·0	(10·7)	13·5	(13·8)	19 2	19·9	18·0	(16·6)	(12·9)	
6			(4·9)	10·9	(13·3)	(14·0)	19·3	19·7	18·2	(16·6)	(12·7)	
7			4·9	11·1	(13 1)	(14·1)	19·1	19·7	(18·4)	(16·7)	(12·6)	
8			4·9	(11·1)	(12·9)	14·2	18·8	19·9	(18·5)	(16·7)	12·5	
9			4·9	(11·0)	(12·7)	14·3	(18·7)	19·9	(18·6)	(16·7)	(12·3)	
10			4·9	(11·0)	(12·6)	14·5	18·5	20·1	(18·6)	(16·7)	(12·1)	
11			5·0	(11·1)	(12·4)	(15·0)	18·5	20 3	(18·7)	(16·6)	(11·9)	
12			5·1	(11·4)	12·3	(15·4)	18·1	20·4	(18·7)	16·6	(11·5)	
13			5·2	(11·6)	12·2	(15·8)	18·0	20·5	(18·7)	(16·5)	(11 2)	
14			5·4	(11·9)	12·2	(16·0)	18·0	(20·6)	(18·7)	(16 5)	(10·8)	
15			(5·5)	(12·2)	12·2	16·0	17·9	(20·7)	(18·6)	(16·5)	(10·5)	
16			(5·7)	(12·5)	12·3	16·1	18·1	(20·7)	(18 6)	(16·4)	(10·2)	
17			(5·9)	(12·7)	12·3	16·2	18·0	(20·8)	(18·6)	16·3	(10·0)	
18			(6·1)	(13·0)	(12·5)	16·3	18·0	(20·8)	(18·5)	(16·0)	(9·9)	
19			6·3	(13 3)	(12·9)	16·4	(18·1)	(20·7)	(18·4)	(15·7)	(9 8)	
20			6·6	13·6	13·4	16·5	18·3	(20·6)	(18·4)	15·2	(9·7)	
21			6·9	(13 8)	13·6	16·6	18·4	(20·4)	(18·3)	(15·0)	(9·8)	
22			7·1	14·0	13·8	16·6	(18·9)	(20·1)	(18·2)	(14·8)	(9·8)	
23			7·1	14·1	14·1	16·7	(19·4)	(19·8)	(18·0)	(14·9)	(10·0)	
24			7·8	14·3	14·1	16·8	30·0	(19·3)	(17·9)	(15·0)	(10·2)	
25			8·0	14·4	14·0	17·2	20·2	(18·9)	(17·7)	(14·8)	(10·4)	
26			8·4	14·4	13·6	(17·3)	20·4	18·5	(17·5)	(14·6)	10·6	
27			8·8	(14·3)	13·4	(17·6)	20·4	(18·2)	(17·3)	14·2	9·6	
28			(9·0)	(14·2)	(13·3)	(17·8)	20·4	(17·9)	(17·1)	(14·1)	(10·0)	
29			(9·2)	(14·0)	(13·3)	18·1	20·2	(17·6)	(17·0)	(14·0)	(9·9)	
30			(9·4)	13·8	(13 3)	18·3	20·0	(17·4)	(16·8)	13·9	(9 5)	
31			(9·7)		(13·4)		20·0	(17·4)		(13·8)		
Mean			6·3	12 4	13·2	15·7	19·0	19 7	18·1	15·7	11·1	

TABLE 37

DAILY MIDNIGHT PLATEAU-ICE TEMPERATURES: 4 M DEPTH
(Minus °C)

1 Date	2 Jan.	3 Feb.	4 Mar.	5 Apr.	6 May	7 Jun.	8 Jul.	9 Aug.	10 Sep.	11 Oct.	12 Nov.	13 Dec.
1			(6·9)	7·4	10·7	(11·3)	12·7	15 0	(16·2)	(16·1)	(15·2)	
2			(6·9)	7·5	(10·7)	(11·3)	12·8	14·9	16·2	(16·1)	(15·2)	
3			(6·8)	7·5	(10·7)	(11·2)	12·8	15·0	(16·2)	(16 0)	(15·1)	
4			6·8	7·6	(10·8)	(11·2)	12·9	15·1	(16·2)	(16·0)	(15·0)	
5			6·7	(7·7)	10·7	(11·1)	13·0	15·1	16 2	(16·0)	(14·9)	
6			(6·7)	7 8	(10·6)	(11·1)	13·1	15·2	16·2	(16·0)	(14·8)	
7			6·7	8·0	(10·6)	(11·1)	13 3	15·2	(16·2)	(16·0)	(14·7)	
8			6·7	(8·1)	(10·5)	11·1	13·4	15·3	(16·3)	(15·9)	14·5	
9			6·7	(8·2)	(10·4)	11·2	(13·5)	15·3	(16·3)	(15·9)	(14·4)	
10			6·7	(8·3)	(10·4)	11·2	13·6	15·4	(16·3)	(15·9)	(14·4)	
11			6·7	(8·5)	(10·4)	(11·2)	13·7	15·4	(16·3)	(15·8)	(14 3)	
12			6·6	(8·7)	10·4	(11·3)	13·8	15·5	(16·3)	15·8	(14·1)	
13			6·6	(8·8)	10·4	(11·4)	14 0	15·5	(16·3)	(15·8)	(14·0)	
14			6·6	(9·0)	10·6	(11·4)	14·0	(15·5)	(16·3)	(15·8)	(14·0)	
15			(6·6)	(9 1)	10 6	11·5	14 0	(15·6)	(16·3)	(15·8)	(13 9)	
16			(6·5)	(9·1)	10·6	11·6	13·9	(15·6)	(16·3)	(15 8)	(13·8)	
17			(6·5)	(3·1)	10·6	11·7	14·2	(15·7)	(16·4)	15·8	(13·7)	
18			(6·5)	(9·1)	(10·7)	11·7	14·1	(15·7)	(16·4)	(15·8)	(13·6)	
19			6·5	(9·1)	(10·7)	11·8	(14·2)	(15·8)	(16·4)	(15 8)	(13·6)	
20			6·5	9·1	10·7	11·8	14·2	(15·8)	(16·4)	15·8	(13·5)	
21			6·7	(9·2)	10·6	12 0	14·3	(15 8)	(16·4)	(15·8)	(13·5)	
22			6·7	9·3	10·6	12·1	(14 4)	(15·9)	(16·4)	(15·7)	(13·4)	
23			6·8	9·4	10·6	12·1	(14·4)	(15 9)	(16·4)	(15·6)	(13·4)	
24			6·9	9·5	10·6	12·2	14·4	(15·9)	(16·4)	(15·5)	(13·4)	
25			7·0	9·6	10·6	12·3	14 4	(16·0)	(16·4)	(15·4)	(13·4)	
26			7·0	9·8	10·8	(12·4)	14·4	16 0	(16·3)	(15·3)	13·5	
27			7 0	(9·9)	11·0	(12·5)	14·4	(16·1)	(16·3)	15·2	13·4	
28			(7·1)	(10·1)	(11·1)	(12·6)	14 5	(16 2)	(16·2)	(15·2)	(13·4)	
29			(7·1)	(10·3)	(11·2)	12·6	14·7	(16·3)	(16 2)	(15·3)	(13·3)	
30			(7·2)	10·5	(11·3)	12·8	14 7	(16·3)	(16·2)	15·3	(13·2)	
31			(7·3)		(11·3)		14 9	(16·3)		(15·3)		
Mean			6·8	8·8	10·7	11·7	13·9	15 6	16·3	15·7	14·0	

TABLE 38

DAILY MIDNIGHT PLATEAU-ICE TEMPERATURES: 8 M DEPTH
(Minus °C)

1 Date	2 Jan.	3 Feb.	4 Mar.	5 Apr.	6 May	7 Jun.	8 Jul.	9 Aug.	10 Sep.	11 Oct.	12 Nov.	13 Dec.
1				9 8	10·0		10·0	10·6				
2				9·9			10·0	10·5	12·0			
3				9·8			9·9	10·6				
4			10·7	9·8			9·9	10·7				
5			10·8		9·6		9·9	10·7	12·0			
6				9·8			10·0	10·8	12·0			
7			10·5	9·8			10·1	10·8				
8			10·2			9·6	10·0	10·8			13·2	
9			10·5			9·6		10·8				
10			10·2			9·5	10·2	10·9				
11			10·4				10·2	10·8				
12			10·5		9·2		10·2	11·0		12·9		
13			10·4		9·4		10·2	11·0				
14			10·2		9·4		10·2					
15					9·4	9·7	10·1					
16					9·4	9·6	10·2				13·2	
17					9·4	9·7	10·3			13·1		
18						9·7	10·3					
19			9·9			9·7						
20			9·9	9 6	9·5	9·7	10·3			12·9		
21			10·0		9·4	9·8	10·4					
22			9·9	9·6	9·4	9·8						
23			10·0	9·6	9·3	9·8						
24			10·0	9·6	9·4	9·8	10·4					
25			10·0	9·6	9·4	9·8	10·4					
26			9·9	9·8	9·5		10·4	11 6			13·2	
27			9·9		9·5		10·5			13·2	13·2	
28							10·4					
29						9·8	10·5				13·1	
30				10·0		9·9	10·5			13·2		
31							10·6					
Mean												

TABLE 39

DAILY MIDNIGHT PLATEAU-ICE TEMPERATURES: NOVEMBER TO DECEMBER
(Minus °C)

1 Date	2 T_0	3 $T_{-0.5}$	4 T_{-1}	5 T_{-2}	6 T_{-4}	7 T_{-6}	8 T_{-8}	9 T_{-11}
				NOVEMBER				
26	5·3	3·6	6·0	9·5	12·4	12·7	12·2	
27	6·8	2·4	4·7	8·5	12·3	12·7	12·1	
28	7·6	2·8	5·0	8·9	12·3	12·6	12·1	
29								
30	8·2	2·6	4·5	8·4	12·1	12·6	12·0	
				DECEMBER				
1								
2	5·5	1·7	3·9	8·3	12·0	12·6	12·1	
3	8·3	2·0	4·1	8·2	12·1	12·6	12·2	10·9
4	5·5	1·4	3·1	7·7	11·9	12·5	12·1	10·9
5	2·3	0·5	3·4	7·7	11·8	12·5	12·0	10·9
6	0·8	1·2	3·3	7·3	11·4	12·3	12·0	10·9
7	0	0·8	3·0	7·1	11·4	12·3	11·9	10·9
8	0	0·3	2·6	6·7	11·2	12·1	11·7	10·9
9	0·8	0	2·3	6·6	11·1	12·1	11·8	10·9
10	3·2	0	2·3	6·6	11·1	12·2	11·8	10·9
11	4·6	0	2·2	6·3	11·0	12·1	11·8	10·9
12	5·4	0	2·0	6·2	11·0	12·1	11·8	10·9
13	2·9	0	2·1	6·1	10·9	12·1	11·9	10·9
14	2·5	0	1·9	5·8	10·7	12·1	11·9	10·9
15	6·8	0	1·8	5·6	10·6	12·0	11·9	10·9
16	5·5	0	1·7	5·5	10·5	11·9	11·8	10·9
17	5·0	0	1·7	5·4	10·4	11·9	11·8	10·9
18	3·6	0	1·6	5·3	10·3	11·8	11·7	10·9
19	2·6	0	1·5	5·2	10·2	11·7	11·7	10·9
20	1·5	0	1·5	5·1	10·1	11·7	11·7	10·9
21	2·9	0	1·4	5·0	10·0	11·6	11·6	10·9
22	3·4	0	1·3	4·9	9·9	11·6	11·6	10·9
23	3·4	0	1·2	4·7	9·7	11·5	11·6	10·9
24	2·3	0	1·2	4·6	9·7	11·5	11·6	10·9
25	5·0	0	1·3	4·6	9·7	11·5	11·6	10·9
26	2·3	0	1·2	4·4	9·5	11·4	11·6	10·9
27	2·3	0	1·2	4·4	9·4	11·4	11·6	10·9
28	2·2	0	1·2	4·3	9·4	11·4	11·6	10·9
29	2·5	0	1·1	4·2	9·2	11·3	11·5	10·9
30	0·4	0	1·1	4·2	9·2	11·3	11·6	10·9
31	1·2	0	1·1	4·2	9·1	11·3	11·6	10·9
Mean	3·2	0·3	2·0	5·7	10·5	11·9	11·8	10·9

TABLE 40

DAILY MIDNIGHT PLATEAU-ICE TEMPERATURES: JANUARY TO FEBRUARY
(Minus °C)

1 Date	2 T_0	3 $T_{-0.5}$	4 T_{-1}	5 T_{-2}	6 T_{-4}	7 T_{-6}	8 T_{-8}	9 T_{-11}
				JANUARY				
1	3·0	0	1·0	4·2	9·2	11·3	11·7	11·1
2	1·0	0	0·9	4·0	9·0	11·3	11·7	11·1
3	2·2	0	0·9	4·0	9·0	11·3	11·7	11·1
4	1·2	0	0·8	3·8	8·8	11·2	11·6	11·0
5	0·5	0	0·8	3·8	8·8	11·2	11·6	11·1
6	1·8	0	0·8	3·7	8·7	11·1	11·6	11·0
7	5·0	0	0·9	3·7	8·7	11·1	11·5	11·1
8	6·2	0	0·8	3·6	8·6	11·0	11·5	11·1
9	4·6	0	0·8	3·6	8·5	11·0	11·5	11·0
10	1·9	0	0·8	3·6	8·5	11·0	11·5	11·1
11	5·3	0	0·8	3·6	8·4	10·9	11·5	11·1
12	3·5	0	0·8	3·5	8·4	10·9	11·5	11·1
13	4·6	0	0·7	3·4	8·3	10·7	11·4	11·1
14	3·0	0	0·8	3·4	8·3	10·7	11·4	11·1
15	4·0	0	0·7	3·3	8·2	10·6	11·4	11·1
16	2·6	0	0·7	3·3	8·1	10·5	11·4	11·0
17	0·3	0	0·8	3·4	8·2	10·6	11·4	11·2
18	1·0	0	0·9	3·4	8·2	10·6	11·4	11·2
19	3·2	0	0·8	3·3	8·1	10·5	11·4	11·2
20	2·5	0	0·6	3·2	7·9	10·4	11·3	11·1
21	3·0	0	0·6	3·2	7·8	10·3	11·3	11·1
22	5·2	0	0·6	3·2	7·8	10·3	11·3	11·1
23	4·5	0	0·4	3·0	7·6	10·3	11·3	11·1
24	5·2	0	0·5	3·1	7·7	10·3	11·3	11·2
25	6·4	0	0·5	3·1	7·7	10·3	11·3	11·2
26	6·0	0	0	2·9	7·5	10·1	11·2	11·1
27	5·8	0·3	0·3	3·0	7·6	10·2	11·3	11·2
28	0	0	0·3	2·7	7·3	10·0	11·1	11·1
29	—	0	0·3	2·7	7·3	9·9	11·0	11·0
30	—	0	0	2·6	7·3	9·9	11·0	11·0
31	—	0	0	2·6	7·2	9·8	11·0	11·0
Mean	3·5	0	0·6	3·4	8·2	10·6	11·4	11·1
				FEBRUARY				
1	—	0	0	2·5	7·1	9·7	10·9	10·9
2	—	0	0	2·5	7·1	9·7	10·9	10·9
3	—	0	0	2·5	7·1	9·7	10·9	10·9
4	—	0	0	2·4	7·0	9·6	10·9	10·9
5	—	0	0	2·3	6·9	9·6	10·9	11·0
6	—	0	0	2·3	6·9	9·5	10·9	11·0
7	—	0	0	2·3	6·9	9·6	10·9	11·0
8	—	0	0	2·3	6·7	9·5	10·7	11·0

TABLE 41

MIDNIGHT HEAT FLUX PLATE READINGS: SEA ICE, 30 CM DEPTH

mV

1 Date	2 June	3 July	4 Aug.	5 Sep.
1		11·4	7·3	6·1
2		9·6	6·2	6·4
3		10·0	3·5	9·5
4		4·1	4·5	11·3
5		3·1	6·8	8·0
6		5·6	8·0	9·8
7		6·5	8·5	10·1
8		6·6	7·8	7·0
9		4·6	9·6	5·0
10		4·8	4·9	7·8
11		4·9	4·3	5·2
12		7·9	6·0	4·0
13		9·6	6·1	4·1
14		7·0	7·1	6·6
15		4·2	7·4	8·2
16		6·5	3·5	5·2
17		6·9	2·0	3·3
18	9·0	8·8	3·1	—0·2
19	9·4	11·0	4·4	3·5
20	9·9	11·1	5·3	7·0
21	12·7	11·5	2·1	3·6
22	12·4	11·9	1·5	6·0
23	12·1	9·0	1·8	6·7
24	9·8	6·5	1·8	9·4
25	10·6	7·7	4·0	
26	12·0	5·5	6·3	
27	12·4	3·4	5·9	
28	10·5	3·6	3·6	
29	11·4	7·0	3·6	
30	11·6	8·6	6·4	
31		8·0	8·5	

TABLE 42

MAXIMUM AND MINIMUM DAILY HEAT FLUX PLATE READINGS
SEA ICE: 30 CM DEPTH
Hours & *mV*

	September				October				November			
1	2	3	4	5	6		8	9	10	11	12	13
Date	Local time	Max.	Local time	Min.	Local time	Max.	Local time	Min.	Local time	Max.	Local time	Min.
1					8	6·6	18	2·7	9	3·7		
2					7	5·7	18	1·7			17	—0·2
3					6	1·8	16	—1·0	4	0·7	16	—2·3
4					7	1·4	17	—1·4	6	0	14	—1·6
5					7	3·9	17	0·8	6	0 8	16	—2·2
6					8	6·7	17	0·2	7	1·9	16	—0·3
7					8	5·8	17	1·0	7	2·1	15	0·4
8					7	7·4	17	1·6	9	7·1	18	0·6
9					8	7·4	18	1·6	8	7·0	17	—0·1
10					8	9·5	17	3·5	7	5·5	17	0·5
11					7	12·2	18	3·6	7	7·1	17	·0·8
12					7	11·8	17	3·3	8	4·6	17	—0·5
13					2	6·4			7	7·0	18	0·0
14									8	7·0	18	—1·0
15							18	—0 2	7	5·0	17	—1·6
16					11	1·0	17	0·8	7	4 5	17	—1·5
17					10	2·1	17	1 8	7	1·1	16	—3·2
18					11	4·8	20	3·5				
19					9	6·2	19	4·8				
20					8	7·5	20	5·0				
21	12	5·4	17	4·7	7	5·7	18	2·4				
22	9	8·3	18	6·1	1	2·6	16	—0·8				
23	11	9·6	18	7·8	7	6·6	18	0·7				
24	8	10·9	23	6·5	7	6·8	18	—0·5				
25	10	9·1	18	6·6	8	6·2	17	—1·1				
26	9	10·0	17	7·2	7	5·8	17	—0·6				
27	9	10·6	18	7·0	7	7·0	17	—1·0				
28	8	10·7	18	6·8	8	5·7	17	0·8				
29			17	2·3	7	4·8	17	—1·9				
30	7	3·7	17	2·0	8	4·4	17	—1·8				
31					8	4·1	17	—1·8				

TABLE 43

MIDNIGHT HEAT FLUX PLATE READINGS: PLATEAU

mV

1 Date	2 F_{-1}	3 F_{-2}	4 F_{-4}	5 Date	6 F_{-1}	7 F_{-2}	8 F_{-4}	9 Date	10 F_{-1}	11 F_{-2}	12 F_{-4}
	March				May				July		
11	0·64	−0·04	− 0·23	1	0·12	0·50	0·27	13	0·95	0·49	
12	0·53	0	−0·24	2	0·68	0·55		14	1·10	0·54	
13	0·79	0·02	−0·23			June		15	0·60	0·60	
14	0·93	0·05	−0·22	16	1·32	1·01		16	0·10	0·63	
20	1·19	0·25	−0·13	17	1·50	1·01		17	0·79	0·60	
21	1·33	0·28	−0·12	18	1·20	1·00		18	1·06	0·59	
23	1·98	0 41	−0·11	19	1·16	0·99		19	1·27	0·59	
24	2·15	0·51	−0·10	20	0·90	1·00		21	2·84	0·82	
25	2·02	0 66	−0·10	21	1·22	0·92		22	3·10	0·92	
26	2 10	0·71	−0·08	22	1·55	0·89		25	1·50	1·31	
27	2·17	0·78	−0·07	23	1·72	0·92		26	1·50	1·25	
	April			24	1·80	0·97		27	0·12	1·20	
				25	1·70	1·01		28	−0·58	1·08	
2	1·66	0·86	0·02	30	2·14	1·15		29	0·08	0·90	
3	1·83	0·87	0·03			July		30	0·98	0·77	
7	0·63	0·89	0·08					31	1·73	0·75	
15	2·14	0·87	0·15	1	2·10	1·19			August		
20	1 90	1·07	0·19	2	2 00	1·21					
22	1·62	1·04	0·21	3	2·00	1·23		1	1·50	0·81	
23	1·22	1·08	0·22	4	1·25	1·25		2	1·32	0·87	
25	−0·40	1·00	0·24	5	−0·30	1·25		3	0·28	0·91	
26	−0·63	0·82	0·24	6	−0·40	1·06		4	−0·45	0·76	
27	−0·42	0·65	0·25	7	0·50	0·90		5		0·66	
28	0·05	0·45	0·25	8	0·13	0·81		7		0·59	
29	0 58	0·45	0·25	9	0·08	0·77		8		0·65	
30	0·55	0·46	0·25	10	−0·38	0·63		9		0·72	
				11	−0·48	0·61		10	1·40	0·70	
				12	0·05	0·53		11	0·50	0·72	
								12	0·54	0·72	
								13	0·72	0·68	

TABLE 44

TEMPERATURE AND HEAT FLUX IN SEA ICE AT 30 CM DEPTH: MONTHLY MEANS OF HOURLY VALUES FOR OCTOBER

1 Hour	2 F_{-30} (mV)	3 T_{-30} $(-°C)$
0	3·85	10·69
1	4·24	10·77
2	4·62	10·89
3	4·97	11·01
4	5·24	11·10
5	5·42	11·06
6	5·38	11·04
7	5·13	10·81
8	4·68	10·50
9	4·09	10·19
10	3·41	9·93
11	2·72	9·62
12	2·10	9·43
13	1·63	9·38
14	1·30	9·39
15	1·14	9·52
16	1·19	9·63
17	1·39	9·83
18	1·65	10·03
19	1·97	10·15
20	2·25	10·28
21	2·56	10·36
22	2·93	10·39
23	3·44	10·65

TABLE 45

LIGHT EXTINCTION IN PLATEAU ICE
(DAILY UNCORRECTED RADIOMETER READINGS AMPLITUDES)
mV

1 Date		2 N_1	3 N_2	4 N_4	5 H_1	6 H_2	7 H_4	8 N_1	9 N_2	10 N_4	11 H_1	12 H_2	13 H_4
				MARCH						APRIL			
1	clear							0·97	0·56	0·14	4·16	2·37	0·59
	o/cast							0·71	0·43	0·11	2·84	1·67	0·41
2								0·60	0·44	0·11	3·02	1·79	0·45
3								0·82	0·56	0·15	3·91	2·22	0·56
4													
5		1·16	0·72	0·07									
6								0·54	0·39	0·08	2·22	1·33	0·43
7		1·14	0·71	0·07									
8		1·67	0·87	0·13	7·12	3·86	0·94						
9													
10													
11	o/cast	1·18	0·62	0·10	4·93	2·80	0·65						
	clear	1·61	0·80	0·14	6·81	3·67	0·90						
12		1·69	0·85	0·15	6·81	3·67	0·91						
13		1·56	0·80	0·15	6·49	3·48	0·88						
14		1·63	0·78	0·16	6·36	3·39	0·86						
15													
16													
17													
18													
19		1·35	0·75	0·06									
20		1·61	0·87	0·11	6·98	3·73	0 93						
21													
22		1·42	0·79	0·12	5·34	3·00	0·73	0·09	0·03	0·01	0·23	0·15	0·05
23		0·44	0·38	0·05	2·59	1·50	0·37	0·20	0·07		0·31	0·22	0·13
24		1·01	0·85	0·13	4·90	2·86	0·71	0·32	0·18	0·05	1·60	0·95	0·31
25		1·03	0·78	0·15	4·86	2·86	0·69	0·49	0·22	0·06	1·59	0·88	0·32
26		1·01	0·71	0·15	4·75	2·76	0·69	0·50	0·25	0·05	1·72	0·94	0·31
27								0·49	0·25	0·07	1·84	0·96	0·32
28								0·50	0·27	0 07	1·75	0·94	0·32
29								0·46	0·20	0·05	1·10	0·65	0·21
30													
31													

TABLE 46

LIGHT EXTINCTION IN PLATEAU ICE
(DAILY UNCORRECTED RADIOMETER READINGS AMPLITUDES)
mV

	MAY		JUNE		JULY							
1	2	3	4	5	6	7	8	9	10	11	12	13
Date	H_1	H_2	H_1	H_2	H_1	H_2	H_1	H_2	H_4	N_1	N_2	N_4
1	1·22	0·68			0·11	0·06						
2					0·12	0·06			DECEMBER			
3					0·10	0·06						
4							9·00	4·00	0·92	2·50	1·15	0·17
5	1·20	0·64			0·12	0·07	8·30	3·90	0·92	2·32	1·12	0·20
6	1·00	0·60			0·13	0·08	8·70	4·05	0·94	2·50	1·18	0·19
7	1·16	0·65			0·13	0·09	8·30	3·90	0·90	2·40	1·12	0·19
8	0·54	0·29			0·14	0·09						
9	0·56	0·30	0·10	0·05								
10	0·80	0·38										
11					0·20	0·12						
12	0·76	0·41			0·20	0·12						
13	0·77	0·42										
14	0 73	0·38			0·15	0·09						
15					0·18	0·12						
16	0·62	0·32	0·07		0·18	0·12						
17					0·23	0·15						
18			0·08	0·04								
19			0·08	0·03								
20	0·41	0·25										
21	0·34	0·19	0·09	0·05	0·37	0·18						
22												
23	0·26	0·14										
24	0·22	0·13										
25			0·07	0·03								
26					0·45	0·23						
27					0·60	0·31						
28					0·61	0·33						
29					0·66	0·35						
30												
31												

TABLE 47

ABLATION: PLATEAU

(Mean values from 6-10 ablation stakes)

	150 m altitude					50 m altitude			
1	2	3	4	5	6	7	8	9	10
Period	Mean Ablation	ΣV_i^2	m	σ	Period	Mean Ablation	ΣV_i^2	m	σ
11/ 2–19/ 2/65	2·4	4 04	0·24	0·71	23/11–30/11/65	1·4	0 09	0·05	0·13
19/ 2– 2/ 3	2·2	0·29	0·06	0·19	30/11– 7/12	3·4	1·66	0·23	0·58
2/ 3– 8/ 3	1·3	0·66	0·10	0·29	7/12–14/12	7·6	0·08	0·20	0·28
8/ 3–22/ 3	1·6	0·65	0·10	0·29	14/12–21/12	3·0	0·71	0·09	0·28
22/ 3–30/ 3	0·3	0·05	0·03	0·08	21/12–28/12	2·2	1·64	0·15	0·45
30/ 3– 7/ 4	0 3	0·10	0·04	0·11	28/12– 5/ 1/66	4·0	3·26	0·18	0·53
7/ 4–15/ 4	0·2	0·09	0·04	0·11	5/ 1–12/ 1	3·8	1·61	0·13	0·42
15/ 4–25/ 4	0·2	0·16	0·05	0·14	12/ 1–19/ 1	4·4	2·23	0·16	0·50
25/ 4– 4/ 5	0·3	0·13	0·04	0·13	19/ 1–26/ 1	4·0	0·82	0·11	0·32
4/ 5–12/ 5	1·3	0·39	0·07	0·22	26/ 1– 2/ 2	3·7	6·74	0·58	1·30
12/ 5–20/ 5	0·2	0·06	0·03	0·09	2/ 2– 9/ 2	2·0	2·28	0·23	0·62
20/ 5–30/ 5	0·5	0·23	0·06	0·17					
30/ 5– 7/ 6	0·3	0·30	0·06	0·19					
7/ 6–18/ 6	0·3	0·10	0·04	0·11					
18/ 6–25/ 6	0·1	0·06	0·03	0·09					
25/ 6– 3/ 7	0·2	0·14	0·04	0·13					
3/ 7–10/ 7	0·2	0·15	0·05	0·14					
10/ 7–20/ 7	0 1	0·12	0·04	0·12					
20/ 7–28/ 7	0	0·07	0·03	0·09					
28/ 7– 4/ 8	0·2	0·08	0·03	0·10					
4/ 8–13/ 8	0·1	0·04	0·02	0·07					
13/ 8–24/ 8	0·8	0·27	0·06	0 18					
24/ 8– 4/ 9	0·5	0·11	0·04	0·12					
4/ 9–14/ 9	0·2	0·08	0·03	0·10					
14/ 9–23/ 9	0·3	0·23	0·06	0·17					
23/ 9– 5/10	0 7	0·19	0·05	0·15					
5/10–12/10	0·4	0·09	0·04	0·11					
12/10–25/10	1·2	0·58	0·09	0·27					
25/10–30/10	0·6	0·17	0·05	0·15					
30/10– 8/11	0·8	0·15	0·06	0·16					
8/11–16/11	1·1	0·14	0·05	0·14					
16/11–23/11	1 3	0·22	0·06	0·18					
23/11–30/11	1·5	0·14	0·05	0·14					
30/11–10/12	7·0	1·57	0·17	0·47					
10/12– 1/ 1/66	6·8	15·99	0·53	1·51					
1/ 1– 4/ 2	12·6	4·48	0·23	0·80					
Total:	48·1								

TABLE 48

ICE DENSITY

All density determinations were made in the winter of 1962, samples coming from the top 50 cm of ice. The density was determined by immersion in kerosine.

No. of samples	*Mean density*	*Locality from which the ice was taken*
4	0·872	
4	0·884	
4	0·851	Plateau, 150 m altitude
4	0·893	Ice cliffs, West Bay
4	0·890	,,
4	0·878	,,
4	0·893	,,
4	0·882	Face of small ice berg
4	0 871	,,
4	0·884	,,
Total: 40	Mean: 0·880	

TABLE 49

SEA ICE SALINITY

Sample No. 1		Sample No. 2		Sample No. 3		Sample No. 4		Sample No. 5	
Depth cm	Salinity ‰	Depth cm	Salinity ‰	Depth cm	Salinity ‰	Depth em	Salinity ‰	Depth cm	Salinity ‰
0–10	6·5	0–15	7	0–15	4	0–16	5·5	0–18	4·5
0–10	8·5	15–30	6	15–30	4	16–32	5·5	18–32	4·5
10–30	7	30–50	6	30–40	5	32–48	6·5	32–49	3·5
10–30	7·5	50–65	5	40–50	5	48–64	4·5	49–66	3·5
40–50	5	65–80	5	50–65	5	67–81	4	66–83	3·5
40–50	6	80–100	4	65–80	5	81–98	4	83–100	4·0
		100–120	4	80–95	6	98–115	4	100–116	3·5
				95–105	8	115–132	4	116–135	3·5
				105–120	4	132–154	4	135–147	3·5
				120–135	4				

Sample No. 1: Taken on 5/5/65 in Mawson Harbour. Mean density from three determinations: 0·935 g cm^{-3}.

Sample No. 2: Taken on 14/7/65 in Mawson Harbour.

Sample No. 3: Taken on 24/9/65 near instrument site in West Bay. Doubtful values since sample was only analysed on 28/9 and brine may have percolated out in the meantime.

Sample No. 4: Taken on 18/10/65 in Mawson Harbour.

Sample No. 5: Taken on 2/12/65 in Mawson Harbour.